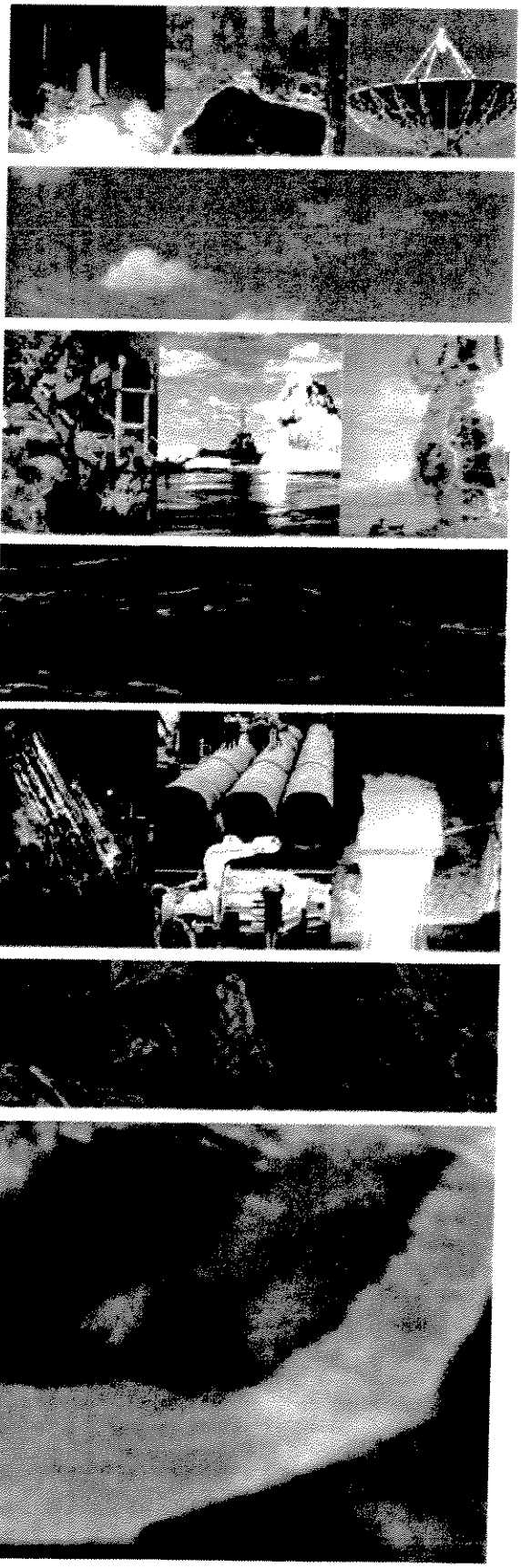

PROJECT OFFSHORE DEEP SLOPES, PHASE I

FINAL REPORT

April 2002
C-CORE Contract Report 01-C12

C-CORE

PROJECT OFFSHORE DEEP SLOPES, PHASE I

FINAL REPORT

Prepared for:

Chevron Canada Resources
Pan Canadian
Murphy Oil
ExxonMobil
Minerals Management Services
Norsk Hydro, Statoil

Prepared by:

C-CORE, OTRC, GSC, NGI

C-CORE Report:

01-C12

April 2002

C-CORE
Captain Robert A. Bartlett Building
Morrissey Road
St. John's, NF
Canada A1B 3X5

T: (709) 737-8354
F: (709) 737-4706

Info@c-core.ca
Www.c-core.ca

The correct citation for this report is:

C-CORE (2002). Project Offshore Deep Slopes – Phase I. Final Report. Prepared for: Chevron Canada Resources, Pan Canadian, Murphy Oil, ExxonMobil, Minerals Management Services, Norsk Hydro and Statoil. Prepared by: C-CORE, OTRC, GSC and NGI. C-CORE Publication 01-C12.

Project Team:

Lars Andersen (NGI)
Jack Clark (C-CORE)
Wayne Dunlap (OTRC)
Peijun Guo (C-CORE)
Richard Hanke (C-CORE)
Jocolyn Grozic (University of Calgary)
Ryan Phillips (C-CORE)
Dick Pickrill (GSC)
David Piper (GSC)
Gary Sonnichsen (GSC)
Abigail Steel (C-CORE)
Skip Ward (OTRC)
Stephen Wright (University of Texas)

EXECUTIVE SUMMARY

In October 1998, at an Associates' meeting in Calgary, industry members directed C-CORE to include deep-water oil and gas development as a priority issue in their offshore research program. Particular attention was drawn to the challenge of deep-water slopes which may experience failures that could affect exploration, production and transportation facilities. It was recognized that several organizations were doing fieldwork, laboratory testing of samples, back analysis of historical slide events and identification of geohazards. Work was being directed by different groups to the unraveling of the processes and mechanisms that trigger slides and how future stability could be predicted and risk assessed.

As a first step, C-CORE set out to bring together those organizations with major programs directed to deep-water slopes and to establish links with other networks willing to share the results of their work which could then be incorporated and considered in the study. The study was titled "Project Offshore Deep Slopes" with the acronym "PODS". The next step was to pull together a program, in consultation with potential sponsors and the partners, that could lead to achievement of the following objectives. The main objective of PODS is to develop a rational method for predicting the stability of submarine slopes under critical loading conditions that may be induced by nature or human activities. A major thrust was to study slides already documented, examining how and why they failed and modeling them numerically. The potential for verification of the numerical models would be demonstrated and assessed by analyzing the equivalent of full-scale events triggered in the C-CORE centrifuge.

Sponsorship of the program was sought from a number of organizations and a funding package was put together to allow the work to proceed. Sponsors of Phase 1 included Chevron, Minerals Management Service, Pan Canadian, Mobil Oil, Murphy Oil and Norsk Hydro and Statoil through NGI.

Phase 2 will include a detailed examination of failure mechanisms and numerical analyses verified by experimental modeling of submarine slopes. Phase 3 will see the production of a numerical model to predict submarine slope stability, based on all of the previous work related to case histories, theoretical analyses and experimental models. It will provide the framework for assessing risk related to exploration, production and operations in regions affected by the stability of submarine slopes.

The Phase 1 Project Team included C-CORE, the Geological Survey of Canada (GSC), the Norwegian Geotechnical Institute (NGI) and the Offshore Technology Research Centre (OTRC) of Texas A&M University.

The Phase I report includes a section on background information including previous work related to submarine slope instabilities and their classification, soil properties and significant indicies, seismic considerations and various analyses conducted.

Well-known case histories of submarine slides worldwide have been selected for study to provide a better understanding of the mechanisms at work when a slide occurs. The physical and

The correct citation for this report is:

C-CORE (2002). Project Offshore Deep Slopes – Phase I. Final Report. Prepared for: Chevron Canada Resources, Pan Canadian, Murphy Oil, ExxonMobil, Minerals Management Services, Norsk Hydro and Statoil. Prepared by: C-CORE, OTRC, GSC and NGI. C-CORE Publication 01-C12.

Project Team:

Lars Andersen (NGI)
Jack Clark (C-CORE)
Wayne Dunlap (OTRC)
Peijun Guo (C-CORE)
Richard Hanke (C-CORE)
Jocolyn Grozic (University of Calgary)
Ryan Phillips (C-CORE)
Dick Pickrill (GSC)
David Piper (GSC)
Gary Sonnichsen (GSC)
Abigail Steel (C-CORE)
Skip Ward (OTRC)
Stephen Wright (University of Texas)

EXECUTIVE SUMMARY

In October 1998, at an Associates' meeting in Calgary, industry members directed C-CORE to include deep-water oil and gas development as a priority issue in their offshore research program. Particular attention was drawn to the challenge of deep-water slopes which may experience failures that could affect exploration, production and transportation facilities. It was recognized that several organizations were doing fieldwork, laboratory testing of samples, back analysis of historical slide events and identification of geohazards. Work was being directed by different groups to the unraveling of the processes and mechanisms that trigger slides and how future stability could be predicted and risk assessed.

As a first step, C-CORE set out to bring together those organizations with major programs directed to deep-water slopes and to establish links with other networks willing to share the results of their work which could then be incorporated and considered in the study. The study was titled "Project Offshore Deep Slopes" with the acronym "PODS". The next step was to pull together a program, in consultation with potential sponsors and the partners, that could lead to achievement of the following objectives. The main objective of PODS is to develop a rational method for predicting the stability of submarine slopes under critical loading conditions that may be induced by nature or human activities. A major thrust was to study slides already documented, examining how and why they failed and modeling them numerically. The potential for verification of the numerical models would be demonstrated and assessed by analyzing the equivalent of full-scale events triggered in the C-CORE centrifuge.

Sponsorship of the program was sought from a number of organizations and a funding package was put together to allow the work to proceed. Sponsors of Phase 1 included Chevron, Minerals Management Service, Pan Canadian, Mobil Oil, Murphy Oil and Norsk Hydro and Statoil through NGI.

Phase 2 will include a detailed examination of failure mechanisms and numerical analyses verified by experimental modeling of submarine slopes. Phase 3 will see the production of a numerical model to predict submarine slope stability, based on all of the previous work related to case histories, theoretical analyses and experimental models. It will provide the framework for assessing risk related to exploration, production and operations in regions affected by the stability of submarine slopes.

The Phase 1 Project Team included C-CORE, the Geological Survey of Canada (GSC), the Norwegian Geotechnical Institute (NGI) and the Offshore Technology Research Centre (OTRC) of Texas A&M University.

The Phase I report includes a section on background information including previous work related to submarine slope instabilities and their classification, soil properties and significant indicies, seismic considerations and various analyses conducted.

Well-known case histories of submarine slides worldwide have been selected for study to provide a better understanding of the mechanisms at work when a slide occurs. The physical and

environmental conditions that are potential slide triggers are examined and the analytical work by others is summarized.

A section of the report is dedicated to Regional In-Depth Studies of the Scotian Slopes, St. Pierre Slope and Gulf of Mexico. The existing loading conditions, geohazards, geotechnical and geological conditions for the eastern Scotian Slope are identified and summarized. The three failures on the Scotian Slope, the Verrill, the Albatross and the Logan, are described in detail through consideration of the slide morphology, sediment types and properties and previous analyses. Transects through each of the failures are analyzed for existing slope stability through use of the infinite slope and limit equilibrium approach. How the existing failure could have evolved is assessed. Next, the effect of excess pore water pressure and seismic loading on the selected profiles is considered. The St. Pierre Slope is analyzed in a similar manner as the Scotian Slope failures.

The report contains a section on the analysis of wave induced sediment movements, with particular reference to the destruction of a platform in the Gulf of Mexico as a result of Hurricane Camille in 1969. This section did not appear in the draft report issued in October 2001. The development of numerical analyses to investigate sediment movement and resulting drag forces on structures is described, along with the parametric validation procedure. A presentation of the geotechnical aspects of gas hydrates is also given, with an examination of its role with respect to the potential instability effects on submarine slopes.

As a contribution by C-CORE to the project, centrifuge demonstration tests were conducted. Demonstration tests were considered necessary because modeling of submarine slope failures had never been carried out before by any centrifuge facility. Two tests were conducted. The first test showed remarkable resemblance to the full-scale failures documented in the literature. Failure occurred at a lower gravitational force than expected but the results were sufficiently encouraging to carry out a second test. The second test showed identical failure mechanisms to the first and the instrumentation functioned without a hitch. This allowed detailed analysis of the slide which has led to the conclusion that a range of mechanisms can indeed be modeled in the centrifuge to help verify potential methods to evaluate critical loading conditions and numerical analyses. This is a major contribution to the ability to conduct realistic risk analyses.

At this stage a framework for risk analysis is presented to identify dominant failure mechanisms and highlight the governing parameters for those mechanisms. The releasing agents are described, the data required for modeling is assessed and the site parameters outlined. Where readily available, mechanistic models governing the effect of the releasing agents are presented as well as data relating to the occurrence of failure triggers. Data and information gaps are outlined.

Results of Phase 1 will be reviewed with industry sponsors to provide a basis from which the program will be designed for Phase 2. A proposal for Phase 2, including recommendations from the team, is presented in Section 11.2 of this report. The project team will seek comments from the sponsors on the proposed program. The proposal focuses on aspects relating to the configuration of the experimental program and approaches recommended for analytical model verification.

EXTENDED ABSTRACT

Section 1 Introduction

Project Offshore Deep Slopes (PODS) was initiated following a C-CORE Associates Workshop in 1998. Industry members directed C-CORE to include the challenges faced in deep water exploration and development in their research program. Slope stability issues were identified as a major concern and an appropriate project for C-CORE to undertake. The over arching objective is to develop a rational method for the evaluation of submarine slopes under critical loading conditions through a study of case histories, experimental modeling and numerical analysis. The critical loading may be induced by nature or human activities. This was done by studying slides already documented, examining how and why they failed, and modeling them numerically. A project team was assembled to include those organizations known to have significant investigation and research programs underway that would contribute to this study. The partners included C-CORE, the Norwegian Geotechnical Institute (NGI), the Geological Survey of Canada - Atlantic (GSC-A) and the Offshore Technology Research Centre (OTRC) of Texas A&M University.

Sponsors for the program included Chevron, Minerals Management Services, Pan Canadian, ExxonMobil, Murphy Oil and Norsk Hydro and Statoil through NGI.

After identifying the major programs that were underway and the requirements to bring together the relevant work and extend it to meet the objectives, the project was divided into three phases.

Phase I consisted of eight main components. First it was necessary to investigate previous work done in this area in order to familiarize the team with background information on geotechnical, geophysical, geological and loading conditions. Next, the case histories were selected and examined to gain an understanding of the nature of submarine slides. Then to gain further knowledge of these elements, regional in depth studies were conducted on the Scotian Slope, the St. Pierre Slope and the Gulf of Mexico. Centrifuge demonstration tests were completed and presented in order to demonstrate the applicability of centrifuge modeling to the mechanics of submarine slopes and their trigger mechanisms. Next came the framework for risk analysis, which was presented in order to identify dominant failure mechanisms and highlight the governing parameters for those mechanisms. Lastly, results of Phase I were reviewed and preparations were made for Phase II and the design of an experimental program. Each of the sections comprising this report are briefly summarized in this extended abstract.

Section 2 Background Information

Data has been collected and summarized for the PODS project from a number of different authors and research programs. Research programs conducted relating to submarine slopes included:

- ADFEX – Arctic Delta Failure Experiment, 1982-1992
- GLORIA – Geological LOng-Range Inclined Asdic, 1984-1991

environmental conditions that are potential slide triggers are examined and the analytical work by others is summarized.

A section of the report is dedicated to Regional In-Depth Studies of the Scotian Slopes, St. Pierre Slope and Gulf of Mexico. The existing loading conditions, geohazards, geotechnical and geological conditions for the eastern Scotian Slope are identified and summarized. The three failures on the Scotian Slope, the Verrill, the Albatross and the Logan, are described in detail through consideration of the slide morphology, sediment types and properties and previous analyses. Transects through each of the failures are analyzed for existing slope stability through use of the infinite slope and limit equilibrium approach. How the existing failure could have evolved is assessed. Next, the effect of excess pore water pressure and seismic loading on the selected profiles is considered. The St. Pierre Slope is analyzed in a similar manner as the Scotian Slope failures.

The report contains a section on the analysis of wave induced sediment movements, with particular reference to the destruction of a platform in the Gulf of Mexico as a result of Hurricane Camille in 1969. This section did not appear in the draft report issued in October 2001. The development of numerical analyses to investigate sediment movement and resulting drag forces on structures is described, along with the parametric validation procedure. A presentation of the geotechnical aspects of gas hydrates is also given, with an examination of its role with respect to the potential instability effects on submarine slopes.

As a contribution by C-CORE to the project, centrifuge demonstration tests were conducted. Demonstration tests were considered necessary because modeling of submarine slope failures had never been carried out before by any centrifuge facility. Two tests were conducted. The first test showed remarkable resemblance to the full-scale failures documented in the literature. Failure occurred at a lower gravitational force than expected but the results were sufficiently encouraging to carry out a second test. The second test showed identical failure mechanisms to the first and the instrumentation functioned without a hitch. This allowed detailed analysis of the slide which has led to the conclusion that a range of mechanisms can indeed be modeled in the centrifuge to help verify potential methods to evaluate critical loading conditions and numerical analyses. This is a major contribution to the ability to conduct realistic risk analyses.

At this stage a framework for risk analysis is presented to identify dominant failure mechanisms and highlight the governing parameters for those mechanisms. The releasing agents are described, the data required for modeling is assessed and the site parameters outlined. Where readily available, mechanistic models governing the effect of the releasing agents are presented as well as data relating to the occurrence of failure triggers. Data and information gaps are outlined.

Results of Phase 1 will be reviewed with industry sponsors to provide a basis from which the program will be designed for Phase 2. A proposal for Phase 2, including recommendations from the team, is presented in Section 11.2 of this report. The project team will seek comments from the sponsors on the proposed program. The proposal focuses on aspects relating to the configuration of the experimental program and approaches recommended for analytical model verification.

EXTENDED ABSTRACT

Section 1 Introduction

Project Offshore Deep Slopes (PODS) was initiated following a C-CORE Associates Workshop in 1998. Industry members directed C-CORE to include the challenges faced in deep water exploration and development in their research program. Slope stability issues were identified as a major concern and an appropriate project for C-CORE to undertake. The over arching objective is to develop a rational method for the evaluation of submarine slopes under critical loading conditions through a study of case histories, experimental modeling and numerical analysis. The critical loading may be induced by nature or human activities. This was done by studying slides already documented, examining how and why they failed, and modeling them numerically. A project team was assembled to include those organizations known to have significant investigation and research programs underway that would contribute to this study. The partners included C-CORE, the Norwegian Geotechnical Institute (NGI), the Geological Survey of Canada - Atlantic (GSC-A) and the Offshore Technology Research Centre (OTRC) of Texas A&M University.

Sponsors for the program included Chevron, Minerals Management Services, Pan Canadian, ExxonMobil, Murphy Oil and Norsk Hydro and Statoil through NGI.

After identifying the major programs that were underway and the requirements to bring together the relevant work and extend it to meet the objectives, the project was divided into three phases.

Phase I consisted of eight main components. First it was necessary to investigate previous work done in this area in order to familiarize the team with background information on geotechnical, geophysical, geological and loading conditions. Next, the case histories were selected and examined to gain an understanding of the nature of submarine slides. Then to gain further knowledge of these elements, regional in depth studies were conducted on the Scotian Slope, the St. Pierre Slope and the Gulf of Mexico. Centrifuge demonstration tests were completed and presented in order to demonstrate the applicability of centrifuge modeling to the mechanics of submarine slopes and their trigger mechanisms. Next came the framework for risk analysis, which was presented in order to identify dominant failure mechanisms and highlight the governing parameters for those mechanisms. Lastly, results of Phase I were reviewed and preparations were made for Phase II and the design of an experimental program. Each of the sections comprising this report are briefly summarized in this extended abstract.

Section 2 Background Information

Data has been collected and summarized for the PODS project from a number of different authors and research programs. Research programs conducted relating to submarine slopes included:

- ADFEX – Arctic Delta Failure Experiment, 1982-1992
- GLORIA – Geological LOng-Range Inclined Asdic, 1984-1991

- STEAM – Sediment Transport on European Atlantic Margins, 1993-1996
- ENAM II, 1996-1999
- STRATAFORM, 1995-2001
- COSTA – Continental Slope Stability, 2000-2002

Several authors have presented classification systems and these are presented in this section. Eight classification systems are described. There were also some ratios and indices provided to assess failure mobility. The indices defined relate to mechanical properties, consolidation characteristics, undrained strength, failure mechanisms, elongation and slide geometrical factors.

Parameters involving sediment strength entail two aspects – normalized and cyclic soil loading. Equations to describe static undrained shear strength, cyclic undrained shear strength of cohesionless soil under seismic loading and critical seismic horizontal acceleration required to cause failure are described. Other analyses carried out include cyclic loading required to cause failure and factor of safety against sliding. Some of the relationships relating to slide characterizations included: water content against k_c, shear strength to overburden stress, wave induced shear stress, cyclic shear strength and critical earthquake acceleration. Sources and authors are all identified in the text.

The background given in this section has been provided to assist with the understanding of the work on the case histories and in depth studies in the following sections. A brief overview has been provided on the various classification methods for submarine slides, as well as an approach to conducting slope stability analysis for a site.

Section 3 Case History Evaluation

A review of six submarine slides was conducted and documented in this section in order to gain a better understanding of the nature of slides and how they should be classified. The six case histories studied were at Kitimat Arm, the Fraser River Delta, the Gulf of Cadiz, Eureka, Kidnappers, and Oahu.

The first case under study was the failure at Kitimat Arm, British Columbia. The triggering mechanisms for this slide could have included excess pore pressure and localized liquefaction, interstitial gas, strong tidal currents, cyclic wave loading and possibly gas hydrates. The slide has a maximum thickness of 30m and a total runout distance of 5km. The estimated volume of failed sediment was 60 x 10^6 m^3. Shear strengths in the area ranged from 11-35 kPa and had water contents of 44 to 60%. The slope's general gradient ranged between 4° and 7°.

Northwest of Gibraltar, in the Gulf of Cadiz, Spain, a failure took place that is suggested to have occurred in two phases. First, a retrogressive rotational slump occurred, then a translational slide. The triggering mechanism is hypothesized to be oversteepening of the slopes due to erosion from bottom currents or gassy sediments. Also, it is a seismically active zone. The failure involved a 12 km^3 volume of soil, with thickness generally between 75-95m. Scarps as high as 6.5m are evident in the area. The upper slope has a gradient of 1.5°, and the middle slope is less steep. The shear strength varies from 2-15 kPa near the surface and 5-10 kPa at 1.5-2mbsl. The water content varies between 25-80% over the whole study area. Plastic index tests were high (26-56%).

The Eureka retrogressive slump failure occurred on the southern part of the Eel River Basin near Eureka, California. It occurred north of the intersection of the Gorda, Pacific and Northern Plates. The failure took place in a segment of shear dominated retrogressive movements. Failure mechanisms are believed to include the reduction in the sediments effective stress levels, the reduction in soil strength, and the short term stresses generated by seismic activity. The volume of failed sediment was on the order of 6 km^3 and has a runout distance of 6-10km, with a depth of 50-65m below the seafloor. The slope angle is approximately 4°. The shear strength ranged from 2-36 kPa with a water content of 35-60%. The bulk density varied from 1.55 to 2.00g/cc and all samples showed overconsolidation.

In early Holocene times, and again in Holocene times, sediments 30km off the coast of Kidnappers, New Zealand, south of Hawke Bay, failed. This area experiences extensive seismic activity and is also affected by tilting and rapid sedimentation. The slide involved 33km^3 of sediment, with its thickness varying between 15-140m. The slope angle ranges from 1-5°. The failure consists of sheet slides and rotational failures, it is retrogressive at the top and includes a number of phases. Many geotechnical properties have been investigated: sedimentation rate (1-3 m/1000yr), shear strength (1.5-5 kPa), water content (48-85%), bulk density (1.38-1.73t/m^3), liquid limits (60-85), plastic limits (25), liquidity index (0.5-1.0), plasticity index (30-70) and cohesion (12-19 kPa).

On November 23, 1982, the Ohau Slide occurred off the coast of Hawaii, west of the island of Kauai. This slide was initiated by the waves generated by Hurricane Iwa. The waves may have caused a series of slump events. Geometry measurements for this slide are not well known. The angle of the slope is 30-40°, the soil density is given an upper limit of 0.15 g/cm^3. These hurricanes may occur every 5-7 years. More frequent events are experienced if earthquakes and tsunamis are considered.

Since an extensive amount of parameters are needed to assess slope stability, it is proposed that an approach be taken to streamline their evaluation. This would include failure classification, initiation and evolution, slope stability analysis and assessment of environmental loads and geohazards.

Section 4 General Characterization of the Scotian Slope

The Scotian Slope is part of the Mesozoic rifted margin of the central North Atlantic Ocean. It is divided into three major regions: East of Verrill Canyon; between Verrill and Mohican Canyon; and west of Mohican Canyon.

The gradient is generally between 1-2°, despite the varied morphology of these areas. The distribution of shallow sediment is the same over most of the slope. Conventional shear vane, water content and bulk density measurements are available for cores in the area. There are no deep-water geotechnical boreholes on the Scotian Slope.

Average undrained shear strength and bulk density profiles in the Verrill Canyon area were used to perform an infinite slope analysis on the Verrill failure area. On 2° slopes, surficial sediment was found to be stable. Previous authors have considered and rejected such triggering

mechanisms as storm wave loading and excess pore pressures alone. It is hypothesized that the failure was probably seismically triggered. Shear strengths were found to be 8-11kPa and bulk density, 1.7gm/cm^3.

The most severe geohazard on the Scotian Slope involves stability. Failure deposits cover approximately 38% of slopes between 500 and 3000mbsl. A further 8% consists of steep erosional slopes. Near surface retrogressive rotational slumps and debris flows are widespread on the Western Scotian margin and debris flow deposits fill many canyon floor on the eastern Scotian Margin. Interstratal deformation is also widespread on the entire margin, as well as shallow gas and gassy sediment. Boulder beds have proved to be a drilling problem, and some geohazards are present in the preglacial section of the slope.

Only sparse data exists on waves and currents on the Scotian Slopes. Peak velocities of 50cm/s are seen at 20m off the seabed at 250mbsl, 30cm/s at 70mbsf and 20cm/s at the tidal frequencies, 1000mbsl. The largest wave height observed is 10m for a ten year period and 17m for a hundred year period. The Eastern continental margin of Canada is relatively seismically active, with two M>7 earthquakes this century. Mean sedimentation rates are of the order of 10-20 cm/ky. Mean heat flow on the margin is about 60 $\pm$14 mW/m^2 with variability resulting from salt diapirsim and fluid migration.

The key data requirements on the Scotian Slope are geotechnical boreholes. This would allow the retrieval of information on sediment properties below the limit that can be reached by piston cores, particularly in decollement zones. Multibeam bathymetry is essential on the eastern Scotian Slope from The Gully eastward and would be desirable on the western Scotian Slope from Mohican Channel westward. Additional high-resolution seismic profiles and deep-water sidescan are necessary to understand particular geohazards. General data coverage of cores and seismic is poor on the Scotian Slope east of The Gully and west of 64°.

Section 5 Description and Analysis of Mass Failures on the Scotian Slope

Presented in this section is a description and analysis of three failures off the coast of Nova Scotia. These failures are the Verrill Canyon Failure (43°N 62°W), the Albatross Failure (42°N 63°W) and the Logan Canyon Failure (43°N 60°W). All these selected profiles were analyzed by C-CORE using the infinite slope stability analysis. The various equations used and the reasons for choosing them can be seen in section 5.6.

The Verrill Canyon area is characterized by progradation and lack of deep canyons, with large scars, slumped diamicts and pockmarks. Its upper slope has a gradient of 5°, while the remainder of the slope averages 2.5°. The failed sediment extends downslope from the 600m isobath to 1200mbsl with the thickest section being 15m.

The Verrill Canyon area is composed of two complex rotational slumps. The eastern slump is between the ages of 14.2ka and 15.4ka. It is located on the east of Verrill Canyon and is 15km wide. The western zone is 5km wide and is bordered by East Acadia Valley. The runout distance is greater than 30km.

The area of the failed sediment was found to contain ice rafted, bioturbated laminated gray mud layers, covering gravelly sand and brown mud. It was also found to have distinctive red-brick layers under these units. The sedimentation rate is 0.05-1.0m/ka, the average density, 1.65-2.0 g/cm^3, the plastic index, 22% to 36%, undrained shear strength 2.0-18.0 kPa, and an OCR of 0.33.

The most probable failure mechanisms for Verrill were earthquakes and excess pore pressure. The factor of safety in this area was calculated as 1.6, occurring at shallow sliding surfaces. The pseudo-static method was used to estimate the influence of earthquake on the factor of safety (for k=0.05). The factor of safety for the sediment in consideration was found to decrease from 1.68 to 1.12. At static condition, FOS went down to less than 1. When gas hydrates or pore pressure was introduced, the FOS was seen to be 4.5% higher in linear sliding surfaces than circular sliding surfaces.

In the undisturbed areas of Verrill, the minimum factor of safety ranged from 3.85 to 5.29, but an earthquake may trigger this area. The FOS for the Western slump ranges from 2.19 to 3.29 with no triggering factors, with possible earthquake loading (I=6) it decreases to 1.8. The FOS for the whole slope in general is 1.02 to 1.40.

The Albatross area is characterized by several small canyons and steep slopes, with the uppermost slope being relatively smooth. The failure is recognized as a series blocky debris flows that occurred throughout the Quaternary to the Late Pleistocene, with the most recent failure occurring during the Late Pleistocene. The source area for the debris flow is most likely the smooth region around Heron and Puffin Valleys.

Within the failed sediment, two major debris near-surface flows were identified. These failures are given the bracketed age of 13-13.3ka. The slide depth averages 120m on the slope and 20m on the lower slope. The slide depth is determined as 50m, with the failure angle being 6° and a runout of 200km. The total volume of the slide is estimated to be 600km^3

The following soil parameters were also determined from cores in the area. The OCR for the undisturbed sediment is 0.22 and the disturbed is 0.26. The shear strength averages 1-20kPa. The profiles analyzed by C-CORE presented the following data: the total unit weight was 14-18 kN/m^3, the minimum factor of safety is 1.23 for 300-400mbsl and 2.34 for 40-900mbsl. With the possibility of earthquake loading (I=6) the FOS for the whole slope is less than 1.2. It is likely that retrogressive failure took place.

Not much is known about the failure southwest of Logan Canyon. The Canyon is one of the largest on the Scotian Margin and indents the shelf edge. Widely spaced canyons, typically 200-500m deep, characterize the area. Downslope, these canyons lead into a major debris flow corridor.

This failure southwest of Logan Canyon is composed of a stacked series of debris flows, with several slump scars. The major slump scar extends more than 300m deep. The main failure is a debris flow and extends to the rise. Some runouts reach 150km. The slope angle is approximately 2-6°.

The total unit weight of the soil is defined as 18 kN/m^3, the minimum FOS is 2.49 at 500-600mbsl, with 4.85 at 600-700mbsl. It was concluded that during earthquake loading, the slope would be unstable and that a slide would occur when the slope angle is greater than 4.5° and the pore water pressure ratio is greater than 0.8.

The failure mechanism for Logan Canyon is unknown but is hypothesized to be related to earthquakes or excess pore pressure. Little is known of the stability of the canyon's walls and the role of major faults is uncertain.

Section 6 Description and Evaluation of Grand Banks Failure

A description and evaluation of the Grand Banks submarine slide failure of November 18, 1929 has been presented in this section. This is based on information provided by Geological Survey of Canada - Atlantic (GSC-A). From the review of this information, support is found for a hypothesis that the GB slide failure was initiated in soil layers of mostly sensitive and strain-softening clay or clayey material by inertia loading from the GB earthquake of the same day.

However, it must be noted that the soil layering and geotechnical parameters are still very uncertain, due to the limited information of the GB area that has been available.

Slide area

The slide area is located on the continental slope off the coast of Newfoundland. The source area of failing soil masses probably covered more than 2500 km^2 of the slope from 500 to 2500m water depth. The upper slope, to about 500m water depth has a mean gradient of about 2°, below this, the slope steepens to about 5°.

Slide evolution and damage

The slide evolved into a turbidity current travelling at a velocity of more than 19 ms^{-1} and deposited greater than 150 km^3 of sediments on the Sohm Abyssal Plain. This indicates a run-out distance of more than 400 km. The turbidity current broke cables up to 13 h after the earthquake.

Soil conditions

The present day soil conditions in the area display clay material from the seabed and down to several tens of meters depth. Evidence of this is found from core sampling. No sampling of material deeper than 20m has been done. No evidence for a source of a liquefaction susceptible sandy sediment is found.

Geotechnical properties

Clay material found in core samples can typically be classified as having low to medium plasticity (IP~14-20), with high liquidity index (IL~1.5), highly sensitive (S_t > 15), being normally consolidated (or possibly lightly over-consolidated). A few tests of soil strength show a friction angle of $\phi = 34°$ with zero cohesion and undrained shear strength in compression $s_u = 0.3\text{-}0.5 \cdot \sigma'_{v0}$. Total unit weight γ_t is typically about 17.5 kN/m^3. The sensitive clay found in the area is believed to display strong strain softening characteristics with a rapid decrease of shear strength for increasing shear strain after passing the peak shear strength.

Morphology
Present day surface sediments over most of St. Pierre slope are affected by the slide and are interpreted as minor scarps or failure ridges and debris flows. These failures show a prominent line of headscarps on the upper slope between 700 and 500 mbsl. Above this the failure did not disturb the sediments.

Trigger source
The failure was triggered by the M_s 7.2 "Grand Banks Earthquake" of the same day. The epicenter of the earthquake was located at 2000 mbsl, central in the slide area. The failure was probably initiated in areas of locally steeper gradients (local gradient up to 10^o is indicated). Slope stability analyses presented herein indicate that an earthquake generated with an up-slope horizontal acceleration of 0.05g to 0.16g would have been sufficient to initiate failures on the 10^o slopes, for the range of undrained shear strength found for the clay layers in question. Earthquake ground accelerations of up to 0.5g is likely for the GB earthquake. It is likely that the failures were initiated in thin clay layers (or interfaces between layers) with slightly less shear strength and shear modulus, or slightly higher sensitivity, relative to the other soil. Such "imperfections" are known to amplify shear straining caused by earthquake loading.

Because of the strain-softening characteristics of the clay, the soil did not re-stabilize after the short time period of earthquake loading. The earthquake loading probably induced large enough plastic shear strains to bring the shear strength down towards the residual strength level (at least in one layer). For this sensitive clay the residual strength is not high enough to withstand the static shear stresses caused by gravity loading. It is found that for sensitivities S_t in the range 2-17, this causes the clay layers of inclination 2^o-10^o to be unstable even after the earthquake loading has vanished.

Failure mechanism
Once initiated, the failure is believed to have spread retrogressively up-slope and laterally, also into areas with seabed gradient much less than 10^o. The strain-softening clay (or clay layers) probably failed by developing thin shear-bands (or slip lines) of intense plastic straining. The slope failure mechanism in such clays may follow "imperfections" of weaker (or more sensitive clay) up-slope, successively exposing steep backscarps (daybreaks).

The initial failure pattern was probably dominated by wedge and trapezoidal blocks of more or less intact clay dissected by the shear-bands. Such failure patterns have been interpreted from seismic profiling of the slide masses at Storegga. A numerical simulation has been presented herein which illustrates this mechanism in strain-softening clay. The ridges observed in the Grand Banks slide area, interpreted as small and large rotational slumps, could also be evidence of such a failure pattern.

The up-slope failure retrogression eventually stopped in areas of more coarse grained material with higher shear strength or less sensitivity.

Section 7 Wave Induced Sediment Movements

A review of the effects of surface waves on seabed sediments is presented in this section. The failure of a platform in the So. Pass area of the Mississippi delta in 1969 has been attributed to

wave-induced mudslides in the soft, underconsolidated sediments, and as a response to this event the development of methods of analysis to help in the design of mudslide resistant platforms in this area is described.

Research into the constitutive relationships for the soft sediments involved, determination of sediment drag forces on platform members and development of the governing equations for sediment movement and numerical solution of these equations is presented. A computer program has been written to allow the numerical solution of the closed form equations to be calculated, and to provide information on:

a. horizontal and vertical sediment movements at desired locations below mudline
b. downslope movement if the sediment is on a slope
c. drag forces against a pile of specified diameter at desired depths below the mudline
d. wave degeneration, i.e. distance required for a wave to lose a percentage of its height due to energy lost while traveling over a deformable bottom.

Program validation and parametric studies have been carried out for a range of water depths, soft clay strengths and seabed slope angles. Complications in site specific soils data, such as cut-back zones of soil strength or strain softening behavior have not been assessed. The results show that in areas of shallow water (less than 200 feet) and underconsolidated soft clays, large sediment movements can be expected, even on flat or very shallow slopes. A number of graphical outputs are presented to provide a guide to whether sediment movement is likely to be a problem

Section 8 Geotechnical Aspects of Gas Hydrates

This section was prepared by Dr. J.L.H. Grozic, P.Eng., University of Calgary.

The presence of gas hydrates around the world has been seen as a potential energy source for a number of years, but is also considered a potential submarine geohazard. This section provides details of the effects of gas hydrates with respect to slope stability issues.

Properties of gas hydrates, such as structure, acoustic and electrical properties and strength are described, along with the formation, stability and dissociation issues of gas hydrates in soils specimens.

Circumstantial evidence suggests that gas hydrates have had a role in a number of submarine slope failures. The reduction in effective stress due to hydrate dissociation is shown from the results of theoretical and laboratory programs, and possible mechanisms are examined. Finally, recommendations are made on areas of future research required to gain a better understanding of the effects of gas hydrates on deep offshore slope stability.

Section 9 Centrifuge Demonstration Tests

The triggering mechanisms for submarine slope failures are not well understood. Physical model tests in a centrifuge can provide insight into, and quantify, the effects of proposed triggering mechanisms. Two centrifuge tests were conducted as part of PODS Phase I to demonstrate this

modelling technique. Significant submarine slope failures were observed in both tests of 8° slope in under consolidated silty clay. The failures were initiated by excess pore pressures in the slope. These observations were confirmed by infinite slope stability analysis. Recommendations are presented for other triggering mechanisms to be studied in future tests.

Section 10 Framework For Risk Analysis

This section provides insight in assessing slope stability using a probabilistic analysis. The development of a risk analysis framework includes four main components: releasing agents, site parameters, mechanistic models and event consequence and frequency.

The releasing agents are broken up into eight categories:
1) Sedimentation (with four sub-types: long term, short term, overloading, oversteepening)
2) Tidal changes
3) Wave loading
4) Tectonics
5) Emergence
6) Erosion
7) Physical/chemical
8) Earthquake

Section 10.4 describes the site characteristics including subsurface stratigraphy, presence of geohazards and bathymetry, that are all used in slide models to determine critical trigger levels for releasing agents.

Five mechanistic models have been identified in the literature for the eight releasing agents mentioned. They are earthquakes, wave loading, sedimentation, erosion, and sea level changes. Section 10.5 briefly describes these models and the literature they were found in.

Where available, data has been collected that is applicable to the study regions, including epicenter location and Richter scale magnitudes. Data for wave loading and slope intensities can be found in the figures of this section. In order to perform a full-scale risk assessment, more data is needed. Further work is required to develop mechanistic models.

Section 11 Summary of Phase I Work and Phase II Proposed Workscope

Section 11 is a summary of the work completed in Phase I of PODS and the proposed work for Phase II. The objective of Phase I was to examine case histories, failure sites on the Scotian Slope, the St. Pierre Slope and in the Gulf of Mexico and also to analyze these failures. Centrifuge tests were also completed to demonstrate the applicability of these types of tests to analyzing submarine failures.

The background information presents many aspects of submarine failures and their classification, along with an approach to analyzing the slopes. The case histories studied were well-known worldwide sites. Failure morphology, loading conditions and failure mechanisms were investigated.

The indepth studies conducted were of the Scotian Slope, the St. Pierre Slope and the Gulf of Mexico. The existing loading conditions, geohazards, geotechnical and geological conditions were identified.

The framework for analysis was presented to identify dominant failure mechanisms and to highlight governing parameters for those mechanisms.

Phase II is directed to quantifying the phenomenological evidence gathered in Phase I. Also, an analytical model needs to be set-up to predict future slides integrated with centrifuge testing of the model. It is proposed that future work be set up into six tasks:

A) Laboratory Testing and Design of Centrifuge Experiments (NGI, GSC, C-CORE)
B) Centrifuge Experiments (C-CORE)
C) Analysis of Centrifuge Results (NGI, C-CORE)
D) Numerical Analysis Work (ORTC, NGI, C-CORE)
E) Gas Hydrate Work (University of Calgary)
F) Risk Analysis Framework (NGI, C-CORE, GSC, other researchers)

Phase II is scheduled to start in September 2001 and will take approximately 18 months. All work under PODS is to remain confidential for an agreed time period. The budget for phase II is $180,000, which will be received by C-CORE, OTRC, GSC, NGI, and others. A description of these companies is given in Section 11.

TABLE OF CONTENTS

LIST OF FIGURES

LIST OF TABLES

1 INTRODUCTION

An in-depth review of submarine slope stability has been initiated by C-CORE in collaboration with the Geological Survey of Canada (Atlantic), the Norwegian Geotechnical Institute (NGI) and the Offshore Technology Research Centre (OTRC) of Texas A&M University. The work was initiated in response to recommendations by associates of C-CORE that the Centre include in its research program the challenges facing the offshore industry in exploration and development of oil and gas reserves in deep water. This led to Project Offshore Deep Slopes with the acronym PODS.

The objective of the project is to develop a rational method to determine the stability of submarine slopes under critical loading conditions that may be induced by natural or human activities. It was decided that a logical progression would be to undertake the work in 2 Phases; Phase I includes an in-depth review of the literature on approaches to evaluating submarine slope stability, the analysis of several historical submarine slide events and site specific study of instabilities identified on the Scotian Slope and a description and analysis of Scotian Slope failures and an in-depth description and analysis of the 1929 Grand Banks failure. A section on wave induced sediment movements and a summary of analyses related to a failure in the Mississippi delta associated with Hurricane Camille has been prepared by OTRC at Texas A&M. A report on Geotechnical Aspects of Gas Hydrates prepared by Dr. J.L.H. Grozic, University of Calgary is included as an extension of Section 8 to provide background information in this important aspect of submarine slope stability.

As a contribution by C-CORE to Phase I, two demonstration tests of submarine slope failures were conducted in the C-CORE centrifuge. It was not known at the outset if a submarine slope failure could be modeled in the centrifuge, as it had never been done before. The tests produced failures that were remarkable to the extent that they mirrored failures observed on most submarine slides. Instrumentation data allowed specific analysis to assess and verify predictive models currently proposed. The triggering method tested was loading due to sedimentation but the results indicated that other mechanisms such as drilling and development activities, gas hydrates, wave loading and increase in pore water pressure can be modeled in the centrifuge to assess stability and assist with a realistic risk analysis.

A brief outline of a potential program for Phase II is presented at the end of the report. This is intended as a basis for discussion with potential sponsors and it will be modified to meet specific sponsor needs.

Sponsors for Phase I included Chevron, Minerals Management Service, Pan Canadian, Mobil Oil, Murphy Oil and Norsk Hydro and Statoil through NGI.

2 BACKGROUND INFORMATION

2.1 Background Information

2.1.1 Data Collection and Classification

Internationally, submarine slope stability has been under investigation primarily by geologists, geophysicists and geotechnical engineers. A number of research and development groups have been formed in an attempt to characterize and understand factors influencing submarine failures all over the world. Research programs that have contributed to this study include:

- ADFEX – Arctic Delta Failure Experiment, 1982-1992
- GLORIA – Geological LOng-Range Inclined Asdic, 1984-1991
- STEAM – Sediment Transport on European Atlantic Margins, 1993-1996
- ENAM II, 1996-1999
- STRATAFORM, 1995-2001
- COSTA – Continental Slope Stability, 2000-2002

Submarine failure sites have been investigated all over the world. These failures can be identified or classified according to many attributes, including the failure mechanism and the resulting morphology. A selection of classification systems is outlined in the following sections to assist with the understanding of the different types of submarine mass movements.

Varnes (1978) classified slides, first according to the type of mass movement and second, by the type of material. He described six mass movements: falls, topples, slides, lateral spreads, flows and complex failures. This breakdown is similar to the ISSMGE Technical Committee Classification shown in Figure 2.1. Varnes (1978) subdivided and described each of the mass movements according to material type: bedrock, coarse soil debris and fine soils earth. These simplified categories are shown on Figure 2.2.

The individual mass movements can be further categorized, for example Schwartz (1982) subdivided slides as follows:

1. Minor Block Slide
2. Rotating Block Slide (slump)
3. Translational Planar Block Slide
4. Convolution Slide

Schwartz's overview of submarine mass movements (Figure 2.3) considers the amount of water in the soil structure and the vertical displacement of the soil (Schwartz, 1982).

Other authors have utilized different classification systems, for example Meunier (1993) showed mass movements in relation to their amount of solid or water content in a matrix at various phases of mixing (Figure 2.4). Nardin et al. (1979) grouped failures into a three part classification according to transport mechanism. The rockfalls and slides represented the elastic transport mechanism, the mass flows deformed plastically and liquefied flows and turbidity currents involved viscous fluid behavior. Nardin et al. further described the failures according to their structure, transport mechanism and acoustic characteristics.

Slope failures can consist of simple slides involving only one set of slide characteristics. Typically however, the slides are mixed, involving a combination of types of slides or a number of similar types of failures. To take the idea of classification one step further, slides can be broken down into groups such as:

1. successive overlapped slumps
2. successive adjacent flows
3. fitted together slides
4. successive "domino-like" slides

Within these groups, slides can be classified in terms of the direction of the slide. Slide direction can occur through progradation (down slope) or retrogradation (upslope).

2.1.2 Triggering Mechanisms

Further classification of failures is often related to its cause. A failure can basically be induced in two ways. Either something occurs to reduce the strength of the sea floor, or there is an increase in stress placed on the sea floor. There are many factors which can cause either one of these occurrences. Table 2.1 adapted from Hampton et al. (1996) shows the various mechanisms that can either reduce the soil stress or increase the stresses of the seafloor. Further information on these mechanisms is provided in Section 8.0 and discussed in Section 3.0 in the evaluation of case histories.

2.2 Approach of Slope Stability

Youd and Perkins (1978) summarized slope stability as a situation where one must compare the anticipated loading to the sediments and the expected resistance to that loading. For example, "ground failure opportunity" was termed as the distribution of anticipated seismic shaking, and "ground susceptibility" was defined as the sediment resistance to strength loss. A failure was deemed to occur when the "ground failure opportunity" exceeded the "ground susceptibility". This type of analogy applies to all factors causing a submarine slide at any time, if the loading condition exceeds the soils ability to support it, a slide will occur. Conversely, any time the strength is reduced, the soil becomes more susceptible to failure.

A systematic process needs to be established in confronting a slope stability analysis. A logical progression of investigative proceedings allows for comparison between findings in different slides. One possible approach adapted from Lee and Edwards (1986) to analyzing slope stability follows.

1. ***Field Investigation in the Area.*** Identify existing data for the study area and determine the extent of site investigation required. Through geophysical surveys, one can gain a perspective of what type of slide has occurred, the general morphology of the slide and its surroundings, the subsurface reflectors and the existence of active faults or other features in the region. Further investigation of the area should reveal the possible slide surfaces, the scarps, and the disturbed material and may suggest possible trigger mechanisms. Sampling should be conducted on the subsurface soils through the depth of the failure and in both disturbed and undisturbed areas.

2. ***Investigate and Correlate Existing Data***. Assimilate all the data on the region. Integrate the historical environmental and human loading conditions and conduct laboratory testing to determine engineering properties of the subsurface soil.

3. ***Map the Geohazards.*** Establish the potential geohazards in the study area and map the location, magnitude and frequency of the hazards.

4. ***Map Possible Trigger Mechanisms***. Establish the potential trigger mechanisms which will include the geohazards and environmental and anthropogenic loads. Establish the location, magnitude and frequency of the triggers.

5. ***Final Calculations***. Determine the effect that the triggers will have on the conditions at the site. Once all factors have been considered, the slope stability can be calculated and mapped for points along the slope. Sensitivity analysis should be carried out on all critical parameters along with back calculations of loads over the failure locations.

6. ***Final Risk Analysis.*** The risk analysis will combine the work on the trigger mechanisms and slope stability in a risk framework.

2.3 Evaluation of Submarine Slides

The evaluation of submarine failures has been approached using several different methodologies. The failure is often described and classified in a geological manner then the soils involved in the mass movement are described and classified. Next the failure can be compared to others through the development of parameters describing the slide. Loading parameters have been used to indicate the magnitude effect of various loads. Finally slope stability analysis has been conducted on the failure area as well as the undisturbed area. Where data is available the slope stability work can be mapped on a regional basis and potentially put in a risk analysis framework. These methods of evaluation have been employed by various researchers and are briefly outlined in the following sections.

2.3.1 Soil and Slide Classification

In order to classify soils and further understand the effect of the soil properties on the failure, various researchers have used several different plots. Listed below is a selection of the frequently used techniques.

- The method used to understand the stress history of the sediments is a graph of plasticity index (Ip) versus the undrained strength over the effective stress (Su/p'_0). The graph developed by Skempton (1948) and Bjerrum (1954) shows that over-consolidated soils usually are above the line and under-consolidated soils are usually below the line. Barnes et al. (1991) used the plot to suggest the stress history of the sampled soils at the failure site (Figure 2.6).
- Booth (1979) developed another method to illustrate the under and over-consolidated sediments. The plots were of the consolidation ratio versus depth below the surface. Normally consolidated sediments typically have an OCR (over consolidation ratio) of close to 1.0. For the Albatross failure a range of 0.8 to 1.2 was used (Mulder et al., 1997). It

should be noted that apparent over-consolidation of sediments often exists near the surface due to bioturbation, this is not the same as true over-consolidation.

- The sediment's tendency for liquefaction is often determined through considering how individual sample water content varies with liquid limit. Locat et al. (1990) used this work to show which sediments have a proclivity to mobilize if the water content was greater than the liquid limit to a substantial depth.
- Lee and Baraza (1999) established site specific empirical relationships between sample water content and mean grain size and plasticity. Dependencies have also been shown to exist between the depth of sample and sample shear strength, water content or mean grain size. As cyclic shear strength measurements are used in the prediction of critical wave or seismic loads for a site, researchers have also derived relationships between sample water content or density and cyclic shear strength (Lee at al. 1999).
- The type of failure likely to occur, either a disintegrative or non-disintegrative failure has been described by Whitman (1985). He indicated that a disintegrative failure that occurs after an event causes a loss in soil strength and the remaining soil strength is less than the gravitational force, therefore there is continued movement. A non-disintegrative failure occurs when the movement happens during a transient loading event but little occurs after the event.
- Poulos et al. (1985) considered plots of void ratio versus effective stress to quantify disintegrative failure that the authors called liquefaction. Figure 2.7 describes the types of failures as given by Poulos et al. (1985). Points above the steady state curve show contractive soils and points below the line indicate dilative soils. If the sediment is contractive, the mobilizing steady-shear strength after failure is lower than the initial-state shear strength, the pore water pressure increases and the effective stress decreases with failure and the failure was disintegrative. If the sediment is dilative, the failure is non-disintegrative and the effective stress increases as failure progresses. These plots can also be created using sample water content or liquidity index values instead of void ratio.

2.3.2 Ratios and Indicies

Failure Mobility

When considering the mobility of a submarine slide, various authors have visited the work by Schneidegger (1973) on subaerial landslides, as well as that by Edgers and Karlsrud (1982) on runout mobility. The model assumes that the material is granular and presents a relationship between the logarithm of slide volume versus logarithm of the ratio of slide height to runout length as indicated in Figure 2.8. The subaerial slides are upper bound over the submarine slides in this plot as shown in Figure 2.9 after Hampton et al. (1996).

The Skempton Ratio has also been used to describe failure mobility. It has been suggested that h/L values less than 0.15 are generally translational slide and ratios greater than 0.33 are generally rotational failures. In addition contractive sediments have smaller h/L ratios than dilative sediments. In this case "h" is the depth to the failure surface and "L" is the same runout distance as indicated in the work by Karlsrud.

Indices

A number of indices, which are used to describe a sub-aerial slide, can be applied to submarine applications provided the variables which are used are corrected to suit the conditions present at the site. Listed below are a selection of the indices as described by Vaunat & Leroueil (1992):

1. Mechanical Index: $I_m = \tau_g/(\sigma_{nf}'\tan\phi')$
2. Consolidation Index: $I_c = \tau_g/\tau_{go}$
3. Undrained Index: $I_u = \tau_{go}/(\sigma_{nf}'\tan\phi')$
4. Failure Index: $I_f = \sigma_{nf}'/\sigma_{nf}$
5. Elongation Index: $I_e = \sigma_{nf}/\sigma_{ng}$
6. Geometrical Index: $I_{geo} = H_G L_T/H_T L_G$

2.4 Normalized Soil Parameter and Cyclic Loading Parameters

There are two aspects related to soil strength that are of interest in this section: the normalized soil parameter and the cyclic loading parameter. Both of these parameters involve sediment strength. Sediment strength can be determined through numerous methods and the values obtained are somewhat affected by both the measurement and sampling methodology.

2.4.1 Normalized Soil Parameter Approach

Ideally researchers would have soil strength information for the sediments at numerous locations in the failure zone and in the unfailed area of the submarine slide. In addition this information would be available through the depth extent of the slide. Unfortunately offshore soil sampling is very expensive thus samples are frequently only available within the top a few meters of the seafloor. Work by Lee and Edwards (1986) describes a methodology by which sediment strength testing information from the near subsurface samples can be used to estimate strength parameters at depth. The soil strength information estimated at deeper locations can then be used in slope stability analyses.

The approach is best suited to locations where the deposition has been fairly steady and uniform, thus the near surface samples will have the same fundamental properties and consolidation state as the deeper sediments.

Lee and Edwards (1986) modified the work by Ladd et al. (1977) and described the static undrained shear strength as:

$$S_{us}/\sigma_v' = S(OCR)^m \qquad (2.1)$$

Where S_{us} static undrained shear strength
σ_v' in place overburden effective stress = $\gamma'H$
S ratio of undrained shear strength to consolidated stress
OCR over-consolidation ratio, determined from odeometer test
m soil constant (m=0.8)

The overconsolidation ratio (maximum past effective stress / effective stress) is determined by oedometer test results. S is determined through triaxial testing or direct simple shear tests. The

vertical consolidation stresses are typically about four times σ_v'. This procedure allows the strength of the soil to be estimated at different depths depending on those inferred through the vertical consolidation stresses.

2.4.2 Seismic Loading (k_c)

Seismic loading has often been represented by a horizontal acceleration applied to the sediment. Morgenstern (1967) presented a version of the infinite slope stability equation for seismic loading (simplified for low angle slopes) as

$$\tau_s /(\gamma' h) = \sin\alpha + (k\gamma/\gamma') \quad (2.2)$$

where τ_s the shear stress induced by seismic or gravitational loading
α the slope angle
k pseudo-static horizontal earthquake acceleration
$\gamma' h$ unit weight of the sediment

This equation assumes the induced stresses, from the horizontal acceleration, are constant.

Lee and Edwards (1986) produced an equation for the cyclic undrained shear strength of cohesionless soil under seismic loading. For earthquake loading usually undrained strength is employed as it is a short term event. This equation was simplified to the following form:

$$S_{ur}/ \gamma' h = A_c A_r S(OCR)^m \quad (2.3)$$

Where S_{ur} cyclic undrained shear strength
A_c correction factor to account for the difference between laboratory and field loading conditions (typically ≈ 0.8, Hampton et al. (1996))
A_r cyclic strength degradation factor (measured by cyclic strength testing in the laboratory, range <0.5 for silt to >1.0 for clay Hampton et al. (1996))
S ratio of undrained strength to consolidation stress for normal consolidation (range <0.3 clayey silt to >1.0 for sand and coarse silt)
OCR overconsolidation ratio (σ_{vm}'/σ_v'), $(OCR)^m \approx 1$ for thick units of normally consolidated sediment, Hampton et al. (1996))
m soil constant ≈ 1

Using equation (2.2) and (2.3) Lee and Edwards (1986) developed an empirical relationship for the critical siesmic horizontal acceleration required to cause failure

$$k_c = (\gamma'/\gamma)[A_c A_r US((\sigma_v' + \sigma_e')/\sigma_v')^m - \sin\alpha] \quad (2.4)$$

where k_c critical seismic horizontal acceleration
γ'/γ ratio of submerged unit weight to bulk unit weight
A_c correction factor
A_r degradation factor (ratio of the cyclic stress to failure in 10 cycles/static undrained strength)
U degree of consolidation
S undrained stress

σ_v' submerged overburden unit weight /unit area
σ_e' excess maxiumum past effective stress
m soil constant
α slope angle

Values of the pseudo critical static acceleration were found to vary between k_c equal to 0.13 and 0.19 g for the failures analyzed by Lee and Edwards (1986).

2.5 Other Analysis

Seed and Idriss (1971), Seed and Rahman (1978) and Lee and Edwards (1986) have considered the cyclic load required to initiate failure of submarine slides. Variations have developed on their work in seismic and wave loading and are outlined in point form below. The factors of safety against sliding as well as slope stability dependencies have been derived for various case histories. The slope stability analysis work will be described in Section 4.0 of this report.

- Lee and Edwards (1986) derived plots of kc versus sample water content showing the critical water contents over which seismic failure may occur. They also indicated, through consideration of two failure sites offshore Alaska and California, that S (ratio of undrained strength to consolidation stress) decreased with increasing water content and A_r increased with increasing sample water content (Figure 2.10).

- Cyclic shear strength tests have been conducted on cores from many submarine failure sites. Seed and Idriss (1971) plotted the ratio of the cyclic shear stress magnitude to the overburden effective stress (i.e. Cyclic Stress Ratio) versus the logarithm of the number of cycles to failure. The plot shows a decrease in the cyclic shear stress ratio as the number of cycles to failure increases (Figure 2.11).

- Seed and Rahman (1978) contributed a form of the following equation of the wave induced shear stress (τ_w) as a function of the depth of the sediment and the wave characteristics which assists with the prediction of the effects of wave induced instability:

$$\tau_w/\gamma' Z = \sin\alpha + [(\pi\gamma_w H)/(\gamma' L\cosh(2\pi d/L)] \quad (2.5)$$

where

γ' submerged unit weight of the sediment
α slope angle
γ_w unit weight of water
H wave height
d water depth
L wave height

- Lee et al. (1999) conducted many cyclic shear strength tests on samples from the Eel River region off the California coast. Plots revealed the cyclic shear strength ratio generally increased with increasing sample water content and decreased with sample grain density. The authors used the modified simple, infinite slope equation by Morgenstern (1967) and applied the special case for a normally consolidated soil where the cyclic shear stress ratio

(Su/ γ'h) in Equation (2.3) equals CSR_{10} (the cyclic shear stress ratio at 10 cycles to failure). The critical earthquake acceleration k_c is expressed as shown in Equation (2.4)

$$k_c = (\gamma'/\gamma)[CSR_{10} - \sin \alpha] \quad (2.6)$$

Where γ'/γ ratio of buoyant density to total density
CSR_{10} cyclic stress ratio needed to cause failure after 10 cycles
α slope angle

- Barnes et al. (1991) utilized graphs of the dynamic strength degradation factor ($\beta S_u/\gamma'h$) versus slope angle to derive the critical horizontal earthquake acceleration for particular samples. This work is modified from Morgenstern (1967) and was applied to the Kidnappers Slide. The earthquake acceleration was expressed as a percentage of gravity (Figure 2.12).

- Rahman and Jaber (1991) plotted depth versus slope distance and slope angle and overlaid probability of failure lines from wave action.

2.6 Summary

Background information on submarine slides has been provided to assist with the understanding of the work on case histories (Section 3.0) and the evaluation of specific slides (Section 5.0 and Section 6.0). A brief overview has been provided on the various classification methods for submarine slides as well an approach to conducting slope stability analysis for a site was presented. Various methods to evaluate slides were summarized, with focus on soil and slide classification, failure mobility and the use of the normalized soil parameter and cyclic loading parameter.

2.7 References

Barnes, P.M., Cheung, K.C, Smits, A.P., Almagor, G., Read, S.A.L., Barker, P.R., Froggatt, P., 1991, Goetechnical analysis of the Kidnappers slide, upper continental slope, New Zealand. *Marine Geotechnology*, 10, 159-188.

Bjerrum, L., 1954.Geotechnical properties of Norwegian marine clays. Geotechnique, v.4, pp 49-59.

Booth, J.S., 1979. Analyses of, and results of laboratory tests on, surficial sediments from the upper continental slope across the northern Gulf of Mexico. Open file report, U.S. Geological Survey.

Edgers, L., and Karlsrud, K., 1982. Soil flow generated by submarine slides –Case studies and consequences. In: C. Chryssostomidis and J.J. Connor (Eds.), Proceedings of the Third International Conference on the Behavior of Offshore Structures, Hemisphere, Bristol, Pa, pp 425-437.

Hampton, M.A., Lee, H.J., and Locat, J., 1996. Submarine Landslides. *Reviews of Geophysics*, 34:33-59.

σ_v' submerged overburden unit weight /unit area
σ_e' excess maxiumum past effective stress
m soil constant
α slope angle

Values of the pseudo critical static acceleration were found to vary between k_c equal to 0.13 and 0.19 g for the failures analyzed by Lee and Edwards (1986).

2.5 Other Analysis

Seed and Idriss (1971), Seed and Rahman (1978) and Lee and Edwards (1986) have considered the cyclic load required to initiate failure of submarine slides. Variations have developed on their work in seismic and wave loading and are outlined in point form below. The factors of safety against sliding as well as slope stability dependencies have been derived for various case histories. The slope stability analysis work will be described in Section 4.0 of this report.

- Lee and Edwards (1986) derived plots of kc versus sample water content showing the critical water contents over which seismic failure may occur. They also indicated, through consideration of two failure sites offshore Alaska and California, that S (ratio of undrained strength to consolidation stress) decreased with increasing water content and A_r increased with increasing sample water content (Figure 2.10).

- Cyclic shear strength tests have been conducted on cores from many submarine failure sites. Seed and Idriss (1971) plotted the ratio of the cyclic shear stress magnitude to the overburden effective stress (i.e. Cyclic Stress Ratio) versus the logarithm of the number of cycles to failure. The plot shows a decrease in the cyclic shear stress ratio as the number of cycles to failure increases (Figure 2.11).

- Seed and Rahman (1978) contributed a form of the following equation of the wave induced shear stress (τ_w) as a function of the depth of the sediment and the wave characteristics which assists with the prediction of the effects of wave induced instability:

$$\tau_w/\gamma' Z = \sin\alpha + [(\pi\gamma_w H)/(\gamma' L\cosh(2\pi d/L)] \quad (2.5)$$

where
γ' submerged unit weight of the sediment
α slope angle
γ_w unit weight of water
H wave height
d water depth
L wave height

- Lee et al. (1999) conducted many cyclic shear strength tests on samples from the Eel River region off the California coast. Plots revealed the cyclic shear strength ratio generally increased with increasing sample water content and decreased with sample grain density. The authors used the modified simple, infinite slope equation by Morgenstern (1967) and applied the special case for a normally consolidated soil where the cyclic shear stress ratio

(Su/ γ'h) in Equation (2.3) equals CSR_{10} (the cyclic shear stress ratio at 10 cycles to failure). The critical earthquake acceleration k_c is expressed as shown in Equation (2.4)

$$k_c = (\gamma'/\gamma)[CSR_{10} - \sin \alpha] \quad (2.6)$$

Where γ'/γ ratio of buoyant density to total density
CSR_{10} cyclic stress ratio needed to cause failure after 10 cycles
α slope angle

- Barnes et al. (1991) utilized graphs of the dynamic strength degradation factor ($\beta S_u/\gamma'h$) versus slope angle to derive the critical horizontal earthquake acceleration for particular samples. This work is modified from Morgenstern (1967) and was applied to the Kidnappers Slide. The earthquake acceleration was expressed as a percentage of gravity (Figure 2.12).

- Rahman and Jaber (1991) plotted depth versus slope distance and slope angle and overlaid probability of failure lines from wave action.

2.6 Summary

Background information on submarine slides has been provided to assist with the understanding of the work on case histories (Section 3.0) and the evaluation of specific slides (Section 5.0 and Section 6.0). A brief overview has been provided on the various classification methods for submarine slides as well an approach to conducting slope stability analysis for a site was presented. Various methods to evaluate slides were summarized, with focus on soil and slide classification, failure mobility and the use of the normalized soil parameter and cyclic loading parameter.

2.7 References

Barnes, P.M., Cheung, K.C, Smits, A.P., Almagor, G., Read, S.A.L., Barker, P.R., Froggatt, P., 1991, Goetechnical analysis of the Kidnappers slide, upper continental slope, New Zealand. *Marine Geotechnology*, 10, 159-188.

Bjerrum, L., 1954.Geotechnical properties of Norwegian marine clays. Geotechnique, v.4, pp 49-59.

Booth, J.S., 1979. Analyses of, and results of laboratory tests on, surficial sediments from the upper continental slope across the northern Gulf of Mexico. Open file report, U.S. Geological Survey.

Edgers, L., and Karlsrud, K., 1982. Soil flow generated by submarine slides –Case studies and consequences. In: C. Chryssostomidis and J.J. Connor (Eds.), Proceedings of the Third International Conference on the Behavior of Offshore Structures, Hemisphere, Bristol, Pa, pp 425-437.

Hampton, M.A., Lee, H.J., and Locat, J., 1996. Submarine Landslides. *Reviews of Geophysics*, 34:33-59.

Ladd, C.C., Foott, Ishihara, K., Scholosser, F., and Poulos, H.G., 1977. Stress-deformation and strength characteristics. Proceedings of the 9th International Conference on Soil Mechanics and Foundation Engineering, 2:421-494.

Lee, H.J. and Edwards, B.D., 1986. Retional method to assess offshore slope stability. *Journal of Geotechnical Engineering Division*, 112:489-509.

Lee, H.J., and Baraza, J., 1999. Geotechnical characteristics and slope stability in the Gulf of Cadiz. Marine Geology. V.155, pp. 173-190.

Lee, H.J., Locat, J., Dartnell, P., Israel, K. and Wong, F., 1999. Regional variability of slope stability: application to the Eel margin, California. *Marine Geology*, 154: 305-321.

Leroueil, S., Magnan, Jean-Pierre, Tavenas, F. (1985). Embankments on Soft Clays (Ellis Horwood Series in Civil Engineering).

Locat, J. and Lee, H.J. 2000. Submarine landslides: advances and challenges. Proc. 8th Int. Symp. on Landslides , Cardiff, U.K., June 2000.

Locat, J., Norem, H., and Schieldrup, N., 1990. Modelisation de la dynamique des glissements sous-marins. In: Proceedings for the 6th Congress of the International Association of Engineering Geology, Amsterdam.

Meunier, M., 1993. Classification of stream flows. In: Proceedings of the Peirre Beghin Int. workshop on Rapid Gravitational Mass Movements, CEMAAGREF, Grenoble, France.

Mulder, T., Berry, J. A. and Piper, D.J.W. 1997. Links between the morphology and geotechnical characteristics of large flow deposits in the albatross area on the Scotian slope (SE Canada). Marine Georesources and Geotechnology, 15: 253-281.

Morgenstern, N.R., 1967. Submarine slumping and the initiation of turbidity currents. *In*: A.F. Richards (Editor), *Marine Geotechnique*, University of Illinois Press, Urbana, Ill., pp. 189-210.

Nardin, T.R., Hein, F.J., Gorsline, D.S., and Edwards, B.D., 1979. A Review of mass movement processes and acoustic characteristics and contrasts in slope and base-of-slope systems versus canyon-fan-basin floor systems: *In* Doyle, L.J., and Pilkey, O.H., (eds), Geology of Continental Slopes, Society of Economic Paleontologists and Mineralogists, Tulsa, Oklahoma, pp.61-73.

Poulos, S.G., Castro, G., and France, J.W., 1985. Liquefaction evaluation procedure. *Journal of Geotechnical Engineering*, 111:772-791.

Rahman, M.S. and Jaber, W.Y., 1991. Submarine landslide: Elements of Analysis, *Marine Geology*, Vol. 10, pp97-124.

Schneidegger, A.E., 1973. On the prediction of the reach and velocity of catastrophic landslides. *Rock Mechanics*. V.5, pp 231-236.

Schwartz, H.U., 1982. Subaqueous slope failures. *Contrib. Sedimentology*, 11, 116 pp.

Seed, H.B. and Idriss, I.M., 1971. Simplified procedure of evaluating soil liquefaction potential, *Journal of Soil Mechanics and Foundation Engineering Division*, V.97, No. SM9, Sept. 1971, pp 1249-73.

Seed, H.B. and M.S. Rahman, 1978. Wave-induced pore pressure in relation to ocean floor stability of cohesionless soils, *Marine Geotechnology*, V.3, pp 123-150.

Skempton, A.W., 1948. Vane tests in the Alluvial plain of the River Forth, near Grangemouth. Geotechnique, V. 1, pp. 111-124.

Varnes, D.J., 1978. Slope Movement Types and Processes. *In*: R. L. Schuster and R. J. Kriezek (Eds.). Landslides, analysis and control. Transportation Research Board, Commission on Sociotechnical Systems, NRC, Washington, pp. 11-33.

Vaunat, J., and Leroueil, S., 1992, Analysis of Post-Slope Movements. *The Canadian Geotechnical Society.*

Whitman, R. V., 1985. On liquefaction, In: A. A. Balkema, Proceedings of the 11th International Conference on Soil Mechanics and Foundation Engineering, Vol. 4, 1923-1926, Rotterdam, Netherlands.

Wood, D.M., 1990. Soil Behaviour and Critical State Soil Mechanics. Cambridge University Press, New York, p. 302.

Youd, T.L, and Perkins, D.M., 1978. Mapping Liquefaction-Induced Ground Failure Potential. *Journal of Geotechnical Engineering* Division, ASCE, Vol. 104, No. GT4, Apr. 1978, pp. 433-446.

Table 2-1: Causes of Submarine Failures (Hampton et al, 1996)

Factor of Safety = Resisting Forces/ Gravitational Forces	
Factors Which Reduce Strength	Factors Which Increase Stress
Earthquakes	Earthquakes
Wave Loading	**Wave Loading**
Tidal Changes	Tides Changes
Sedimentation	Sedimentation
Gas	Gas
Erosion	Erosion
Weathering	Diapirs

Note: processes in bold are thought to be more significant.

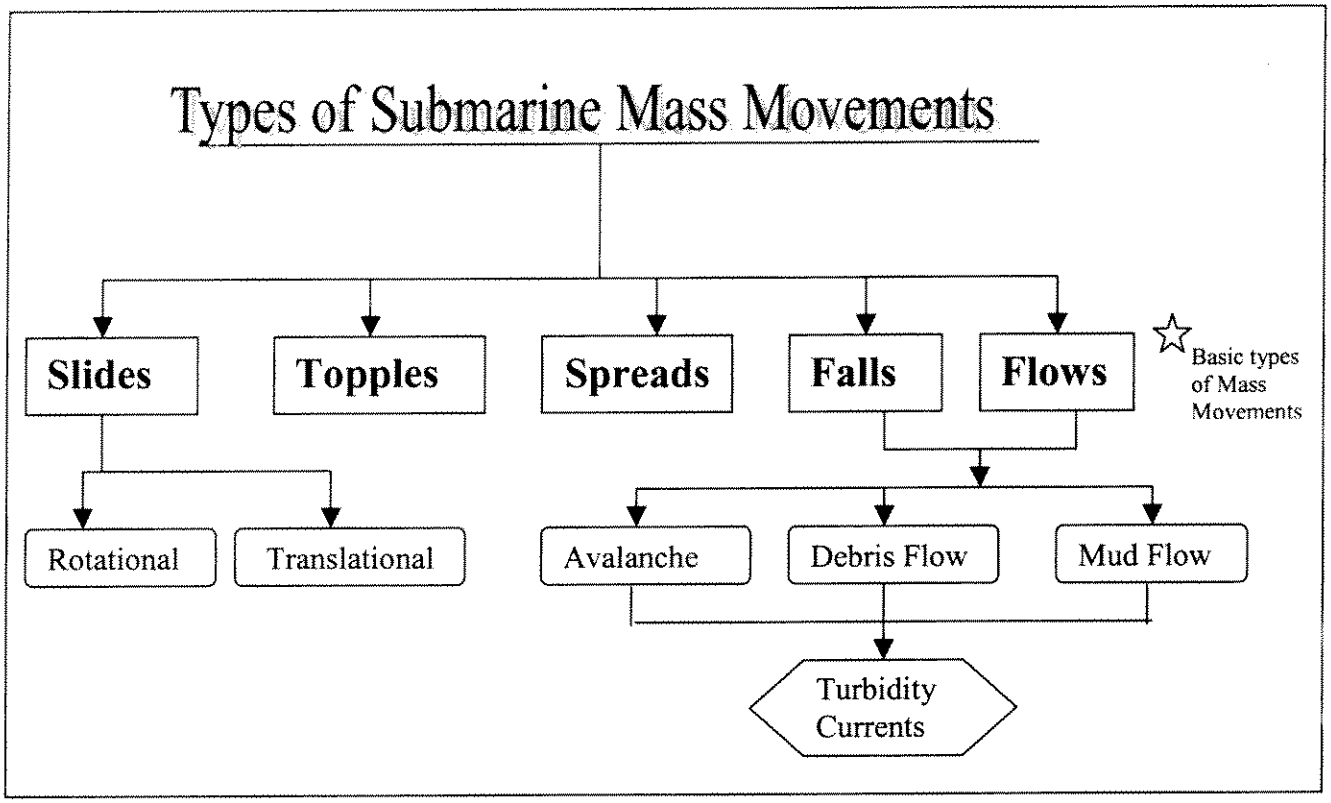

Figure 2-1: Submarine mass movement class. Adapted from Locat and Lee (2000)

Type of Movement			Type of Material		
			Bedrock	Engineering soil	
				Predominately coarse	Predominately fine
Falls			Rock fall	Debris fall	Earth Fall
Topples			Rock topple	Debris topple	Earth topple
Slides	Rotational	Few units	Rock slump	Debris slump	Earth Slump
	Translational	Many units	Rock block slide Rock slide	Debris block slide Debris slide	Earth Block slide Earth slide
Lateral Spreads			Rock Spread	Debris spread	Earth Spread
Flows			Rock flow (deep creep)	Debris flow (soil	Earth flow creep)
Complex			Combination of two or more principal types of movement		

Figure 2-2: Classification and slope movements according to material. Adapted from Varnes, 1978.

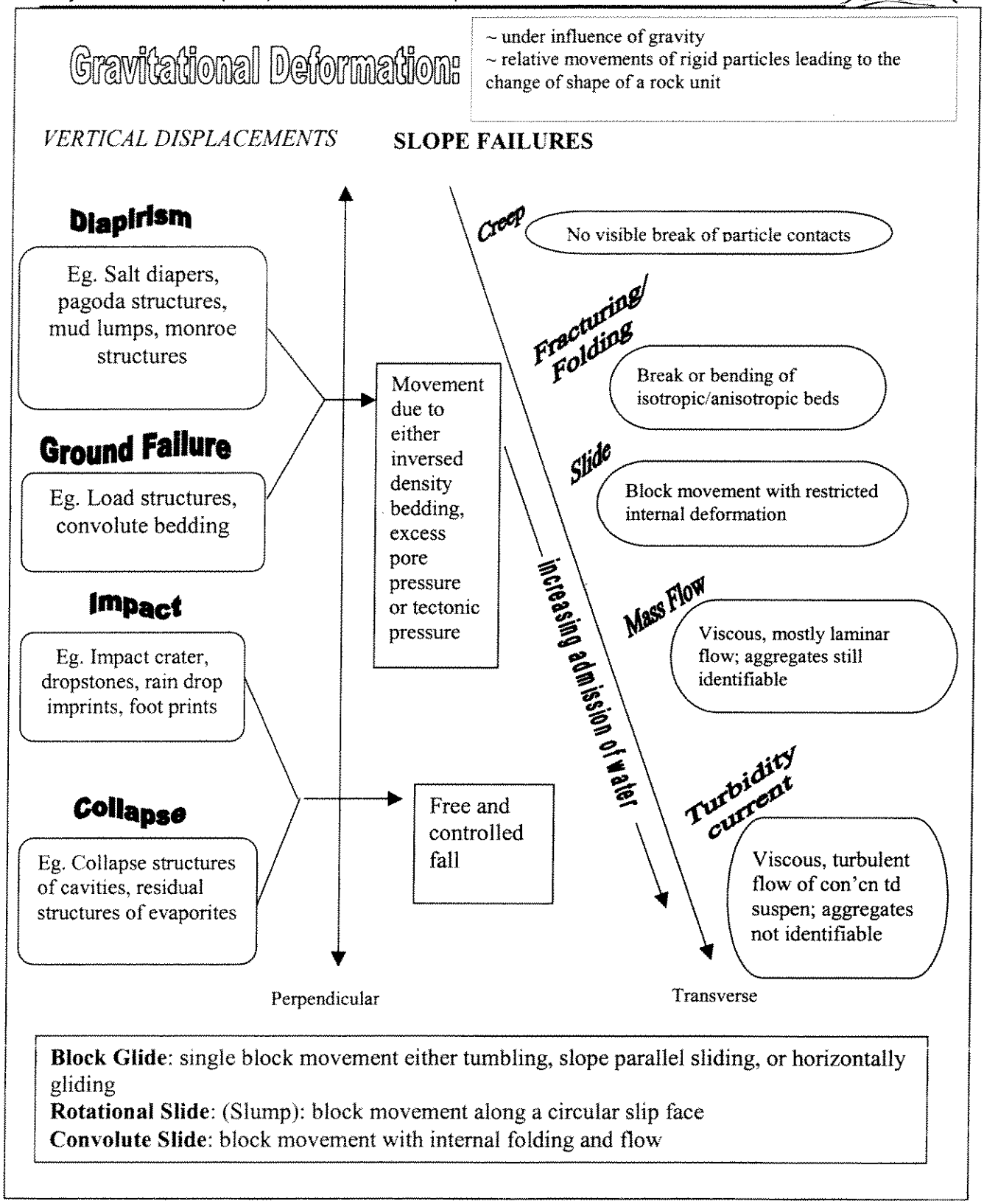

Figure 2-3: Classification and definition of gravitational deformation of sediments. Adapted from Schwartz, 1982.

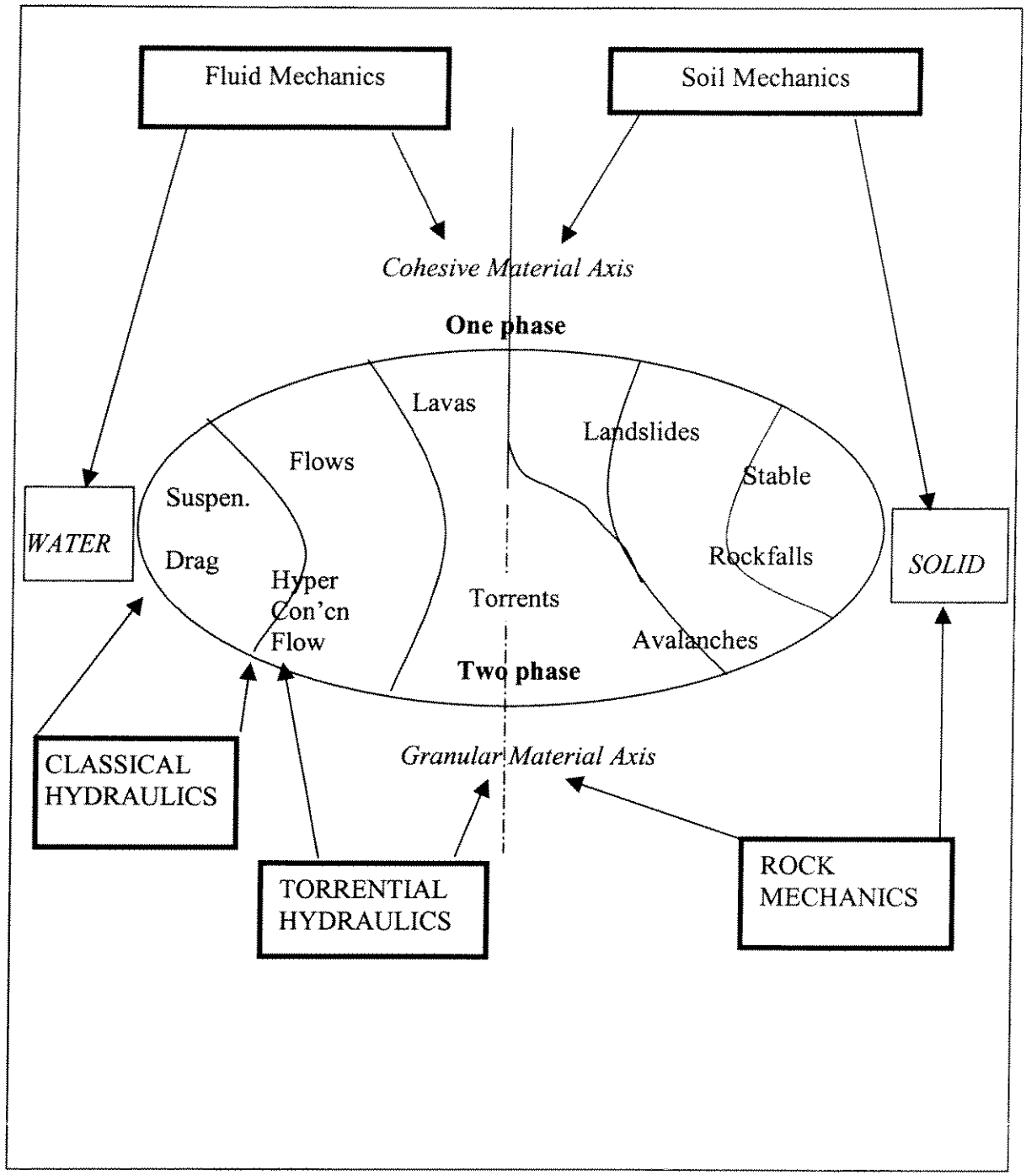

Figure 2-4: A schematic view of mass movements made of mixtures of solid and water at various stages of mixing and as a function solid characteristics with the indication of the physics involved in the phenomena. Adapted from Locat and Lee (2000).

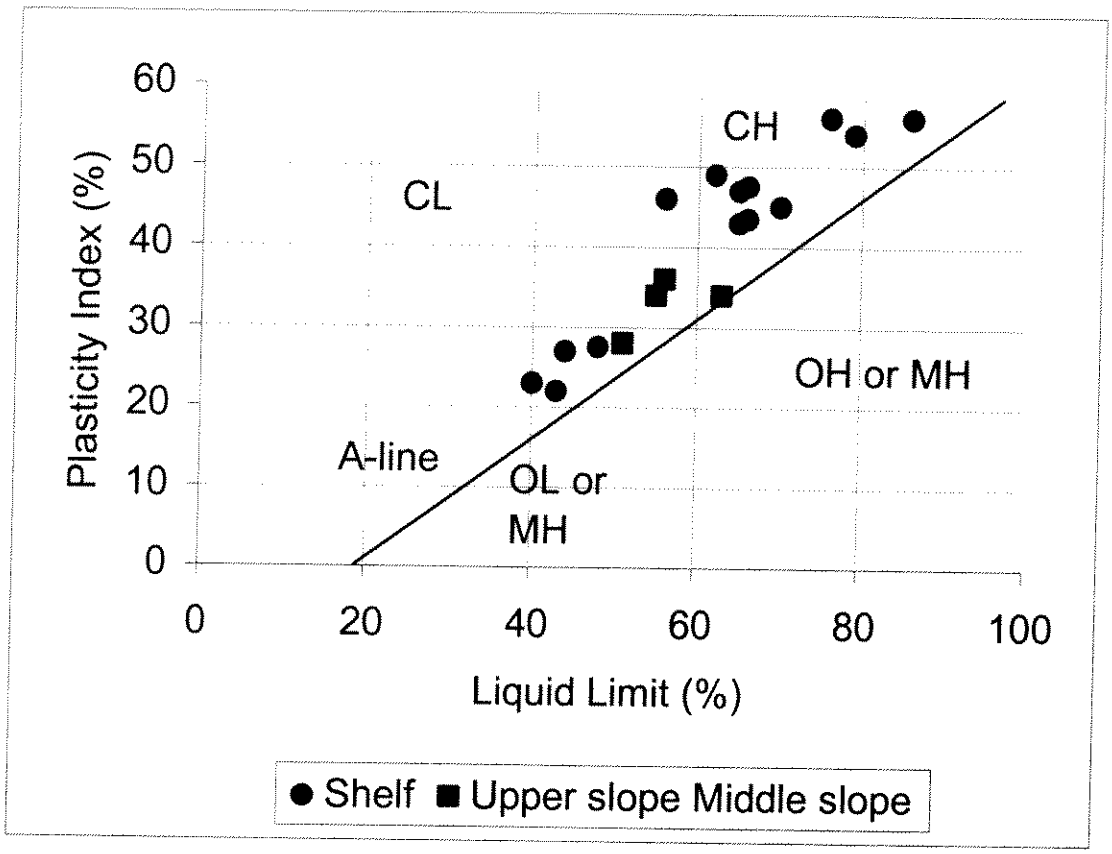

Figure 2-5: Plasticity vs liquid Limit. Adapted from Lee and Baraza (1999).

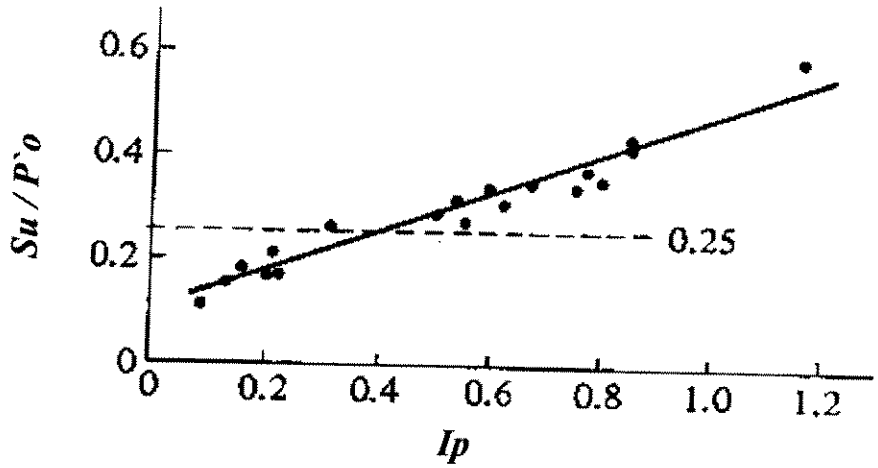

(a)

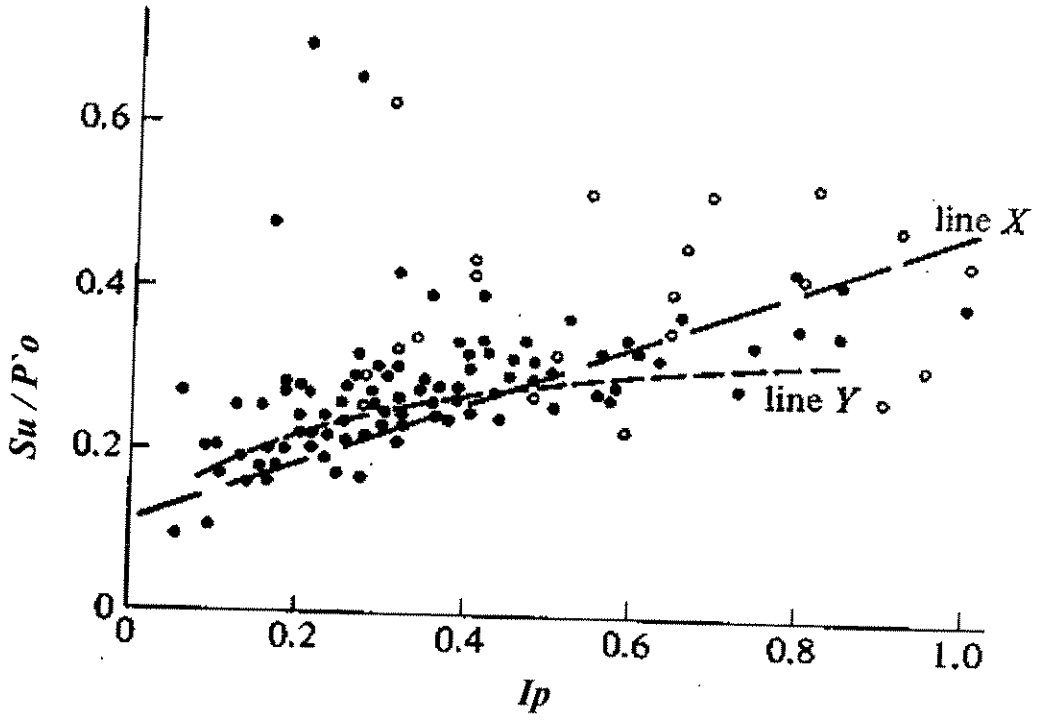

(b)

Figure 2-6: Adapted from Wood (1990). Data of ratio of undrained strength to vertical effective stress (Su/P'o), and Plasticity index Ip. (a) after Skempton (1948); (b) after Leroueil et al. (1985), with relationships proposed by Skempton, Line X and Bjerrum (1954), Line Y.

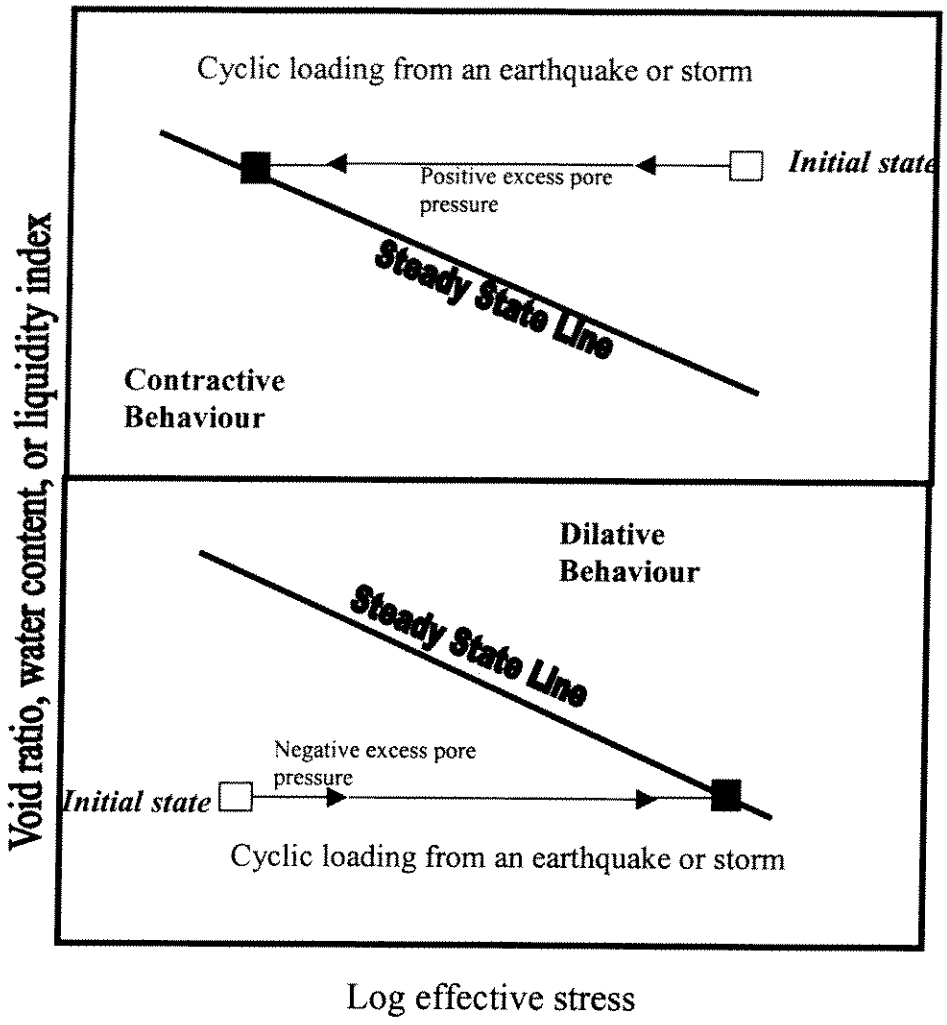

Figure 2-7: Two ways in which sediment state can change during undrained failure induced by a transient loading event such as an earthquake or a storm.

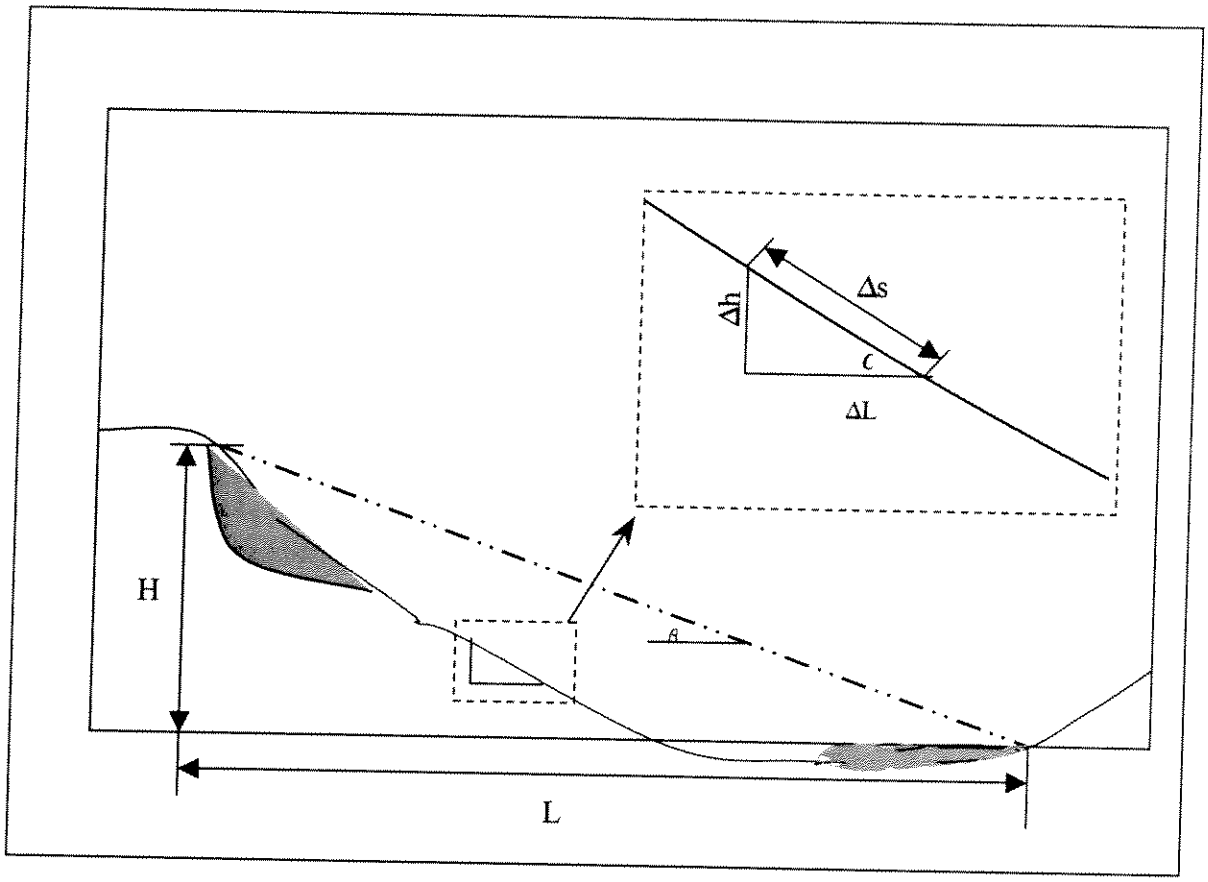

Figure 2-8: Adapted from Hampton et al. (1996). Runout model of submarine slides. h~ elevation difference between top of failed mass in both starting and depositional zones, β ~ slope of the line connecting these points, s ~ travel distance, L ~ ordinate for lateral displacement.

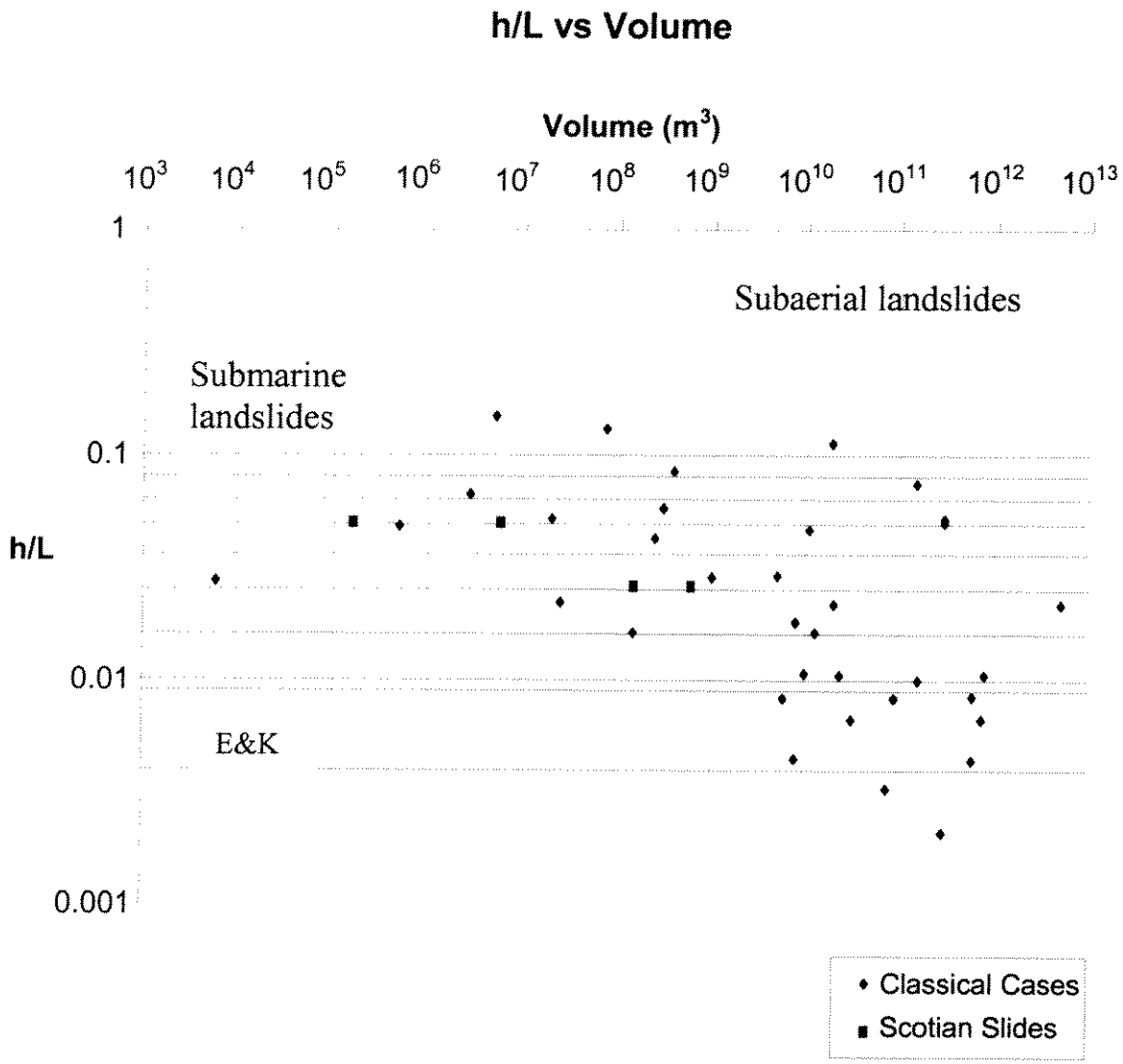

Figure 2-9: Adapted from Hampton et al. (1996). Height to runout distance vs. Volume of failed mass for the classical cases studied and the Scotian Slope slides. Upper bound values are from Edgers and Karlsrud (1982) are given with the upper cure proposed for submarince landslides and the lower curve for quick clay slides (subaerial), along with the average value for suberial landslides proposed by Scheidegger (1973).

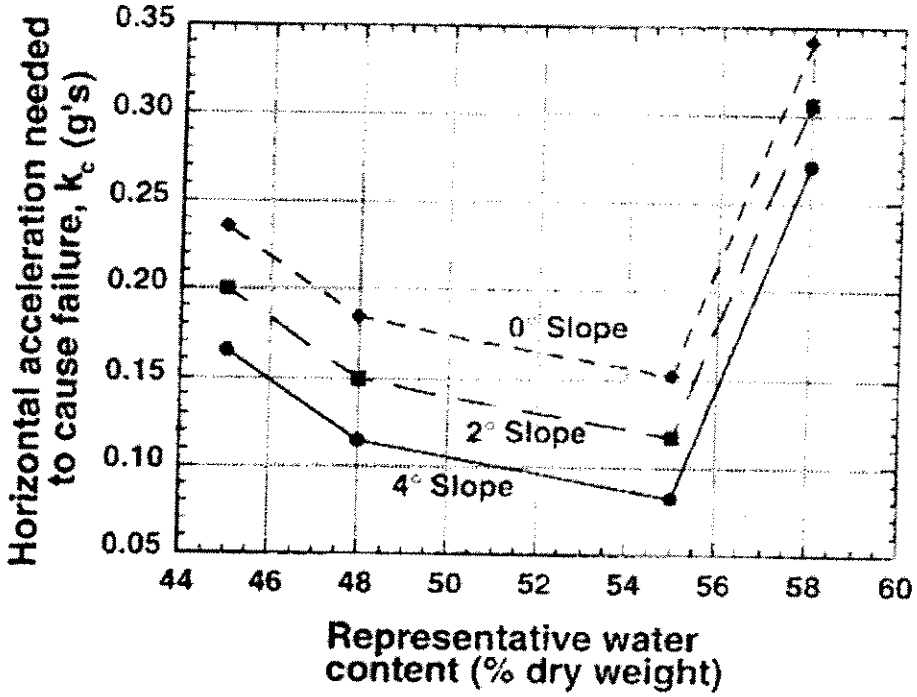

Figure 2-10: Calculated values of k_c as a function of the representative water content for the four cores analyzed for advanced geotechnical strength properties (Lee and Baraza, 1999).

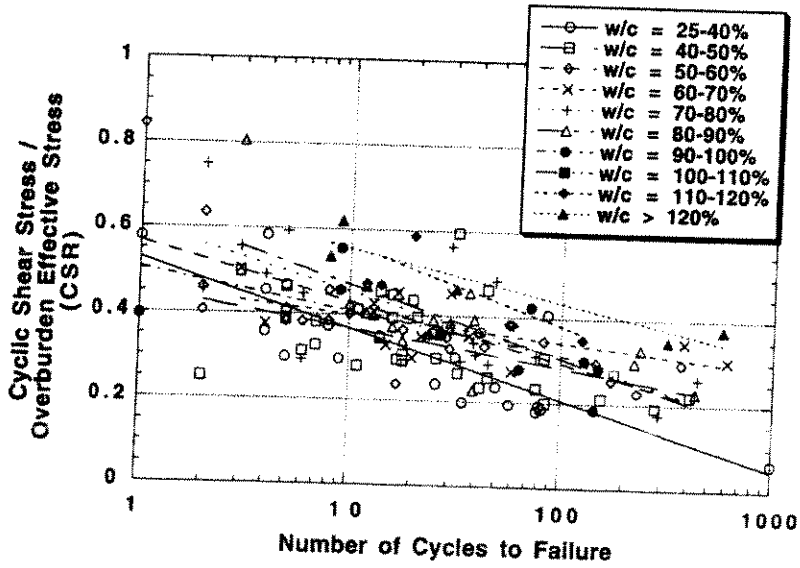

Figure 2-11: Adapted from Lee and Baraza (1999). Cyclic shear stress normalized by consolidation stress (CRS) versus the number of cycles to failure. (15%) strain from 144 cyclic triaxial tests performed on sediment from ten marine study areas distributed worldwide. Data points are identified according to initial water content (w/c) of the sediment tested.

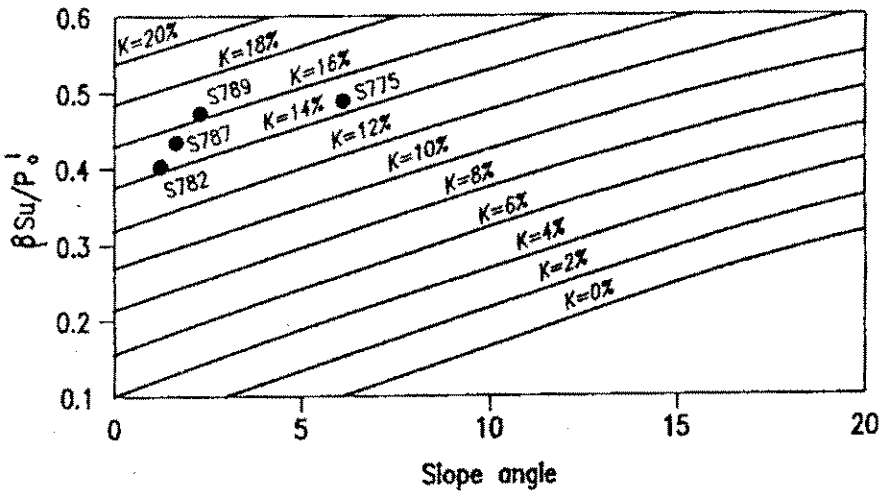

Figure 2-12: Plot adapted from Barnes et al. (1991). Theoretical relationship of metastable angle to undrained strength for and infinite slope subject to earthquake horizontal acceleration K (% gravity) line. Points correspond to properties of core samples and actual slopes.

3 CASE HISTORY EVALUATION

3.1 Objectives

The objective of this section is to gain a better understanding of the nature of submarine slides through an evaluation of case histories. Six slides have been reviewed for this work and a further four slides on the Scotian slope and Grand Banks that have been considered in detail are included in Sections 5 and 6. To perform the case history evaluation a summary of the submarine slide conditions has been provided and the applied loading conditions and failure mechanisms have been described. Next the methods of analysis for each slide is outlined. Finally, an evaluation process for submarine failures has been investigated and presented.

Information for each of the slides is summarized in Table 3.1 and detailed information is provided in Appendix 1. The slides selected for review included a variety of environments: a fjord, an active river delta, a submarine canyon, oceanic ridges and continental slopes. The focus of our work will be on the continental slopes; however, site conditions, failure types and triggering mechanisms from other environments are in many cases similar and are important to consider.

3.2 Kitimat Slump failure

A slump failure occurred in 1975 in Kitimat Arm of the Douglas Channel, British Columbia (Figure 3.1). Several other events are also believed to have occurred in the area in 1952, 1968, 1971 and 1974. The 1975 slide occurred 53 minutes after a low tide. The delta front and sidewall area of the fjord were believed to be the location of the start of the failure. The triggering mechanism was thought to be the excess pore water pressures in the clay, induced from the extremely low tides and the saturated soil conditions from the spring run-offs. In addition there was a reduction in the local effective stress due to dredging for a breakwater that could have caused localized liquefaction. The failure could have begun at the sidewall near the breakwater and extended from this area to the delta front (Johns et al., 1986). The slide involved the fjord wall, which has a gradient of up to 10° and the delta front with a gradient of 4 to 7°. The slide depth was on average 7.5m thick with a maximum of 30m and the total run-out distance was approximately 5km (Prior et al., 1982). The estimated total volume of material involved was 60×10^6 m^3 (Figure 3.2).

The sediments involved in the failure included finely stratified gravels, sands, silts and marine clays near the lower delta slope. Sediments contain a high percentage of silt. Silty sands exist close to shore, while clayey silts are found in deeper water (Johns et. al., 1986). Cores approximately 500cm deep were taken at six locations in the delta front, the distal debris flow and the undisturbed basin floor. The delta front clays exhibited shear strength of 11-35kPa and water contents of 44-60%, while the distal debris flow showed strengths of 11-21kPa and water contents of 56-80%. The seafloor morphology as depicted by Prior et al. (1984) indicates shallow channels in the delta front (at 4-7°) with downslope depositional lobes (at 1-2° slope). An elongated depositional area causing a ridged seafloor and blocky and hummocky lobes extending 3.2 km with slopes of less than 1°. Longitudinal shears exist throughout the failure zone and both the shallower and deeper depositional lobes contain sediment blocks. From the cores tested, the water content of the samples generally decreased with depth except for a sample in the undisturbed basin floor in which the water content varied between 75 and 95%.

Analysis Conducted

The following points are conclusions from analysis conducted by Johns et al. (1986):

- Conventional analysis was conducted to look at the effect of loading due to the construction of a shoreline structure and low tide: Total stress analysis provided a factor of safety 0.7 and 0.8 for low and high tide conditions respectively.
- Effective stress/infinite slope analysis showed the slope was stable prior to construction.
- Back calculation of sediment shear strength gave reasonable results.
- The delta front has numerous shallow, rotational and translational slide events. High factors of safety were obtained using conventional methods. Therefore, additional loading mechanisms, e.g. locally oversteepened slopes, rapid tidal drawdown, effect of tsunami and nearby sidewall failure are required to propagate failure.
- In order to achieve the intact outrunner sediment blocks on the relatively undisturbed fjord floor; high pore water pressures were necessary.

3.3 Fraser River Slide

The Fraser River Delta, located immediately southwest of Vancouver, British Columbia, experienced a submarine flow slide in 1985 (Figure 3.3). It resulted in the recession of the submarine sea valley to a point 100m offshore of the Sand Heads lighthouse. The cause of the failure is thought to be liquefaction due to high sedimentation rates at the delta in combination with tidal drawdown (Christian et al, 1994). McKenna et al. (1992) hypothesized that the slide could also have been attributed to the presence of interstitial gas, strong tidal currents, cyclic wave loading and possibly seismic activity. McKenna et al. (1992) estimated the volume of soil involved in the Fraser slide to be at least $1x10^6$ m^3 and to cover an area of 7 km wide by 5 km long. In some places, the thickness was up to 100m. The slope of the Fraser Delta fore-slope ranges from 0.5 to greater than 23°. The western delta slope averages 2-3°. The slides at the delta appear to be self-limiting, they stop when the front reaches denser soil located about 300m from the canyon area. The slide occurred in water depths between 100 and 300m. The morphologic evidence of seafloor failures includes: collapse depression, seafloor scarps, displaced rotational slide blocks, a submarine channels system, distal debris lobes, fans and aprons (Prior and Coleman, 1984, Prior et al.1984).

The sediments involved in the failure consist of interbedded silty sands and clayey silts of the Holocene age. The coarsest sediments occur on the upper slope near the mouth of the distributary channels and over most of the southern slope of the Main Channel. The Fraser delta has been the focus of several offshore and onshore investigations including geophysical, geotechnical work and installation of monitoring systems. Boreholes on the delta region have been extended as deep as 367m with several boreholes 80m in depth. Offshore piston cores, vibrocores and grab samples were taken during two cruises. These cores appear to extend 3 to 4.5m in depth.

Analysis Conducted

The infinite slope formulation was used with digital bathymetric data to present a map of the factor of safety against sliding. In doing this work a single value ($6kN/m^3$) was assumed for the soil unit weight and the undrained shear strength was taken to be $0.2\sigma_{vo}$' (Christian et al., 1994).

This work predicted the areas along the crest of Roberts Banks slope where translation of sediment may still occur.

Key Failure Regions (Christian et al, 1994)

- At Sand Head, the liquefaction triggered by rapid sedimentation and tidal draw down evolved into a retrogressive flow slide which created the submarine valley system. The channel acts as a conduit for turbidity currents and contributes to the dynamic behavior of the delta slope.

- The shallow rotational slide area appears to be a result of movements due to localized slope oversteepening.

- The Foreslope Hills may be compressional folds caused by progressive failure or creep of weak clays at the base of the delta.

- The Roberts Bank Failure Slump complex may exist due to liquefaction of the upper foreslope or stacked delta front failure deposits.

Luternauer et al. (2000) conducted work on seismic geohazards at the Fraser River delta. The sediment response to seismic shaking includes ground motion amplification, shifts in spectral frequency and cyclic liquefaction. A simple first-order technique was used to determine the ground motion amplification factor from sediment shear wave velocities. The sediment response due to cyclic loading is primarily dependent on the intensity and duration of the loading and the behavior of the sediment. A plot of shear wave velocity versus depth and liquefaction potential versus depth from Robertson et al. (1992) indicated the depth of potential sand liquefaction from a design-earthquake.

3.4 Gulf of Cadiz

A seafloor failure occurred in the Gulf of Cadiz, Spain, northwest of the Gibral Strait on the edge of the continental shelf (Figure 3.4). Lee and Baraza (1999) suggested that the failure might have taken place in two phases. Initially a retrogressive rotational slump occurred resulting probably in rotated blocks and then a translational slide leaving a fairly smooth seafloor.

The triggering mechanism could have been oversteepening of the slopes due to erosion from bottom currents and/or the presence of interstitial gas or gas seeps at a depth of about 20m in the sediments (Baraza et al., 1999). Seismic records show evidence of gas in the near surface sediment and possibly active gas seepage as indicated by pockmarks on the subsurface (measuring 360-580m in diameter) and inferred below the seafloor (Baraza and Ercilla, 1996, in Lee & Baraza, 1999).

In addition, the Gulf of Cadiz is in a seismically active zone as it is near the convergence of two major tectonic regions, the African and Eurasian plates. Locally, effects of the active zone are revealed through evidence of faulting, folding and diapirism (Baraza et al., 1999).

Morphological features related to the failure include: the slump with step-like internal structure that denotes weakly developed shear planes in the soil and distal parts of the slump revealed slight hummocky surface a mobile seafloor composed of bedform fields.

The failures involved approximately 12 km^3 of soil and occurred in water depths from 157m to 440m. There are a number of slumps in this area from 200 to 750m in length and with a total thickness of 75 to 95m covering an area 12km long and 3 to 8 km wide. Baraza et al. (1999) indicated that there exist single and multiple slumps occupying an area of 147km^2. Scarps as high as 6.5m are evident. The upper slope, at the 120m shelf break to 440mbsl, has a uniform gradient of 1.5°. The middle slope is less steep.

In total 37 boreholes were put down in three different sediment environments: within the mapped submarine slump in 275m of water, in unfailed sediment on the continental slope and on the continental shelf at 3mbsl. On the slope, the samples consisted of 10 to 25cm of fine sand overlying clay. Bioturbation is common throughout. The shear strength varied from 2-15 kPa near the surface and 5-10 kPa at 1.5-2.0 m depth. The water content varied from 25-80% in the whole study area. Plasticity indexes indicated that most of the samples are inorganic soils of high plasticity and ranged from 26 to 56 %.

Analysis Conducted

Slope stability analysis of the Gulf of Cadiz and synthesis of geotechnical information was completed by Lee and Baraza (1999). An outline of the work completed is provided below:

- Mapping of mean grain size, water content, shear strength and plasticity index over the slope region.
- Derivation of the cyclic strength ratio and then the peak seismic acceleration for failure kc.
- Characterize the sediments with depth by plotting water content and vane shear strength with depth. Development of a model such that soil parameters could be related to water content.
- Infinite slope analysis indicated that the maximum stable slope was greater than 16° under static loading conditions. The stable slope angle could well be affected by interstitial gas.
- Lee and Edwards (1986) derived the wave height required to cause storm wave induced instability on the shelf as 16m based on the work by Seed and Rahman (1978) and Morgenstern (1967). However evidence of such failures on the shelf was not apparent.
- Ground failure susceptibility was expressed as kc (critical earthquake acceleration needed to cause failure). It was found that kc was lowest over a sample with water content of 50-56%. This implies that these sediments are most susceptible to seismically induced failure.

3.5 Eureka Retrogressive Slump

A retrogressive slump failure on the southern part of the Eel River Basin near Eureka, California has been well documented. The slide occurred within the Eel River Basin north of the intersection of the Gorda, Pacific and North American plates. The contributing factors to the failure are thought to include: the reduction in sediment effective stress levels due to high pore water pressures caused by heavy sedimentation rates from the Eel River; the reduction in soil strength due to methane gas seeps as is evident from the pockmarks near the failure area; and the short term stresses generated by seismic activity (Gardner et al. 1999, Lee et al. 1981). Gardner et al. (1999) indicated that the failure occurred during the late Pleistocene or early Holocene period.

The volume of failed soil is estimated at 6 km^3 covering an area of 150 to 200 km^2 within a shallow bowl-shaped depression on the seafloor. This complex slide has a runout distance of 6 to 10 km and a depth of 50 to 65m below the seafloor. The water depth in which the slide occurred is 200 to 500m. The slope angle is approximately 4° (Gardner, 1999, Field and Edwards, 1980). It is thought that the failure initiated at a water depth of about 500m (Lee et al., 1980).

A map showing the failed zone is shown in Figure 3.4. The evident morphological features suggest that the failure occurred as a sequence of shear dominated retrogressive movements. Initially the central portion of the slide failed by extension creating folded and back-rotated blocks. The failure progressed upslope and the downslope sediment became compressed creating a series of folds. It is thought that a later date translational sliding occurred at the top of the slope (Gardner et al, 1999).

The slide site is mainly composed of silt. The sediment is gassy and contains plant and wood debris (Field and Edwards, 1980). The older sediments are composed of thin-bedded clayey silts and occasional sandy layers (Gardner et al., 1999). This region including failed and unfailed areas has been extensively sampled including 70 box samples taken near the seafloor and 31 piston cores to a depth of approximately 2.5m. Samples indicated that the shear strength ranged from 2 to 36 kPa, while the sample water content varied from 35 to 60%. The bulk density varied from 1.55 to 2.00 g/cc and all samples showed some degree of overconsolidation (Lee et al., 1981).

Analysis Conducted

Lee et al. (1981, 1999) completed considerable analysis on the Eel Margin. The driving forces or the factors that influence downslope shearing stress, as suggested by Lee and Edwards (1986) include: gravity, seismic loading, wave loading and other authors have included seepage forces from pore fluid flow. Lee et al. (1981) estimated the value of k (earthquake horizontal acceleration) using the simplified formula after Morgenstern (1967). For slope instability the k term was estimated to be in the range of 0.26 to 0.39, this is 3 to 4 times the gravity term, thus indicating gravity is unlikely to be the only factor causing failure.

In order to more accurately assess slope instability, the strength of the soil at depths greater than the sample measurements was required. The normalized shear strength parameter allowed for this estimation. This procedure was developed by Ladd et al. (1977) and was outlined in Section 2 of this report. The over consolidation ratio was assumed to be constant and the shear strength at a depth of 50mbsf was estimated using the equation 2.1.

The stability of the slope was then determined using the pseudo-static infinite slope analysis approach. This method was able to predict lower stability in the slump region as well as in other areas of the Eel River Basin.

Lee and Locat (1999) considered the ground failure opportunity due to seismic loading and the ground failure susceptibility from the sediment strength for this site. This work was completed by evaluating the lithology and consolidation state of the sediments and through determination of the sediment cyclic shear strength. Consolidation testing of the erosion surfaces near the seafloor indicated past stresses of 124 kPa, representing removal of approximately 15m of sediment. The determination of the cyclic shear strength for approximately 200 samples allows for the

estimation of the critical horizontal earthquake acceleration (k_c). As the majority of the samples were taken near the surface, correlations were made between water content, sample density and cyclic shear strength so that estimations of cyclic shear strength could be made for various depths below the seafloor.

As a great deal of data exists for this area, the values of k_c were mapped through a GIS (Geographic Information System) program thus areas with lower k_c values were evident.

3.6 Cape Kidnappers

In early Holocene times, metastable sand and silty layers failed approximately 30 km off the coast of Cape Kidnappers, New Zealand. The slide is situated south of Hawke Bay. In late Holocene time, again, this area experienced slight failure and sediment flow movement (Barnes and Lewis, 1991). Seismic activity has been observed in this region with earthquake magnitudes reaching 7 on the Richter scale ever since researchers began recording seismic activity, 150 years ago (Barnes, 1989).

The submarine slide at Cape Kidnappers involved approximately 33 km^3 of material. This volume is distributed over an area of 720 km^2, over which approximately 19km^3 moved within the central area of the slide and 14 km^3 moved in the northern section. The slide thickness varies greatly from 15m to 140 m. The slide extends 70 km along slope and up to 22 km downslope from the shelf edge at 180 m water depth (Barnes, 1991).

The average water depth along the slide at Cape Kidnappers ranges from 200 – 900m. The slope angle changes along the slide surface depending on geographic location. In the northern section of the slide, the slope angle is less than 2°, at the centre, the slope angle is 1°, while in the south, the slide angle increases to 4 - 5° (Barnes and Lewis, 1991).

Prominent, actively growing, anticlinal folds control slopes along the Cape Kidnappers area (Barnes et al., 1991). The triggering mechanism in this case appears to be due to seismic loading. Evidence of other triggering mechanisms has led researchers to believe however that the slide may also have been affected by tilting or rapid sedimentation (Barnes and Lewis, 1991).

The submarine slide at Cape Kidnappers consists of sheets of slides and rotational failures. The slide is retrogressive at the top and includes a number of phases, ranging from buried slumps to deep rotational slumps. The sediments involved in the slope failure were mostly metastable sands and silty layers of late Quaternary age (Barnes and Lewis, 1991). Cores that were retrieved from the site contained greyish olive clay and silt with minor sand and ash layers (Barnes et al., 1989). The slide is believed to have occurred in three phases; relatively small failures of only a few square kilometers, early Holocene and deeper penetrating rotational slumps, and two smaller failures of the transparent surface veneer.

A number of geotechnical properties have been assessed from the sampling that has taken place at the Kidnappers site. A maximum sedimentation rate was found to be between 2 and 3 m/1000yr with the average falling between 1 – 3 m/1000yr. Other properties were assessed both at the seabed surface and 2 m, below this surface. Shear strengths ranged from 1.5 – 5 kPa over this depth. Water content ranged from 85% at the surface down to 48%. Bulk density varied from

1.38 t/m^3 - 1.73 t/m^3 at 2 m below the surface. Atterberg limits were also determined for this same depth. The liquid limit ranged from 85 – 60, while the plastic limit remained constant at approximately 25. The liquidity index ranged from 1.0 – 0.5 at 2 m below the surface. The plasticity index ranged 30 – 70. The maximum friction angle was found to be 25 - 27°. The values of cohesion ranged from 12 to 19 kPa.

Analysis Conducted

A number of the classical approaches to slope stability have been applied to the slide at Cape Kidnappers. Due to the translational nature of the slide, a psuedo-static approach has been applied to the slide where the slide was considered to have an infinite slope. When analyzing the effect of external seismic forces, the variable "k" has been used to represent horizontal acceleration. Calculations can be made to examine the effect that seismic loading with various "k" values would have on the slope, and thus, develop a maximum seismic loading which the slope can endure before failure. As previously mentioned, portions of the Cape Kidnappers slide failed as deep rotational slides. In these areas the use of a finite element slope model was chosen. Similarly to the infinite slope model, the goal was to generate the threshold value of "k".

3.7 Kahe Point, Oahu Slide, Hawaii

On November 23, 1982, a submarine slide occurred off the coast of Hawaii, just west of the Island of Kauai (Normark et al., 1993). In this case, turbidity currents and/or slumps appear to have resulted from the large storm-generated waves off the coast of Oahu, Hawaii. Hurricane Iwa generated waves at a significant wave height of 5 m, with a maximum height of 9 m (Noda, 1983; Dengler et al., 1984). The movement of current sensor moorings, located along a proposed pipeline route proves this soil failure. It is believed that Hurricane Iwa generated a series of slump events that resulted in the creation of turbidity currents. These currents were responsible for the movement of seafloor moorings (Dengler et al, 1984).

It is believed that rapid loading and unloading of the slope sediment due to the large hurricane-induced storm waves moving over the area could have caused a significant loss of strength within the sediment. This reduction in strength would have generated downslope directed forces to move the sediment (Normark et al, 1993). Noda (1983) suggested that the strong currents produced by the advancing storm could have eroded and put into suspension sufficient sediment to generate a turbidity current directly (Normark et al., 1993).

Specific geometry measurements are not well known for the slide at Kahe Point. Observations by HECO divers however, indicate that most of the reef surface was swept clean of sediment (Tsutsui et al., 1987). The sediment moved moorings that were originally located 10 m above the seafloor, proving that the slide was at least 10 m thick (Normark et al., 1993).

Immediately offshore from Kahe Point, the shelf is narrow and steep at an average slope of 30 ° to 40°. Farther offshore, at a water depth of approximately 1500 m, the slope decreases to about 20° (Normark et al., 1993). There are several volcanoes in the study area. Slumping of volcanic bedrock has been used to explain the irregular bathymetric configurations off portions of Oahu and the other various Hawaii submarine slopes (Tsutsui et al., 1987). Sensors located on the slope were recorded as having total water depth changes of up to 220 m, which translates to downslope movement as much as 2.4 km (Dengler et al., 1984) Movement of soil and

telecommunication cables was observed in water depths greater than 1,100 m (Chui et al., 1983; Normark et al., 1993)

The general area appears to be composed of predominantly silt and clay sized sediment, with a relatively thick upper sequence of fine-grained sediment overlaying a coarse-grained layer. There are areas comprised of poorly sorted, angular, coarse sand and gravel with a minimum thickness of 2.5 m. The shallowest telecommunication cable was broken and partially buried in the area immediately downslope from where two zones of coarse sediment converge. This evidence suggests it is likely that some, or perhaps all, of this coarser sediment was displaced (through slumping and turbidity currents) during Hurricane Iwa (Normark et al., 1993).

The density difference between the turbidity current and the ambient water is given a theoretical upper limit and an empirical lower limit. It is suggested that the theoretical upper limit reaches 0.15 g/cm^3, while the empirical lower limit is 0.0005 g/cm^3. A typical range found in turbidity currents is 0.003 to 0.11 g/cm^3 (Dengler et al., 1984).

It was suggested that several debris flows triggered by rapid changes in pore pressure due to the hurricane-induced waves were responsible for the movements and deep-water cable damage (Tsutsui et al., 1987). Fornari (1983) found no evidence of recent bedrock movement and therefore suggested that slumping is not responsible for the events recorded during the passage of Hurricane Iwa. He believed that breaking internal waves caused the damage to the cables (Tsutsui et al., 1987)

Tsutsui et al. (1987) suggest that events such as Hurricane Iwa, which lead to submarine slope failures, may occur as frequently as every 5-7 years, the approximate recurrence interval for an El Nino related hurricane event. This interval could be even shorter if you include the possibility of other major events such as earthquakes and tsunamis, which could also trigger submarine slides and turbidity currents.

3.8 Characterization of Failures

After reviewing the literature on a number of submarine failures it is apparent that to cost effectively quantify the risk of slope instability at a site, which may or may not involve failed sediments, a streamlined approach for the site investigation and analysis would be beneficial. The approach used to evaluate sites could include the classification of the failure, the initiation and evolution of the failure, the slope stability analysis and the environmental loads and geohazards. Towards this end, the process used in the presented case histories has been reviewed and an outline has been compiled from the case histories that describes how information can be attained on the classification, slide initiation and evolution, and slope stability analysis of a submarine failure area. In Section 5 of this report, the data gaps will be identified for the Scotian Slope using this outline and the approach for slope stability analysis will be evaluated in detail on a case specific basis.

3.8.1 Classification

When considering a previously studied or an unstudied region, it is necessary to understand the types of failures that have occurred at the location in the past and the triggers for those failures.

Usually geophysical surveys, both bathymetric and of near surface sediments, are conducted to determine the type and age of failure, depth of failure surfaces, volume of disturbed sediments, type and structure of disturbed sediments and source of sediments. Then the geotechnical investigation is used to ascertain the nature of sediments (disturbed and undisturbed) through shallow samples augmented with a few deeper sampled locations. Analysis of the soil samples should lead to determination of the strength, strength history, water content, sensitivity, plasticity, grain size, void ratio, and bulk density of the soils at the site.

Examples of effective diagrams used to assist with the interpretation of the sample information are listed below. The A-line plot of liquid limit versus plasticity index is used to classify sediments according to grain size and organic content (Figure 2.5) The plot of the stress path on the axes of sample void ratio versus effective stress provides information on whether the soils tend to be dilative with increasing stress or contractive. This information will show the tendency towards whether the soils will fail in the form of flow rather than a slide (Figure 2.7).

The graph of plasticity index versus the ratio of soil strength to effective overburden pressure indicates how the soils plot in relation to the Skempton correlation line (Figure 2.6). Overconsolidated sediments plot above the line while underconsolidated sediments plot below the line. If the sediments are overconsolidated it indicates that soils have been removed from the area potentially by mass failures.

In order to compare the failure under consideration with other submarine or subaerial failures, the relationship between the volume of the slide and the logarithm of h/L (Height /runout distance) has been derived. Figure 2.9 (adapted from Hampton et al 1996) indicates the number of mass failures and the Scotian submarine failures.

3.8.2 Initiation and Evolution

As similar types of failures often occur in the same region it is worthwhile to consider the initiation and evolution of existing failures. The initiation of the failure can be investigated by reviewing the environmental loads, geohazards and features in the region. This work is explored in more detail in Section 4.0. The evolution of the failure has been studied through using several approaches, one of which is to consider the sediments within and outside of the disturbed areas. The following information has been included in understanding the evolution of the slide and its sediments:

- Evidence of failure surfaces and shape and character of the surfaces,
- The condition of the sediments in the failed and the unfailed zones,
- The change in the sediments properties with depth, and
- The change in the surface morphology, scarps, block size, sediment properties with distance from the centreline of the failure and along the length of the failure.

Graphs used to portray the information given above have included depth below seafloor versus soil shear strength, water content, bulk density, grain size, LL, PL, PI, void ratio, sensitivity and OCR. These plots should be given at various locations in disturbed and undisturbed soils to indicate depth dependencies and variations. In addition, maps of surface morphology, scarps, block size and sediments properties should be used to indicate real variations.

3.8.3 Slope Stability

In general, two cases should be reviewed:

1. The stability of the existing slope, and
2. The conditions required to cause any existing failures.

For each case a number of parameters need to be selected then applied to either the infinite slope or limit equilibrium analysis. An integrated approach used for assessing the stability of an existing slope is provided below.

a) Select the range of soil parameters (unit weight, shear strength, OCR) based on laboratory and field testing.
b) If necessary use the normalized soil parameter approach (see Section 2.4.1) to estimate soil strengths at depths greater than that sampled.
c) Determine range of environmental loads at the site.
d) Where wave or seismic loading should be considered, determine the cyclic shear strength ratio for samples at various locations and depths on the slope.
e) Where seismic loading should be considered, determine the critical horizontal seismic acceleration required to cause failure for several locations on the slope (k_c).
f) Determine the factor of safety for various slope angles and graph factor of safety versus slope angle for various depths of failed sediment (using infinite slope analysis). Assume a translational failure.
g) Determine the factor of safety for various locations along selected slope transects and graph factor of safety versus depth below mean sea level (using infinite slope analysis). Assume a translational failure.
h) Use limit equilibrium approach to consider rotational type failures. Show the relationship between the factor of safety versus slope angle.
i) Conduct parametric analyses using the range of soil properties, slope angles, and pore water conditions.
j) If cyclic loading is a concern, plot k_c for various locations versus water content, grain size, PI etc. to determine the soil conditions which are most susceptible to seismic loading.
k) Develop empirical relationships such that cyclic strength values can be related to parameters that are assessed more readily in the field or lab.
l) If cyclic loading is a concern, construct a contour map of the k_c values for the region of interest.
m) Construct a contour map of the factor of safety on the slope for various site conditions.

To assess the stability of a previous failure, the following steps are provided below.

a) Reconstruct the bathymetry to before failure conditions to ensure mass balance of sediments.
b) Estimate the soil parameters based on the existing soil conditions.
c) If necessary, use the normalized soil parameter approach to estimate soil strengths at depths greater than that sampled.
d) Conduct back calculations to determine loads, sediment properties or excess pore water pressures required to initiate failure. This failure may occur at a single location that retrogrades up the slope or propagates down-slope.
e) Assess how the failure(s) could have progressed to the present state.

3.9 References

Baraza, J. and Ercilla, G., 1996. Gas charged sediments and large pockmarklike features on the Gulf of Cadiz (SW Spain). Marine and Petroleum Geology. Vol. 13, pp 253-261.

Baraza, J., Ercilla, G., and Nilson, C. H. 1999. Potential geologic hazards on the estern Gulf of Cadiz slope (SW Spain). Marine Geology, Vol. 155, pp. 191-215.

Barnes, P.M. et al, 1989. Off shore Failures and Geotechnical Assessment Near Cape Kidnappers, North Island, New Zealand. 9th Australasian Conference Coastal and Ocean Engineering, December 4-8. Pp 214-218.

Barnes, P.M. and Lewis, K.B., 1991. Sheet slides and rotational failures on a convergent margin: The Kidnappers Slide, New Zealand. Sedimentology, v. 38, pp 205-221.

Barnes, P.M., 1991. Geotechnical Analysis of the Kidnappers Slide, Upper Continental Slope, New Zealand. Marine Geotechnology, v. 10, pp. 159-188.

Christian, H. A. et al, 1994. Slope instability on the Fraser River Delta Foreslope Vancouver, British Columbia. Proceedings of the 47th CGS Conference in Halifax. pp 115-165.

Chui, A.N.L., Escalante, L. E., Mitchell, J.K., Perry, D.C., Schroeder, T.A. and Walton, T. 1983. Hurricane Iwa, November 23, 1982: National Academy Press, Washington D.C., 68 p. offshore of Kahe Point,

Dengler, A.T., Wilde, P., Noda, E.K and Normark, W.R., 1984. Turbidity currents generated by Hurrican Iwa. Geo-Marine Letters. v. 4, pp 5-11.

Field, M.E., Edwards, B.D., 1980. Slopes of the southern California boderland: a regime of mass transport, in processes of the Quaternary depositional environments of the Pacific Coasts. In: Field, M.E., Bouma, A.H., Colbourn, I.P., Douglas, R.G.,Ingle, V.V. (Eds.) Pacific Coast Palentology Symposium 4. Soc. Enoc. Misc. Publ., Pac., Sect, Bakersfield, CA, pp 169-184.

Fornari, D.J. 1983. Final report, DSV turtal dives off Kahe Point, Hawaii: Offshore Investigations Ltd., Chatham, NY, 39p.

Gardner, J.V., Prior, D.B. and Field M.E., 1999. Humbolt Slide - a large shear-dominated retrogressive slope failure. Marine Geology. V.154. pp 323-338.

Golder Associates, 1975. Report to British Columbia Resources Service on investigation of seawave at Kitimat, B.C., Vancouver, Golder Associates, 9p.

Hampton, M.A., Lee, H.J., and Locat, J., 1996. Submarine Landslides. *Reviews of Geophysics*, 34:33-59.

Johns, M. W., Prior, D. B., Bornhold, B. D., Coleman, J. M. and Bryant, W. R., 1986, Geotechnical aspects of a submarine slope failure, Kitimat Fjord, British Columbia: Marine Geotechnology, v. 6, n. 3, p. 243-279.

Ladd, C.C., Foot, Ishihara, K., Scholosser, F., and Poulos, H.G., 1977. Stress-deformation and strength characteristics. Proceedings of the 9th International Conference on Soil Mechanics and Foundation Engineering, 2:421-494.

Lee, H.J., Edwards, B.D. and Field, M. 1981. Geotechnical Analysis of a Submarine Slump, Eureka, California. 13th annual Offshore Technology Conference, Houston, TX, May 4-7. pp 53-65.

Lee, H.J., and Baraza, J., 1999. Geotechnical characteristics and slope stability in the Gulf of Cadiz. Marine Geology. V.155, pp. 173-190.

Lee, H.J. and Edwards, B.D. 1986. Retional method to assess offshore slope stability. *Journal of Geotechnical Engineering Division*, 112:489-509.

Lee, H.J., Locat, J., Dartnell, P., Israel, K. and Wong, F., 1999. Regional variability of slope stability: application to the Eel margin, California. *Marine Geology*, 154: 305-321.

Luternauer et al, 2000. Fraser River Delta: Geology , geo hazards and human Impact, Southwestern British Columbia, (ed) J.W.H Monger: Geological Survey of Canada, Bulletin 481, p. 197-220.

Mckenna, G.T. et al, 1992. Large Scale Mass-wasting events on the Fraser River Delta front near Sand Heads, British Columbia; Canadian Geotechnical Journal, v.29, p. 2-33 to 2-40.

Morgenstern, N.R., 1967. Submarine slumping and the initiation of turbidity currents. *In*: A.F. Richards (Editor), *Marine Geotechnique*, University of Illinois Press, Urbana, Ill., pp. 189-210.

Murty, T. S. and Brown, R.E., 1979. The submarine slide of 27 April, 1975 in Kitimat Inlet and the water wave that accompanied the slide, Pacific Marine Science Report 79-11.

Noda, E. K. 1983. Effects on the Hurricane Iwa, November 23, 1982, offshore of Kahe Point, Oahu: Technical Report for Research Corporation, University of Hawaii, Honolulu, Hawaii, 56 p.

Normark, W. R., Wilde, P., Campbll, J.F., Chase, T.E. and Tsutsui, B. 1993. Submarine slope failure initiated by Hurricane Iwa, Kahe Point, Oahu, Hawaii. In: Submarine Landslide: Selected Studies in the U.S. Exclusive Economic Zone (Eds. Schwab, W.C., Lee, H.J. and Twichell, D.C.), U.S. Geological Survey Bulletin 2002, pp. 197-204.

Prior, D.B. and Coleman, J.M., 1984. Submarine slope instability. In: Brunsden, D., Prior, D.B. (Eds), Slope Instability. Wiley, Chichester, pp. 419-455.

Prior, D.B., Bornhold, B.D., Coleman, J.M. and Bryant, W.R., 1982. Morphology of a submarine slide, Kitimat Arm, British Columbia. Geology, v. 10, November, p. 588-692.

Prior, D.B., Bornhold, B.D. and Johns, 1984. Depositional characteristics of a submarine debris flow. Journal of Geology. V. 29, pp707-727.

Robertson, P.K. et al, 1992. Seismic techniques to evaluate liquefaction potential: Proceedings, 45th Canadian Geotechnical Conference, Toronto Ontario, p 5-1 to 5-9.

Seed, H. B. and Rahman, M.S., 1978. Wave-induced pore pressure in relation to ocean floor stability of cohesionless soils. Marine Geotechnology. v. 3, pp 123-150.

Tsutsui, B., Campbell, J.F. and Coulbourn, W.T. 1987. Storm-generated, episodic sediment movements off Kahe Point, Oahu, Hawaii. Marine Geology. V.76, pp. 281-299.

Table 3-1: Classification and Description of Case Studies

Slide Type	Soil Type	Density	PI (%)	Su (kPa)	Water Depth(m)	Amount of soil	Depth of slide	Angle (°)
1. Kitimat inlet Soil failure was due to slumping and can be attributed to the shear failure of the soft marine clay	Sediments involved in the slope failure were gravels, sands, silts, and marine clays. Sediments contained a high percentage of silts	2.66-2.76 Mg/m^3 Wet Bulk Density	5-25 (Plots from John et al)	Delta front 11-35 Undisturbed Basin 7-17 Distal Debris Flow 11-21	Kitimat arm as an average water depth of 200m	$60x10^6$ (Golder Assoc.,1975) 10^7 (Casagrande, 1977) $26x10^6$ all in m^3.	The slide has an average thickness of 7.5m, with a max of 30m.	Short steep slope on delta front 4-7°. Intermediate blocky zone, 1-2°. A large area has slopes <1°.
2. Eureka California The failure was a shear dominated retrogressive movement, occurring as a sequence of events. The central portion failed by extension upslope, while down slope failure became compressional, creating folds. At the top of the slide translational sliding is thought to have occurred	Slide sediments are mainly composed of silt. It is noted as gassy and enriched with plant and wood debris.	Bulk Density 1.55-2.0 g/cc	8.9-16.3 (Lee et al, 1981)	2-36	200-500	$6km^3$	50-65m	4

3. Gulf of Cadiz, Spain Corresponds to a slump taking place in two phases. First, a retrogressive rotational slump, and secondly, translational sliding.	Within the slump and on the continential margin adjacent to the slump, there is a thick greenish brown fine sand layer lying above [illegible]y grey mud.	For the slump 1.709 g/cc contin. Shelf 1.791 g/cc Contin.shelf, outside slump 1.688-1.765 g/cc	26.5-56.2 Avg. 37.9	Near surface 2-15 depth of 1.5-2m 5-10	The head of the slump is 157 m of water. Slide extends down to a depth of 440m		75-95	The upper slope., to 440m of water depth is 1.5°. The middle slope, 440 to 600mbsl is 0.5-1°
4. Ohau Slide, Hawaii The slide occurred as turbidity currents and/or slumps as a result of Hurricane Iwa	The general area is composed of silt and clay sediments	A typical range found in turbidity currents is 0.003. to 0.11 g/cc			>1100m	There is no quantitative estimate of the total amount of soil involved.	10m	Immediately offshore there is an average slope of 30 to 40°.At depths of 1500m the slope increases to 20°
5. Fraser River The cause of this failure is believed to be liquefaction due to high sedimentation rates at the delta in comb'n with tidal drawndown.	Interbedded silty sands and clayey silts of the Holocene age.	??	??	??	100-300	$1x10^6$ m^3	Estimated to be 10-20m.	Fore-slope 0.5->23° Western delta slope, 2-3°.

6.Cape Kidnappers The triggering mechanism seems to be seismic loading. The slide is retrogressive at the tops and includes a number of phases ranging from buried slumps to deep rotational slumps.	Metastable sand and silty layers of the Quarternary age.	Bulk density varies from 1.38t/m^3 to 1.73 t/m^3	Approx. 25	1.5-3	200-900	33 km^3 total with: 19 km^3 from central area. 14 km^3 from northern section.	15-140m	Northern section, <2° Centre, 1° South, 4-5°.

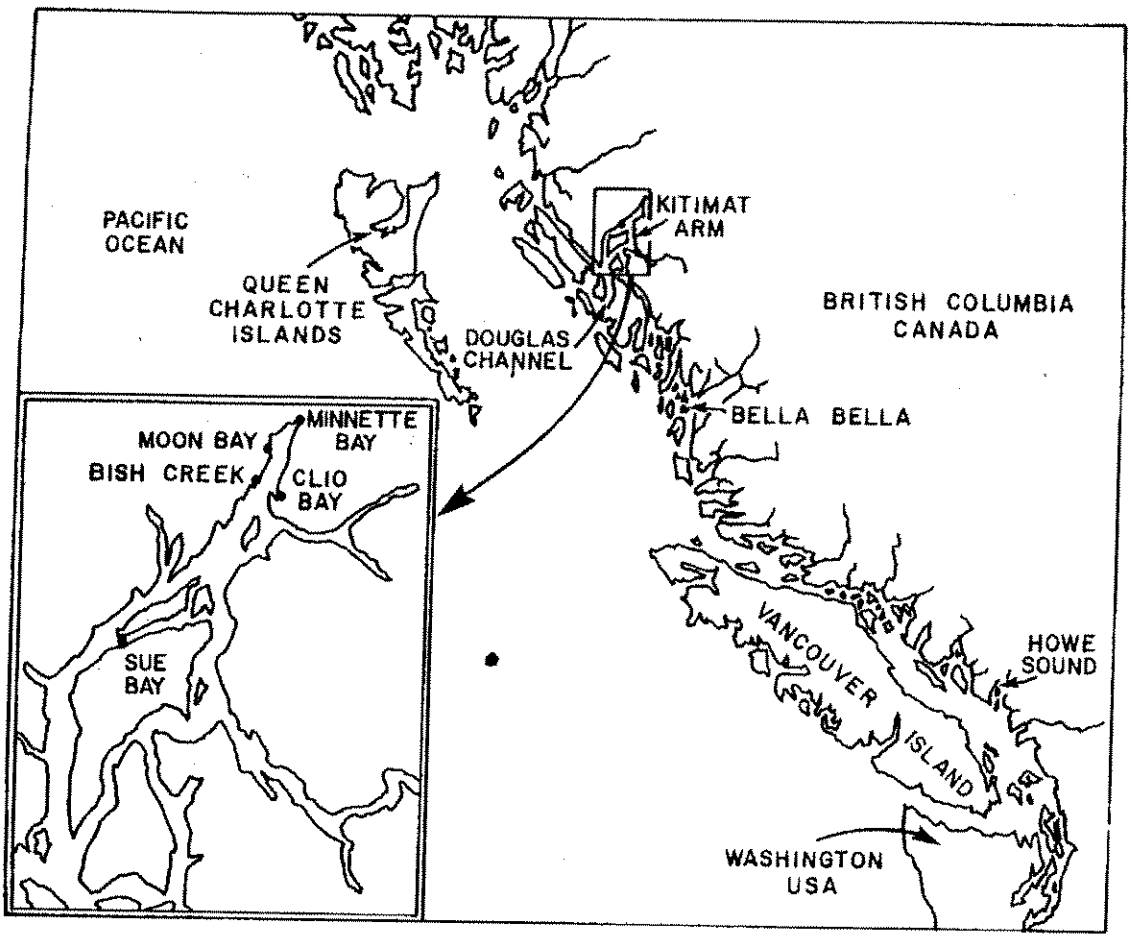

Figure 3-1: Location Map, Kitimat Arm (Murty and Brown, 1979).

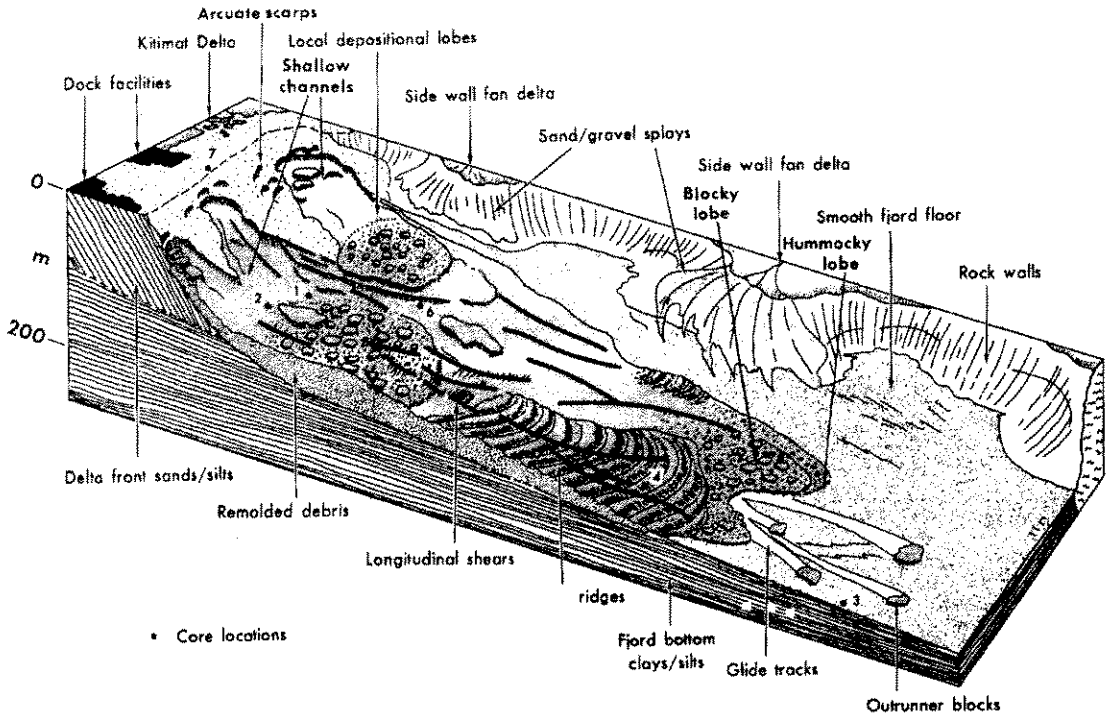

Figure 3-2:Logical map of Kitimat arm failure (Prior, et al., 1984).

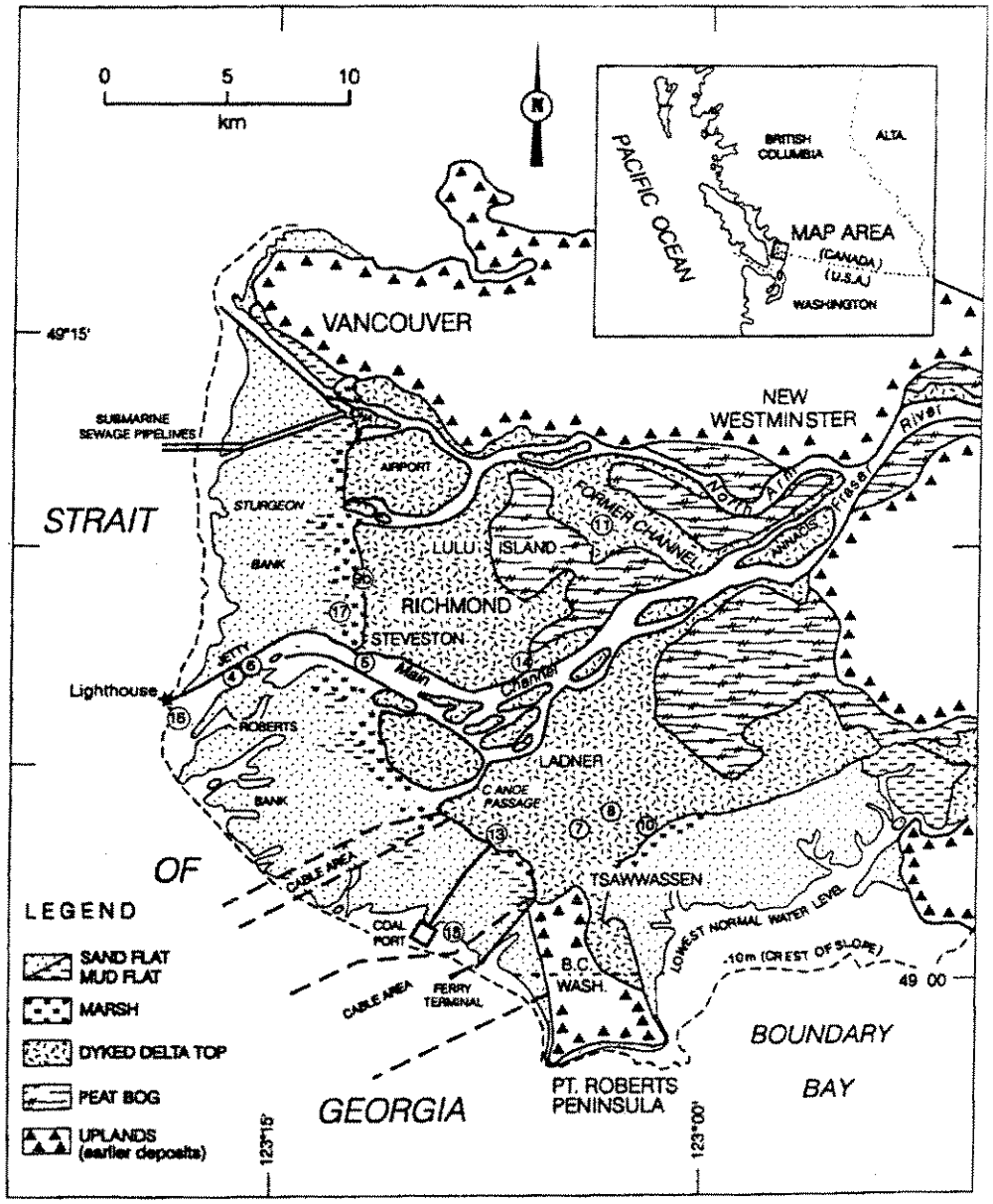

Figure 3-3: Fraser River Delta location map. (Luternauer et al, 2000)

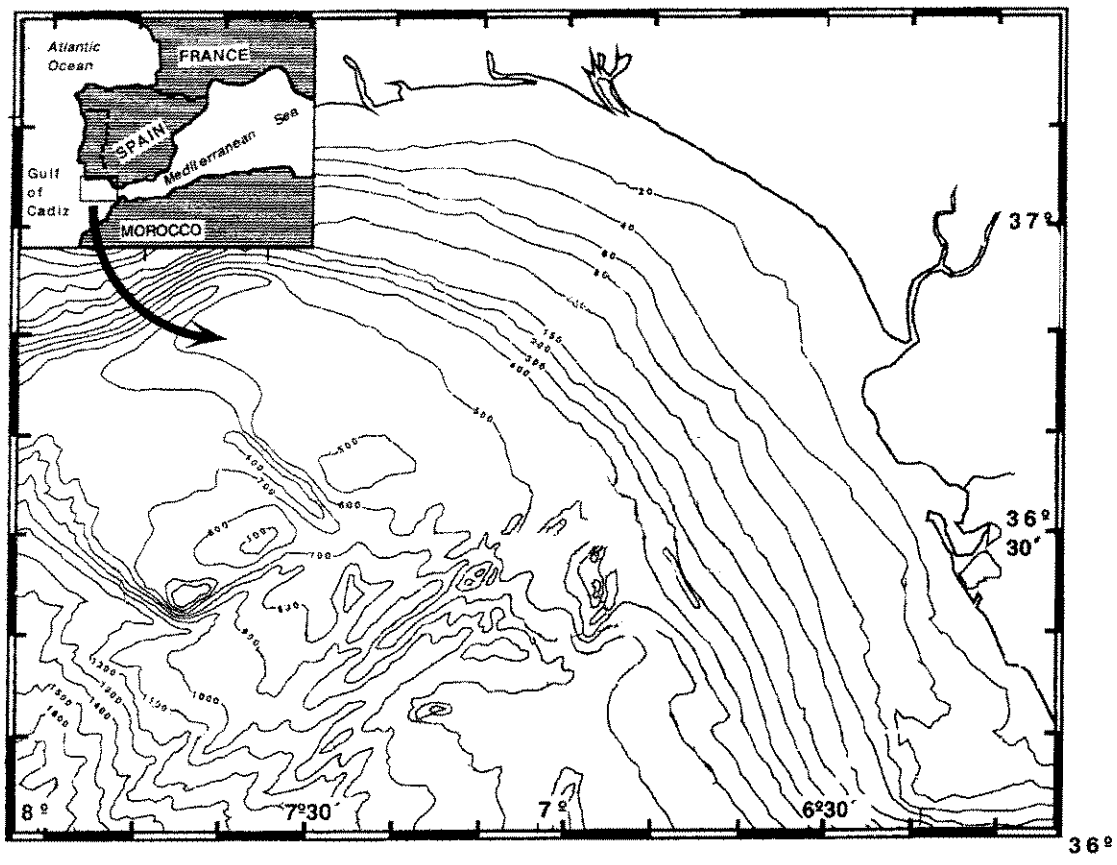

Figure 3-4: Bathymetery of the northeast Gulf of Cadiz. (Baraza et al.,1999)

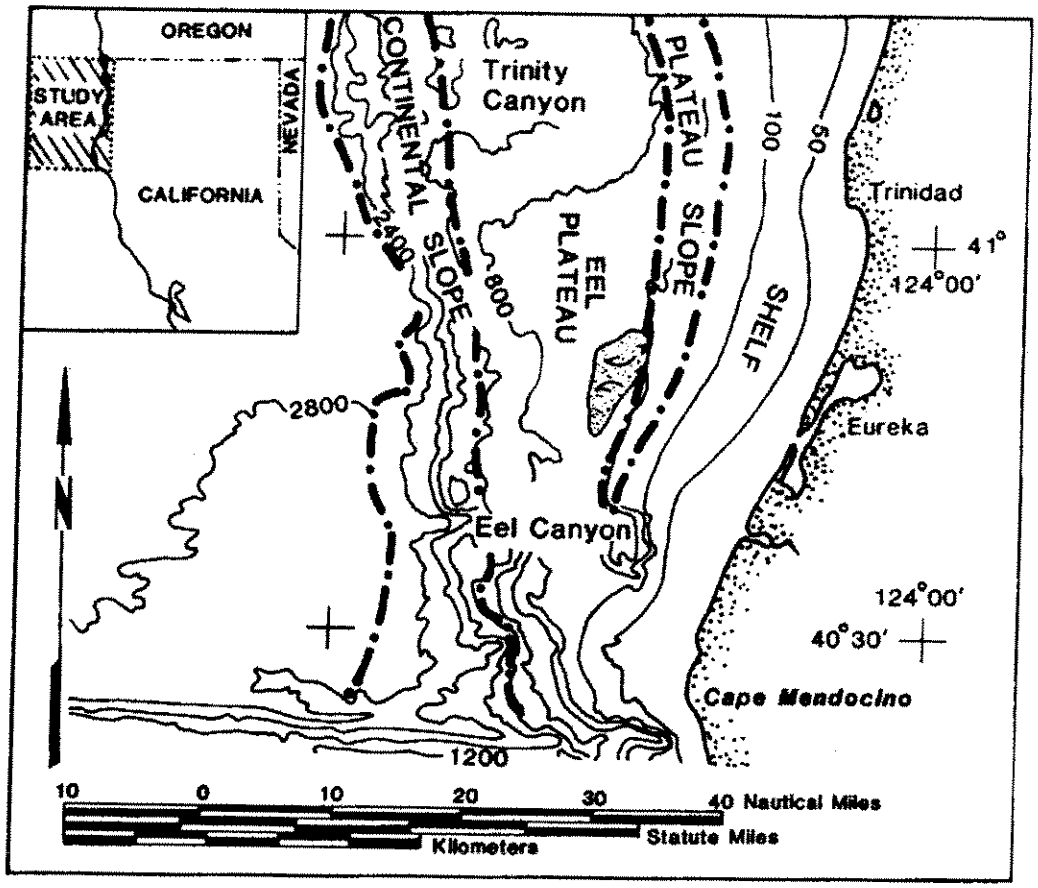

Figure 3-5: Location Map for Eureka Slide (Lee et al, 1981).

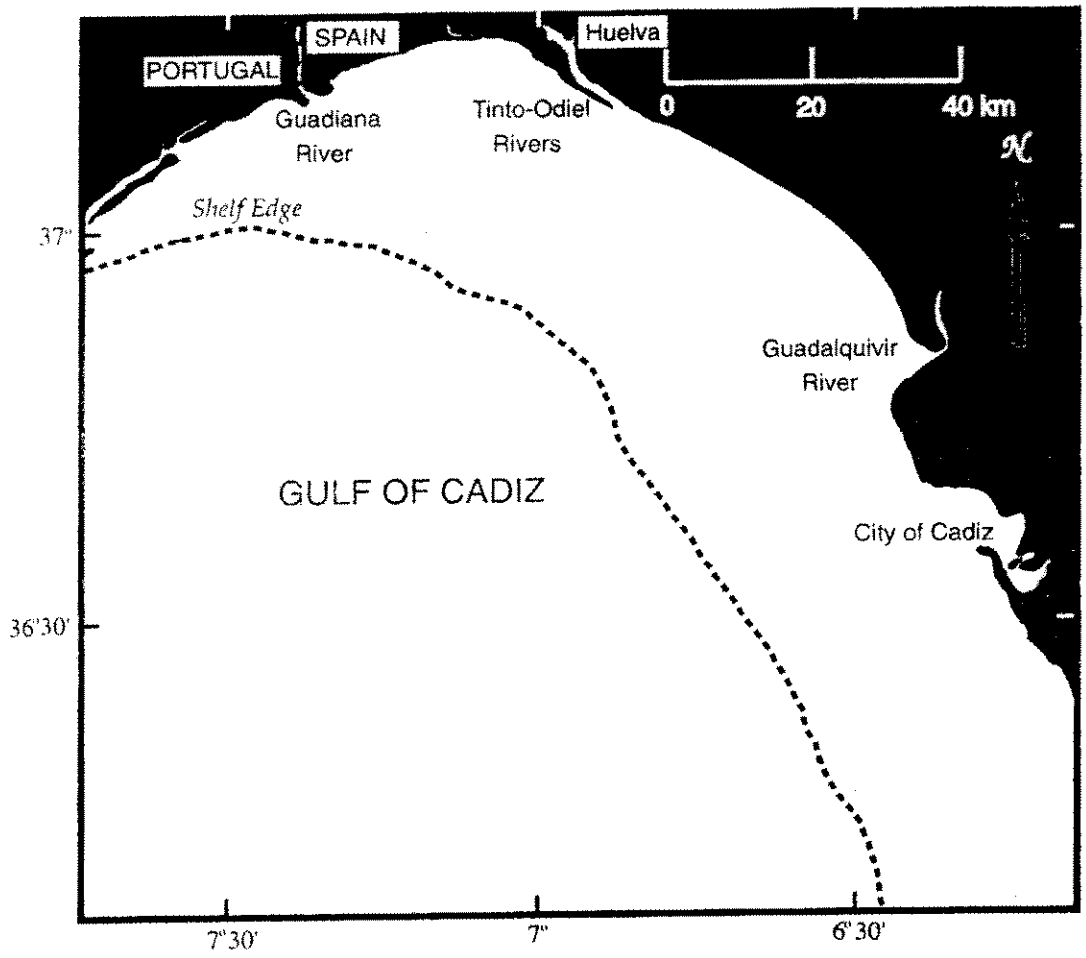

Figure 3-6: Location Map of Gulf of Cadiz, Spain (Lee and Baaraza, 1999).

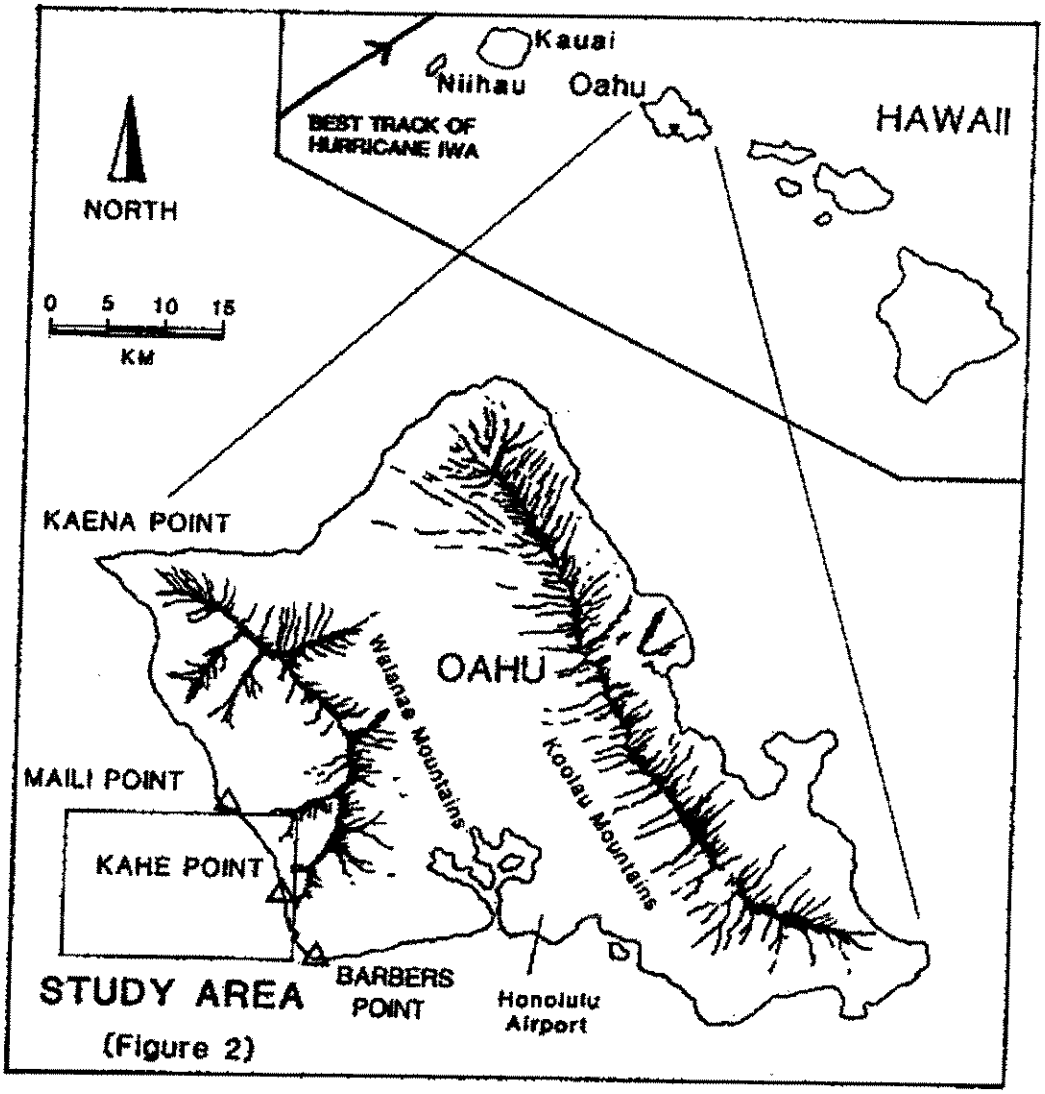

Figure 3-7: Location map, Kahe Point, Oahu slide, Hawaii (Tsutsui et al, 1987)

4 GENERAL CHARACTERIZATION OF THE SCOTIAN SLOPE

4.1 Geological overview

The Scotian Slope is part of the Mesozoic rifted margin of the central North Atlantic Ocean, with thick Jurassic and Cretaceous strata overlying Triassic salt (Wade and MacLean, 1990). Throughout the Tertiary, the Scotian margin accumulated prodeltaic and hemipelagic shales, in places modified into sediment drifts, and was deeply incised by canyons during major sea level lowstands. With the onset of terrestrial glaciation and general lowering of sea levels globally by many tens of metres in the Pliocene (5 to 2 Ma), more sand and mud were supplied to the margin, including the development of the large Laurentian Fan depocentre. Widespread gully cutting took place in the early Pleistocene (1.5 Ma), but the overall style of sedimentation was prodeltaic. Glacial ice first crossed the Scotian Shelf at about 0.5 Ma and since that time the continental slope has been dominated by proglacial sedimentation (Figure 4.1).

Morphologically, the Scotian Slope can be divided into three main regions (Figure 4.2).

(1) East of Verrill Canyon (62°W) the slope is highly dissected by canyons with sidewall slopes of up to 40° (typically 20°). Intercanyon areas are generally completely erosional in <1000 mbsl, but in deeper water canyons converge and intercanyon areas become broader and flatter (Pickrill et al., 2001). Much of the canyon cutting appears to have taken place in the mid to late Quaternary and is related to glacial outburst floods through tunnel valleys on the Scotian Shelf (Flynn, 2000).

(2) Between Verrill Canyon and Mohican Channel, the Scotian Slope is relatively smooth with only shallow gullies and widespread debris flows, summarized by Piper et al. (1985), Mosher et al. (1991, 1994), Gauley (2001) and Pickrill et al. (2001). Gradients are generally between 1° and 2°. Gullies head upslope in low headscarps at 500 - 700 mbsl.

(3) West of Mohican Channel, large areas of the upper slope have shallow canyons or gullies that lead downslope into widespread debris flows and shallow channels. The shallow water morphology is summarized by Piper and Sparkes (1987), Shor and Piper (1989), Baltzer et al. (1994) and Piper (2000) and the deeper water morphology by Hughes Clarke et al. (1992). Canyons and gullies mostly head upslope at about 400 mbsl.

Despite this varied morphology, the distribution of shallow sediments follows the same broad patterns over most of the Scotian Slope. Much of the upper continental slope is underlain by glacial till, which fingers out downslope in water depths of about 500 mbsl forming features termed till tongues (Mosher et al., 1989). In parts of the margin as many as 6 stacked till tongues may be present. Till appears to be overconsolidated preventing penetration by piston corers and multibeam imagery shows widespread iceberg scours and pits (Pickrill et al., 2001). The till tongues interfinger downslope with massive proglacial muds with sparse dropstones that could include the occasional boulder. In deeper water, the proglacial muds become thinner and interbed with mud turbidites. In places, particularly near channels, thin sand beds interbed with the muds. Canyon floors consist of thick sand beds interbedded with mud clast conglomerates of debris flow origin. All the margin is draped with a veneer of Holocene sediment typically 0.5 to 3 m thick, consisting of sorted sand down to 400 mbsl on the upper slope (greater water depths on isolated ridges), muds down to 2000 mbsl and muddy foam ooze in greater water depths. A few

canyons have a central active narrow channel (Baltzer et al., 1994, Pickrill et al., 2001) that appears to periodically transport small sandy turbidity currents in the Holocene.

The geology of much of the Scotian margin is dominated by salt tectonics (Wade and Maclean, 1990). Salt diapirs are less prominent morphological features than in the Gulf of Mexico and only a few have a visible morphological expression, generally in about 3000 m water depth. Faulting associated with salt diapirs is widespread and uplift rates on diapirs are of the order 10-50 m/Ma. High-resolution seismic profiles show at least one fault that slipped at least twice in the past 30 ka, with throws of 2 m. Failure scarps tens of metres high are widespread on the continental rise in the area of salt domes and appear related to faults (Pickrill et al. 2001).

4.2 Geotechnical Overview

Conventional shear vane, water content and bulk density measurements are available for some piston cores (<10 m penetration) from the Scotian margin (Figure 4.3): some results are presented by Mosher et al. (1994) and Mulder et al. (1997). Most of these measurements have been made on the normal stratigraphic section recovered in cores. They consist of 1-2 m of Holocene mud that become sandier near the base, overlying 1-2 m of brownish muds with sand and gravel beds that then overlies greater than 10 m of proglacial muds with rare dropstones. Ten Atterberg limit determinations have been made on sediment in the upper 15 m on the Scotian Slope (Figure 4.4). There are no deep-water geotechnical boreholes on the Scotian Slope.

Mosher et al. (1994) used average undrained shear strength and bulk density profiles in a normal stratigraphic section near Verrill Canyon to perform an infinite slope analysis. They found that on the regional 2° slopes, surficial sediments are stable. They considered and rejected triggering mechanisms such as storm wave loading and excess pore pressure due to shallow gas. Excess pore pressures of 6-11 kPa would be required for failure. Such excess pore pressures have not been measured on the Scotian Slope, although excess pore pressures of 2.5 kPa in gassy sediment and 6.7 kPa in debris flows have been measured on St Pierre Slope (Christian and Heffler, 1993). Mosher et al. (1994) concluded that failure was probably seismically triggered. Other authors have used geological arguments to conclude that seismicity was probably the cause of observed failures (Piper et al., 1985; Moran et al., 1990; Piper and Skene, 1998), although the relationship of failures to glaciation has also been modelled (Mulder and Moran, 1995). Moran and Hurlbut (1986) demonstrated that wave loading was unlikely to trigger failure.

On the eastern Scotian Slope, thick sticky red clays accumulated during the last glacial maximum, as a result of a plume of suspended sediment issuing from the Gulf of St Lawrence. There are anecdotal reports of problems with "sticky clays" when drilling the Tantallon M-41 well. Given that outwash plumes have issued from the Gulf of St Lawrence for at least the last 0.5 Ma (Piper et al., 1994), this facies may be several hundred meters thick. Geomechanical properties can be compared with those near Verrill Canyon. Average shear strengths of 8-11 kPa are found at 3-5 m subbottom at Verrill Canyon; similar shear strengths occur in sediments inferred to have originally been buried about 16 m at Tantallon, implying a strength ratio of about 0.2. Likewise, bulk density at 8 m depth near Verrill Canyon is about 1.8 gm/cm^3 and is only 1.7 gm/cm^3 at Tantallon. We have not completed a new infinite slope stability analysis but these data show that sediment at Tantallon is substantially less stable than for Verrill Canyon.

Downcore variation in shear strength in the normal stratigraphic section on the central and western Scotian Slope implies a strength ratio of about 0.33. This may indicate some slight cementation by early diagenetic iron monosulphides. Clay minerals are dominantly illite, with minor kaolinite and chlorite and large amounts of rock flour of quartz and feldspar. Baltzer et al. (1994) made in situ measurements with a 2m piezocone penetrometer and obtained more precise shear strength data that confirms measurements made on cores. The authors showed that the upper 1.5 m of sediment had an apparent overconsolidation as a result of partial cementation by burrowing organisms (Christian et al., 1991).

Mulder et al. (1997) used shear vane and bulk density measurements on debris flow deposits near the Albatross well site to calculate the degree of overconsolidation and hence the depth of failure in the source area. They concluded that some debris-flow clasts had been previously buried to depths of up to 50 m.

4.3 Geohazard Overview

The most severe geohazards on the Scotian margin involve slope instability. Instability is recognized from both the erosional remnants of failed material and from the deposition products of failures. Piper (1991) estimated that surficial failures or failure deposits covered 38% of the seabed between 500 mbsl and 3000 mbsl and that a further 8% consisted of steep erosional slopes. Pickrill et al. (2001) documented the styles of failure visible in regional multibeam bathymetric images. Information is first presented on types of mass movement and failure, then other geohazards such as shallow gas and boulder beds are discussed.

Near surface retrogressive rotational slumps and debris flows are widespread on the western Scotian margin and debris flow deposits fill many canyon floors on the eastern Scotian margin. Large areas of the lower slope and upper rise have tens of metres of "missing" sediment, apparently removed along bedding planes (Campbell, 2000). Pickrill et al. (2001) suggest that much of this sediment was lost by retrogressive failure initiated at fault line scarps associated with salt tectonics on the upper rise. Radiocarbon dating summarized by Piper and Skene (1998) shows that most near surface failures occurred in the interval between 15 ka and 12 ka and that there is no evidence for significant failure younger than 10 ka on the Scotian margin. Pickrill et al. (2001) report that many of the larger failures on the lower slope and upper rise are draped with tens of metres of sediment and are thus tens of thousands of years old.

Interstratal deformation is widespread on the entire Scotian margin. It is best known from Huntec sparker profiles near the Shubenacadie H-100 well, where 50 m thick slabs of sediment show spreading creep above a decollement surface developed at the same stratigraphic horizon as an upper slope till tongue (Gauley, 2001). The slab of sediment showing creep features is unsupported laterally at valley walls and unsupported downslope as a result of older failure scarps up to 100 m high. Similar features are known elsewhere on the Scotian Slope and also on St. Pierre Slope (MacDonald, 2001), where no observed failure took place along the decollement surface in the M=7.2 1929 earthquake. Evidence on the Scotian Slope suggests that occasional failure along such decollement surfaces is responsible for creating at least some of the thick debris avalanche deposits described on the Scotian Rise by Piper et al. (1999), as a result of the collapse of a 50-100 m thick sediment section above the decollement plane. Smaller debris flow deposits on the rise may result from upper slope failure in canyon heads (e.g. as documented for the Albatross debris flow: Mulder et al., (1997)). Major debris deposits on the Scotian Rise date

back to at least the upper Pliocene (~3 Ma) and are therefore unlikely to be genetically related to glaciation (Piper et al. 1999).

Shallow gas has been interpreted to be widespread on the Scotian Slope (Campbell, 2000) and a few piston cores have recovered very gassy sediment (Figure 4.5). Pockmarks 10-40 m in diameter are widespread on the mid slope below the limit of till but are less common in deeper waters (Baltzer et al., 1994): knowledge of their distribution is limited by the availability of deep-water high-resolution sidescan data and no data is available on the distribution of pockmarks near salt diapirs. Although the physical conditions on the Scotian Slope are suitable for the presence of gas hydrates, gas hydrates have not been sampled and no BSRs have been recognised in seismic profiles from the Scotian margin. A gas kick was recorded near the bottom of casing in the Shubenacadie H-100 well.

Boulder beds proved to be a drilling problem at the Albatross G-13 well and similar problems could be expected in any well drilled on a canyon or channel floor. In intercanyon areas, there are probably isolated ice-rafted boulders, but winnowed beds are not to be expected.

Some geohazards are present in the pre-glacial section on the Scotian Slope, in particular, mud diapirism occurs in the vicinity of the Shelburne G-29 well, apparently sourced in Pliocene shales (Piper and Sparkes, 1987). Maximum rates of uplift are of the order 50 m/Ma.

4.4 Geophysical Information

The distribution of high-resolution seismic reflection profiles is shown in Figure 4.6. Data consists principally of single-channel small sleeve-gun records (vertical resolution ~10 m) and Huntec boomer or sparker records (vertical resolution ~1 m), both used for assessment of shallow geohazards. The resolution of the Huntec system allows correlation with piston cores. 3.5 kHz echosounder profiles are available over much of the Scotian margin and allow a classification of seabed conditions (Campbell, 2000). Long-range GLORIA sidescan is available from west of 63°W in water depths <2000 m (Hughes Clarke et al., 1992). Small areas of the Scotian Slope have been surveyed with the SeaMARC I 5-km swath deep-towed sidescan (Piper et al., 1985; Piper and Sparkes 1987; Shor and Piper, 1989) and the SAR 1-km swath deep-towed sidescan (Baltzer et al., 1994).

4.5 Environmental conditions and loads

Only sparse data is presently available on waves and currents (Gregory and Bussard, 1996) on the Scotian Slope. Long-term current meter records at longitude 63°W (reported in part by Hill and Bowen 1983) show peak velocities at 20 m off the seabed of 50 cms^{-1} at 250 mbsl and 30 cms^{-1} at 700 mbsf. Preliminary data from a deep water mooring at 1100 mbsl shows near-bed currents of 20 cms^{-1} at tidal frequencies. Bottom photographs show that deeper water areas generally lack current-produced structures above water depths of about 4000 mbsl (Tucholke et al., 1985). Winnowing of Holocene sediment on ridges in water depths to 1500 mbsl is evidence for currents of >20 cms^{-1}. Evidence of current erosion is seen in seismic reflection profiles from the heads of some canyons. The largest annual significant wave height is 10 m, the largest 100-year significant wave height is 17 m (Neu, 1982).

Earthquake risk concepts on the East Coast of Canada are summarized by Keen et al. (1990) and updated numerical estimates are available from *www.seismo.nrcan.gc.ca*. The eastern continental margin of Canada is relatively active compared to many passive continental margins, with two M>7 earthquakes occurring this century (1929 off the Laurentian Channel and 1933 in Baffin Bay). The instrumental record of earthquakes is 30-70 years for this region. Historical records suggest that off Nova Scotia there were no earthquakes comparable to the 1929 earthquake in the previous 150 years. Piper and Normark (1982) and MacDonald (2001) suggested that the recurrence interval for earthquakes similar to the 1929 earthquake, off the Laurentian Channel was hundreds of thousands of years. The geological record on the Scotian margin suggests that there has been no large earthquake in the last 10 000 years, but that there were significant earthquakes in the late Pleistocene. The abundance of failures in the 12-15 ka time interval might be a consequence of more frequent earthquake activity due to glacial unloading (Dehls et al., 2000 in Norway).

Mean sedimentation rates can be estimated for a range of timescales. Mean sedimentation rates in the Holocene (the last 10 000 years) are of the order of 10-20 cm/ky, with silts and muds largely swept off the outer banks. Where data exists, the early Holocene sedimentation rates appear much higher than those in the late Holocene. Sedimentation rates during the last glacial maximum are probably regionally variable, depending on the proximity of the site to ice margins. In the Shubenacadie-Acadia area, principally muddy sediments accumulated in the 12-18 ka interval at about 60-100 cm/ky and in the 12-36 ka interval at 100 cm/ky. At the Tantallon well site, radiocarbon dates indicate a sedimentation rate of 450 cm/ky in the sticky red muds. Near the Shelburne well, a radiocarbon date of 28.1 ka implies a glacial sedimentation rate of only 15 cm/ky, again principally in muds, perhaps because of erosion. Over the last 0.5 Ma, the mean sedimentation rate is about 40 cm/ky and since the base Quaternary (1.8 Ma) is about 30 cm/ky.

Mean heat flow on the margin is similar to that measured in mainland Nova Scotia, about 60±14 mWm^{-2}, with variability resulting from salt diapirism and fluid migration (Keen and Beaumont, 1990).

4.6 Data requirements

The key data requirement on the Scotian Slope is geotechnical boreholes to obtain information on sediment properties below the limit that can be reached by piston coring, particularly within decollement zones. Multibeam bathymetry is essential on the eastern Scotian Slope from the Gully eastward and would be desirable on the west Scotian Slope from Mohican Channel westward. Additional high-resolution seismic profiles and deep-water sidescan are necessary to understand particular geohazards. General data coverage of cores and seismic is poor on the Scotian Slope east of the Gully and west of 64°W.

4.7 References

Baltzer, A., Cochonat, P. and Piper, D.J.W., 1994. In situ geotechnical characterisation of sediments on the Scotian Slope, eastern Canadian continental margin. Marine Geology, V. 120, p. 291-308.

Campbell, D.C., 2000. 3.5 kHz sub-bottom profiler seabed classification along selected ship's tracks on the Scotian Slope, offshore Nova Scotia; Geological Survey of Canada, Open File 3928, 15 pages (3 sheets).

Christian, H., Piper, D.J.W. and Armstrong, R., 1991. Geotechnical properties of seabed sediments from Flemish Pass. Deep Sea Research, V. 38, p. 663-676.

Christian, H.A. and Heffler, D.E., 1993. Lancelot - a seabed piezometric probe for geotechnical studies. Geo-Marine Letters, V. 13, p. 189-195.

Dehls, J.F., Olesen, O., Olsen, L., and Blikra, L.H., 2000. Neotectonic faulting in northern Norway; the Stuoragurra and Nordmannvikdalen postglacial faults. Quaternary Science Reviews, V. 19, p. 1447-1460.

Flynn, R.F.J., 2000: Tunnel Valleys under the Southeastern Scotian Shelf. B.Sc. (hons) thesis, Saint Mary's University, Halifax, N.S.

Gauley, B.J.L., 2001. Sediment stratigraphy and failure on the central Scotian Slope. Unpublished M.Sc. thesis, Dalhousie University, Halifax, N.S.

Gregory, D.N. and Bussard, C., 1996. Current statistics for the Scotian Shelf and Slope. Canadian Data Report of Hydrography and Ocean Sciences, 144, 167 p.

Hill, P.R. and Bowen, A.J., 1983. Modern sediment dynamics at the shelf slope boundary off Nova Scotia; in The Shelfbreak. Critical Interface on Continental Margins, eds. D.J. Stanley and G.T. Moore; Society of Economic Palaeontologists and Mineralogists Special Publication No. 33, p. 265-276.

Hughes Clarke, J.E., O'Leary, D. and Piper, D.J.W., 1992. The relative importance of mass wasting and deep boundary current activity on the continental rise off western Nova Scotia. Geologic evolution of Atlantic continental rises, ed. C.W. Poag and P.C. de Graciansky, van Nostrand Reinhold, New York, p. 266-281.

Keen, C.E. and Beaumont, C., 1990. Geodynamics of rifted continental margins. Chapter 9, in Geology of the continental margin off eastern Canada, ed. M.J.Keen and G.L.Williams. Geological Survey of Canada, Geology of Canada, no. 2, (also Geological Society of America, The Geology of North America, v. I-1), p. 391-472.

Keen, M.J., Adams, J., Moran, K., Piper, D.J.W. and Reid, I., 1990. Earthquakes and seismicity. in Geology of the continental margin off eastern Canada, ed. M.J.Keen and

G.L.Williams. Geological Survey of Canada, Geology of Canada, no. 2, (also Geological Society of America, The Geology of North America, V. I-1), p. 793-798.

MacDonald, A.W.A., 2001. Late Cenozoic geology framework of St Pierre Slope, offshore eastern Canada. B.Sc. (hons) thesis, Saint Mary's University, Halifax, N.S.

Moran, K. and Hurlbut, S.E., 1986. Analysis of potential slope instability due to wave loading on the Nova Scotian Shelf. Proceedings of the Third Canadian Conference on Marine Geotechnical Engineering, St Johns, Nfld.

Moran, K., Keen, M.J., Piper, D.J.W. and Adams, J., 1990. Slope stability. in Geology of the continental margin off eastern Canada, ed. M.J.Keen and G.L.Williams. Geological Survey of Canada, Geology of Canada, no. 2, (also Geological Society of America, The Geology of North America, V. I-1), p. 798-802.

Mosher, D.C., Piper, D.J.W., Vilks, G., Aksu, A.E. and Fader, G.B., 1989. Evidence for Wisconsinan glaciations in the Verrill Canyon area, Scotian Slope. Quaternary Research, V. 31, p. 27-40.

Mosher, D.C., Moran, K. and Hiscott, R.N., 1994. Late Quaternary sediment, sediment mass-flow processes and slope stability on the Scotian Slope. Sedimentology, V. 41, p. 1039-1061.

Mosher, D.C., Moran, K. and Zevenhuizen, J., 1991. Surficial Geology and Physical Properties 18. Slope: Verrill Canyon. in East Coast Basin Atlas Series: Scotian Shelf; Atlantic Geoscience Centre, Geological Survey of Canada, p. 145.

Mulder, T. and Moran, K., 1995. Relationship among submarine instabilities, sea-level variations and the presence of an ice sheet on the continental shelf: an example from the Verrill Canyon area, Scotian Shelf. Paleoceanography, V. 10, p. 137-154.

Mulder, T., Berry, J.A. and Piper, D.J.W., 1997. Links between geomorphology and geotechnical characteristics of large debris flow deposits in the Albatross area on the Scotian slope (E. Canada). Marine Georesources and Geotechnology, V. 15, p. 253-281.

Pickrill, R., Piper, D.J.W., Collins, J.T., Kleiner, A. and Gee, L. 2001. Scotian Slope Mapping Project: The benefits of an integrated regional high-resolution multibeam survey. Offshore Technology Conference, Houston, Texas, 30 April-3 May 2001, paper OTC 12995, 10 p.

Piper, D.J.W. 2000. Pleistocene ice outlets on the central Scotian Slope, offshore Nova Scotia. Current Research 2000-D7, 8 p.

Piper, D.J.W., 1991. Surficial Geology and Physical Properties 6. Deep water surficial geology. in East Coast Basin Atlas Series: Scotian Shelf; Atlantic Geoscience Centre, Geological Survey of Canada, p. 121.

Piper, D.J.W. and Normark, W.R., 1982. Effects of the 1929 Grand Banks earthquake on the continental slope off eastern Canada. Geological Survey of Canada Paper 82-1B, 147-151.

Piper, D.J.W. and Skene, K.I., 1998. Latest Pleistocene ice-rafting events on the Scotian margin (eastern Canada) and their relationship to Heinrich events. Paleoceanography, V. 13, p. 205-214.

Piper, D.J.W. and Sparkes, R., 1987. Proglacial sediment instability features on the Scotian Slope at 63°W. Marine Geology, V. 76, p. 1-11.

Piper, D.J.W., Farre, J.A. and Shor, A.N., 1985. Late Quaternary slumps and debris flows on the Scotian Slope: Geological Society of America Bulletin, V. 96, p. 1508-1517.

Piper, D.J.W., Mudie, P.J., Aksu, A.E. and Skene, K.I. 1994. A 1 Ma record of sediment flux south of the Grand Banks used to infer the development of glaciation in southeastern Canada. Quaternary Science Reviews, V. 13, p. 23-37.

Piper, D.J.W., Skene, K.I and Morash, N., 1999. History of major debris flows on the Scotian Rise. Geological Survey of Canada Current Research, 1999-E, p. 203-212.

Piper, D.J.W., Mudie, P.J., Fader, G.B., Josenhans, H.W., MacLean, B. and Vilks, G., 1990. Quaternary Geology. Chapter 10 in Geology of the continental margin off eastern Canada, ed. M.J.Keen and G.L.Williams. Geological Survey of Canada, Geology of Canada, no. 2, (also Geological Society of America, The Geology of North America, V. I-1), p. 475-607.

Shor, A.N. and Piper, D.J.W., 1989. A large Pleistocene blocky debris flow on the central Scotian Slope. Geo-Marine Letters, V. 9, p. 153-160.

Tucholke, B.E., Hollister, C.D., Biscaye, P.E. and Gardner, W.D., 1985. Abyssal current character determined from sediment bedforms on the Nova Scotian continental rise. Marine Geology, V. 66, p. 43-58.

Wade, J.A. and MacLean, B.C., 1990. Aspects of the geology of the Scotian Basin from recent seismic and well data. Chapter 5, in Geology of the continental margin off eastern Canada, ed. M.J.Keen and G.L.Williams. Geological Survey of Canada, Geology of Canada, no. 2, (also Geological Society of America, The Geology of North America, V. I-1), p. 190-238.

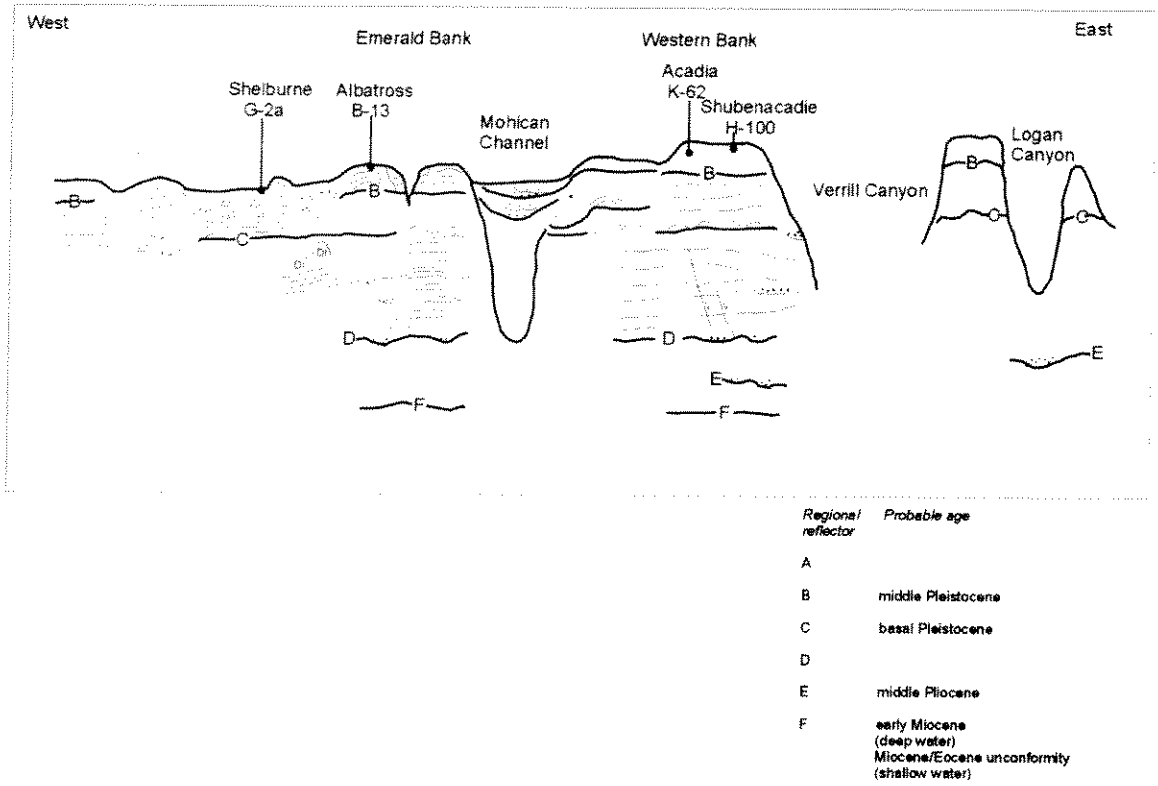

Figure 4-1: Cartoon cross-section showing the upper few hundred metres of sediment on the Scotian Slope.

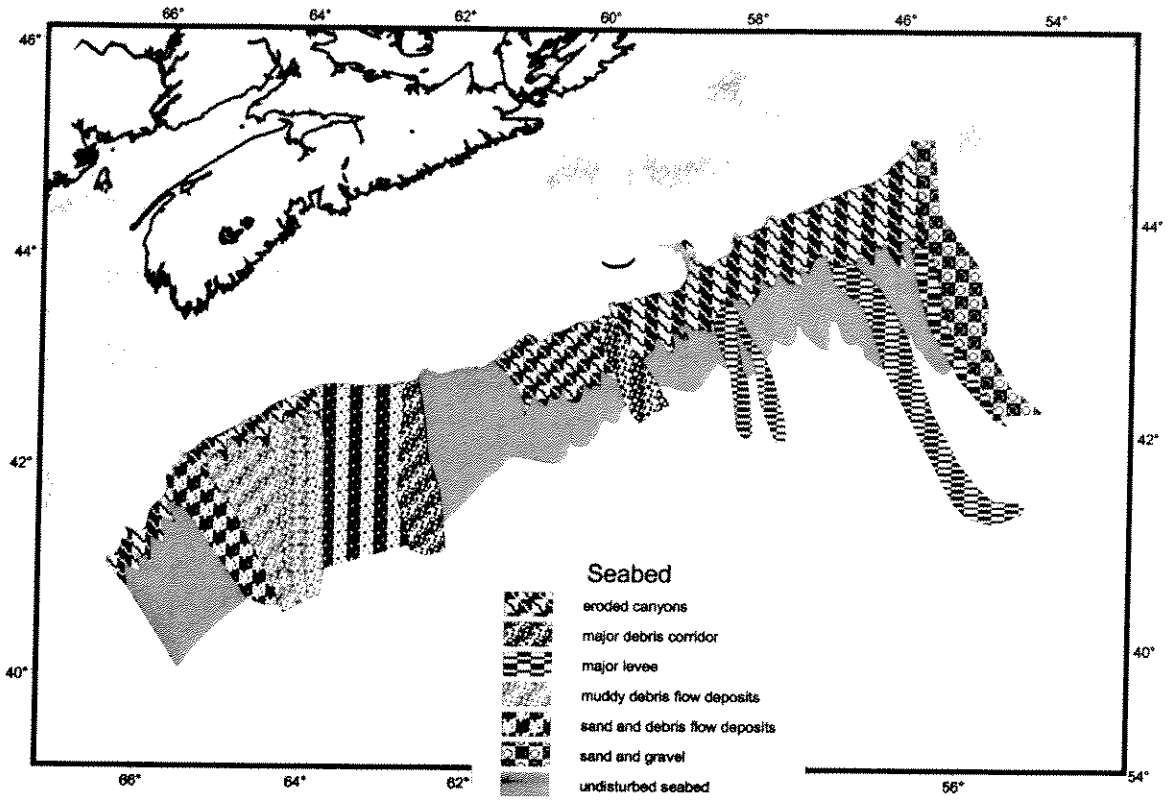

Figure 4-2: Generalized classification of seabed types on the Scotian margin.

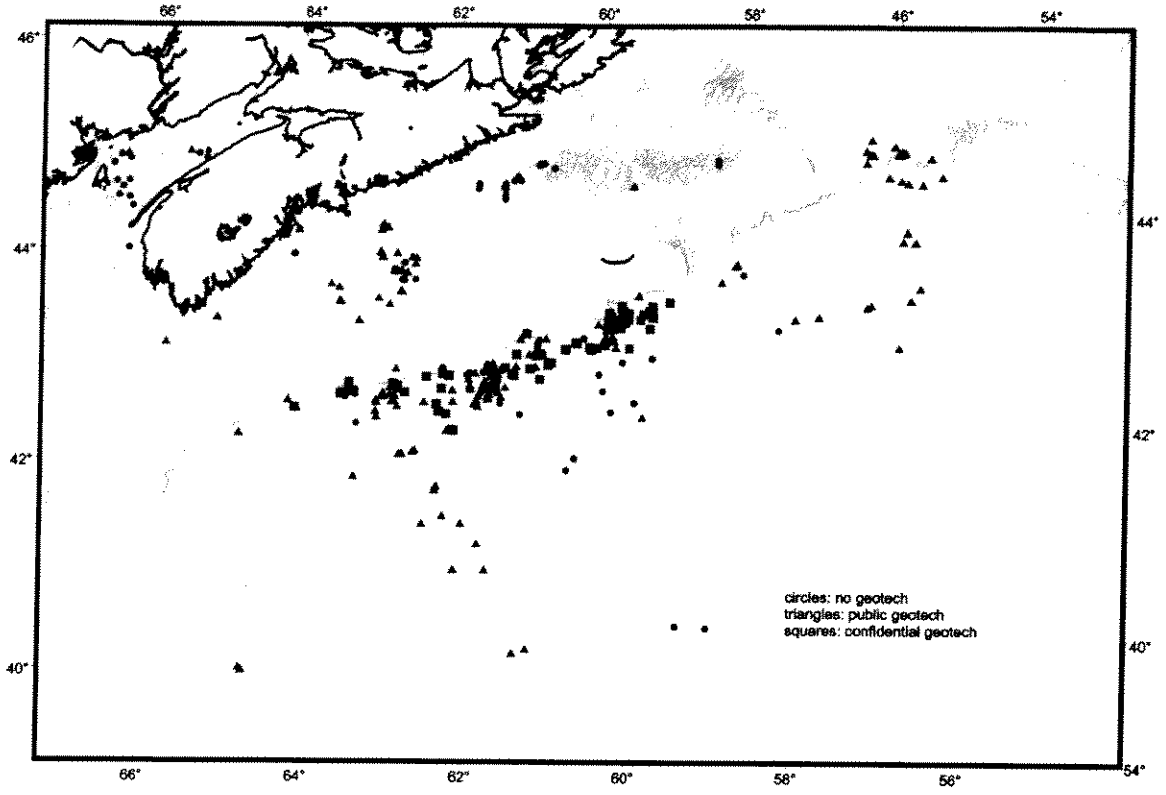

Figure 4-3: Map showing available seabed samples on the Scotian margin.

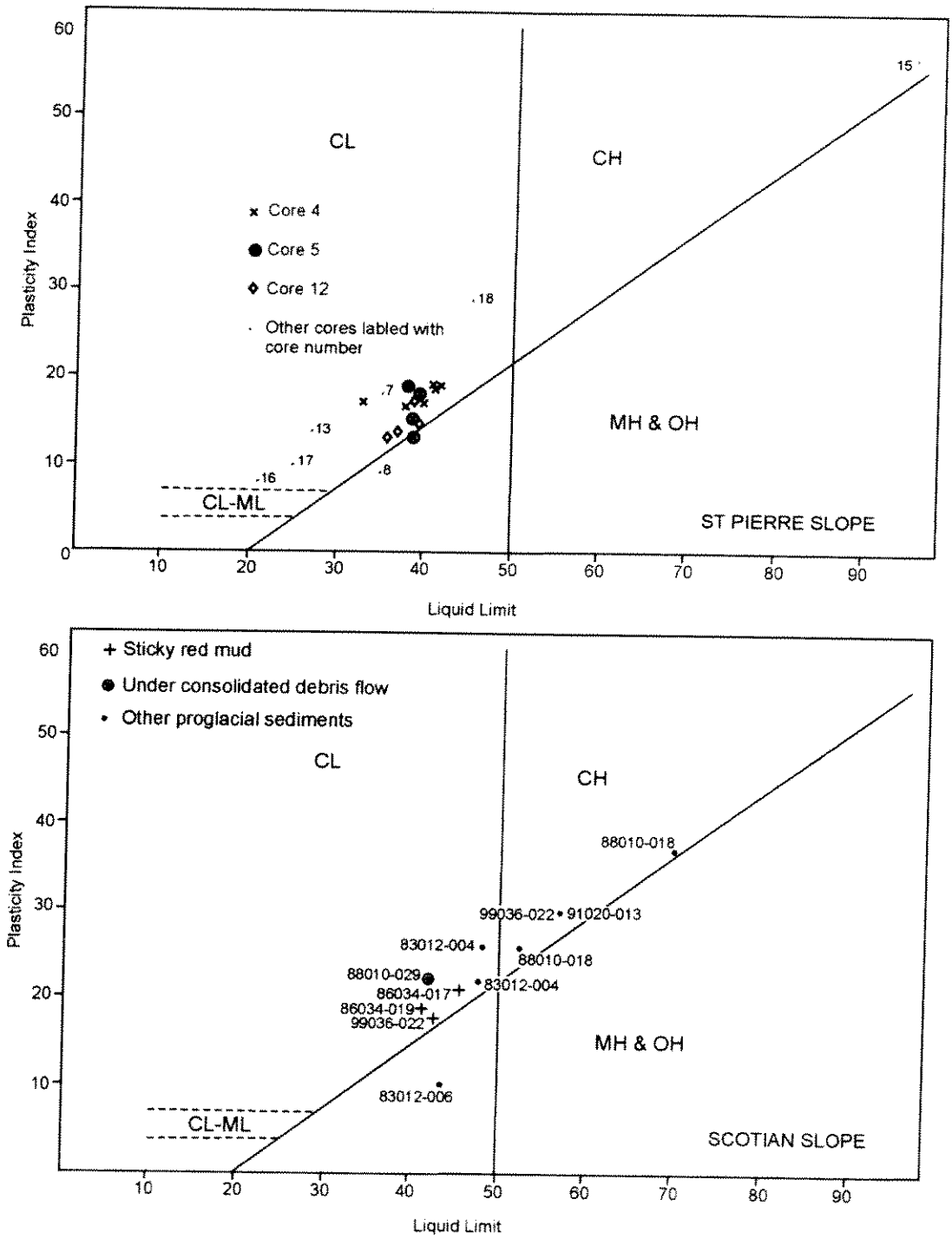

Figure 4-4: Atterberg limit determinations from the Scotian margin and St Pierre Slope.

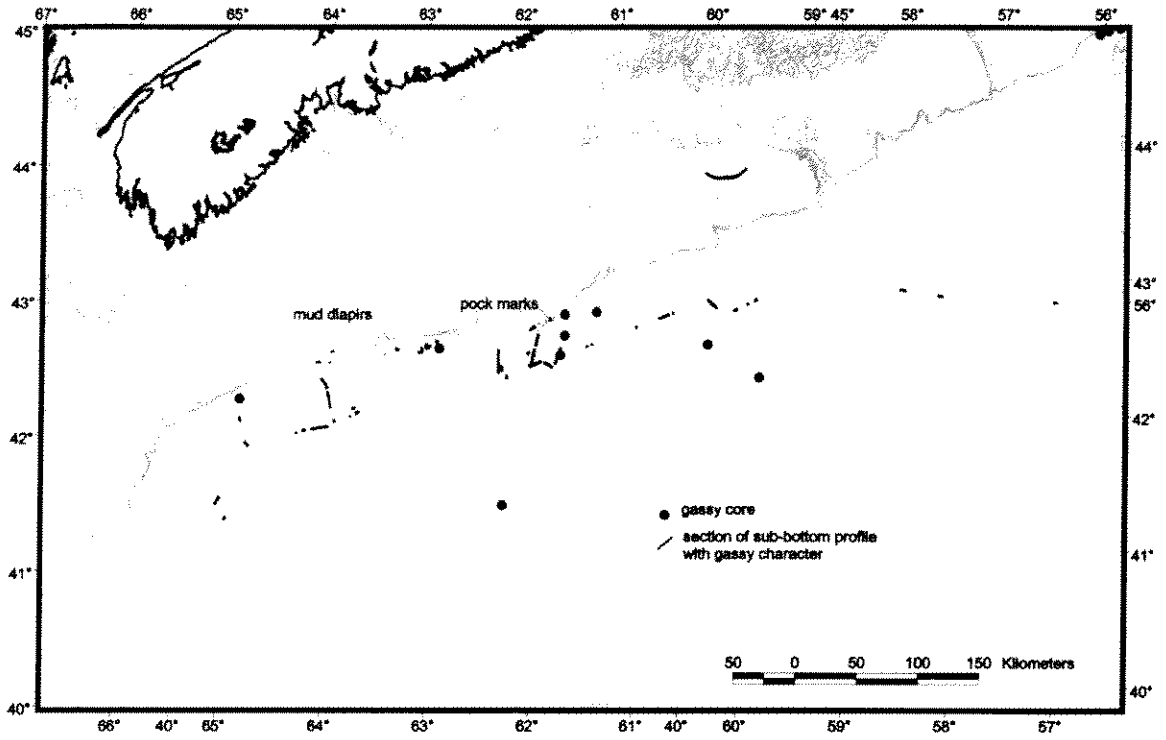

Figure 4-5: Map showing evidence of shallow gas on the Scotian margin.

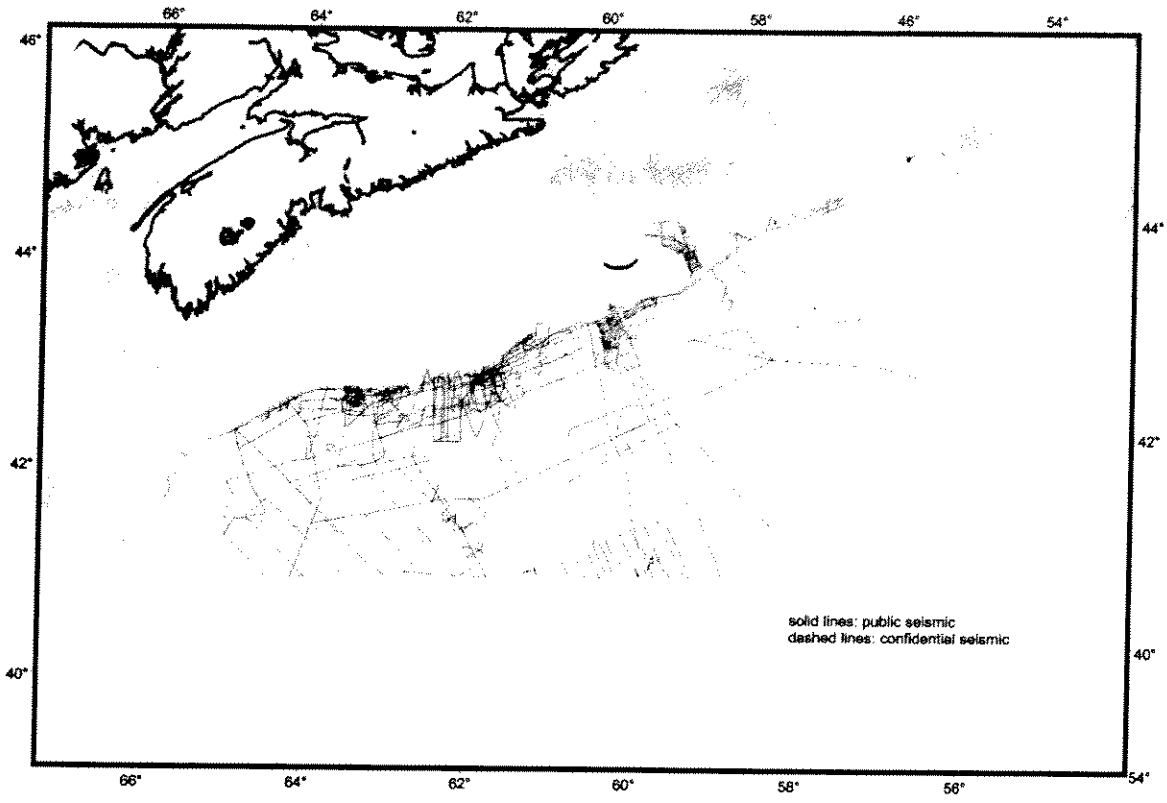

Figure 4-6: Map showing available high-resolution geophysical data from the Scotian margin.

5 DESCRIPTION AND ANALYSIS OF MASS FAILURES ON THE SCOTIAN SLOPE

5.1 Objectives

General information on the geohazards, geological setting, geotechnical information and environmental loads on the Scotian Slope was presented in Section 4.0. The objective of this section is to consider specific mass failures on the Scotian Slope in detail through a review of what is known of the failures and by analyzing the stability of the failed areas. The three failures considered in this section are: the Albatross debris flow, the Verrill Canyon rotational slumps and the Logan Canyon debris flow series. First, information is presented from the literature on each failure, the data gaps are highlighted and then the slopes are analyzed through use of the infinite slope method and limit equilibrium methods. The analysis includes the existing slope stability conditions, the initiation of the slide, the evolution of the failure and the effect of environmental loading.

Section 5.2 presents a general study and the case histories of four sediment failures along the Scotian margin and Grand Banks. Sections 5.3 through 5.5 are a collation of information on the three failures from various publications without further interpretation, mainly focusing on geotechnical related issues. Information on each slide is summarized in Table 5.3 and core data is provided in Tables 5.1 and 5.2.

5.2 Case Histories of Four Sediment Failures Along the Scotian Margin and Grand Banks

5.2.1 Introduction

In order to understand why and where sediments fail along continental slopes, known failures are being studied. By determining the lithologic controls and failure mechanisms behind the failures, it might be possible to find similar areas that have not yet failed. The ability to determine areas of possible slope failure could be important to industries that are moving into deeper water with their exploration.

Along the Scotian Slope, there are three well known failures that are being studied: the Albatross Debris Flow, the Verrill Canyon Rotational Slumps, and the Logan Canyon Debris Flow. These failures are all located on the central portion of the slope, which is smoother and easier to study than both the highly dissected eastern and western sections. This report also looks at a fourth well-known failure at the western edge of the Grand Banks: the Grand Banks Failure of 1929.

5.2.2 Albatross debris flow

Location:

The sediment failure is located on the central portion of the Scotian Slope south of Emerald Bank and west of Mohican Canyon between Heron and Puffin Valleys (62° 45'W and 63° 05'W to 42° 45'N and 41° N). The source area is inferred from 5 km sidescan and consists of several small canyons on the middle slope. The headwall scarp is 550-700 mbsl.

Detailed bathymetry

Above 500 mbsl, the upper slope is relatively smooth. From 500 mbsl to 1,000-1,200 mbsl, the slope is dissected by submarine canyons (Shor and Piper, 1989). Below this, the slope is divided into valleys with high levees and ridges (Mulder et al., 1997). The lower slope to upper rise is smooth.

Type of slide/Type of sediment failure

The late Pleistocene failure is recognized as a blocky debris flow that averages 120m thick on the slope to 20m thick on the lower slope (Mulder et al., 1997). There are two possible debris flows that Piper and Skene (1998) recognized in cores that compose the Albatross Debris Flow. They are termed debris flow 1 (DF1) and debris flow 2 (DF2). DF1 is thin, < 1 m, and not recognized acoustically. It appears to have been deposited close to the time of the deposition of brick red mud (brm 'b') (Piper and Skene, 1998)[1]., which might have been eroded by the flow, because this layer is seen neither above nor below DF1. DF2 is thicker than DF1, older than brm b, but younger than brm d. Piper and Skene suggest that DF2 was found in the dated core 90-015-19, but it might more likely be DF1 (Piper, 2000, personal communication).

Age

In the Albatross area, there have been debris flows throughout the Quaternary. The most recent failures occurred in the Late Pleistocene. Debris flow 1 occurred at the same time or soon after brm 'b' was deposited Debris flow 2 occurred before brm b was deposited but after brick red mud "d" (brm d) was deposited. Brm b is bracketed by radiocarbon dating of a 12.74 +/- 0.2 ka gastropod from core 82004-2 above (Piper and Skene, 1998) and by radiocarbon dating of 13.3 +/- 1.1 ka foraminifera below (Keigwin and Jones, 1995)[2]. Brm d is bracketed by radiocarbon dating of foraminifera (Keigwin and Jones, 1995) and was deposited 14.0-14.1 ka (Piper and Skene, 1998). These dates are supported by the radiocarbon dates of the resedimented shells found within debris flow 1.

Failure mechanism

The failure mechanism is unknown but is hypothesized to be an earthquake or related to gas hydrates (Berry, 1992). Support for the earthquake hypothesis is the similar aged failure near Verrill Canyon. No direct evidence is known for gas hydrates here, but Pockmarks near the failure indicate that gas or gas hydrates might also be a cause for failure.

Geometry of slide

Amount of soil: > 600 km^3 (Mulder et al., 1997)
Depth of slide: ~ 50 m, based on consolidation testing of blocks (Mulder et al., 1997)
Slope angle within source area: approximately 6°
Run out distance of debris flow: 200 km

[1] Along the Scotian Slope, four correlative brick red sandy mud layers associated with glacial retreat and iceberg rafting have been documented. They are termed a, b, c, and d, and they have been well dated by Piper and Skene (1998).
[2] All dates within the text of the report have been reservoir corrected (-0.4ka).

Slide sediment lithology

The lithology of the failed sediment is only known from examining the blocks from the debris flows, which consist of a wide range of muds. No long cores are available from the source area.

Sedimentation rate

In this general area the postglacial sedimentation rate is estimated to be 0.185 m/ka (Berry and Piper, 1993). The Late Wisconsinan sedimentation rate is 0.85 m/ka.

Subsurface stratigraphy

The piston cores that have been collected have only sampled the debris flows and not the stratified sediment around the failure. The piston cores from the debris flow deposits contain bioturbated, hemipelagic, Holocene muds over a layer of sandy/muddy fine turbidities. The distinctive brick red sandy mud layers are found within this unit. Below the thin turbidite sequence, the cores have penetrated a mud-clast conglomerate with a mud matrix that represents the debris flows (Shor and Piper, 1989).

Geotechnical properties

The sediment in the undisturbed areas and on the levees down slope from the slide area tends to be slightly underconsolidated (Mulder et al., 1997). The blocks within the debris flows are overconsolidated. Some of the debris flows within channels on the continental rise are underconsolidated or normally consolidated and the suggested reason is that there was whole flow entrainment of water (Berry and Piper, 1993). The shear strength of the debris flow sediment decreases away from the source area indicating that the failure turned into a slurry (Mulder et al., 1997).

Atterberg Limits

Location	Core	Depth	LL	PL	PI	Description
Albatross	88010 29	700-750 cm	42	20	22	Under-consolidated debris flow
Albatross	91020 13	600-650 cm	52	26	26	Stratified muds on rise

Nature of constant loads

The upper slope sediment might contain glacial tills that pinch out at 500 mbsl based on the similarity to other regions along the slope but seismic profiles only display a delta-type progradation. Thus, the nature of the upper slope is unclear and requires more field work.

Regional features and effects

On the upper rise (2,500-3,000 mbsl) there is the Sedimentary Ridge Province, composed of Triassic salt diapirs (Mulder et al., 1997). The ridge could have acted as a dam for the debris

flows moving down slope and it also channeled flows south of the ridge (Berry, 1992). Pockmarks are found within the sediment failure region and could indicate the release of gas.

Tsunami

None known

Source, type, quality of data

Sidescan
SeaMARC 1 survey (1000 m^2): 27 and 30 kHz sidescan sonar system with a 5 km swath (simultaneous 3.5 kHz and 40-cu-in. airgun seismic profiles) (Kosalos and Chayes, 1983);

Système Acoustique Remorqué (IFREMER SAR): high-resolution (vertical resolution of 75 cm with ability to penetrate 80m in soft sediment) deep-towed sidescan system, 170 and 190 kHz sidescan transducers towed 80-100m off the seafloor, 1000-1500m swath with a pixel resolution of 0.3m – positioned by range and bearing from ship using IFREMER Distob system (Baltzer et al., 1994)

Geotechnical Equipment
Module géotechnique (Geotechnical Module): acquires cone resistance and excess differential pore pressure measurements every 2 cm as well as a 2 m long piston assisted push core – positioned with Oceano short baseline transponder system (Baltzer et al., 1994)

Seismic
HU88010 and HU91-020: 40-cu-in. sleeve gun fired at 3 sec. rate and a NSRFC model LT-06 streamer filtered to 120-850 Hz (927 line-km); 3.5 kHz seismic profiles (1165 line-km) (Berry and Piper, 1993)

Piston Cores (cruise numbers)
86034; HU88010; 90015; HU91020; PAR93026

5.2.3 Verill canyon rotational slumps

Location

The Verrill canyon rotational slumps are located on the central Scotian Slope west of Verrill Canyon (43° N and 42° 30'N to 61° W and 62° W).

Detailed bathymetry

Two discrete rotational slumps are located west of Verrill Canyon. The western slump is 5km wide and bordered on the west by East Acadia Valley (Piper et al., 1985a). The eastern slump zone is 15km wide and is bordered on the east by the Verrill Canyon. There is a 5km wide section of undisturbed sediment between the two disturbed zones. In contrast to the bathymetry of the Albatross area, the slope is smooth in the region around the rotational slumps. Large (≥ 80 m), arcuate scarps are found south of the disturbed zone and are evidence for bedding plane slides and rotational failures (Piper et al., 1985a).

Type of slide/Type of sediment failure

The failure is principally composed of complex rotational slumps. Down slope the slumps are overlain by and pass into debris flows (Piper et al., 1985a). Turbidity currents are inferred from erosional features. The rotational slumps head in 500-600 m of water.

Age

The minor debris flow overlying the eastern slump contains a 10.4 ka gastropod in core 82004-7. This is the maximum age of the failure. Sediment overlying the main failure sediments in core 82004-2 contains a 14.7 ka shell. The sediment immediately overlying the failure sediment contains 15.4 ka mollusk fragments. Both brm b and brm d appear to overlie the failure sediments. Thus the eastern rotational slump is bracketed by the dates 14.7 ka and 15.4 ka. In the western slump, there are no brick red mud layers above the failure sediment but there is an 11.9 ka gastropod immediately overlying the failure sediments in core 82004-11. This indicates that the western failure occurred at approximately 11.9 ka.

Failure mechanism

The failure was triggered externally, most likely by an earthquake with possible excess pore pressure involvement (either from gas hydrates or rapid sedimentation) (Mosher et al., 1994).

Geometry of slide

Amount of soil: 5.75 km^3 (Mosher et al., 1994)
Depth of slide: 10-20 meters (Piper et al., 1985a)
Slope angle: At 700 mbsl, the slope changes from 5° to 2.5° (Mosher et al., 1989; Mulder and Moran, 1995)
Run out distance: The western slump is approximately 30 km long. Down slope from the slide the slope is eroded, either from debris flows of bedding plane sliding. In this sense, the run out distance of distal deposits is not known.

Slide sediment lithology

According to the Piper et al. (1985a) stratigraphy, the failed sediment is composed of bioturbated, hemipelagic sandy muds that contain ice rafted material, bioturbated, laminated gray muds, and units of brown sediment. Resedimented muddy sands and gravelly, sandy muds immediately overlie these failed sediments. Above this unit are bioturbated olive grey Holocene sediments.

Sedimentation rate

Above the brown reflector, the sedimentation rate was determined to be 0.05 m/ka (Mosher et al., 1989). Between the brown and the pink reflectors, the sedimentation rate was estimated at 1.0 m/ka. The rates were calculated by determining the youngest and oldest ages of sediment within the stratigraphy and then measuring the thickness of the sediment. By dividing the two values, an average rate of sedimentation was determined.

Subsurface stratigraphy

By describing and studying cores from areas around the failure and within the failure itself, the lithostratigraphy can be determined. Piper and Wilson (1983) determined a stratigraphy based on the core 82004-05 and Mosher (1994) developed a similar stratigraphy. The upper part of the section is an olive gray, bioturbated, silty mud that represents the Holocene. This layer also contains some red-brown mud. This is underlain by brownish muds and gravelly sands. The distinctive brick red mud layers are found within this unit. Below this are monotonous dark brown muds that contain some sand and gravel layers. The base of the units is a dark olive gray unit that is slightly bioturbated and contains scattered granules. Mosher et al. (1994) explains that laminated silt and clay layers as well as sandy/silty layers represent turbidites. The clay layers containing sand and gravel represent debris flows.

Six acoustic reflectors have been selected within the seismic profiles: brown, orange, green, yellow, red, and pink (Mosher, 1987). Within core 88010-18, taken from the undisturbed section between the two debris flows, the acoustic reflectors can be tied to the lithostratigraphy. The upper unit of the core is composed of olive-gray, bioturbated silty mud, representing the Holocene. Below this is a condensed section containing the brick red sandy mud layers. A unit of brownish muds is beneath the condensed layer. Beneath the brownish muds are olive-grey and dark grey muds. These tend to be higher in organic carbon. Brownish muds and sands are next in the lithostratigraphy. The brown reflector is located between the olive-grey and brownish mud units and the orange and green reflectors are located within the brownish mud unit. Cores 83012-04 and 83012-06, which were taken in areas where the upper sediment was stripped off so that deeper sediment could be sampled, contained brownish mud with ice-rafted sand and granules. Reflectors yellow through pink are found within this unit. Pink is found approximately 32 m beneath the sediment/water interface (Campbell, 2000).

The sediments tend to fail between the green and red reflectors. The red and green reflectors correlate to sandy or silty intervals that are overlain and underlain by finer sediment (Campbell, 2000).

Mosher et al. (1989) dated mollusc shells within cores to determine the dates of the various reflectors. Based on the youngest and oldest dates, they determined a sedimentation rate and then from that rate, they extrapolated the ages of the reflectors. Brown is 14 ka, orange is 21 ka, green is 24.5 ka, yellow is 26 ka, and pink is 32 ka. The sediment thickness between reflectors decreases 50% from 500-1300 mbsl.

Geotechnical properties

The Holocene sediments have a higher water content (60-70%) and a decreasing shear strength with depth (10-15 kPa at the surface and < 5 kPa at depth) (Mosher et al., 1994). The surface overconsolidation appears to be related to biologic activity (Baltzer et al; 1994). In the western disturbed zone, there is an increase in bulk density and a decrease in water content with depth. The disturbed and deformed units show little change in geophysical properties with depth.

The Late Pleistocene sediments range from 4-20 kPa shear strength, 1.5-2.0 g/cm^3 bulk density, and 1470-1680 m/s acoustic p wave velocity (Mosher et al., 1994).

Atterberg Limits

Location	Core	Depth	LL	PL	PI	Description
Verrill	88010 18	480-530 cm	70	33	37	stratified sediment
Verrill	88010 18	800-850 cm	52	26	26	stratified sediment
Verrill	83012 06	350-400 cm	43	23	19	stratified sediment (below pink reflector)
Verrill	83012 04	400-450 cm	48	26	22	stratified sediment (between yellow and red reflectors)

Nature of constant loads

The gravitational loading of the region is stable (Mosher et al., 1994).

Regional features and effects

Wedge shaped units of sediment tapering out at 400 to 500 mbsl are seen within the seismic profiles. They are thought to represent slumped diamicts and outwash from glacial ice. The youngest wedge is located beneath the green reflector (Piper et al., 2000). Pockmarks are found throughout the region down to 2200 mbsl but are most abundant from 500-900 mbsl.

Tsunami

None known

Source, type, quality of data

Sidescan
SeaMARC 1 survey (1500 m^2): 27 and 30 kHz sidescan sonar system with a 5 km swath (simultaneous 250 line km of 4.5 kHz seismic profiles) – positioned with Loran-C and transit satellite, instruments positioned by acoustic range and wire-out (Kosalos and Chayes, 1983).

Système Acoustique Remorqué (IFREMER SAR)
high-resolution (vertical resolution of 75 cm with ability to penetrate 80 m in soft sediment) deep-towed sidescan system, 170 and 190 kHz sidescan transducers towed 80-100 m off the seafloor, 1000-1500 m swath with a pixel resolution of 0.3 m – positioned by range and bearing from ship using IFREMER Distob system (Baltzer et al., 1994).

Geotechnical Equipment-
Module géotechnique (Geotechnical Module): acquires cone resistance and excess differential pore pressure measurements every two cm as well as a 2 m long piston assisted push core – positioned with Oceano short baseline transponder system (Baltzer et al., 1994).

Seismic:
1980's-1999 - 3.5 kHz sub-bottom profiler, deep towed sparker, and Huntec Deep Tow System (Campbell, 2000).

Huntec DTS boomer and NSRF sparker in water depths <1200 m (Mosher, 1989)
SeaMOR: deep towed boomer and side-scan system – Loran-C and satellite navigation (BIONAV) (Dodds and Fader, 1987)

Piston Cores (cruise numbers):
82004; 83012; 85001; 88010; 90015

5.2.4 Logan canyon debris flow

Location

The Logan Canyon debris flow is located west of Logan Canyon and found within what is called the Logan Canyon debris flow corridor. The head of the failure is in 400 m of water. Several slump scarps are located within the corridor (Piper et al., 2000).

Age

The failure is composed of a stacked series of debris flows; the youngest failed during the latest Pleistocene.

Detailed bathymetry

The upper slope is smooth. The failure originates in a region of scalloped valleys and head scarps. The smooth debris flow is bordered on the east and west by low stratified ridges. On the opposite side of the ridges than the debris flow are canyons. Glacial tills extend to 400-500 mbsl. They are overlain by 5 meters of stratified sediment.

Type of slide/ type of soil failure

It is unknown whether the upper region of the failure is a rotational slump because no cores or sidescan data have been collected. The main failure is a debris flow that extends to the rise.

Failure mechanism

Unknown; probably similar to Verrill Canyon (earthquake or related to pore pressure)

Geometry of slide

Run out: some of the deposits traveled at least 150 km

Slide sediment lithology

It is possible to determine the average thickness of three individual debris flows. Debris flow one is approximately 16 m thick. It overlies stratified sediment. Debris flow two is approximately 9m thick. It fills the contours and overlies debris flow one. Debris flow three appears to be the thinnest of the three failure sediments at 8 m thick. It does not completely blanket debris flow two but only fills in the contours.

Subsurface stratigraphy

The sediment thickness decreases 50% from 900-1350 mbsl. The lithostratigraphy of the immediate area of the failure is based on piston cores collected during cruise 99036 (Piper et al., 2000). The upper sections of the cores tend to contain olive gray Holocene mud. Below this are two signature brick red sandy mud layers. Below these layers is a section of alternating reddish brown and brown muds. These are the muds that failed. One core penetrated a section of olive gray mud below this section.

Two acoustic reflectors have been traced through the high-resolution Huntec records: blue and black (Piper et al., 2000) . They are both located within the alternating reddish brown and brown mud package. The black reflector indicates a decrease in the red-green color of the sediment (according to spectrophotometer measurements) as well as a slight decrease in bulk density. It tends to appear between the changes from red-brown mud to brownish-grayish mud. The blue reflector indicates a larger change in bulk density.

Atterberg Limits

Location	Core	Depth	LL	PL	PI	Description
Logan	99036 22	250-350 cm	42	24	18	redder sediment
Logan	99036 22	350-400 cm	57	27	30	grayer sediment

Tsunami

None known

Source, type, quality of data

Seismic:
HU99036 – Huntec Deep-Tow System and 3.5 kHz seismic profiles (Piper, 1999)

Piston Cores (cruise number)
HU99036

5.2.5 Grand Banks failure

Location

The Grand Bank sediment failure is located on the St. Pierre Slope, between the Eastern Valley of the Laurentian Channel and Halibut Canyon. The head wall of the failure is located 500-700 mbsl.

Age

The failure occurred November 18, 1929 and is well documented due to the severing of trans-Atlantic telegraph cables.

Type of slide/ type of soil failure

The sediment failed as rotational slumps and slides, debris flows, and a turbidity current. There are two types of rotational slides: small and large (Piper et al., 1999). The small rotational slides are found on slopes of 2°-3°. The failed sediment is Holocene and is 2-5 meters thick. The large rotational slides are 5-30 meters thick. Debris flows are found immediately down slope from slides or within St. Pierre Valley. Rotational slumps and debris flows are found from 700-1400 mbsl. The transition between debris flows and turbidity current occurred at 700-1500 mbsl. The turbidity current, which severed trans-Atlantic telegraph cables, had a flow thickness of hundreds of meters, travelled at speeds up to 19 m/s, and flowed from 4-13 hours.

Failure mechanism

Earthquake (magnitude 7.2, epicenter at 2000 mbsl)

Geometry of slide

Amount of soil: >150 km^3 (Piper et al., 1999)
Depth of slide: 20-25 m of proglacial sediment (Piper et al., 1999)
Slope angle: 100-500 mbsl = 2 ° slope; >500 mbsl = 5 ° slope (Piper et al., 1999)
Run out distance: >100 km^2 (Piper et al., 1999)

Regional features and effects

Pockmarks, as large as 30-50 m in diameter, are found from 400-1700 mbsl (Piper et al., 1999). They appear in undisturbed sediment as well as on rotational slides. From 1600-4500 mbsl gravel waves with a wavelength of 50-100 m and heights of 2-5 m are found (Piper et al., 1985b). The waves most likely represent glacial relicts instead of features formed from the sediment failure. They have no modern day analog.

Tsunami

A tsunami occurred along areas of the southern coast of Newfoundland. The wave was from 4-12 m in height and 27 people were killed (Driscoll et al., 2000). Associated sea level effects were seen in Nova Scotia (< 1 m change in sea level).

Source, type, quality of data

Cores
various cruises

Sidescan
1983 and 1984 - SeaMARC 1 survey: 27 and 30 kHz sidescan sonar system with a 5 km swath (40-cu-in. airgun seismic profiles) (Piper et al., 1999)

Système Acoustique Remorqué (IFREMER SAR):
High-resolution deep-towed sidescan system (simultaneous 3.5 kHz subbottom profiling) (Piper et al., 1999)

Seismic:
1991 - Huntec Deep-Tow System seismic profiles (Piper et al., 1999)

Submersible dives:
4 dives in 1985 (Hughes Clarke et al., 1989), subsequent dives in 1986

5.3 Description of Verrill Canyon Failure

The Verrill Canyon rotational slumps are located west of Verrill Canyon on the central Scotian Scope (43° N to 42° 30' N and 61° W to 62° W) (Figures 5.2 and 5.3). Here, two discrete rotational slumps can be identified: the western slump and the eastern slump. The eastern slump can be given a maximum age through minor debris flow and other sediment overlying the slump and is given a bracketed age of 14.7ka to 15.4ka. The western slump is identified to occur at approximately 11.9ka (Gauley and Piper, 2000).

In general, the slide involved a 5.75km^3 volume of soil, based on the number and size of scarps and escarpments in the area. The depth of the slide was 10-20 meters with a run out distance on the western slump of approximately 30km long. Downslope from the slide the slope was eroded either by debris flow or bedding plane sliding, meaning the actual run out distance is unknown. Samples in this area were found to have a plastic index (PI) of 22 % to 36% and an undrained shear strength (Su) of 2.0kPa to 18.0kPa (Gauley and Piper, 2000). The average density of the soil was 1.65-2.0 g/cm^3.

Net Late Quaternary progradation and a lack of deep canyons characterize the Verrill Canyon area. The upper slope has the steepest gradient (5°) and extends from the shelf break to the 700m isobath. The gradient of the remainder of the slope averages 2.5° (Gauley and Piper, 2000). The upper slope appears erosional and small downslope trending gullies occur at 500-700 mbsl. Two small valleys (East and West Acadia) extend across the area and dissect the upper slope, they are approximately 1km wide and 100m deep (Piper and Sparkes, 1987).

Principally, the failure is composed of complex rotational slumps that downslope are overlain by and pass into debris flows (Gauley and Piper, 2000). The western slump is 5km wide and bordered on the west by East Acadia Valley. The eastern slump is located on the east of Verrill Canyon and is 15km wide. These large deformational zones extend downslope from the 600m isobath to a maximum of approximately 1200mbsl (Baltzer et al., 1994). The thickest parts of the disturbed zones are greater than 15m and are located on the upper slope near the mouths of steep upper slope gullies that open out in 800mbsl (Piper et al., 1985). Between these two zones a 5km section of smooth, undisturbed sediment exists. In the region around the slumps, the slope is smooth. Large curved scarps, greater than 80 meters, are found south of the disturbed zone (Figure 5.3) and are evidence for bedding plane slides and rotational failures (Gauley and Piper, 2000). The rotational slumps head in 500-600 meters of water. At 450-550mbsl, wedge shaped units of sediment can be seen tapering out, which are thought to represent slumped diamicts and outwash from glacial ice (Baltzer et al., 1994). Also, there are pockmarks found throughout the region down to 2200 mbsl but are most abundant from 500-900 mbsl. The effects of the pockmarks deep below the seafloor are not known.

Gauley and Piper (2000) determined the following subsurface stratigraphy from cores in the area. The upper part was composed of an olive grey, bioturbated, silty mud that represents the Holocene and also some red-brown mud. Brownish muds and gravelly sands underlie this upper part and distinctive red brick layers are found within this unit. Below this are monotonous dark brown muds containing some sand and gravel layers. The base of the unit is a dark olive grey unit that is slightly bioturbated and contains scattered granules. Turbidities are represented by the silt and clay layers and the sandy/silty layers. Debris flow is represented by the clay layers that contain sand and gravel (Gauley and Piper, 2000).

Mosher et al. (1994) reported that the slide sediment consists of bioturbated hemipelagic sandy muds containing ice rafted materials, bioturbated laminated gray muds, and units of brown sediment. Immediately above these sediments lie resedimented muddy sands and gravelly, sandy muds. Above this unit are bioturbated, olive grey Holocene sediments. The dominance of both bioturbated mud and biogenic material is consistent with relativelyslow rates of sedimentation. The dominant sedimentation process is argued to be passive settling from suspension. The sedimentation rate varies from 0.05 to 1.0m/ka.

A core has been taken in the undisturbed area of the region between the two debris flows and is labeled 818 on Figure 5.3. This core (88010-18) was found to have a top unit composed of olive grey, bioturbated, silty mud, representing the Holocene. The next unit is a condensed section that contains brick red sandy mud layers. A unit of brownish muds follows the condensed layer, beneath which olive-grey and dark grey muds can be found. These tend to be higher in organic carbon. After this unit comes brownish muds and sands. Some of the brown muds have ice-rafted sand and granules. (Gauley and Piper, 2000).

Sediment recovered in the cores from areas of undisturbed seabed has been correlated with the observed failure planes beneath the rotational slumps and in the bedding plane slides. This analysis shows that failures seem to be localized at horizons with abundant sand beds (Piper, 2000). The sediment tends to fail in the sandy or silty intervals that are overlain and underlain by finer sediment (Gauley and Piper, 2000).

The Holocene sediments have a higher water content (60-70%) and decreasing shear strength with depth. The decrease in shear strength of the sediment with depth is contrary to typical marine sediment observations. Hence, Holocene sediments do not display normal consolidation behavior (Gauley and Piper, 2000). Also, it was found by Piper (2000) that the downcore variation in shear strength implies an overconsolidation ratio of 0.33. At the surface, the shear strength ranges from 10-14kPa, while at its depth the shear strength is less than 5kPa. The over consolidated surface appears to be related to biological activity.

In the western disturbed zone, there is an increased bulk density and a decrease in water content with depth (Gauley and Piper, 2000. While the upslope portions of the slope were only disturbed to a small degree in several thin horizons, cores from the midslope (54 and 55) had extensive deformation. A large change in shear strength is found within core 54 at about 4m, which may represent a shear zone within the slumped sediment. As noted by Mosher et al. (1994), core 54 shows slightly increasing shear strength, decreasing water content and increasing bulk density with depth, even though there is little variability within the sediment. This implies that failure did not remould the sediment, nor disrupt the stratigraphy, supporting a slump interpretation for this event (Mosher et al., 1994). Deformation structures within the sediment include: tilted

laminae and bedding surfaces, microfaults, irregular laminae, convoluted laminae, overturned folds, stretched mottles and eyelet and roll balls (Mosher et al., 1994). The deformation structures in core 55 are only observed to about 5.5m and lack any trend in physical property data. This suggests that the sediment sequence within the entire core was subject to failure (Mosher et al., 1994).

Several cores in the Verrill Canyon area were examined by Baltzer et al. (1994) to determine the consolidation of the sediment. Transects of five stations on the midslope were investigated (noted T1 on Figure 5.3). The authors divided five cone resistance (Q_c) and undrained shear strength (S_u) profiles into three units. The uppermost unit thins downslope from 25-10 cm and corresponds to Holocene mud, which is not consolidated at all. The cone resistance (Q_c) curve showed no gradient in this unit. Under this unit, down to a subbottom depth of 150 cm, they found a highly resistant area. The lowest unit generally had a relatively normal consolidation of 80kPa.

A transect from the section on the northern edge of East Acadia Valley (noted T2 on Figure 5.3) to the east of the failure area, between the 2000 and 2100m isobaths, exhibits an apparent over consolidation of 210kPa in the upper 90cm, corresponding to Holocene olive-grey muds. The Late Pleistocene sediments become increasingly over consolidated down slope, corresponding to the increasing depth of erosion in the area. The late Pleistocene sediments range from 4-20kPa in shear strength, have 1.5-2.0g/cm^3 bulk density, and 1470-1680m/s acoustic p wave (compressional) velocity.

A transect located across the headscarp (noted T3 on Figure 5.3) of the western slump was also conducted. The area was covered by a thin debris flow, with a surficial mud that has a Q_c of less than 5kPa. Within a core in this area there was an initial layer of sandy silt, under which the core showed a weak cone resistance, indicating almost no increase in depth. The apparent under consolidated state is probably due to the remolding of the sediment induced by debris flow (Baltzer et al., 1994).

Generally this area off the Scotian Slope shows mass failure deposits that form a significant part of the sedimentary column, even on very low slope angles. From acoustic evidence, it is seen that mass flow processes are probably common and have affected a large portion of the seafloor. There are a wide variety of possible failure mechanisms for the bathymetrically smooth region near the Verrill Canyon. Turbidities appear to be related to ice margin conditions, which can be inferred from erosional features. Due to the low amounts of coarse sand or gravel it can be assumed that transport processes were unable to carry sand and gravel, therefore ice rafting was minimal. Most of the coarse material that is present conforms to the fabric of the beds suggesting that it was transferred by a turbidity current (Mosher et al., 1994). Slumping may be indicative of tectonic activity in the region. Seismic thinning supports progradation hypotheses, but from this evidence alone it is not possible to distinguish the mechanism of transport.

The two most probable mechanisms of failure of the sediment in this area are earthquake loading and the development of excess pore fluid pressure. It is likely that earthquakes triggered the thin-skinned failures. The failures are quite widespread and show a range of structures similar to those associated with the 1929 Grand Banks earthquakes. The slope stability analysis done in the area indicates that an earthquake of magnitude 5.0 within 40km of the site would be necessary to actuate a failure.

Gauley and Piper (2000) determined the following subsurface stratigraphy from cores in the area. The upper part was composed of an olive grey, bioturbated, silty mud that represents the Holocene and also some red-brown mud. Brownish muds and gravelly sands underlie this upper part and distinctive red brick layers are found within this unit. Below this are monotonous dark brown muds containing some sand and gravel layers. The base of the unit is a dark olive grey unit that is slightly bioturbated and contains scattered granules. Turbidities are represented by the silt and clay layers and the sandy/silty layers. Debris flow is represented by the clay layers that contain sand and gravel (Gauley and Piper, 2000).

Mosher et al. (1994) reported that the slide sediment consists of bioturbated hemipelagic sandy muds containing ice rafted materials, bioturbated laminated gray muds, and units of brown sediment. Immediately above these sediments lie resedimented muddy sands and gravelly, sandy muds. Above this unit are bioturbated, olive grey Holocene sediments. The dominance of both bioturbated mud and biogenic material is consistent with relativelyslow rates of sedimentation. The dominant sedimentation process is argued to be passive settling from suspension. The sedimentation rate varies from 0.05 to 1.0m/ka.

A core has been taken in the undisturbed area of the region between the two debris flows and is labeled 818 on Figure 5.3. This core (88010-18) was found to have a top unit composed of olive grey, bioturbated, silty mud, representing the Holocene. The next unit is a condensed section that contains brick red sandy mud layers. A unit of brownish muds follows the condensed layer, beneath which olive-grey and dark grey muds can be found. These tend to be higher in organic carbon. After this unit comes brownish muds and sands. Some of the brown muds have ice-rafted sand and granules. (Gauley and Piper, 2000).

Sediment recovered in the cores from areas of undisturbed seabed has been correlated with the observed failure planes beneath the rotational slumps and in the bedding plane slides. This analysis shows that failures seem to be localized at horizons with abundant sand beds (Piper, 2000). The sediment tends to fail in the sandy or silty intervals that are overlain and underlain by finer sediment (Gauley and Piper, 2000).

The Holocene sediments have a higher water content (60-70%) and decreasing shear strength with depth. The decrease in shear strength of the sediment with depth is contrary to typical marine sediment observations. Hence, Holocene sediments do not display normal consolidation behavior (Gauley and Piper, 2000). Also, it was found by Piper (2000) that the downcore variation in shear strength implies an overconsolidation ratio of 0.33. At the surface, the shear strength ranges from 10-14kPa, while at its depth the shear strength is less than 5kPa. The over consolidated surface appears to be related to biological activity.

In the western disturbed zone, there is an increased bulk density and a decrease in water content with depth (Gauley and Piper, 2000. While the upslope portions of the slope were only disturbed to a small degree in several thin horizons, cores from the midslope (54 and 55) had extensive deformation. A large change in shear strength is found within core 54 at about 4m, which may represent a shear zone within the slumped sediment. As noted by Mosher et al. (1994), core 54 shows slightly increasing shear strength, decreasing water content and increasing bulk density with depth, even though there is little variability within the sediment. This implies that failure did not remould the sediment, nor disrupt the stratigraphy, supporting a slump interpretation for this event (Mosher et al., 1994). Deformation structures within the sediment include: tilted

laminae and bedding surfaces, microfaults, irregular laminae, convoluted laminae, overturned folds, stretched mottles and eyelet and roll balls (Mosher et al., 1994). The deformation structures in core 55 are only observed to about 5.5m and lack any trend in physical property data. This suggests that the sediment sequence within the entire core was subject to failure (Mosher et al., 1994).

Several cores in the Verrill Canyon area were examined by Baltzer et al. (1994) to determine the consolidation of the sediment. Transects of five stations on the midslope were investigated (noted T1 on Figure 5.3). The authors divided five cone resistance (Q_c) and undrained shear strength (S_u) profiles into three units. The uppermost unit thins downslope from 25-10 cm and corresponds to Holocene mud, which is not consolidated at all. The cone resistance (Q_c) curve showed no gradient in this unit. Under this unit, down to a subbottom depth of 150 cm, they found a highly resistant area. The lowest unit generally had a relatively normal consolidation of 80kPa.

A transect from the section on the northern edge of East Acadia Valley (noted T2 on Figure 5.3) to the east of the failure area, between the 2000 and 2100m isobaths, exhibits an apparent over consolidation of 210kPa in the upper 90cm, corresponding to Holocene olive-grey muds. The Late Pleistocene sediments become increasingly over consolidated down slope, corresponding to the increasing depth of erosion in the area. The late Pleistocene sediments range from 4-20kPa in shear strength, have 1.5-2.0g/cm^3 bulk density, and 1470-1680m/s acoustic p wave (compressional) velocity.

A transect located across the headscarp (noted T3 on Figure 5.3) of the western slump was also conducted. The area was covered by a thin debris flow, with a surficial mud that has a Q_c of less than 5kPa. Within a core in this area there was an initial layer of sandy silt, under which the core showed a weak cone resistance, indicating almost no increase in depth. The apparent under consolidated state is probably due to the remolding of the sediment induced by debris flow (Baltzer et al., 1994).

Generally this area off the Scotian Slope shows mass failure deposits that form a significant part of the sedimentary column, even on very low slope angles. From acoustic evidence, it is seen that mass flow processes are probably common and have affected a large portion of the seafloor. There are a wide variety of possible failure mechanisms for the bathymetrically smooth region near the Verrill Canyon. Turbidities appear to be related to ice margin conditions, which can be inferred from erosional features. Due to the low amounts of coarse sand or gravel it can be assumed that transport processes were unable to carry sand and gravel, therefore ice rafting was minimal. Most of the coarse material that is present conforms to the fabric of the beds suggesting that it was transferred by a turbidity current (Mosher et al., 1994). Slumping may be indicative of tectonic activity in the region. Seismic thinning supports progradation hypotheses, but from this evidence alone it is not possible to distinguish the mechanism of transport.

The two most probable mechanisms of failure of the sediment in this area are earthquake loading and the development of excess pore fluid pressure. It is likely that earthquakes triggered the thin-skinned failures. The failures are quite widespread and show a range of structures similar to those associated with the 1929 Grand Banks earthquakes. The slope stability analysis done in the area indicates that an earthquake of magnitude 5.0 within 40km of the site would be necessary to actuate a failure.

It was also suggested that excess pore pressures would promote failure. Such excess pore pressure might result from rapid deposition of proglacial sediment or might be associated with the melting of gas that hydrated as bottom waters warmed up after glaciation. Additional pore pressures would be created by the deposition of the distal parts of "till tongues" beyond the ice limit, but the effect would have been unimportant in water depths of more the 600m (Piper, 2000). Dissipation of excess pore pressure could take up to 8000 years. Due to the low slope angles in this area of the Scotian Slope it is unlikely that pore pressure would induce a large-scale failure (Mosher et al., 1994).

Other considerations were made as well. From the available core data, Holocene sediment failures are not found. Bearing capacity analysis showed that loading of the outer shelf by ice could cause failure in water depths in excess of 1000m, but these failures would also involve large areas of the outer shelf. Therefore, this analysis does not account for the observed styles of thin-skinned failure in water depths of 600-200m. Also, during the Wisconsian glaciation, a lower sea level was known, and this could have resulted in shelf erosion and offshelf transportation of sediment. (Mosher et al., 1994). Meltwater bursts could have enhanced the failure, which may be indicated by slightly lower pore water salinities in the Pleistocene.

Analysis

The following analysis was conducted by Mosher et al. (1989) and Mosher et al. (1994).

- Sedimentation rates were determined by Mosher et al. (1989), by locating the youngest and oldest sediments and then measuring the thickness of the sediment. Dividing the two values determined an average rate of sedimentation.

- Standard geotechnical tests were preformed by Mosher et al. (1994) to determine sediment consolidation.

- The stability of Holocene and late Pleistocene sediments was evaluated using the infinite slope analysis (Mosher et al., 1994). Average undrained shear strength and bulk density profiles with depth were assumed for both Holocene and late Pleistocene sediments, based on core 818 (Mosher et al., 1994). The analyses were preformed over the range of seafloor slope angles that occur in the study region (1°-12°) and over a range of failed sediment thickness (0.5 -25m). A factor of safety greater than one, where the sediment resisting forces are greater than the loading forces, indicated stable conditions. The study region was found to be stable under gravitational loading conditions.

- Earthquake loading was evaluated by calculating a pseudo-seismic coefficient that represents the earthquake induced horizontal acceleration additionally required to load the sediment and cause slope failure (Mosher et al., 1994).

- Possible excess pore fluid was also assessed. Excess pore fluid pressure required to decrease the shear strength to failure was calculated by plotting the slope angle against the seismic coefficient and the excess pore pressure. It was found the pore pressures required for failure range from 6.5kPa for Verrill Canyon, to 11kPa for the western disturbed zone (Mosher et al., 1994).

5.4 Description of Albatross Failure

The Albatross sediment failure occurred south of the Emerald Bank and west of Mohican Canyon (42°N 63°W) with a shelf break at 200m. It is on the central portion of the Scotian Slope, between Heron and Puffin Valleys (Figures 5.1 and 5.5). This source area consists of several small canyons and slopes and has had debris flows throughout the Quaternary, with the most recent of the failures occurring in the Late Pleistocene.

This slide is recognized as blocky debris flow. It averages 120 m thick on the slope, to 20 m thick on the lower slope (Gauley and Piper, 2000). The slide depth, based on consolidation testing blocks, was found to be approximately 50m (Mulder et al., 1997). The surface width is variable, with blocks and depressions 50 to 200m wide and relief of 5 to 20m (Shor and Piper, 1989). The slope angle at which the failure occurred was approximately 6° and the total run out distance of debris flow was 200km, with the volume of soil being greater than 600km^3. The rate of postglacial sedimentation in the general area is estimated to be 0.185m/ka, while the Late Wisconsinan sedimentation rate is 0.85m/ka.

The headwall scarp of the area was detected at 550-700mbsl (Figure 5.5). The middle slope reaches 1,000mbsl in the east and 1,200mbsl in the west (Section A, Figure 5.5). It is dissected by shallow canyons that extend upslope to the 500m contour, where the uppermost part of the slope is relatively smooth and not indented by canyon heads (Shor and Piper, 1989). This slope was probably cut when the sandy shelf break was emergent at sea level lowstands in the Pleistocene. The shallowest part of the middle slope is from 600 to 1000mbsl. The slope here is dissected by canyons and smaller gullies, with typical spacing of 500m or less in the eastern part of the area and up to 1000m near Egret Valley in the West. Canyon relief over this section is typically 50 to 300m. A significant decrease in relief is observed west of 63° 00' W, where relief stays below 50m, while the gully spacing remains about 300 to 500m (Shor and Piper, 1989). The canyons on the upper slope have pinnate gully patterns and complex tributary systems, with main valley talwegs being characteristically straight. Research places the incision of the canyons to the mid-to-late Pleistocene strata (Shor and Piper, 1989).

The midslope (between 1,100 and 1,300m) has a very different pattern compared to the immediate middle slope (Section B, Figure 5.5). A major break in gradient occurs, from 4° to 2°, at a 1,000-1,200 mbsl. In the west, transverse gullying can be seen on both flanks of the Albatross Ridge. Elsewhere, shallow valleys representing continuation of the upper slope canyons can be seen. Between Heron and Tern valleys, at 1,200-1,350 mbsl, there is another relatively smooth slope that is interrupted by clusters of blocks that become increasingly prominent as the slope goes into deeper waters.

This blocky pattern is interpreted by Shor and Piper (1989) to be that of the debris flow which transported slabs of consolidated sediment from the upper slope. Places of reduced relief within the depressions are thought to be due to preferential filling by subsequent coarse turbidite sediments. Shor and Piper (1989) state that the most probable source area for the debris flow is the unusually smooth region around Heron and Puffin valleys on the upper slope. A map of the superficial debris flow suggests that the debris flows originated on the continental slope between Albatross Ridge and Tern Valley (Piper, 2000). In this area the normal dendritic pattern of minor gullies on the inter-canyon ridges seem to be absent (Shor and Piper, 1989).

The lower slope, west of the blocky debris flow, show little evidence of surface texture (Section C, Figure 5.5). Here, the trend of the middle slope gullies is continued. Below 1650mbsl, there is evidence of rotational slides and local failures, which can be interpreted from the scarps in the area. In some sections of this region, a 1-2m surface drape of acoustically transparent sediment is observed which postdates the debris flow.

Since no long cores are available from the source area the lithology of the failed sediment is only known from examining blocks from the debris flows which consist of a wide range of muds. The piston cores collected have only sampled the debris flows and not the stratified sediment around the failure. The piston cores from the debris flow deposits contain bioturbated, hemipelagic, Holocene muds over a layer of sandy/muddy fine turbidities. The distinctive brick red sandy mud layers are found within this unit. Below the thin turbite sequence, the cores have penetrated a mud-clast conglomerate with a mud matrix that represents debris flow (Shor and Piper, 1989). A summary of the core descriptions and depth of sampling is presented in Table 5.1.

There are two possible debris flows recognized by Piper and Skene (Gauley and Piper, 2000) in the Albatross debris flow cores (Figure 5.3). They are termed Debris Flow One and Debris Flow Two. There were many cores taken in the vicinity of the Albatross debris flow that were analyzed by Shor and Piper (1989) and then further analyzed by Piper (2000) (Figure 5.6). The available core data for Albatross is from three main settings. The first area is the Albatross Ridge (Core 88010-23, 7m) which contained bioturbated sediment scattered with ice-rafted detritus. A brick red mud horizon at 30cm is evidence of a thin Holocene section. Interbedded with the muds are some thin fine sand beds. Debris Flow One appears to have occurred at the time this brick red layer was deposited, with its source area being the upper slope (Piper, 2000). The slope west of Albatross Ridge (Core 86034-41, 2m) was found to contain Holocene Olive gray mud that overlies 0.5m of brown mud with abundant clasts of both mud and rock pebbles and also rare shell fragments. This interval is interpreted as a debris flow deposit since it also overlies 0.4m of red brown mud that could represent a diluted brick red sandy mud interval (Mulder et al., 1997). As with some other cores in the area, this core has a red brown upper section and a dark brown lower section. Debris Flow Two is thicker and older than Debris Flow One. It is older than brick red mud layer at 30cm, but younger than the brick red mud layer found at 40 cm (Piper, 2000; Mulder et al, 1997). Shear strengths and water contents of sediments in this region were also available (Figure 5.4).

Mud clast conglomerate, overlain with a few thin sand to mud turbidities, and then olive grey muds, are found in cores from the blocky Late Pleistocene debris flow (Core 86834-35). The major two debris flows are evident in a core from the smoother area (Core 86034-36). From one core (86034-31) shells have been recovered that date 14.3ka while similar debris flow deposits in other cores, such as core 86034-41, have shells of 13.3ka (Piper, 2000).

Various other shells were found and dated and from the chronology it is suggested that the debris flows date from around 13 to 13.3ka. A core collected in August 1999 (Piper, 2000) suggests the last debris flow down the Mohican Channel to be dated 14ka and one 10 cm thick sand bed deposited at about 12ka. In the past 1000 years, one or more sand deposits have been made; suggesting the transport of sand on the shelf may occasionally initiate small turbidity currents that flow down the slope.

The sediment in the undisturbed areas and on the levees down slope from the slide area tends to be slightly underconsolidated (0.22) (Gauley and Piper, 2000). The blocks within the debris flows are over consolidated (0.26). Most blocks in the Albatross Debris flows have shear strength values that range from 1kPa to 20kPa. But, some reach as high as 70kPa for sediment located at only 3 to 5mbsf (Piper, 2000). This indicates that the flows in the highly overconsolidated area were already consolidated before the debris flow began (Mulder et al., 1997). Piper (2000) notes that these high values coincide with low water content values (40-60%) and the thickness of the sediment involved in the failure at the source suggests that the failure occurred at large depths under the seafloor (greater than 50m).

Some of the debris flows within channels on the continental rise are underconsolidated or normally consolidated. The source area had shear strength values typically ranging from 20-50kPa, which is consistent with peak shear strength values measured in undisturbed sediments. A decrease in this shear strength can be seen as distance from the source area increases. This behavior is not normal and is interpreted by Mulder et al. (1997) to be related to a progressive transformation of the flow slide into a slurry by the increase in pore pressure.

The triggering mechanism of the Albatross sediment failure is hypothesized to be either seismic triggering of slopes that were steepened by canyon erosion (Shor and Piper, 1989) or possibly gas hydrates. The earthquake hypothesis is supported by the similar aged failure, Verrill Canyon, but pockmarks near the failure indicate that the failure mechanism may have been gas or gas hydrates. The pockmarks occupy an area of over 4000km on the Scotian Shell and Slope. Recent surveys of the slope show that pockmarks are complex and widespread. However, the densest areas within the Emerald Basin, where some studies indicate that the pockmarks are active (Fader, 1991). On the upper rise (2,500-3,000 mbsl) there is the Sedimentary Ridge Province, which is composed of Triassic salt diapirs (Mulder et al., 1997). The ridge could have acted as a dam for the debris flow moving down slope and it also channeled flows south of the ridge (Gauley and Piper, 2000).

Analysis

- Geotechnical measurements of the Albatross Debris flow (Mulder et al., 1997) were taken using the down hole variation of shear strength with depth to distinguish four groups of sediment, based on the basis of degree consolidation. A summary is found in Table 5.2.

Mulder et al. (1997) also used the following analysis:

- Plots of depth versus shear strength to determine consolidation.
- Plots of sample density, water content, and undrained shear strength / effective stress ratio verses depth, and the relationships that are evident from these plots.
- Plots of p-wave velocity and acoustic impedance versus density.
- Plots of distance from the source versus max clast size, yield strength, dynamic viscosity, block size, viscosity
- An equation to estimate the depth of the failure at the origin of debris flow deposits using undrained shear strength (S_u) values measured from the overconsolidated blocks:

  $H=[S_u/(0.25\ \gamma')]$ where γ' is the effective unit weight of soil.

- Plots of viscosity vs. yield resistance.

- Plots of eroded thickness versus distance from the source.

Baltzer et al. (1994) used a Geotechnical Module, designed to measure geotechnical properties of fine-grained sediments to determine *in-situ* conditions in the upper 2m.

- They measured excess pore pressure (u_t) and compared it to cone resistance Q_c. A simplified equation

  $$Q_c = N_k \, x \, S_u$$

  is used, where N_k is a characteristic parameter of the cone piezometer and Su is the shear strength. N_k linearly increased from 13 to 18.5 as the Plastic Index increases from 0% to 50%. It was also considered that an average of N_k=15 does not give significant error to Qc values.

- In addition, an assumed mean value of 5kPa at 2m depth was used to illustrate "normal" consolidation on the down core plots of Q_c. This corresponds to a strength/effective stress ratio of $S(v) = 0.31$. Over consolidated sediments are characterized by a ratio $S(v) > 0.40$. Under consolidated sediments show a ratio $S(v) < 0.20$. Mass physical and geotechnical properties were determined from lab analyses on cores, including grain size distribution, bulk unit weight, gamma density, water content, Atterberg limits, acoustic velocity and vane shear strength (Figure 5.7).

5.5 Description of the Failure at Logan Canyon

The Logan Canyon debris flow occurred west of Logan Canyon and is located within the Logan Canyon debris corridor. Logan Canyon is one of the largest on the Scotian Margin and like others in the area indents the shelf edge.

East of Logan Canyon the outer shelf gradually steepens seawards. It has an abrupt break in slope at 350-450 mbsl, which corresponds to the heads of a series of small submarine canyons. The canyons at 1000 mbsl have an average spacing of 2km and are typically 200 to 500m deep. West of Logan Canyon the smaller canyons are deeper and more widespread but head again in 400mbsl. Downslope they lead into a major debris flow corridor. Glacial tills extend to 400-500mbsl and are overlain by 5 meters of stratified sediment.

The failure southwest of Logan Canyon heads in 400m of water and is composed of a stacked series of debris flows with several slump scarps within the corridor (Gauley and Piper, 2000). The major slump scar extends more than 300 m deep and the main failure is a debris flow that extends to the rise with some of its deposits having runouts of at least 150km. The upper slope of the failure is smooth and its origin is a region of scalloped valleys and head scarps. It is unknown whether the upper region of the failure is a rotational slump since no cores or sidescan images have been collected in this area.

This smooth debris flow on the upper slope is bordered on the east and west by low stratified ridges, which have been probably preserved due to the canyon permitting drainage of excess pore pressure. Canyons can be found on the opposite side of these ridges. How the failure occurred is unknown but it is hypothesized to be an earthquake or related to pore pressure. There have been several cores collected in the area (but not fully analyzed yet) and so far Piper (2000)

has found that none of the failures are of the Holocene age. The youngest slide is believed to have occurred during the late Pleistocene.

A core off the Western Bank (Core 87-07) was analyzed by Piper (2000) and was correlated with the Huntec record. He found that the upper 5m of the core showed alternate olive green and slightly browner intervals, whose base is dated to 10.77ka above and 14.63ka below. Below 523cm, three lithological units were distinguished. The first was coarse-grained graded beds with varying amounts of mud which are interpreted by Piper (2000) to be proximal turbidities. The second was composed of red-brown muds with abundant clay clasts, then sporadic pebbles and some sandy laminae, this is interpreted as an ice-rafted debris flow facies. The last was a bioturbated greenish brown silty mud with scattered stones, interpreted as glacially influenced hemipelagic sediment that could represent spillover of coarse turbidities from the channel. Little is known about the stability of the canyon walls and the role of major faults in the canyoned area is uncertain.

Analysis
None noted.

5.6 Data Gaps for the Scotian Mass Movements

In order to characterize the failure as described in Section 3.8, information relating to the the classification, the initiation and evolution and the slope stability of the area under investigation is required. In addition data pertaining to environmental loads and geohazards is necessary. In this section the data gaps relevant to the three failures on the Scotian Slope are highlighted as shown in Table 5.4.

The information required for the study of the failures is focused on the end product of formulating a methodology for the determination of the risk of submarine slope instability in a selected region. The classification of the failure will provide background information on the type of mass movement and failure mechanism. Information on the initiation of the failure may be derived in part from understanding the sediments involved in the failure, the source of the sediments, the surface morphology and the subsurface geophysical characteristics of the sediments and failure surfaces. A limited understanding of the evolution of the failure can be accepted by considering the changes in soil properties across the site and through the extent of the failed soils as well as by evaluating the nature subsurface reflectors. The slope stability analysis requires knowledge of sediment properties, detailed bathymetric information and potentially specific laboratory tests related to field conditions.

For the Scotian failures described in Section 5.2 through Section 5.4 in general there were few cores taken and fewer which extended through the failed sediments, and limited public domain bathymetric data. The basic soil properties were derived at the sampled sites, however additional sampling and soils testing would allow for more accurate parametric analysis of the slope stability and a better comprehension of the effect of environmental loads and geohazards. In addition, more specific triaxial testing would enable a better interpretation of the effect of cyclic loading on the sites.

In the following Section 5.7 the stability analysis of the existing slopes on the three Scotian failures is provided. Further information may be become available for the Scotian Slope failures

either through further testing of the existing samples, additional sampling, further geophysical work, or a greater understanding of the failures due to centrifuge testing and numerical modeling. When the incremental data exists a more comprehensive analysis of the Scotian Slope failures will be possible.

Generally, submarine slopes extend across large expanses of the seafloor, typically from several to more than 10 km. The variation of the geological condition over the area of interest makes the assessment of slope stability complicated.

The normal methods used for assessing slope stability are based on limit equilibrium analysis. These methods involve locating the potential sliding surface, either by trial and error searches, or based on *in-situ* soil conditions. Slope stability analysis has been well developed for onshore applications. The dimensions of the slopes are usually small and soil conditions can be well estimated therefore, a unique critical sliding surface with a minimum factor of safety for the whole slope can be found. However, these methods do not work well for seabed slopes where stability varies spatially without any unique sliding surface for the whole slope. Special procedures have to be used to evaluate the factor of safety along seabed slopes.

It must be noted that the slope geometry, soil layering and geotechnical properties are still very uncertain, due to the limited information available in the study areas. In the area of the Scotian Slope slides, soil samples are available only from cores down to a maximum of 10m below the seabed.

5.7 Evaluation of Verrill Failure

5.7.1 Slope profiles

Three profiles are selected for the slope stability analysis. They are from the west and east sliding slumps and the middle stable zone, as shown in Figure 5.9. The corresponding slope profiles are given in Figure 5.10. The overall slope angle changes from 5° to 2.5° (Mosher et al., 1989; Mulder and Moran, 1995) while the local slope angle may reach as large as 12.5°, with increasing water depth, the slope angle will decrease.

5.7.2 Soil geotechnical properties

Details of soil properties are referred to Section 5.2. According to the downcore variation of undrained shear strength and bulk density, the distribution of shear strength ratio s_u/σ_z' in Core 88-017 and 88-018 is presented in Figure 5.11. Since the scale of original undrained shear strength distribution is very small, errors could be significant in the curve for Core 88-017. As such, the results for Core 88-018 will be used. When the soil depth is more than 1 m from seabed, the shear strength ratio s_u/σ_z' is almost constant with an average of 0.36 and a standard deviation of 0.07.

5.7.3 Linear shear surface: Infinite slope analysis

Infinite-slope stability analysis is the most reliable method available to assess seabed sediment stability. The slopes in the study area, including many of the walls of the valleys and canyons,

are long and are made of fairly continuous thin lobate sediment sheets that are conformable over great distances. In this method the force equilibrium between the shearing stress exerted by the buoyant weight of the soil mass and the shear resistance of the soil along a potential failure plane is calculated. When the shearing stress becomes equal to or exceeds the shearing resistance of the soil along the failure surface, a submarine slide or slumping is initiated.

In the infinite slope analysis procedure, the sliding surface is assumed to be parallel to the slope surface (linear) at a depth that is relatively shallow compared to its length. The factor of safety is calculated as

$$F = s/\tau \tag{5.1}$$

where F is the factor of safety, s is the available soil shear strength (shear resistance), and τ is the shear stress (driving force) exerted by the weight of the soil mass. In terms of effective stress, the shear strength of soil is expressed as

$$s = c' + \sigma' \tan\phi' \tag{5.2}$$

where σ' is effective normal stress, ϕ' friction angle and c' cohesion in terms of effective stresses. For a linear slope with angle β, the shear stress and the normal stress acting on the sliding plane at a depth z below the seabed are

$$\tau = \gamma z \cos\beta \sin\beta \qquad \sigma = \gamma z \cos^2\beta \tag{5.3}$$

Then Equation (5.6.1) is rewritten as

$$F = (c + \gamma z \cos^2\beta \tan\phi) / (\gamma z \cos\beta \sin\beta) \tag{5.4}$$

Depending upon the analyzing methods (effective or total stress method), c, γ and ϕ in Equation (5.4) should take the appropriate value.

If the undrained condition is considered at failure, i.e. $\phi = 0$, the factor of safety becomes

$$F = s_u / (\gamma' z \cos\beta \sin\beta) = 2 s_u / (\gamma' z \sin 2\beta) \tag{5.5}$$

Or

$$F = 2 s_u / (\sigma_z' \sin 2\beta) \tag{5.6}$$

Using the shear strength ratio derived from Figure 5.11, the factor of safety along the eastern slope at Verrill is given in Figure 5.12. The variation in factor of safety with respect to the slope angle is further explained in Figure 5.13.

It should be mentioned that the results in Figures 5.12 and 5.13 are correct only for shallow sliding surfaces. The effect of topology of the slope surface is not reflected in these results. Further, since the undrained shear strength of soil increases almost linearly with depth, or more exactly, with vertical effective stress, the factor of safety for infinite slope analysis is independent of the depth of sliding surface.

5.7.4 *Using the limit equilibrium approach, the use of a circular sliding surface*

Methods for searching sliding surfaces

As discussed before, some special procedures have to be used to evaluate the factor of safety along seabed slopes. The following methods are proposed for the analysis of eastern slump at Verrill:

Method 1: Restricting lateral coordinate of the center of the circle

The first search method consists of varying the radius and vertical position of the circles centre for a given lateral coordinate (horizontal position) until a minimum factor of safety is found. This method is illustrated in Figure 5.15(a). The results of such calculations yield minimum values of the factor of safety for various selected horizontal coordinates.

As illustrated in Figure 5.14(a) and 5.15 (a), a part of the sliding surface obtained using Method 1 may provide resistance to sliding, hence the corresponding factor of safety might not be the minimum. This can be eliminated using searching method 2.

Method 2: Restricting failure surface pass beneath the center point

Searching Method 2 is basically the same as Method 1, except that the sliding surface is forced to pass beneath the centre point Figure 5.14(b). Comparisons of results from Method 1 and Method 2 show that when the horizontal coordinates of the centre of sliding surfaces are the same, the factor of safety given by searching Method 2 is larger than that given by Method 1, see Figure 5.15 to 5.17 for details.

Method 3: Restricting range of sliding soil

Another disadvantage of Method 1 is that the sliding surface could be far away from its centre, especially when the radius is large or a steep segment of slope is met, as shown in Figure 5.18. In this case, the centre of the sliding surface is the same as Location 3 (x = 15.35 km), however, the sliding surface is 970 m ahead of its centre. Even though the factor of safety (fs = 1.961) is less than the two cases shown in Figure 5.17, it is meaningless to use this as the factor of safety at Location 3. In order to avoid this disadvantage, Method 3 can be used (Figure 5.14(c)). In this Method, the sliding soil is restricted to a certain range, reflecting the geometrical change in slope surfaces.

Method 4: Restricting the depth of failure surface

Method 4 shown in Figure 5.14(d) is the same as Method 3 except that the maximum depth of the sliding surface is restricted in order to investigate the effect of thickness of sliding soil on the stability of slope stability.

Factor of safety of east slump at Verrill

Figure 5.19 presents the variation of factor of safety along east Verrill slump, calculated from circular sliding surfaces. The average undrained shear strength ratio $s_u / \sigma_z' = 0.36$ is used in this

calculation. The results from linear sliding surfaces are also given in the Figure. The horizontal coordinates of all symbols represent the centre of sliding blocks. Calculating the factor of safety from circular sliding surface methods using the average shear strength of soil is almost the same as the average of those calculated from linear sliding surfaces using upper and lower limits of soil strength. In other words, when the same shear strength of soil is used, the factors of safety calculated using circular surfaces are the same as those from linear sliding surfaces. This is because in all calculations with circular sliding surfaces, the ratios of length to depth for the sliding blocks are less than 0.03, consequently, and the curvature of circular sliding surface has a very small effect on the factor of safety.

The effect of the shape of sliding surface on factor of safety is further investigated by assuming the sliding surface to be triangle at the slope segment of L = 14.02 to 14.46 km (Figure 5.20). Here the maximum depth of 14 m for circular sliding surface is used. Most other smooth sliding surfaces with different shapes lay between the linear and the triangle sliding surfaces. When the average shear strength ratio $s_u / \sigma_z' = 0.36$ is used, the factor of safety for the triangle sliding surface is found to be $f_{s(triangle)} = 1.604$, while the factor of safety for linear and circular surfaces are $f_{s(linear)} = 1.680$ and $f_{s(circular)} = 1.611$. Since the difference of f_s is less than 5%, it is concluded that the shape of sliding surfaces has no significant effect on the calculation of f_s.

In stability analysis of small-scale slopes, the depth of sliding surface has significant effect on the calculated factor of safety. However, for the east slump of Verrill, when the depths of sliding surfaces are restricted to 20 m and 50 m respectively, no remarkable difference in the factor of safety is found (Figure 5.21), while the minimum factor of safety occurs at shallow sliding surfaces. This may suggest that the thickness of sliding soil mass may vary in a certain range (15 to 50m in west slump of Verrill) if the sliding is initialized.

Based on the results of stability analysis for the east slump at Verrill, it is concluded that at current geological and geotechnical conditions, this area is stable, with the minimum local factor of safety along the slope being 1.6 using assumed soil strength parameters.

5.7.5 Failure mechanisms

Sliding initialization

Earthquake

There are two basic lines of approach to studying slope stability under the influence of earthquake, namely pseudo-static method and dynamic analysis. In Phase 1 of this project, the pseudo-static method is used to estimate the influence of an earthquake on the stability of the Verrill slope, assuming linear sliding surfaces.

In the Pseudo-static method, seismic action is estimated by adopting an equivalent static horizontal force applied in the centre of the potentially unstable soil mass. It is usually expressed as a percentage of the force of gravity, according to a seismic coefficient k. It thus follows that

$$F_h = kmg \tag{5.7}$$

Where F_h = pseudo-static earthquake force, m = mass of sliding soil, g = acceleration due to gravity. If the sliding surface is assumed to be linear and undrained condition is considered, the factor of safety can then be expressed as

$$F_s = s_u / (\gamma' z \cos\beta \sin\beta + k\gamma z \cos^2\beta) \tag{5.8}$$

The selection of seismic coefficient is empirical. Representative values for k in terms of earthquake intensity I is given in Table 5.5 derived from the work of Hunt (1984). However, it should be mentioned that the value of k is greatly influenced by local geological conditions and soil properties.

The stability of the east slump at Verrill is presented using different seismic coefficients in Figure 5.22. When the average shear strength of soil is used and the seismic coefficient $k = 0.05$ (or I = 5), the local factor of safety at L = 14.02-14.46 km (distance along the slope) decreases to 1.12 from 1.68 at static condition. When k = 0.10, the factor of safety at several locations decreases to less than 1. Figure 5.23 further shows the variation in the factor of safety with respect to slope angle at different seismic coefficients.

Gas hydrates or excess pore pressure

Pore water and gas pressure reduce effective stress in soil and hence shear strength which may also trigger slope failure. In cohesive sediments, excess pore pressures may be built up by tectonic displacements inclusive earthquake, high sedimentation rates, sudden change of hydrostatic pressure by wave action, and development of free gas within the sediment. For the particular case of Verrill, the depth of water is more than 500 m, the effect of wave action can be neglected. The pore pressure could be induced by either earthquake or gas hydrates.

It is assumed that pore pressure exists only in a small range. The slope segment L = 14.02~14.46 km is selected to investigate the effect of pore pressure. Excess pore pressure is applied to lengths L_p = 50m, 150m, 250m and all areas of the slope respectively, while its magnitude is quantified using excess pore pressure ratio $r_u = u/\sigma_z$, as shown in Figure 5.24 Figure 5.25(a) gives the variation of the minimum factor of safety with pore pressure ratio at different distribution lengths L_p. The factor of safety decreases with both pore pressure ratio r_u and the length of pore pressure zone. When excess pore pressure reaches about 40% of effective stress, i.e. $r_u = 0.4$, the factors of safety are almost 1 with L_p larger than 100m and 1.16 with L_p = 50m. Since the maximum depth of sliding surfaces is approximately 15m, which corresponds the effective stress of 117kPa, $r_u = 0.4$ leads to the maximum pore pressure along sliding surface of u_{max} = 46.8 kPa. When pore pressure exists in the whole range of this slope segment, $r_u = 0.25$ or u_{max} = 29.3 kPa brings the factor of safety to 1.2.

When excess pressure exists in a large area, the effect of pore pressure on marine slope stability can also be estimated using the infinite slope analysis method. The shear strength of normally consolidated sediments can usually be expressed as

$$s_u = \lambda\sigma_z' = \lambda\gamma' z \tag{5.9}$$

When excess pore pressure exists, we have

$$s_u = \lambda(\gamma' z - u) = \lambda\gamma' z(1 - r_u),, \quad r_u = u/\sigma_z' \tag{5.10}$$

According to Equation (5.6), the factor of safety can be calculated as

$$F = 2\lambda\gamma' z(1 - r_u)/(\sigma_z' \sin 2\beta) = 2\lambda(1 - r_u)/\sin 2\beta \tag{5.11}$$

The results at the slope segment L = 14.02 to 14.46 km is given in Figure 5.25(b). The factor of safety for linear sliding surfaces is 4.5% larger than that for circular sliding surfaces.

Successive sliding/flowing

Attempts are made in this section to illustrate the possible mechanisms of slide development when the initial sliding is triggered. The effect of slope kinematics is not considered. In other words, the development of successive slope failure is simplified as a static process.

Retrogressive

It is assumed that the failure of slope segment L = 14.02~14.46 km is triggered by one of the mechanisms discussed above. When the first sliding block is removed, the soil mass above loses some support and sequent failure takes place. As illustrated in Figure 5.26, retrogressive sliding of slope is obtained until a stable state is reached at 12.92 km. The total length of sliding zone is 1.54 km, while the sliding depth varies between h = 20m and 40 m.

Quick sedimentation

When a local slope failure is initiated at a specific location (usually a segment of slope with large angle), the sliding soil mass will move down to the next slope segment which is still stable, and the weight of the sliding soil mass becomes a surcharge. Since undrained condition is maintained during such a short period of time, the shear strengths of soil in the downstream slope segments remain unchanged. Consequently, failure could be triggered in the down-stream slope segments.

Assume the unit weight and the thickness of the sliding soil mass to be $\gamma_{sliding}$ and $h_{sliding}$ respectively, the factor of safety of a down-stream slope segment can be estimated using infinite slope analysis, which leads to

$$f_s = \frac{c}{(\gamma' z + \gamma_{sliding} h_{sliding}) \sin 2\beta} = f_{s0} \frac{\gamma' z}{\gamma' z + \gamma_{sliding} h_{sliding}} \tag{5.12}$$

where $f_{s0} = c/(\gamma' z \sin 2\beta)$ is the initial factor of safety, β the slope angle, γ' the effective unit weight of soil. Then the critical depth of the triggered sliding zone can be calculated as

$$z_{cr} = \frac{1}{f_{s0} - 1} \frac{\gamma_{sliding} h_{sliding}}{\gamma'} \tag{5.6.13}$$

As already known, the slope segment L = 14.02 to 14.46 km fails first. For the slope segment L = 14.46 ~ 15.35 km, the initial factor of safety f_{s0} = 3.25 when the average shear strength of soil is used. At the onset of slope failure, the value of $\gamma_{sliding}$ is very close to the original effective unit

weight of soil, i.e. $\gamma_{sliding} \approx \gamma'$, the thickness of the trigged sliding soil mass is then estimated as $Z_{cr} = h_{sliding}/2.25$. Here $h_{sliding}$ depends on the slope angle and the total volume of upper stream sliding soil mass. The dependency of Z_{cr} on $h_{sliding}$ and slope angle β is presented in Figure 5.27. For slope segments with initial factors of safety much larger than 1, sliding can be triggered by the overflow of upper-stream sliding soil mass. The thickness of the triggered sliding soil zone increases with slope angle and the thickness of overflowing soil.

5.7.6 Undisturbed area at Verrill

As illustrated in Figure 5.9, a profile is chosen in the historically undisturbed zone at Verrill to investigate the stability of that area. The stability obtained from infinite slope analysis is shown in Figure 5.28. The minimum factor of safety is $f_{smin} = 4.81$ when the average shear strength of that area is used, while f_{smin} may vary between 3.85 and 5.79. Any slope with the factor of safety on this level is stable. However, large earthquakes may trigger sliding in this area. As shown in Figure 5.29, an earthquake with the intensity of $I = 7$ (the seismic coefficient $k = 0.1$) decreases the factor of safety to the range of 1.2 ~ 1.5 along the whole slope.

5.7.7 Western slump at Verrill

As shown in Figure 5.10, the average slope angle of the profile at western slump of Verrill is between that of the eastern slump and the undisturbed zone. When the properties are the same, it is expected that the stability of the western slump should also be in the middle of all three slopes. Figure 5.30 presents the overall slope stability calculated assuming linear sliding surfaces. The minimum factor of safety in the range of 2.19 ~ 3.29 is obtained at $L = 5.0 \sim 5.74$ km (or water depth 700 ~ 800 m). When no other triggering factors exist, slopes in this area are stable. However, when an earthquake of $I = 6$ (or the seismic coefficient $k = 0.05$) occurs, a local factor of safety at water depth 700 ~ 800 m can be decreased to 1.50 with $s_u/\sigma_z' = 0.36$. If the lower limit of soil strength $s_u/\sigma_z' = 0.29$ is considered, f_s will be decreased to 1.21, which indicates that the slope is very close to the critical state. If the intensity of earthquake is of $I = 7$ (corresponding to the seismic coefficient $k = 0.1$), the factor of safety along the whole slope is in between 1.02 and 1.40 with $s_u/\sigma_z' = 0.36$. It means that sliding will be triggered either locally or globally when the variation in soil strength is considered.

5.8 Evaluation of Albatross Failure

5.8.1 Slope profiles

Two slope profiles selected for the calculation of the slope stability (Figure 5.32) are given in Figure 5.33. The overall slope angle at Albatross is approximately 6° with the maximum local slope angle larger than 10°. Not much difference is observed between these two slope profiles. All analyses will then be performed using data of slope profile 2.

5.8.2 Soil geotechnical properties

Details of soil properties are referred to Section 4.3 or Mulder et al. (1997). The variation of shear strength ratio s_u/σ_z' is presented in Figure 5.34. When the depth is larger than 4 m, s_u/σ_z' is almost constant, which means that soil is normally consolidated. The total unit weight for all the

cores ranges between 14 and 18 kN/m^3, and the value of 16.2 kN/m^3 is considered significant for the normally consolidation sediments.

5.8.3 *Slope stability*

As already discussed in Section 5.5, for slopes of large dimension, the shapes of sliding surfaces have less effect on the calculated factor of safety. This is again proved in the stability analysis for Albatross slope. The variation of stability along slope profile 2 is given in Figure 5.35. The minimum factor of safety (fs_{min} = 1.23) appears at the water depth of 300 to 400 m. The factor of safety is approximately 2.34 in the water depth of 400 to 900 m. The variation of f_s with slope angle is further given in Figure 5.36. Critical states are reached at slope angles of approximately 15°. However, Figure 5.37 shows that slope angles along both Profiles 1 and 2 are generally less than 10, except some specific locations at the water depth between 300 to 400 m. It is hence concluded that Albatross slope is stable if no other triggering forces exist.

5.8.4 *Failure mechanisms*

Sliding initialization

Earthquake
The stability of slopes at Albatross during earthquake is analyzed using a quasi-static method. As shown in Figure 5.38, when k = 0.05 (or earthquake intensity I = 5), the factor of safety at water depth of 300 ~ 900 m is less than 1.2. When I = 6, f_s is less than 1.2 in the whole slope. Figure 5.39 further shows the variation in the factor of safety with respect to slope angle at different seismic coefficients.

Gas hydrates or excess pore pressure
As discussed in section 5.6.5.1, the influence of excess pore pressure, u, can be estimated using infinite slope stability method when u exists in a large area.

Successive sliding/flowing

Retrogressive
As shown in Figures 5.35 and 5.37, failure will first take place at water depths of 300 ~ 400 m. Retrogressive failure may take place, as shown in Figure 5.38. If only static conditions are considered, the retrogressive process proceeds only 86 m when a stable state is recovered. The total sliding length is 550 m with the depth of 33 m.

Quick sedimentation
When a local slope failure is initialized at a specific location (usually a segment of slope with large angle), the sliding soil mass will move down to the next slope segment which is still stable, and the weight of the sliding soil mass becomes a surcharge. Since the undrained condition is maintained during such a short period of time, the shear strengths of soil in the downstream slope segments remain unchanged. Consequently, failure could be triggered in the down-stream slope segments. The critical depth of triggered sliding soil mass Z_{cr} depends on the thickness of overflowing slump, $h_{sliding}$, and the slope angle, β, as shown in Figure 5.41. For slope segments with initial factors of safety much larger than 1, sliding can be triggered by the overflow of

upper-stream sliding soil mass. The thickness of the triggered sliding soil zone increases with slope angle and the thickness of overflowing soil.

5.9 Evaluation of Logan Failure

5.9.1 Slope profiles

One slope profile was selected for the stability analysis (Figure 5.43). The overall slope angle at Logan is approximately 2-6°, with the maximum local slope angle larger than 10°, where the water depth is 500-600m. The bathymetry map used for defining the slope profile is small-scaled, so the water depth value could have some error. In the later research, the detailed bathymetry map should be provided.

5.9.2 Soil geotechnical properties

Details of soil properties are referred to in Section 5.4 or Mulder et al. (1997). The geotechnical profile is presented in Figure 5.44. When the soil depth is larger than 1 m, s_u/σ_z' is almost constant signifying that soil is normally consolidated. The total unit weight is defined 18 kN/m^3.

5.9.3 Slope stability

From the geometry of the features that have been identified, the slope stability of Logan is assessed by the method of infinite slope stability analysis. The variation of stability along slope profile is given in Figure 5.45. The minimum factor of safety (fs_{min} = 2.49) appears at the water depth of 500-600m. The factor of safety is approximately 4.85 in the water depth of 600 to 700m. It is hence concluded that the Logan slope is stable under gravity conditions, but when taking earthquake loading into account, the calculated results show that the slope will be unstable when the earthquake coefficient is less than 0.1g.

5.9.4 Failure mechanisms

The determination of the precise conditions responsible for the slope instability is difficult. The instability threshold appears to result from the interaction of several variables rather than a single factor. The major factors that appear to combine to influence the stability of the seabed sediment include earthquake, gas hydrate and methane gas, and excess pore water pressure. According to the analysis result and the geological conditions, the earthquake and pore water/gas pressure are the main factors in assessing slope instability.

Earthquake

The stability of slopes during an earthquake is analyzed using quasi-static method. As shown in Figure 5.45, when k = 0.05g (or earthquake intensity I = 5), the factor of safety at water depth of 500 ~ 600 m is less than 1.0. When k = 0.1g (I = 6), f_s of the slope where water depth is less than 1300m is less than 1.2. When k = 0.15g (I = 8), f_s of the whole slope is less than 1.2. Figure 5.46 further shows the critical slope degree for slope slide occurring with respect to different seismic coefficient.

Gas hydrates or excess pore pressure

As discussed in Section 5.7.5, the influence of excess pore pressure, u, can be estimated using infinite slope stability method when u exists in a large area.

Pore water or gas pressures reduce the effective stress in soil and hence the shear strength, which may trigger a slope failure. According to the areas environmental and geological conditions, an earthquake or the development of free gas within the sediment may build up excess pore pressure. Thus far, without available data on excess pore water pressures, we can only do general calcuations for the stability on the slope (Figure 5.47). Figure 5.47 tell us the Logan slope will slide only when the slope angle is more than 4.5° and the pore water pressure ratio r_u more than 0.8. If the slide depth is 20m, the excess pore water pressure should be as large as 96kpa.

Conclusion

In order to understand the triggering mechanisms for the submarine slides observed on the Scotian margin, the factor of safety (FOS) of the slopes when subjected to gravity loading is evaluated. The geological setting (slope geometry) of the study area and soil's geotechnical properties were used. The calculation was carried out using an infinite slope method, under gravity loading and for the undrained condition. The calculation results show that the static stability of the Scotian slopes are satisfactory with the minimum factor of safety on the upper slopes being greater than 1.2. With increased water depth the safety factor of the slide area tends to increase.

The calculation of the factor of safety is based on geotechnical properties, the soil's physical parameters, and on the morphology of the area. This calculation allows us to conclude that in the absence of external factors, the Scotian slopes are presently safe and that the gravity loading cannot be at the origin of the observed slide.

Earthquakes are the cause of three risk factors on slope instability: 1) the horizontal acceleration, which increases the driving forces, 2) the build up of pore pressure, which can decrease the resisting forces and generate a liquefaction of the soil, and 3) the decrease of the shear resistance under cyclic loading. Due to lack of geotechnical data considering the effect of the cyclic loading on the soil behavior, only the effect of the horizontal acceleration on the slope stability was considered here. Several calculations were carried out at different horizontal accelerations (different seismic coefficients 0.05g, 0.10g, 0.15g). The calculation results revealed that when the horizontal acceleration is more than 0.10g the slopes in the study area will lose their stability and failure will occur. When the horizontal acceleration is 0.05g, the upper slope near the head scarp in Albatross and Logan area will tend to lose their stability. One can conclude from the above results that earthquakes can generate sliding in the area. The earthquake is the major factor for the initiation of the submarine slides in this area.

Excess pore pressure in the area could be generated by shallow gas, dissociation of gas hydrates or fluid flow and could trigger instability by generating seepage forces, inducing excess pore pressures. Although the relationship between instability and the excess pore pressure cannot be determined, the scenario of failure due to excess pore pressure is supported by the coincidence between the pockmarks and slide scar. According to the calculation results, the slopes with

degrees more than 2 , 6, or 8 will lose their stability when the pore pressure ratio is 0.8, 0.6, or 0.2 respectively under gravity loading.

The results show that failure occurs on the upper slope near the slide scarp corresponding to the pockmark area. This confirms the scenario of instability due to an upward fluid flow in the pockmarks field. So, the gas or gas hydrates would be another contributing factor for the submarine slide in the research area.

Submarine slope instabilities that occur in the Scotian Slope region are mainly caused by earthquake and shallow gas or gas hydrate. Detailed mapping of the location and geometry of bottom failures are needed for the accurate analysis of the instability process and the research results show that each slope failure involves several related mechanisms, with considerable spatial and temporary variability.

5.10 References

Baltzer, A., Cochonat, P, and Piper, D.J.W., 1994. In Situ Geotechnical Characteristics of Sediments on the Scotian Slope, Eastern Canadian Continental Margin. *Marine Geology*, v. 120, p. 291-308.

Berry, Jacqueline A. 1992. A Detailed Study of a Debris Flow System on the Scotian Rise. unpublished M.Sc. thesis. Dalhousie University, 202 p.

Berry, J.A. and Piper, D.J.W. 1993. Seismic Stratigraphy of the Central Scotian Rise: A Record of Continental Margin Glaciation. Geo-Marine Letters, 13: 197-206.

Campbell, D. Calvin. 2000. Relationship of Sediment Properties to Failure Horizons for a Small Area of the Scotian Slope. Geological Survey of Canada Current Research 2000.

Dodds, D.J. and Fader, G.B. 1987. A Combined Seismic Reflection Profiler and Sidescan System for Deep Ocean Geological Surveys. In: Progress in Underwater Acoustics. H.M. Merklinger, ed. Plenum: New York, 169-180.

Driscoll, Neal W., Weissel, Jeffrey K., and Goff, John A. 2000. Potential for Large-Scale Submarine Slope Failure and Tsunami Generation Along the U.S. Mid-Atlantic Coast. Geology, 28: 407-410.

Gauley B. and Piper, D.J.W, 2000.A Study of Failures Along the Scotian Margin and Grand Banks. Draft report for PODS. GSC (Atlantic), May 29,2000.

Hant, R. E., 1984, Geotechnical engineering investigation manual. New York, Toronto, McGraw-Hill, c1984.

Hughes Clarke, J.E., Mayer, L.A., Piper, D.J.W., and Shor, A.N. 1989. Pisces IV Submersible Operations in the Epicentral Region of the 1929 Grand Banks Earthquake. Geological Survey of Canada Paper 88-20, p. 57-69.

Keigwin, L.D. and Jones, G.A. 1995. The Marine Record of Deglaciation from the Continental Margin off Nova Scotia. Paleoceanography, 10:973-985.

Kosalos, J.G. and Chayes, D. 1983. A Portable System for Ocean Bottom Imaging and Charting. In: Oceans '83 (IEEE conference proceedings of the third working symposium on oceanographic data systems), 2: 649-653.

Mosher, D.C., Moran, K. and Hiscott, R.N., 1994. Late Quaternary Sediment, Sediment Mass Flow Processes and Slope Stability on the Scotian Slopes. *Sedimentology*, v. 41, p. 1039-1061.

Mosher, D.C, Piper, D.J.W., Vilks, G., Asku, A.E. and Fader, G.B., 1989. Evidence for Wisconsinan Glaciations in the Verrill Canyon Area, Scotian Slope. *Quaternary Research*, v. 31, p. 27-40.

Mosher, D.C., 1987. Late Quaternary Sedimentology and Sediment Instability of a Small Area on the Scotian Slope. Unpublished M.Sc Thesis, Memorial University of Newfoundland, St. John's Newfoundland. 249 p.

Mulder, T., and Moran K., 1995. Relationship among submarine instabilities, sea-level variations and the presence of an ice sheet on the continental shelf: an example from the Verrill Canyon area, Scotian Shelf. *Palenoceanography*, v.10, p.137-154.

Mulder, Thierry, Berry, Jacqueline A., and Piper, David J.W. 1997. Links Between the Morphology and Geotechnical Characteristics of Large Debris Flow Deposits in the Albatross Area on the Scotian Slope (SE Canada). Marine Georesources and Geotechnology, 15: 253-281.

Piper, D.J.W. 1999. Cruise Report, Hudson 99-036. Unpublished report, Geological Survey of Canada (Atlantic), Bedford Institute of Oceanography, 49 pp. + appendices.

Piper, D.J.W. 2000. Personal Communication.

Piper, D.J.W., 2000. The Geological Framework of Sediment Instability on the Scotian Slope: Studies to 1999. GSC (Atlantic). Open File 3920, 202 pp..

Piper, David J.W. and Skene, Kenneth I. 1998. Latest Pleistocene Ice-Rafting Events on the Scotian Margin (Eastern Canada) and Their Relationship to Heinrich Events. Paleoceanography, 13: 205-214.

Piper, D.J.W. and Wilson, E. 1983. Surficial Geology of the Upper Scotian Slope West of Verrill Canyon. G.S.C. Open File 939.

Piper, David J.W., Campbell, D.C., and MacDonald, A.W.A. 2000. Report on Properties of Nine Piston Cores Near Logan Canyon. GSC (Atlantic) Internal report.

Piper, David J.W., Cochonat, Pierre, and Morrison, Martin L. 1999. The Sequence of Events Around the Epicentre of the 1929 Grand Banks Earthquake: Initiation of a Debris Flow and the Turbidity Current Inferred from Sidescan Sonar. Sedimentology, 46: 79-97.

Piper, D.J.W., and Shor, A.N.,1985. Later Quaternary slumps and debris flows on the Scotian Slope: Geological Society of America Bulletin, v.96, p.1508-1517.

Piper, D.J.W., and Sparkes, R., 1987. Proglacial Sediment Instability Feature on the Scotian Slope at 63° W. *Marine Geology*, v. 76, p. 1-11.

Piper, David J.W., Farre, J.A., and Shor, A. 1985a. Late Quaternary Slumps and Debris Flows on the Scotian Slope. Geological Society of America Bulletin, 96: 1508-1517.

Piper, David J.W., Shor, Alexander N., Farre, John A., O'Connell, Suzanne, and Jacobi, Robert. 1985b. Sediment Slides and Turbidity Currents on the Laurentian Fan: Sidescan Sonar Investigations Near the Epicenter of the 1929 Grand Banks Earthquake. Geology, 13: 538-541.

Shor, Alexander N. and Piper, David J.W. 1989. A Large Late Pleistocene Blocky Debris Flow on the Central Scotian Slope. Geo-Marine Letters, 9: 153-160.

Table 5-1: Summary of core descriptions

Core #	Location	DF	Description	Depth	Date (ka)
88010-23	Muddy Albatross ridge	/	Bioturbated, ice rafted detritus brick red mud, 30 cm deep thin holocene layer	7m	
86034-41	tubidite plain, lower slope west of Albatross	1	2m of Holocene mud overlie 0.5m of brown mud. Abundant Clasts of mud and rock pebbles, overlies 40 cm of red brick mud	7m	13.2 at 2m 16.05-6.9m
86034-39	tubidite plain, lower slope west of Albatross	1	Both brick red sandy mud (noted as b and d) present.	8.3	
	Low levee on continental rise	1	Thin debris flow. Foraminiferal ooze overlying early holocene muds and late Pleistocene brown mud turbidities		20.9at base
86034-35	Lower slope		Mud clast conglomerate overlain by thin sand to mud turbidities and olive grey mud	3.5m	
86034-36	Smoother area	both	DF1: coarse sand, mud clast shell fragments similar to 86034-41. Overlies fine sand and bioturbated brownish mud. This overlies blocky mud clast conglomerate seen as DF2.	4.6m	14.3 ka 13-13.3 ka
90015-19	Head of debris flow	2	Proximal DF of mud clasts	7m	12-13.35ka
	Lower Mohican Channel	2	10 cm thick sandbed		12ka

Table 5-2: Description of consolidation.

Area	Description	Consolidation
Lower slope not within flow, 3900 m isobath	Muddy debris flow	Under (OCR<=0.8)
Lower slopes, 4600m isobath, within thin debris flow	Proglacial muds	Normal (0.8<OCR<=1.2)
Lower western side of failure	Debris flow matrix	Normal
Lower on the midslope, in the debris flow, between 3800and 3900m isobath	Eroded seabed flow matrix	Over (2<OCR<=4)
Within the Debris Flow,2700m isobath	Blocky debris flow	Over
Within the Debrs Flow, cores taken from the midslope,2600m isobath, and much lower,4200m isobath	Blocky debris flow	Very Over (OCR>4)

Table 5-3: Summary of Scotian Slope Slides

Slide Type	Soil Type	Density (g/cm^3)	PI (%)	Su (kPa)	Water Depth (m)	Amount of soil (km^3)	Depth of slide (m)	Angle (degrees)	Run out distance (km)	Features
1. Albatross Blocky Debris flow Debris flow 1, 12.7ka Debris flow 2, 14ka	A wide range of muds	1.2 - 1.8 (Plots from Mulder et al.., 1997)	22% (under consolidated debris flow) 26% (stratified muds on rise)	1.2 - 1.8 (Plots from Mulder et al.., 1997)	Head wall scarp is 550 - 700 mbsl.	> 600	50 (120m on slope) (20m lower slope)	6 Slope angle is within the source area.	200	Upper rise (2500 - 3000 mbsl) is composed of Triassic salt diapirs. Pockmarks within sediment failure region, indicating possible gas release. Sedimentation rate 0.185-0.85 m/ka Failure mechanism: unknown, earthquake, or related to gas hydrates
2. Logan Canyon Stacked series of Debris Flows. (Three individual flows.) Sediment dated to 16.77 ka to 14.63 ka	Olive grey Holocene mud. Below it, two brick red sandy mud layers. Below this, alternating reddish brown and brown mud. These are the muds that failed.	1.5 - 2.5	18% Redder sediment 30% Greyer sediment		The head of the failure is in 400m of water.		DF1 = 16.40 DF2 = 8.83 DF3 = 7.57 (Thickness of 3 individual debris flows.)		150	Failure mechanism: unknown probably similar to Verrill
3. Verrill Canyon There are two discrete Rotational Slumps. Western Slump 5km wide (11.9ka) Eastern Slump 15km wide (10.4ka) These Slumps pass into Debris Flow.	Bioturbated, hemipelagic sandy muds, containing ice rafted material. Bioturbated, laminated Grey muds, and units of brown sediments.	1.65 - 2.0	22% - 37%	2.0 - 18.0 10-15kPa surface <5kPa at depth	Rotational slumps head is 500 - 600.	5.75	10.0 - 20.0	700 mbsl changes from 5 degrees on the upperslope to 2.5 degress on the lower slope.	Western Slump 30km.	Wedge shaped units of sediment at 700 mbsl, represents slumped diamitics and outwash from glacial ice. Pockmarks down to 2200 mbsl, most abundant from 500 - 900 mbsl. Sedimentation rate: 0.05-1.0m/ka Bedding plane slides exist and rotational failures to the south Failue mechanism: external, earthquake?, with possible excess pwp from gas hydrates or rapid sed.

Table 5-4: Information Required for Submarine Mass Movement Assessment and Data Gaps for the Scotian Failures Considered

	Information Required	Verrill Mass Movement	Albatross Mass Movement	Logan Mass Movement
Classification	Detailed bathymetric maps	L	L	N/A
	Near surface geophysical	A	L	L
	Shape, depth and character of failure surfaces	L	L	L
	Sediment Samples (from disturbed areas through failed sediments and undisturbed areas)	VL	L	VL
Evolution and Initiation	Sediment Parameters (with depth and distance from centreline)	N/A to VL	N/A to VL	N/A to VL
	Soil strength (*In-situ* and Lab)	VL	VL	VL
	OCR	VL	VL	VL
	Water content	VL	VL	VL
	Sensitivity	N/A	N/A	N/A
	Plasticity	Partial	Partial	Partial
	Grain size	N/A	N/A	N/A
	Bulk density	VL	VL	VL
	Void Ratio	N/A	N/A	N/A
	Insitu excess pwp	N/A	N/A	N/A
	Surface Morphology	L	L	L
	Scarps, block size, sediment characteristics	L	L	L
	Subsurface Morphology	L	L	L
Slope Stability	Sediment properties (as given above)	VL	VL	VL
	Triaxial testing (at higher cell pressures where deeper samples are not available)	N/A	N/A	N/A
	Cyclic triaxial testing	N/A	N/A	N/A
Environmental Loads and Geohazards	Sedimentation	L	L	L
	Seismic loading	L	L	L
	Wave loading	L	L	L
	Free Gas	VL	VL	VL
	Gas Hydrates	N/A	N/A	N/A
	Excess Pore Water Pressures	N/A	N/A	N/A
	Erosion	N/A	N/A	N/A
	Tidal Changes	N/A	N/A	N/A
	Diapirs	N/A	N/A	N/A

Note: N/A - not available or not applicable; VL- very limited information available; L – limited information available; A–Adequate information available

Table 5-5: Seismic coefficient *k*, representative values (Hunt, 1984)

k	Intensity *I*
0.00	I-IV
0.05	V-VI
0.10	VII
0.15	VIII-IX
0.25	X or greater

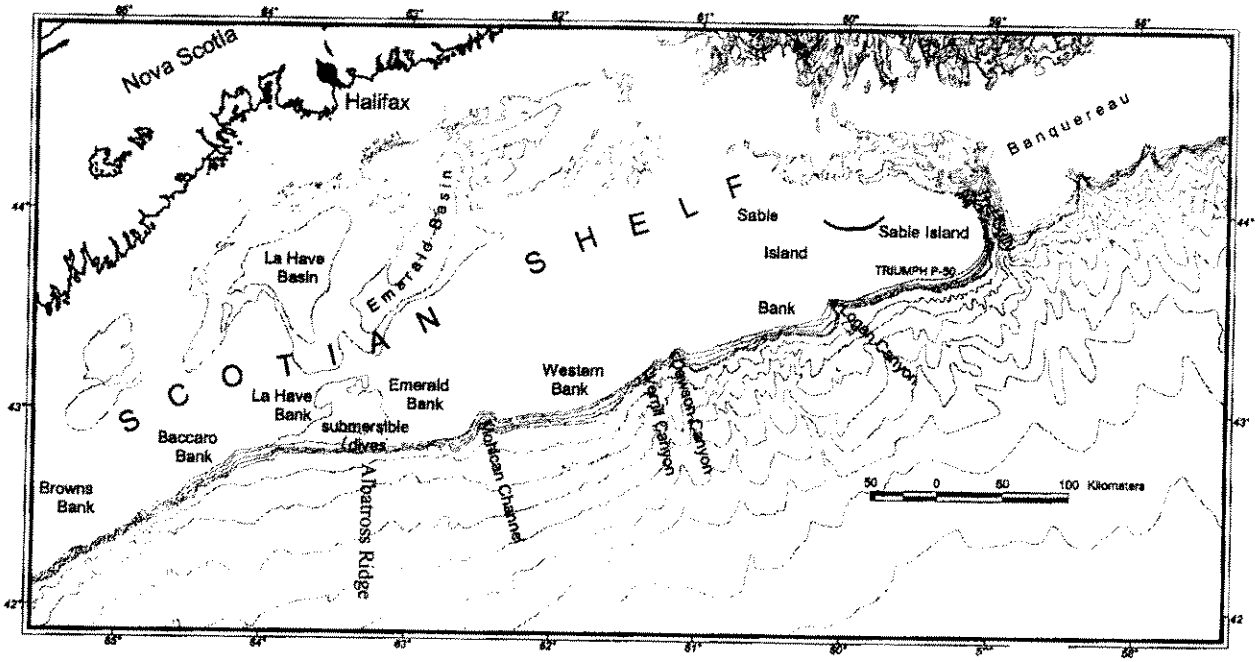

Figure 5-1: Overview of the Scotian Slope (Piper, 2000).

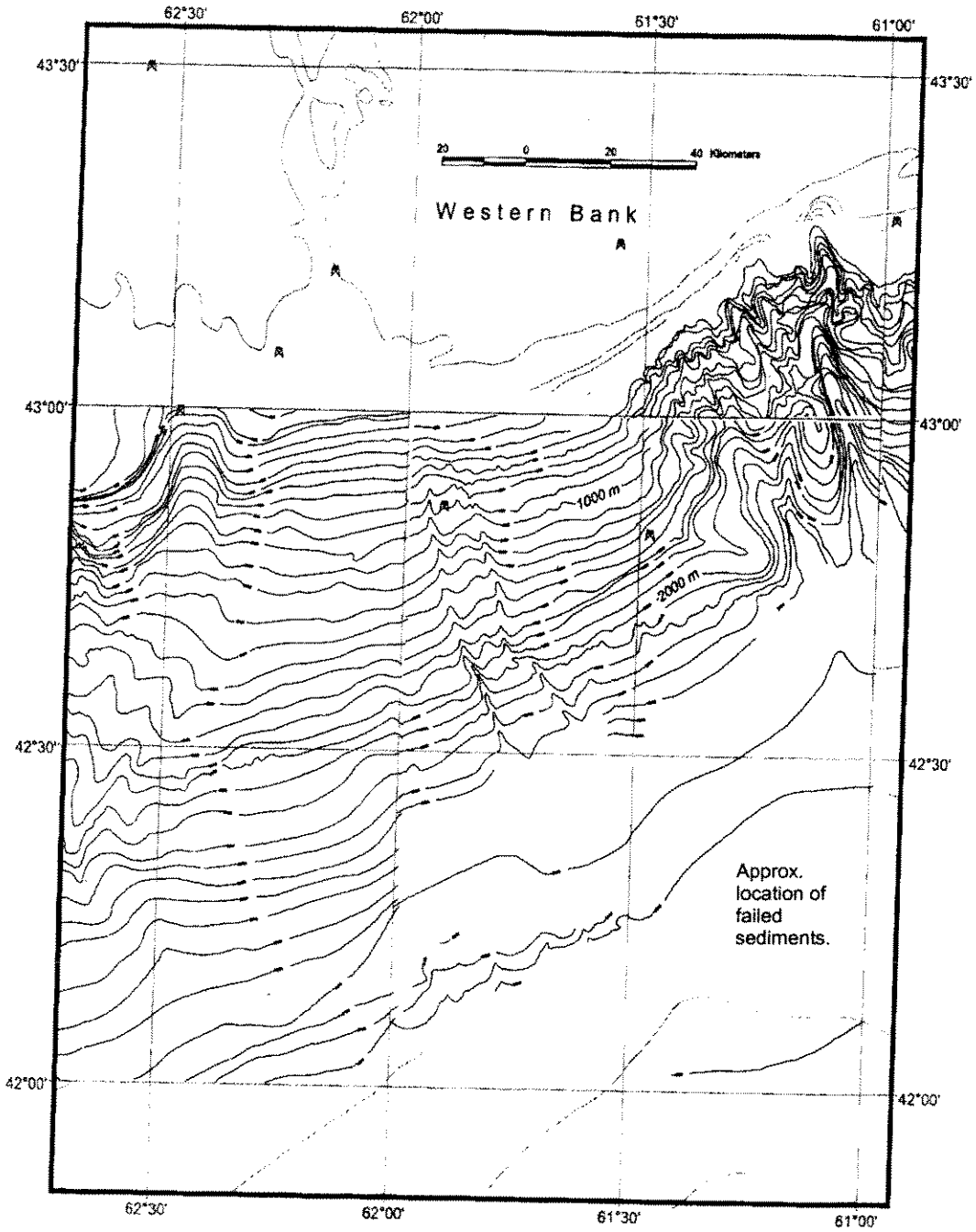

Figure 5-2: Bathymetry of the Verrill Canyon Area. (Piper,2000)

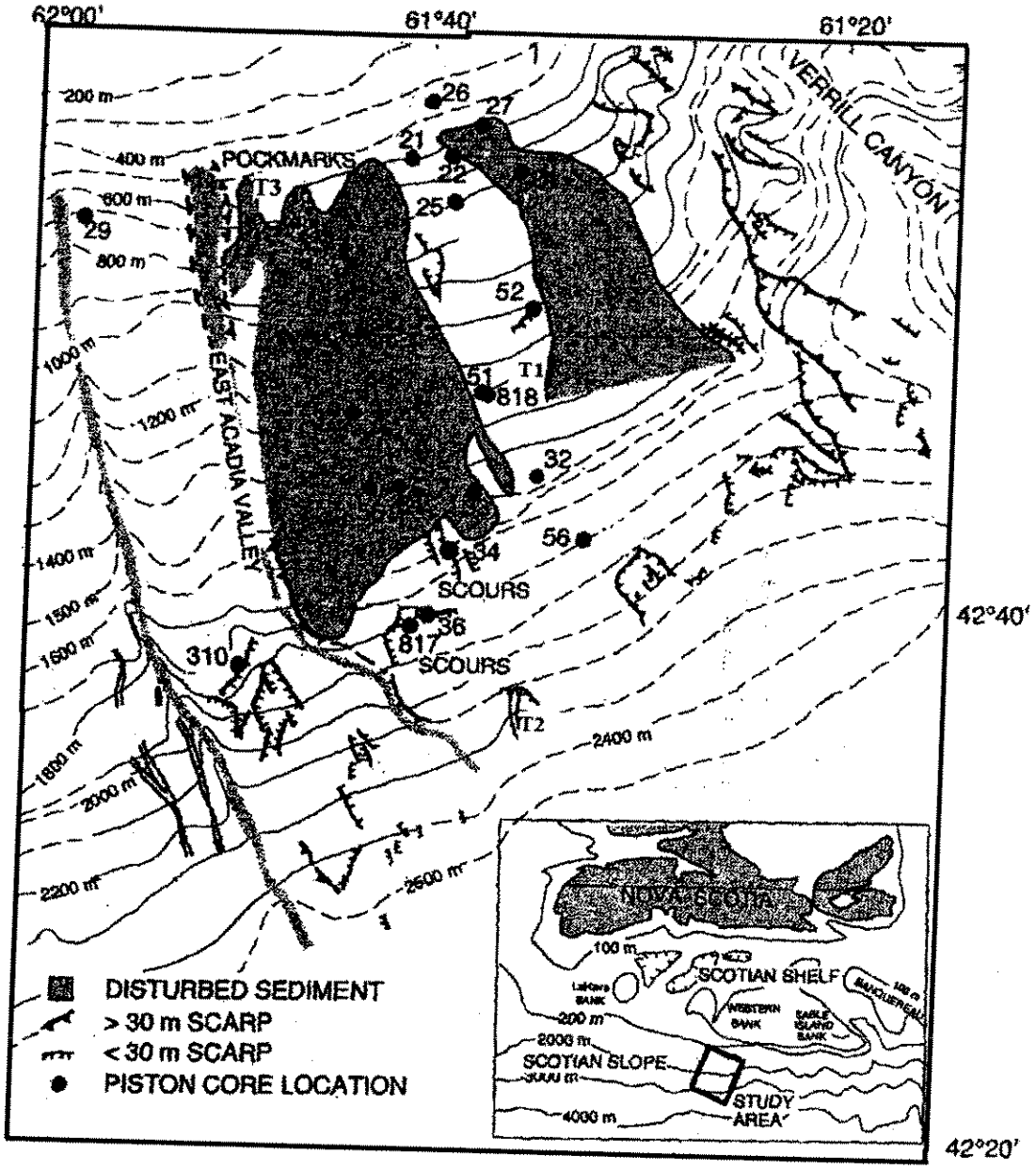

Figure 5-3: Overview of the Verrill Canyon failure (Piper, 2000).

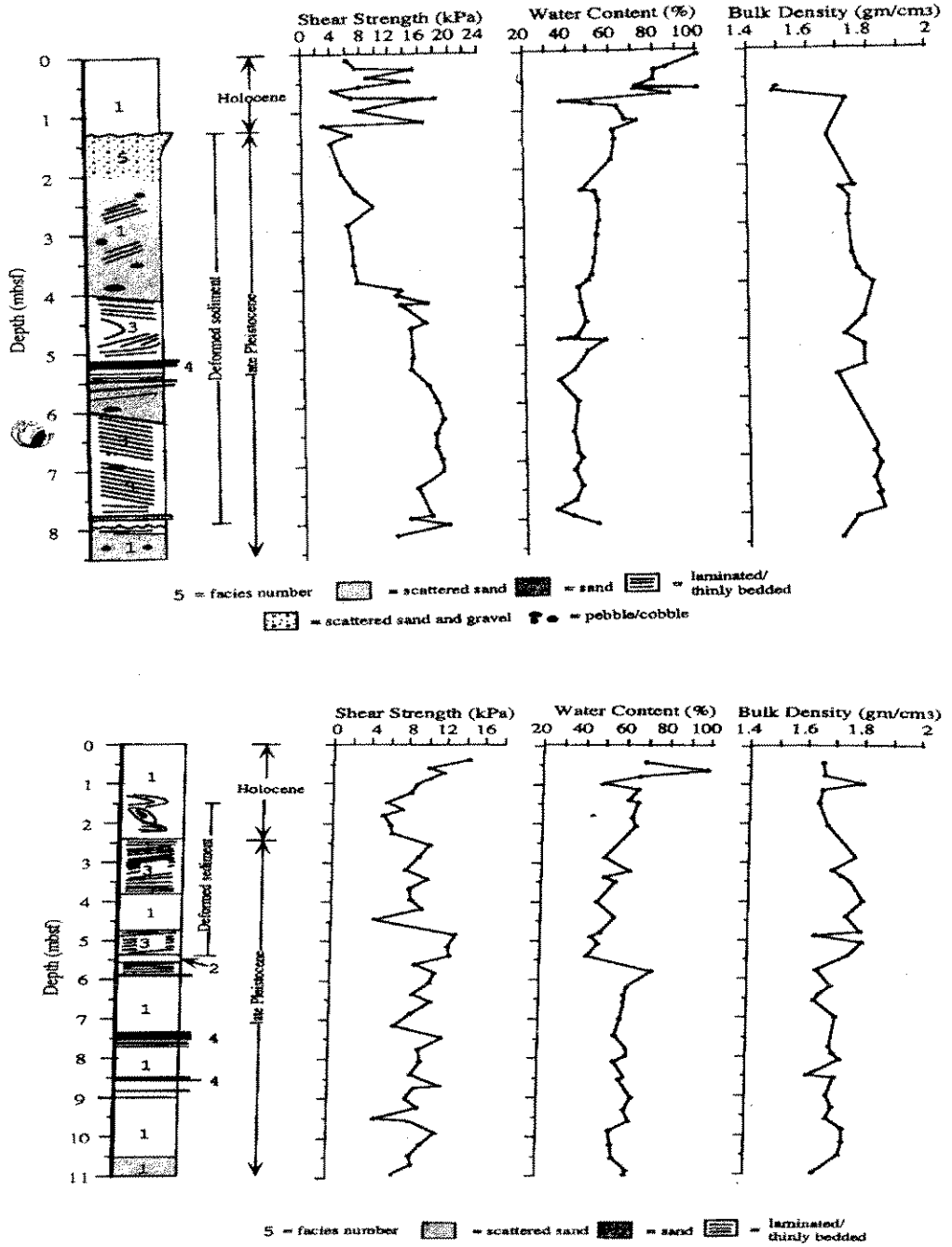

Figure 5-4: Cores 54 and 55, from the western slump (Mosher, 1994).

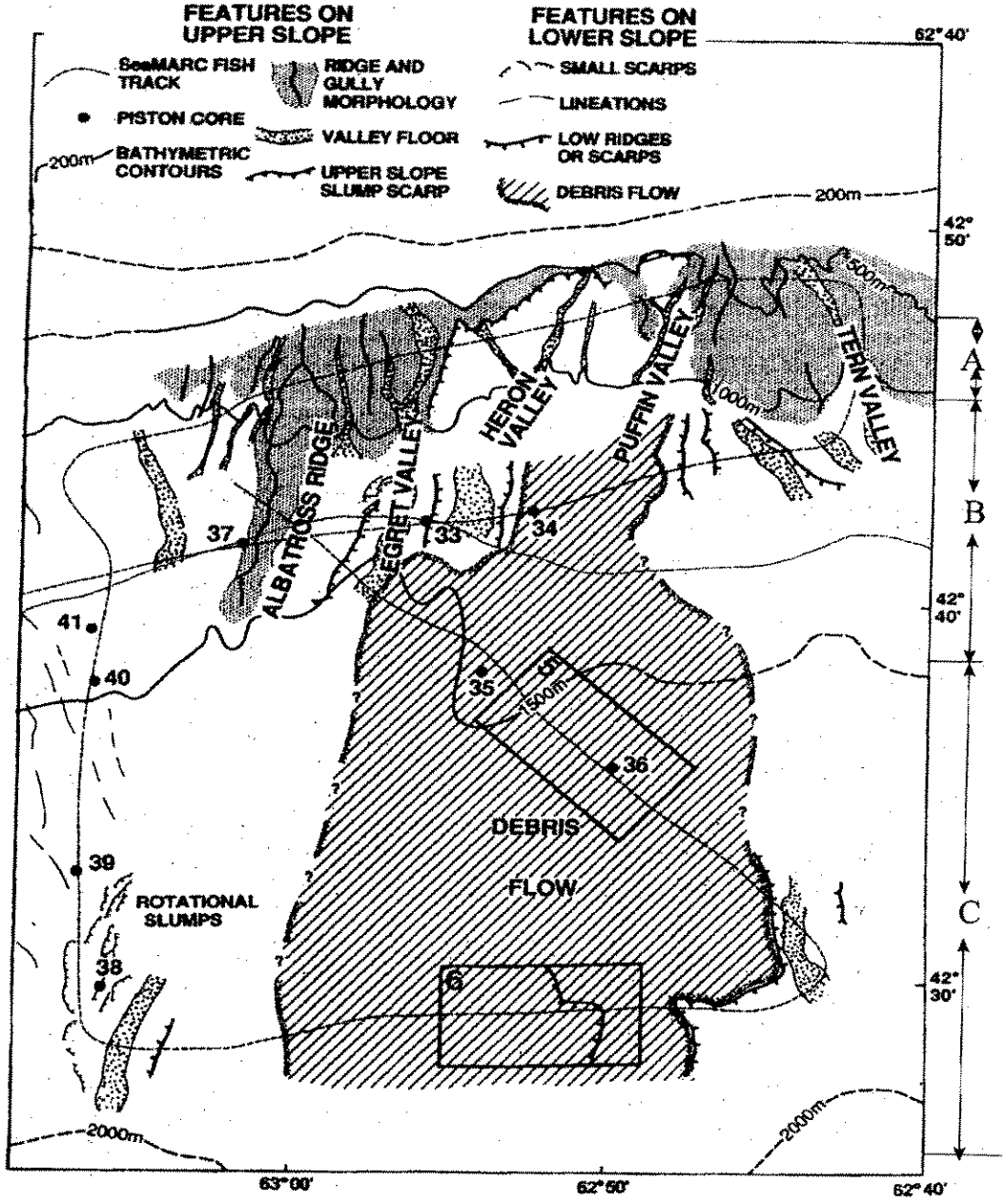

Figure 5-5: The Albatross debris flow failure (Piper, 2000).

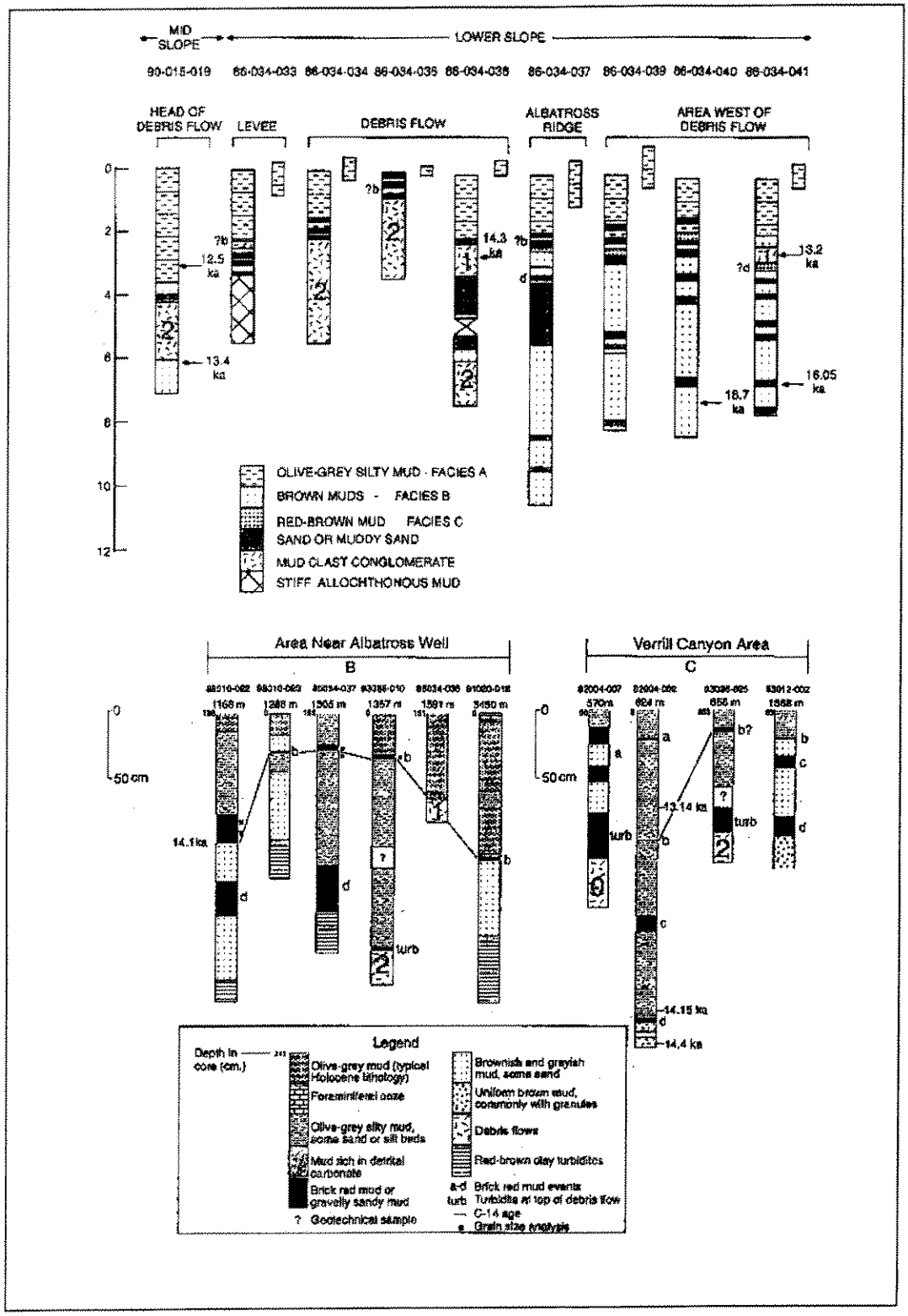

Figure 5-6: Cores from the Scotian Slopes (Piper, 2000).

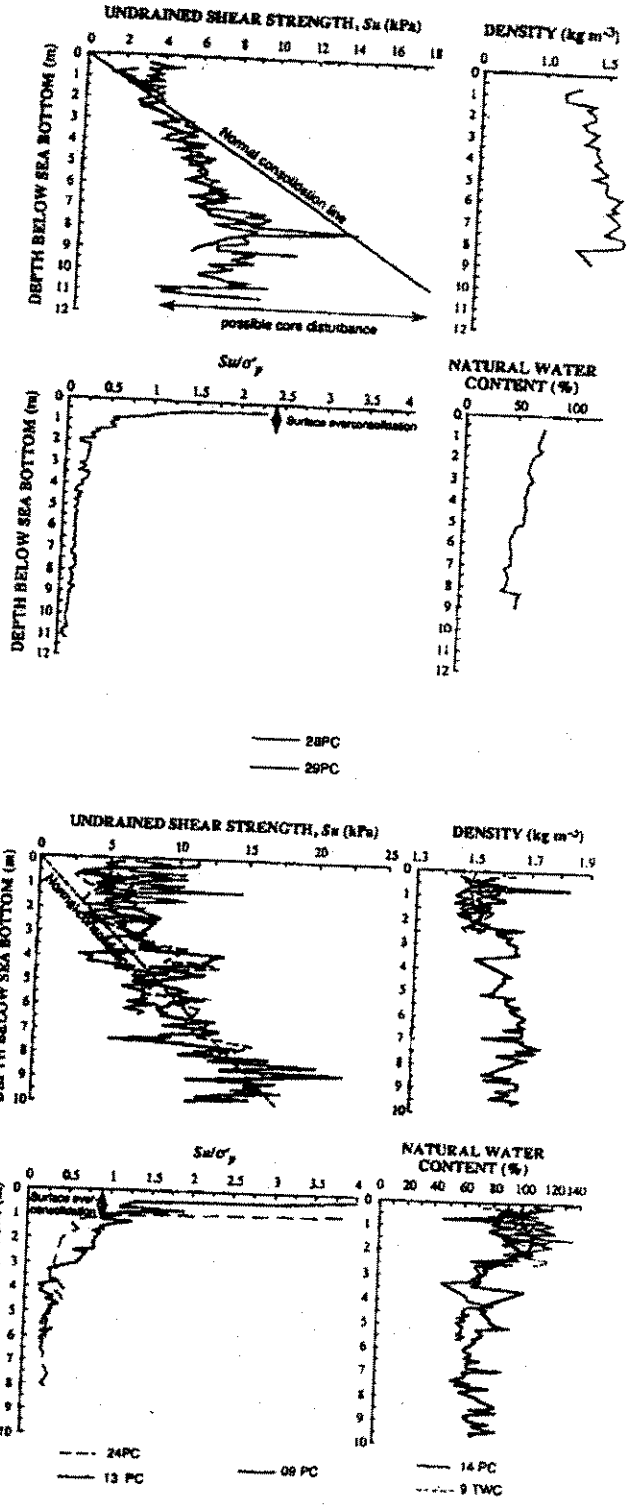

Figure 5-7: Downcore variation of shear strength ratio in cores from stratified sediment (Piper, 2000).

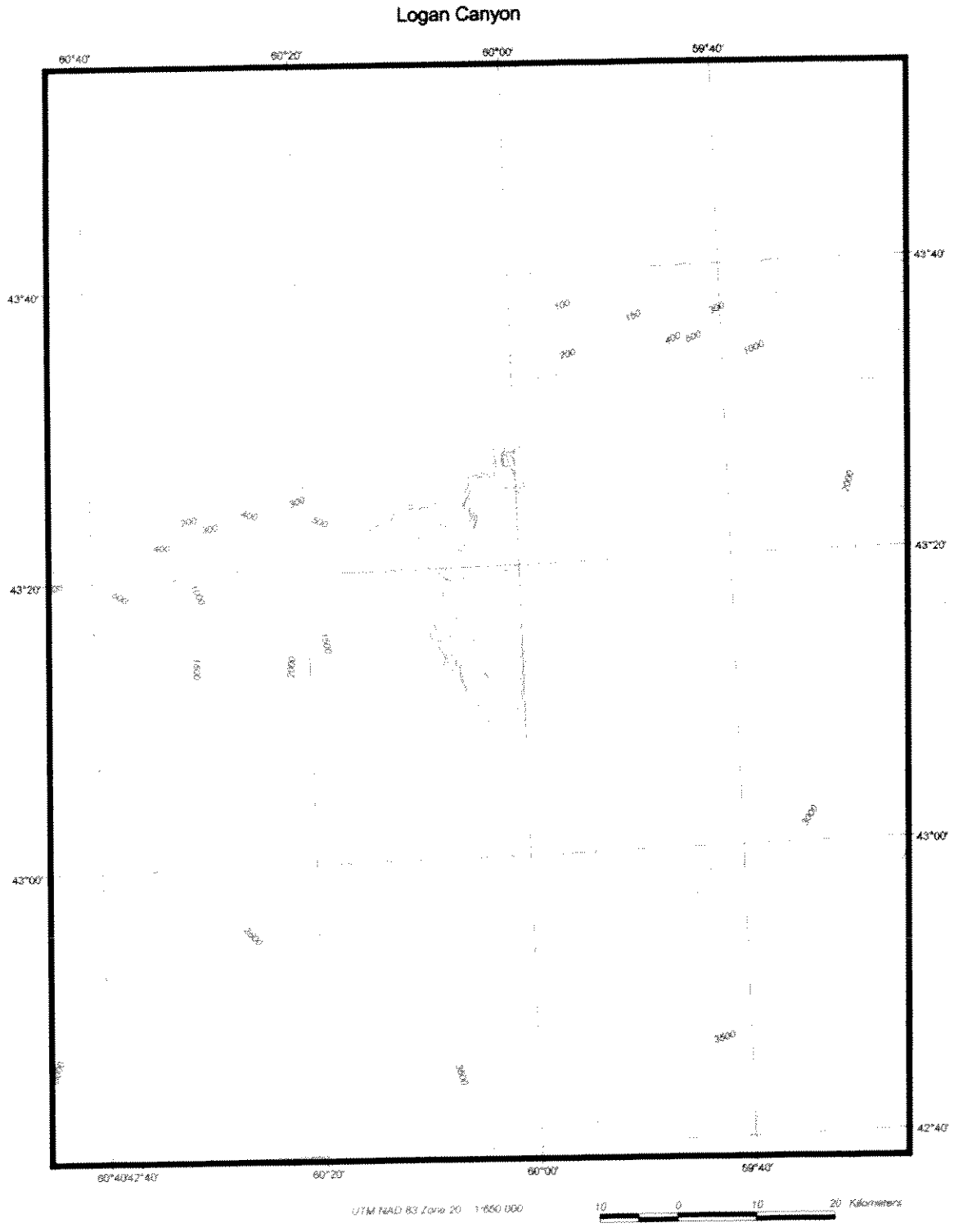

Figure 5-8: Overview of the Logan Canyon area (Piper, 2000).

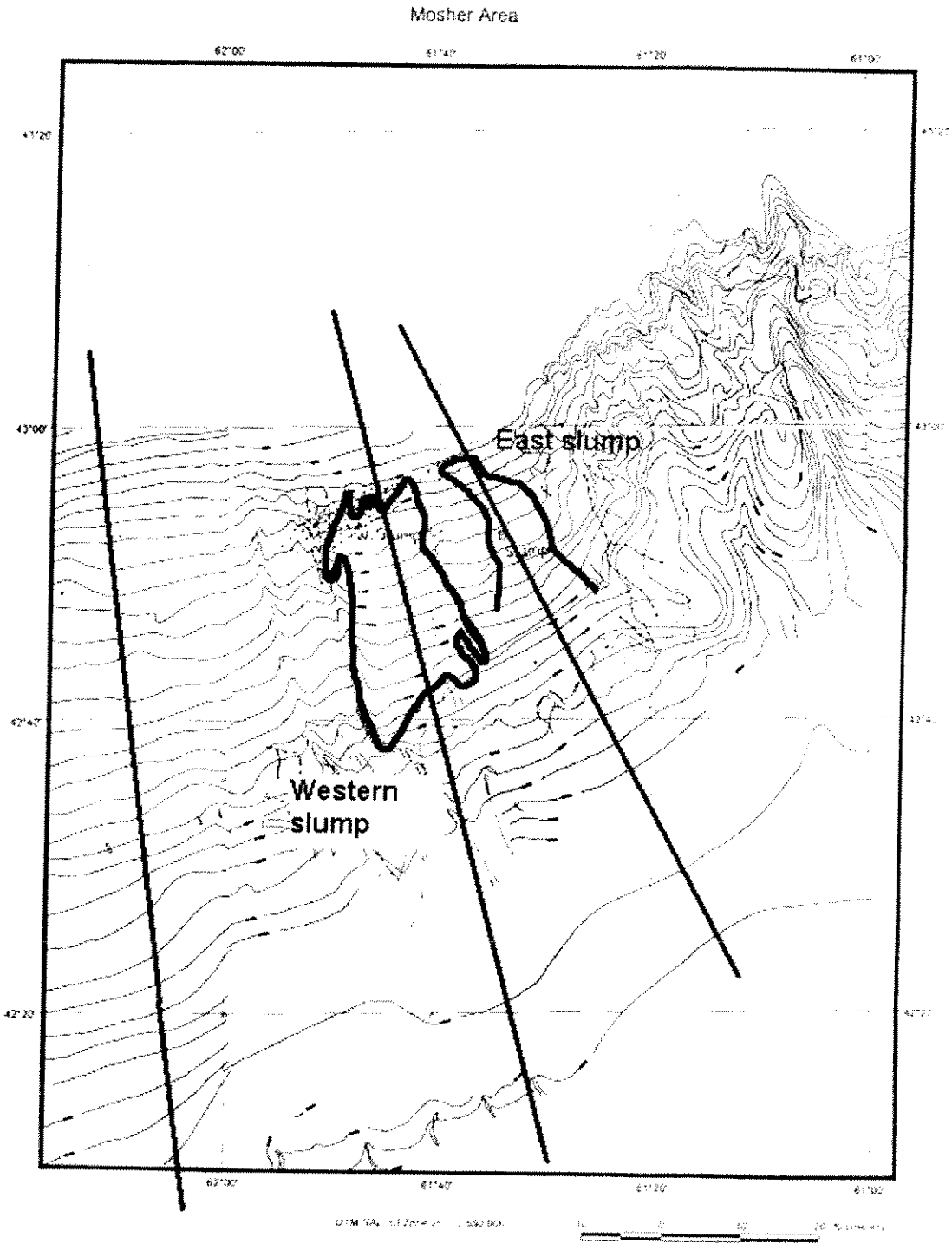

Figure 5-9: Locations of selected slope profiles at Verrill.

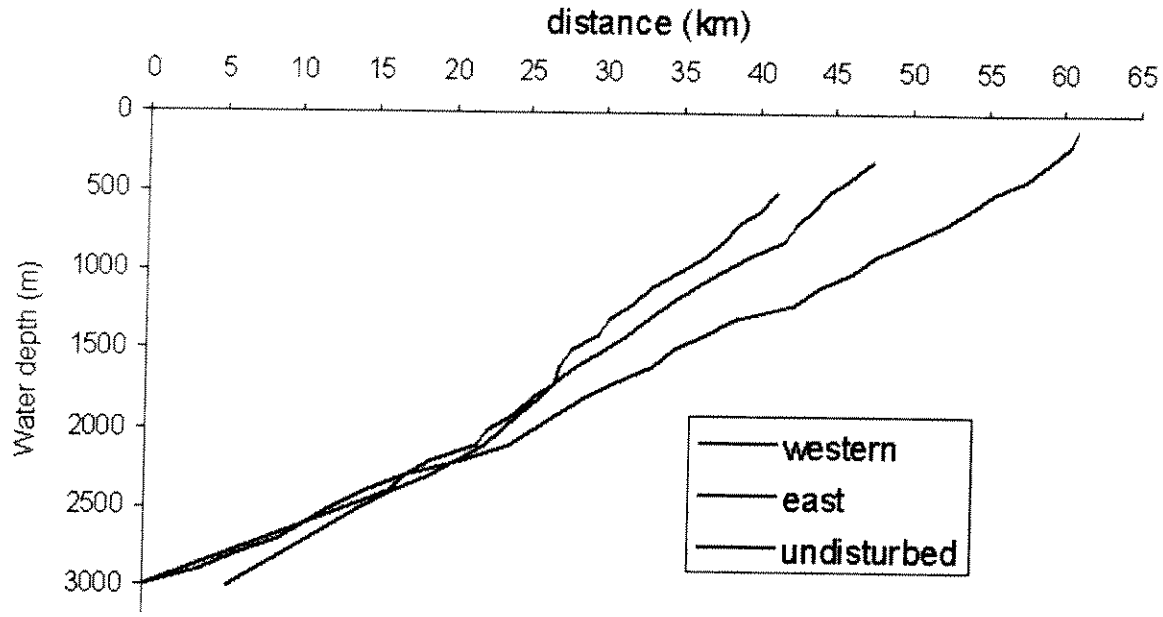

(a) Water depth

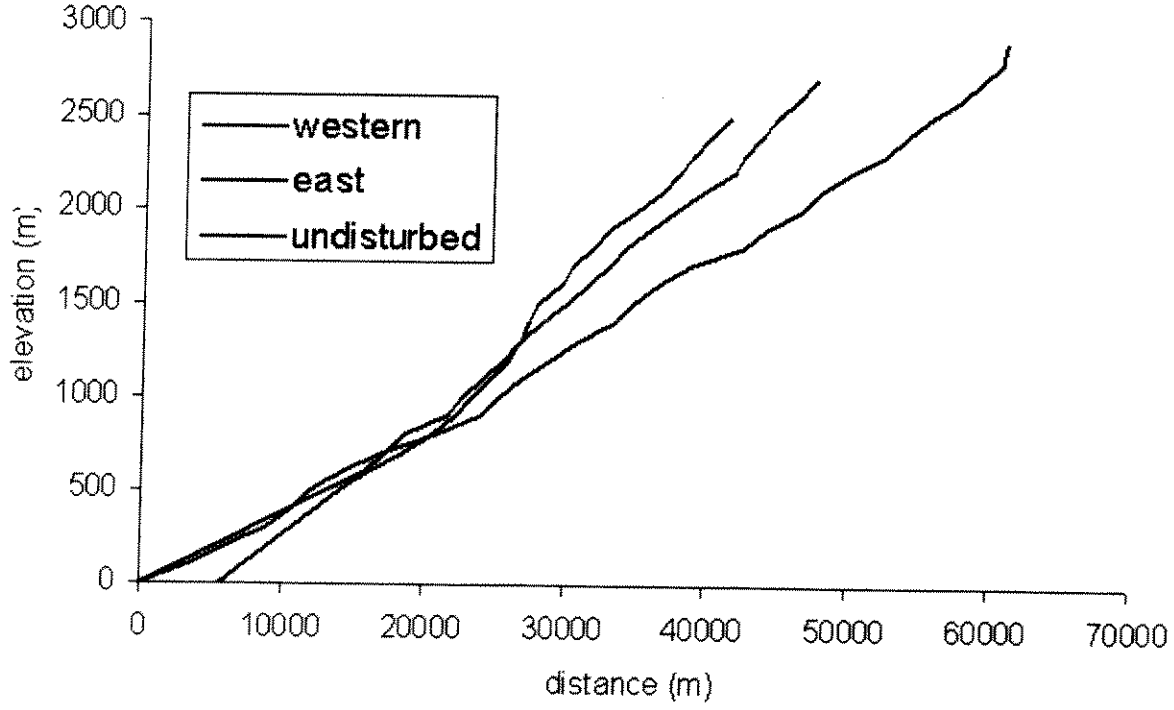

(b) Relative slope elevation

Figure 5-10: Slope profiles.

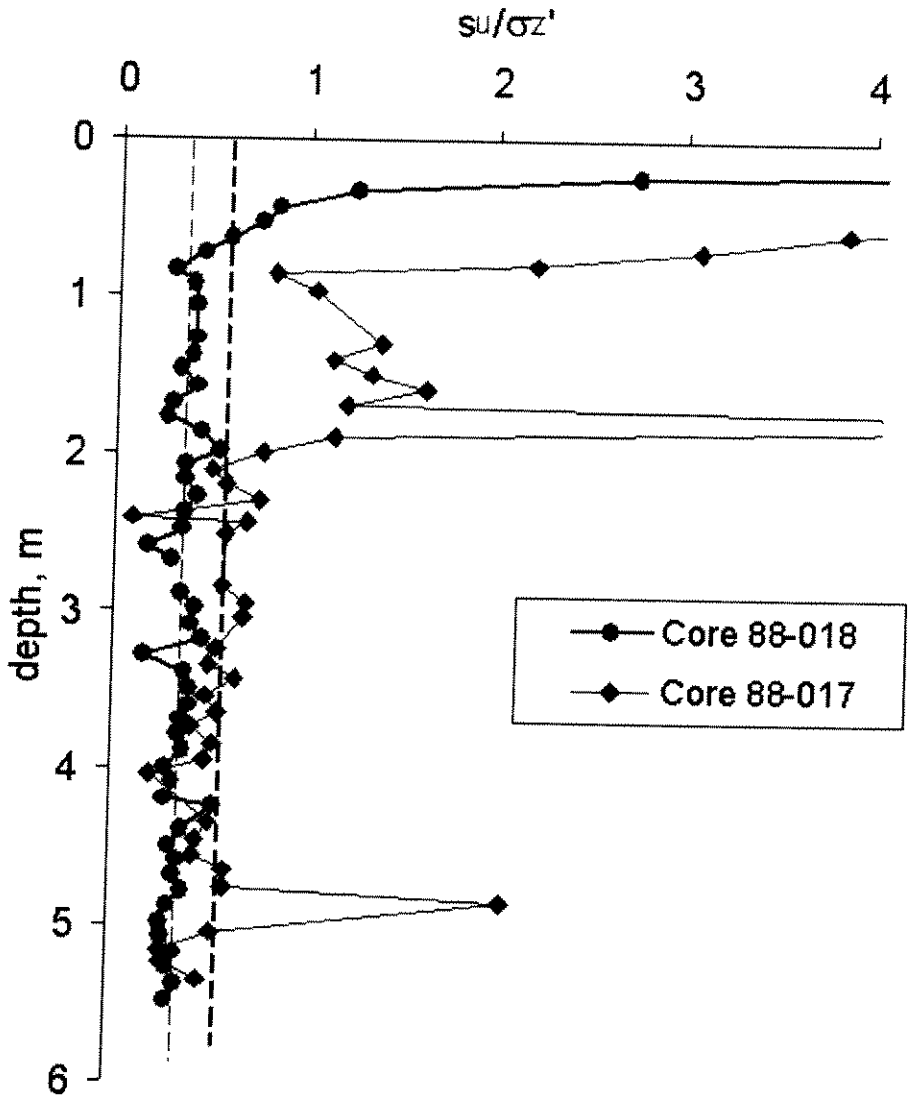

Figure 5-11: Down-core variation in shear strength ratio in cores.

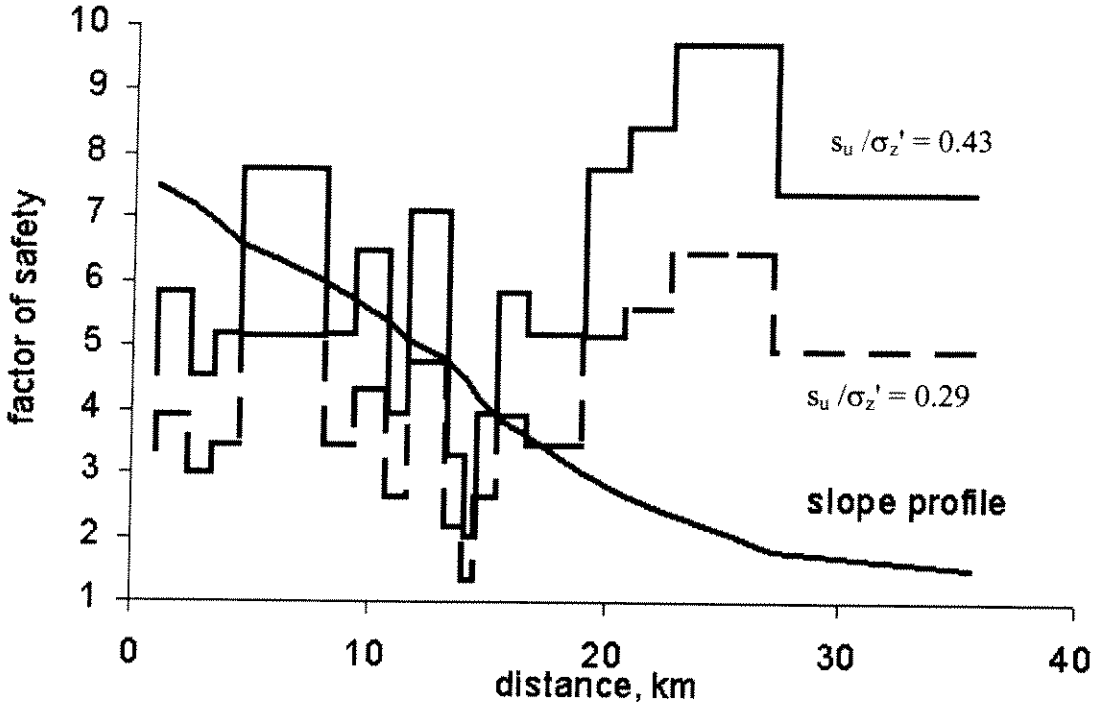

Figure 5-12: Factor of safety: linear sliding plane, eastern Verrill slump.

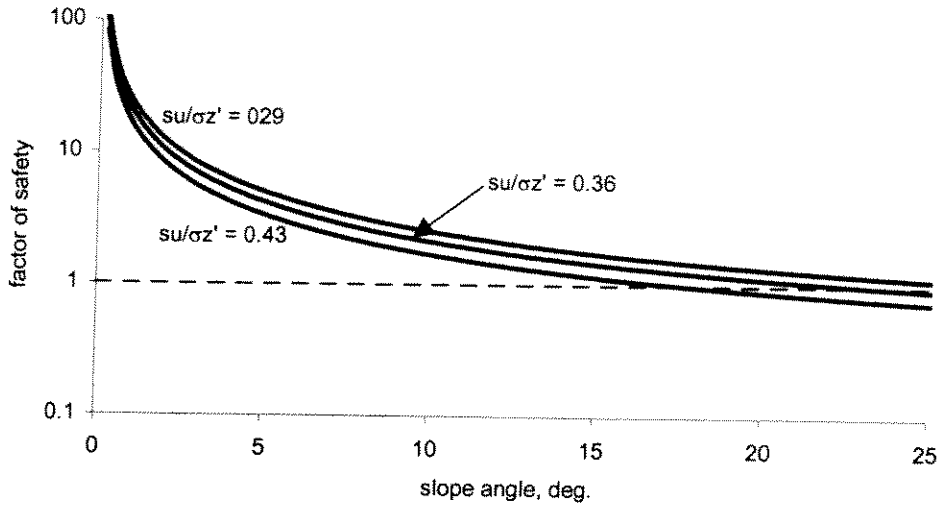

Figure 5-13: Factor of safety: linear sliding plane, Verrill.

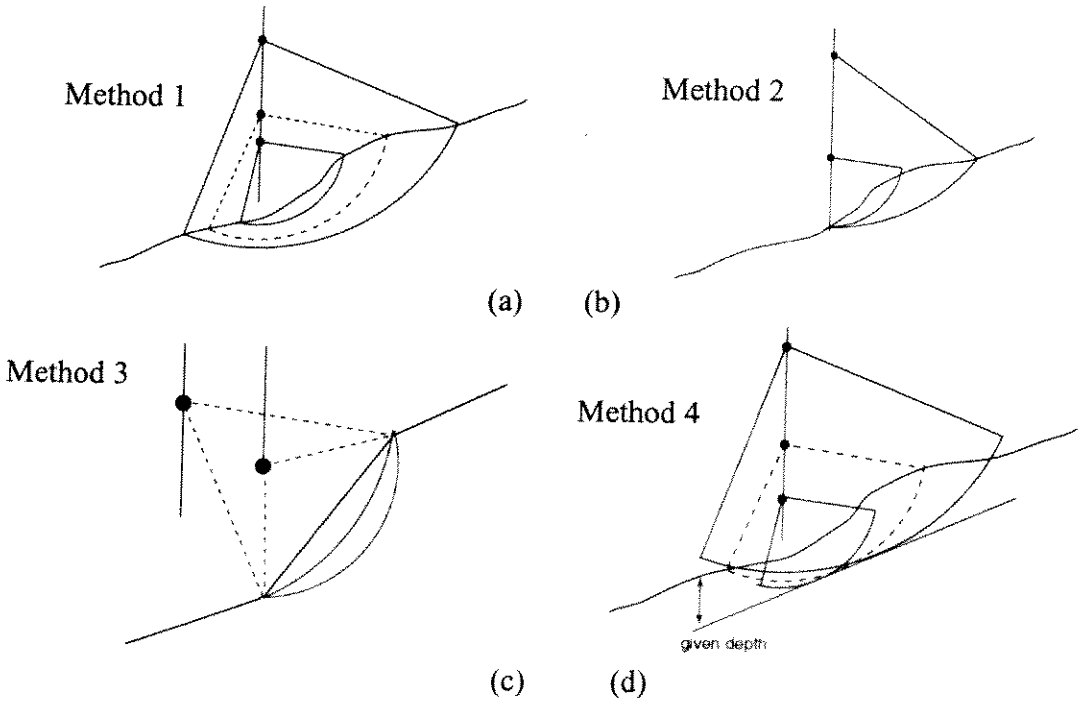

Figure 5-14: Illustration of various searching methods.

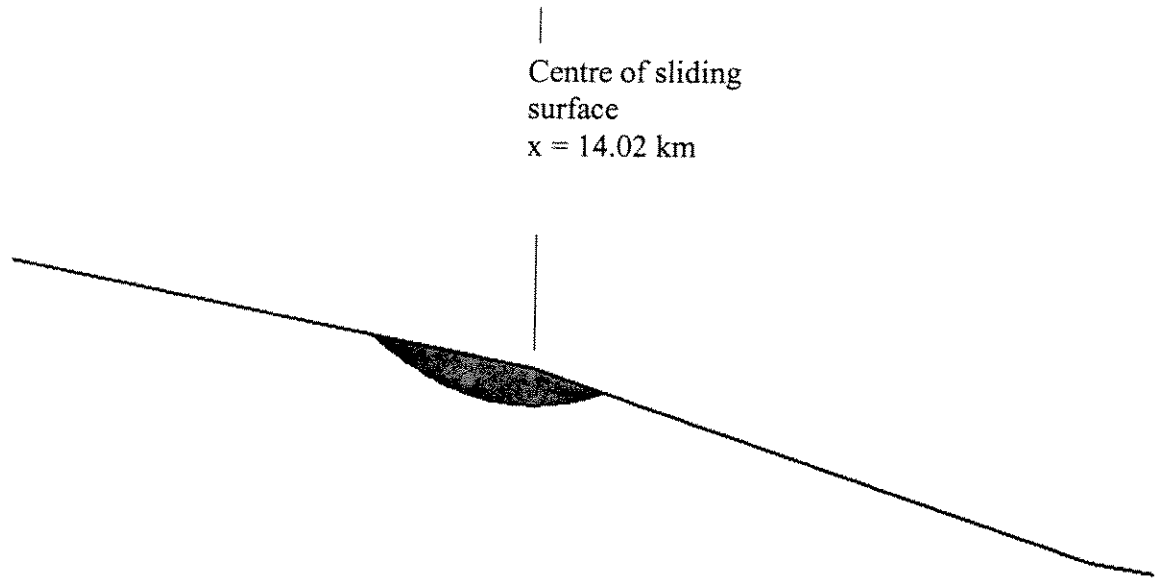

(a) Method1: fs=2.474

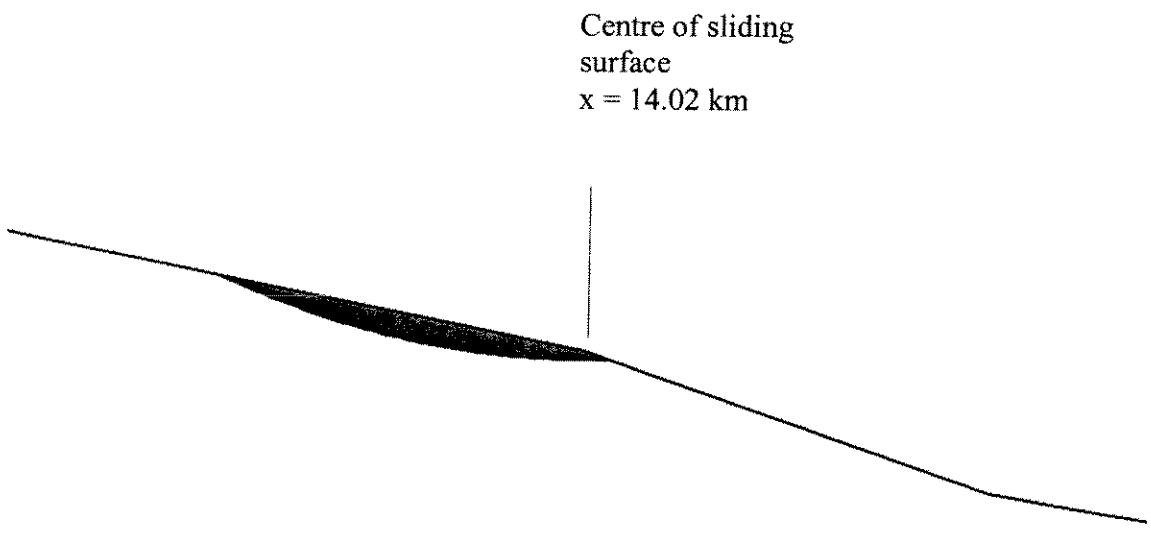

(b) Method 2: fs = 2.686

Figure 5-15: Comparison of Method 1 and Method 2 at location 1.

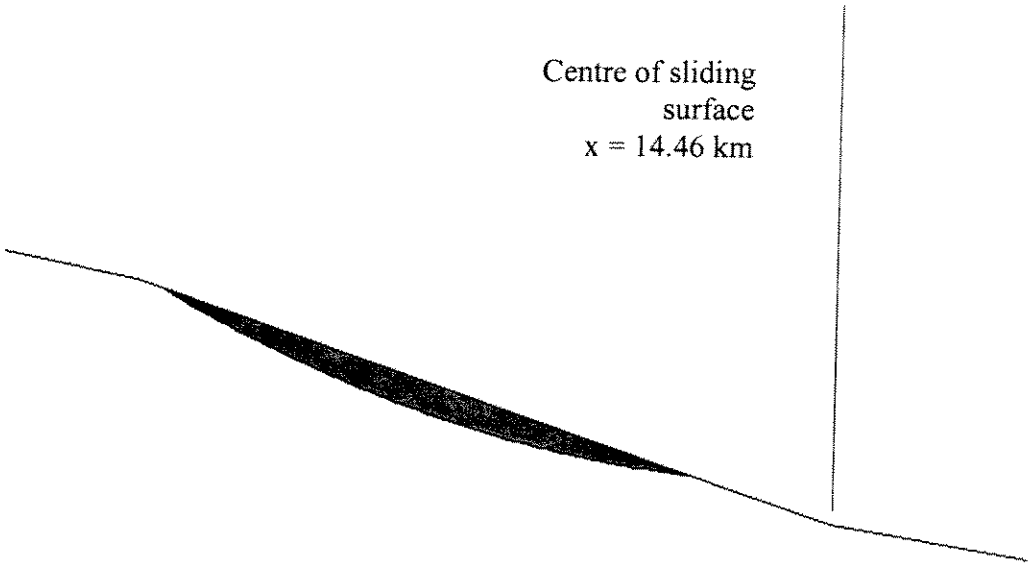

(a) Method 1: fs=1.612

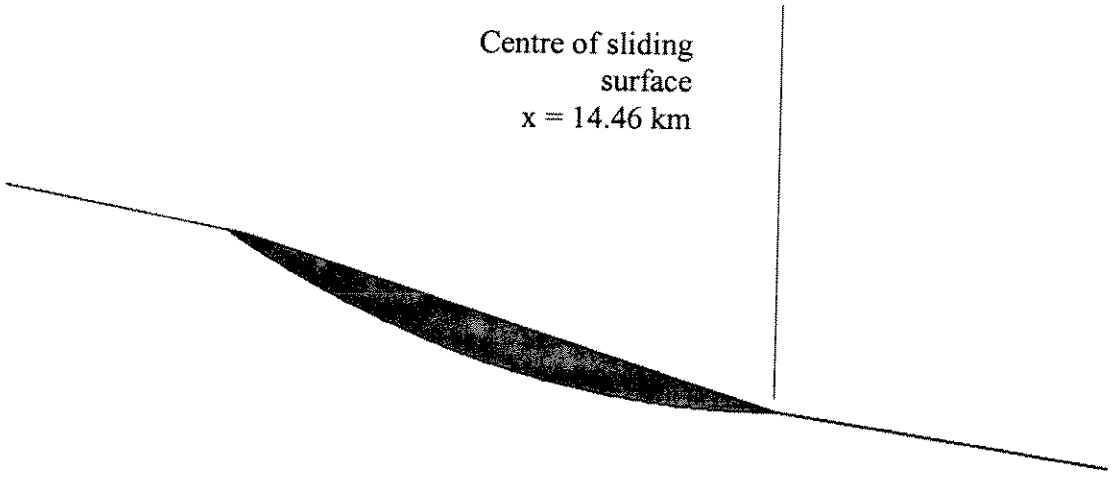

(b) Method 2: fs = 1.634

Figure 5-16: Comparison of Method 1 and Method 2 at location 2.

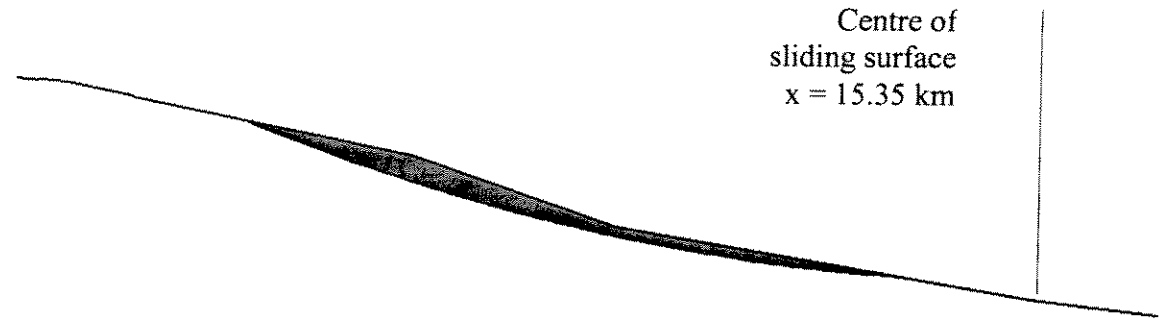

(a) Method 1: fs = 2.126

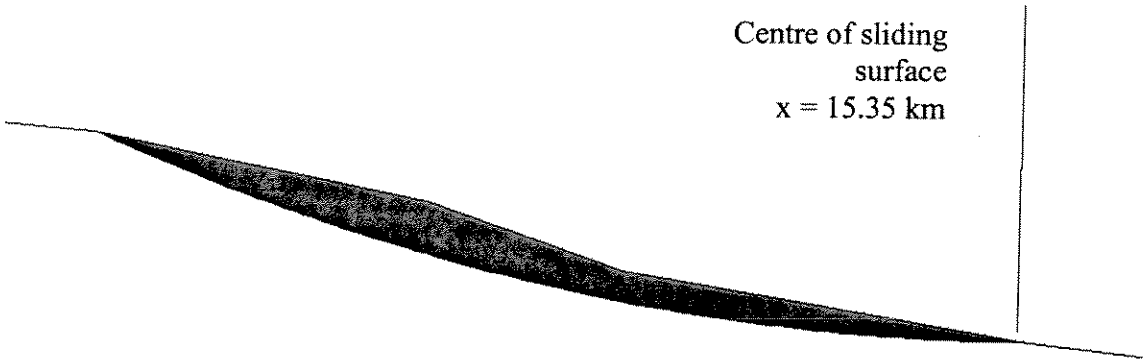

(b) Method 2: fs = 2.335

Figure 5-17: Comparison of Method 1 and Method 2 at location 3.

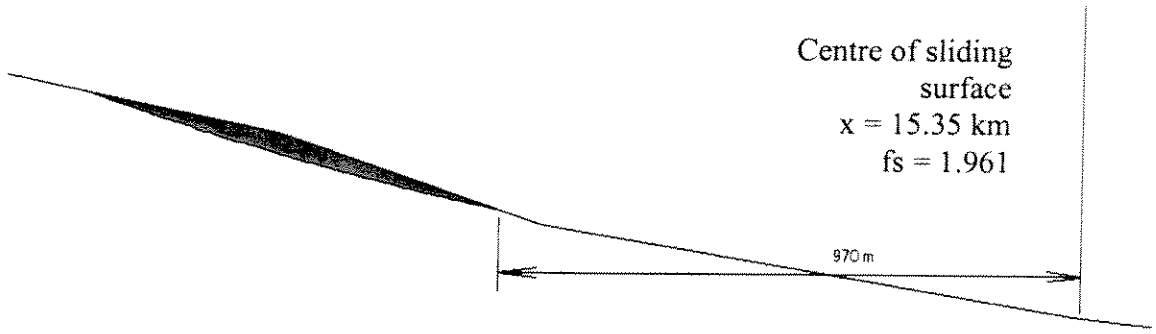

Figure 5-18: Disadvantage in Method 1.

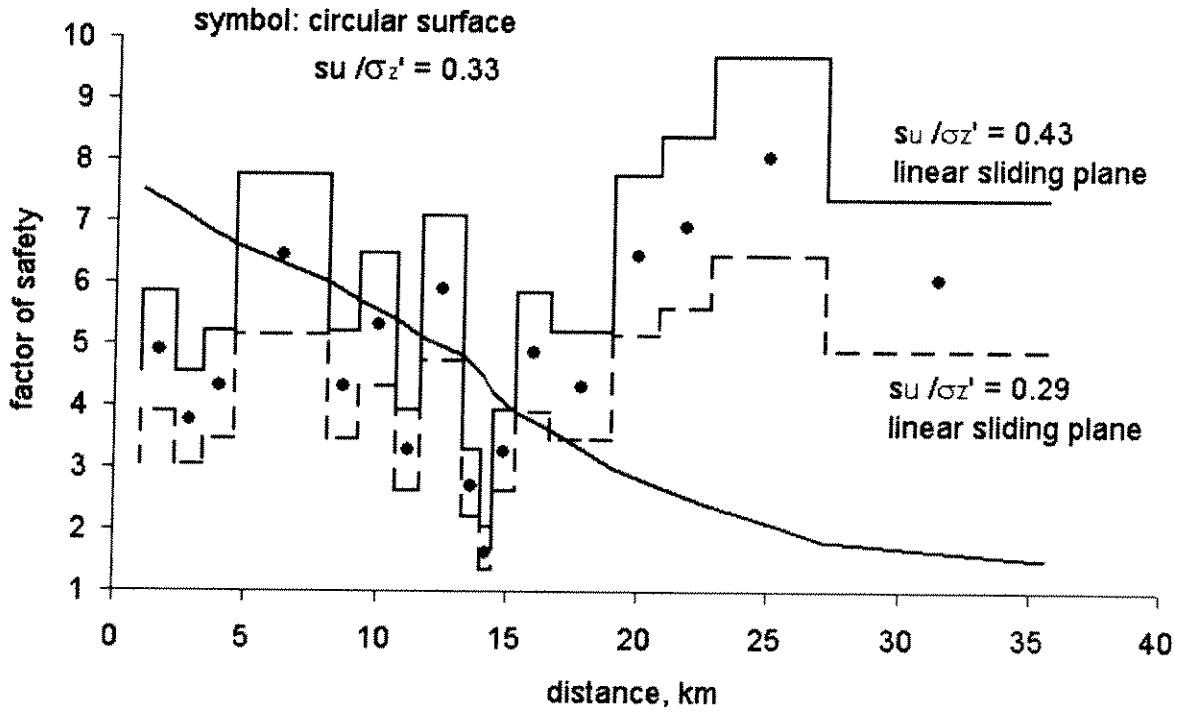

Figure 5-19: Factor of safety along east slump of Verrill.

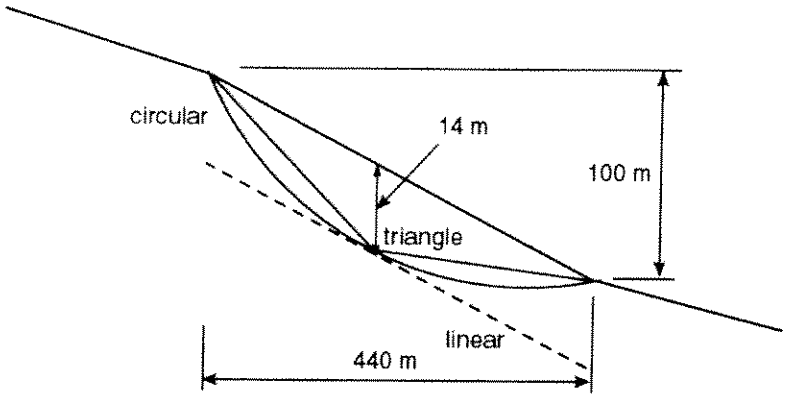

Figure 5-20: Different sliding surfaces at L = 14.02~14.46 km.

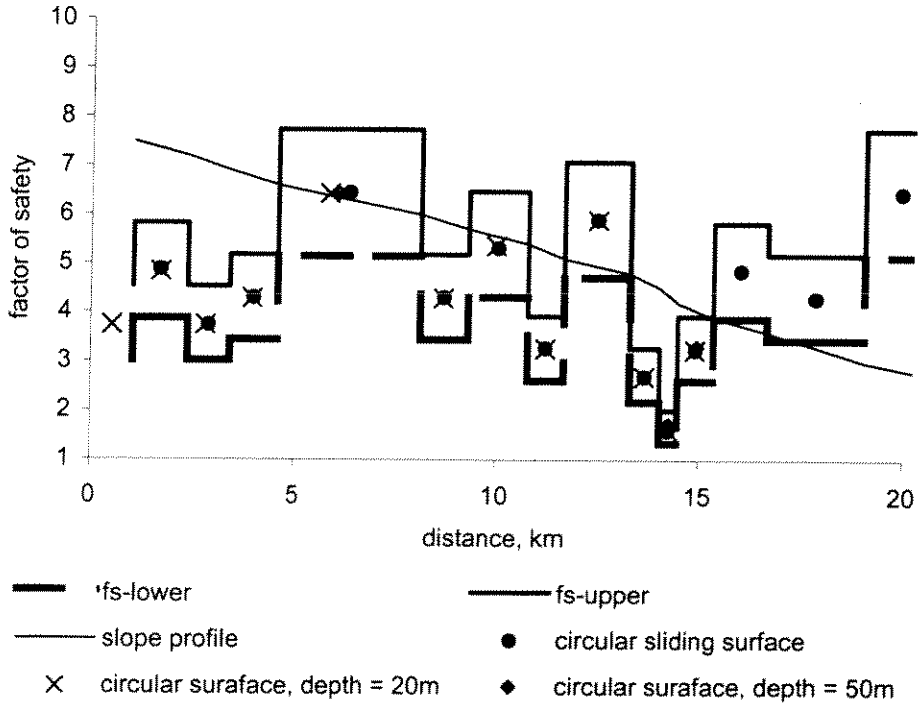

Figure 5-21: Effect of the depth of circular sliding surface on the factor of safety.

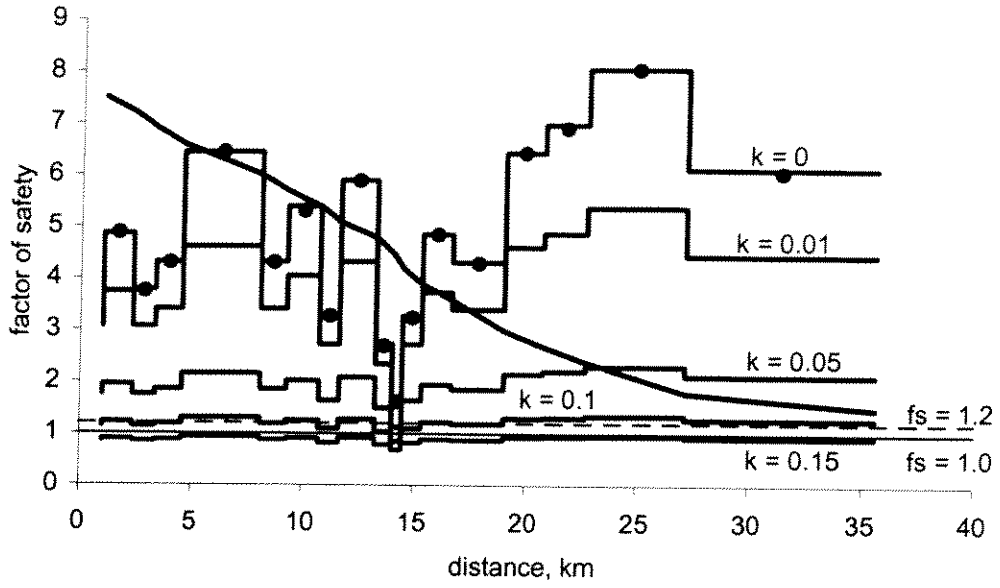

Figure 5-22: Effect of earthquake on the factor of safety of east slump at Verrill: linear sliding surfaces.

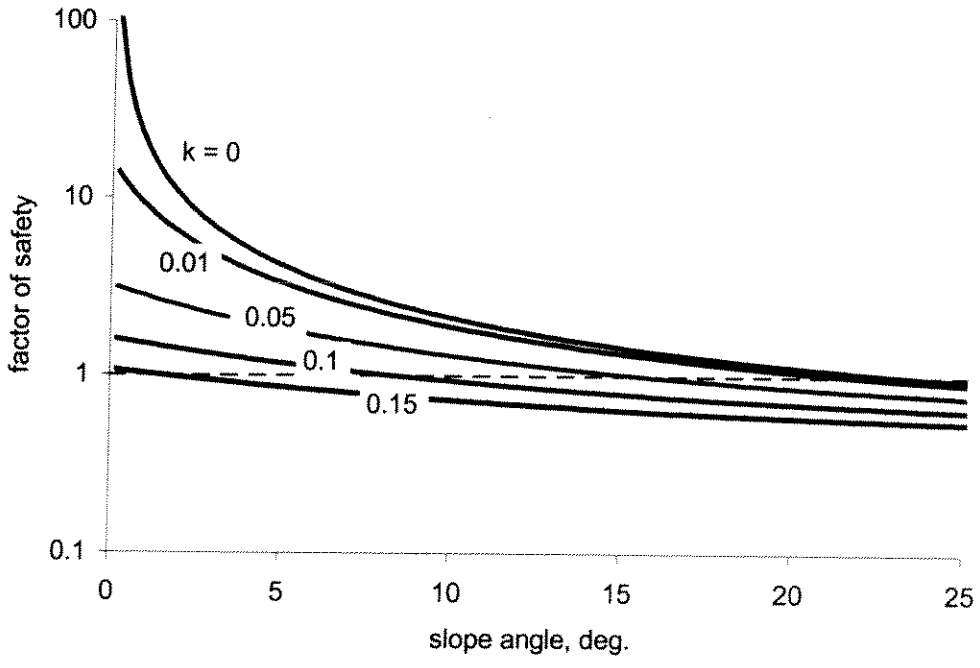

Figure 5-23: Effect of earthquake on the factor of safety with respect to slope angle: linear sliding surfaces.

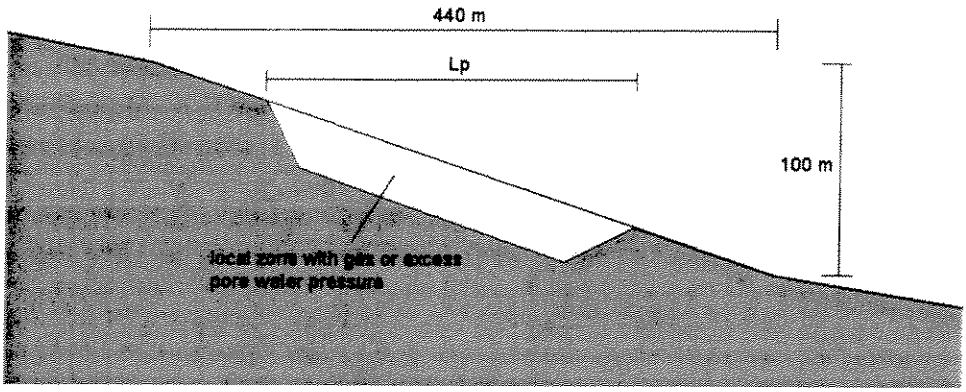

Figure 5-24: Local zone with gas pressure due to gas hydrates, or excess pore water pressure due to earthquake.

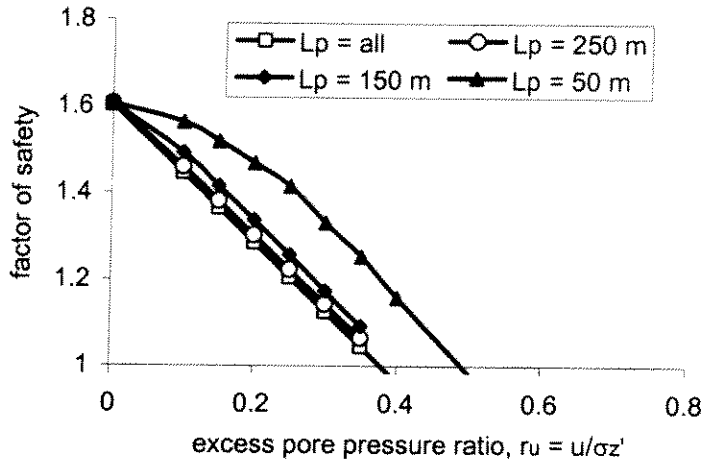

(a) Circular sliding surface with various excess pore pressure zone

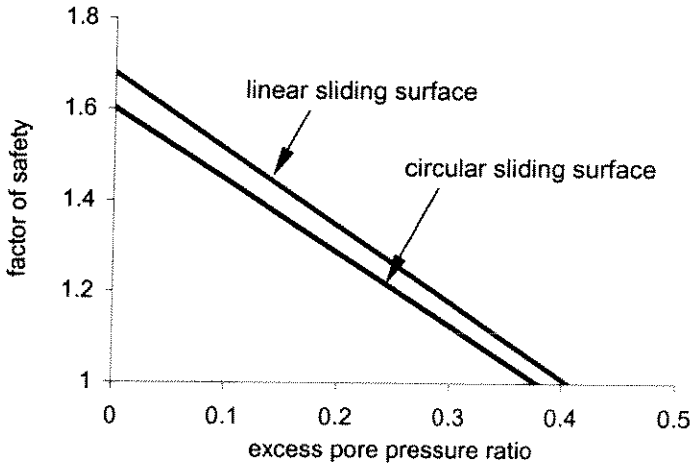

(b) Difference between linear and circular sliding surfaces

Figure 5-25: Effect of local gas or pore water pressure on local stability.

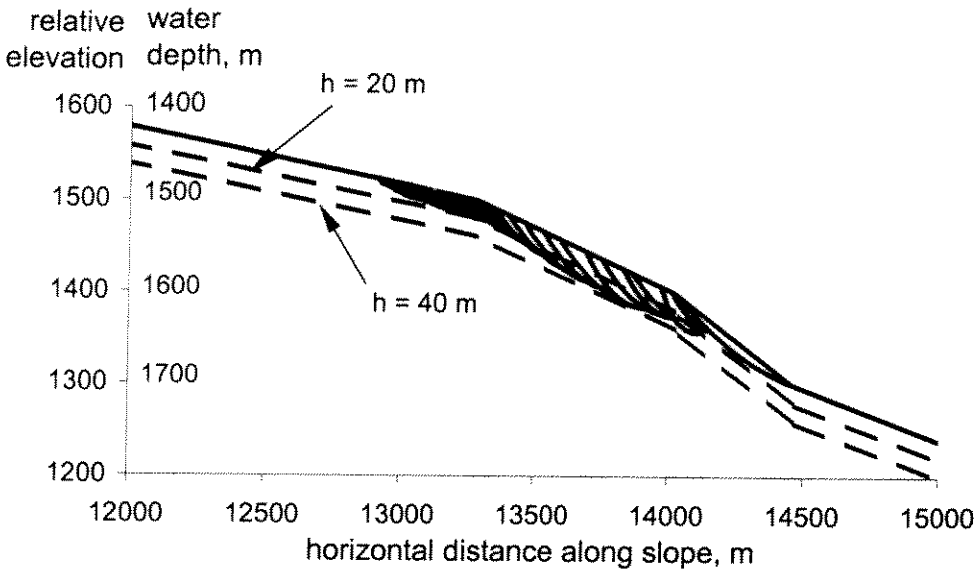

Figure 5-26: Progressive sliding along east slump of Verrill.

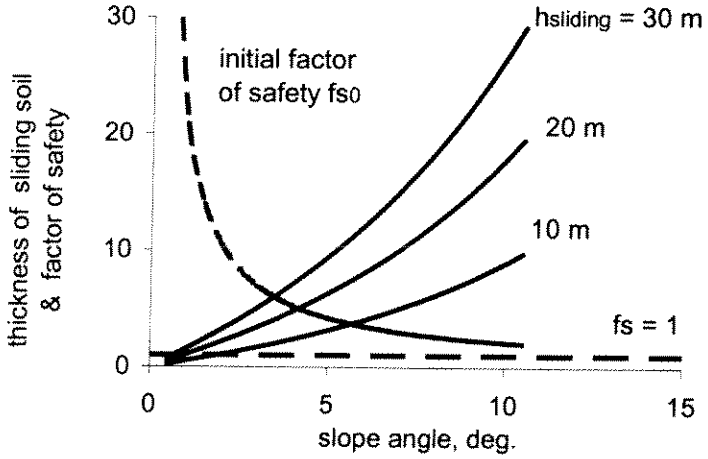

Figure 5-27: Thickness of triggered sliding soil due to upper stream slope failure.

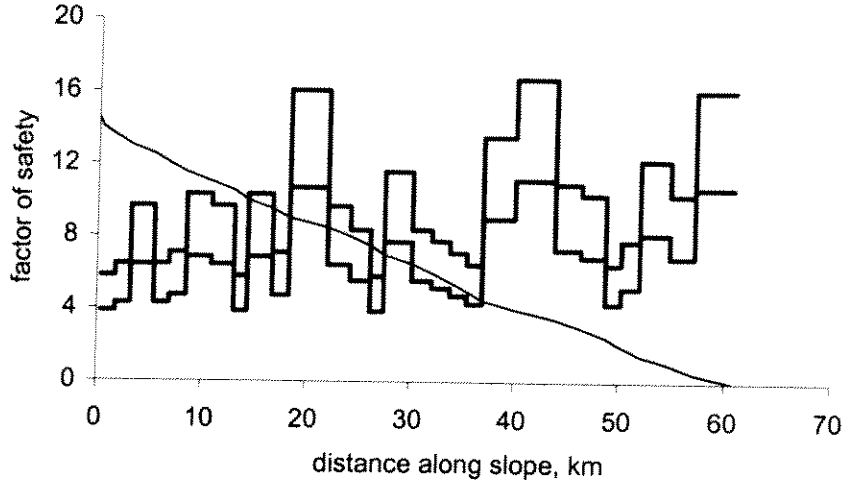

Figure 5-28: Linear sliding surface stability analysis: stable zone at Verrill.

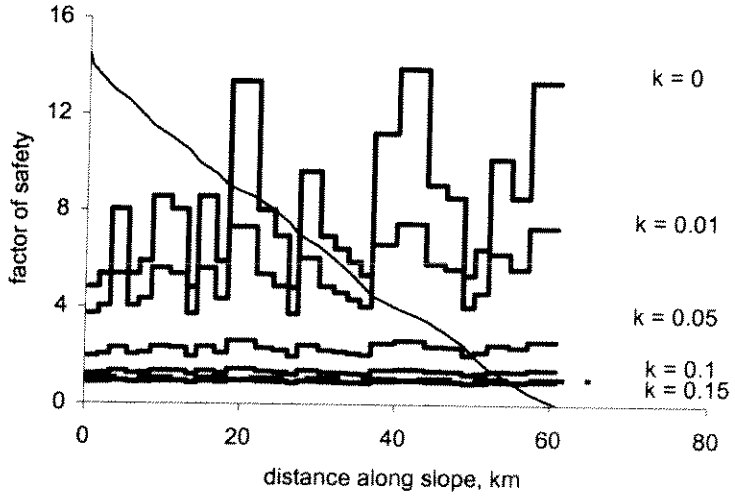

Figure 5-29: Effect of earthquake on the stable area at Verrill.

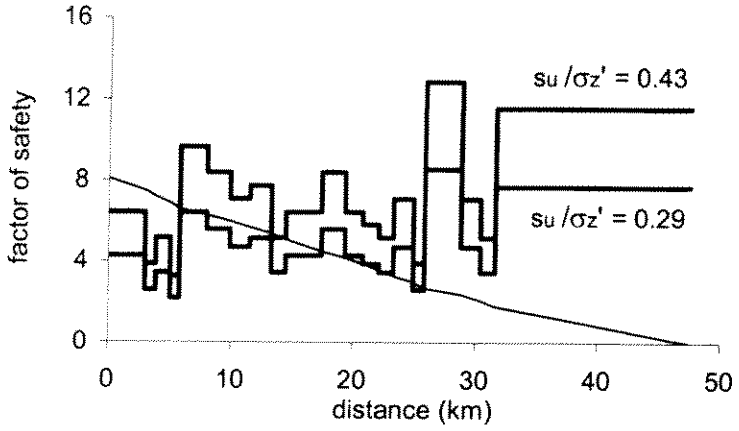

Figure 5-30: Linear sliding surface stability analysis: western slump at Verrill.

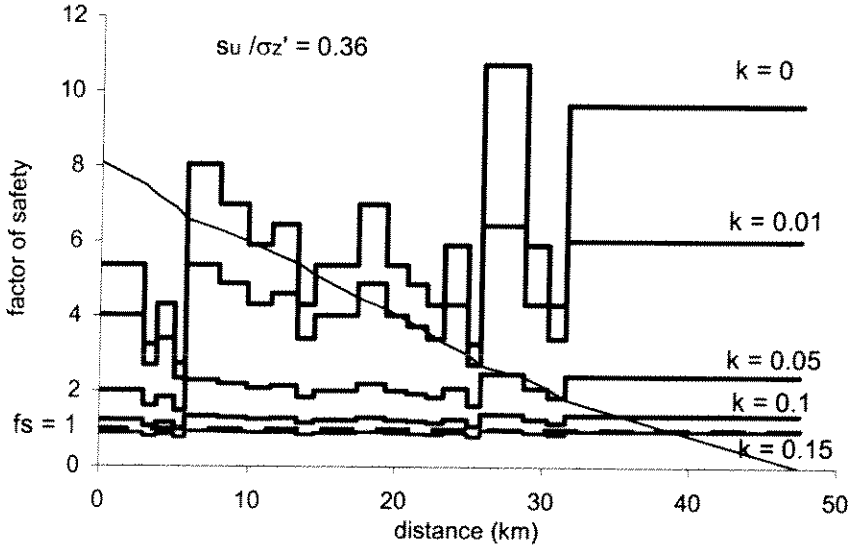

Figure 5-31: Effect of earthquake on the stability of western slump at Verrill.

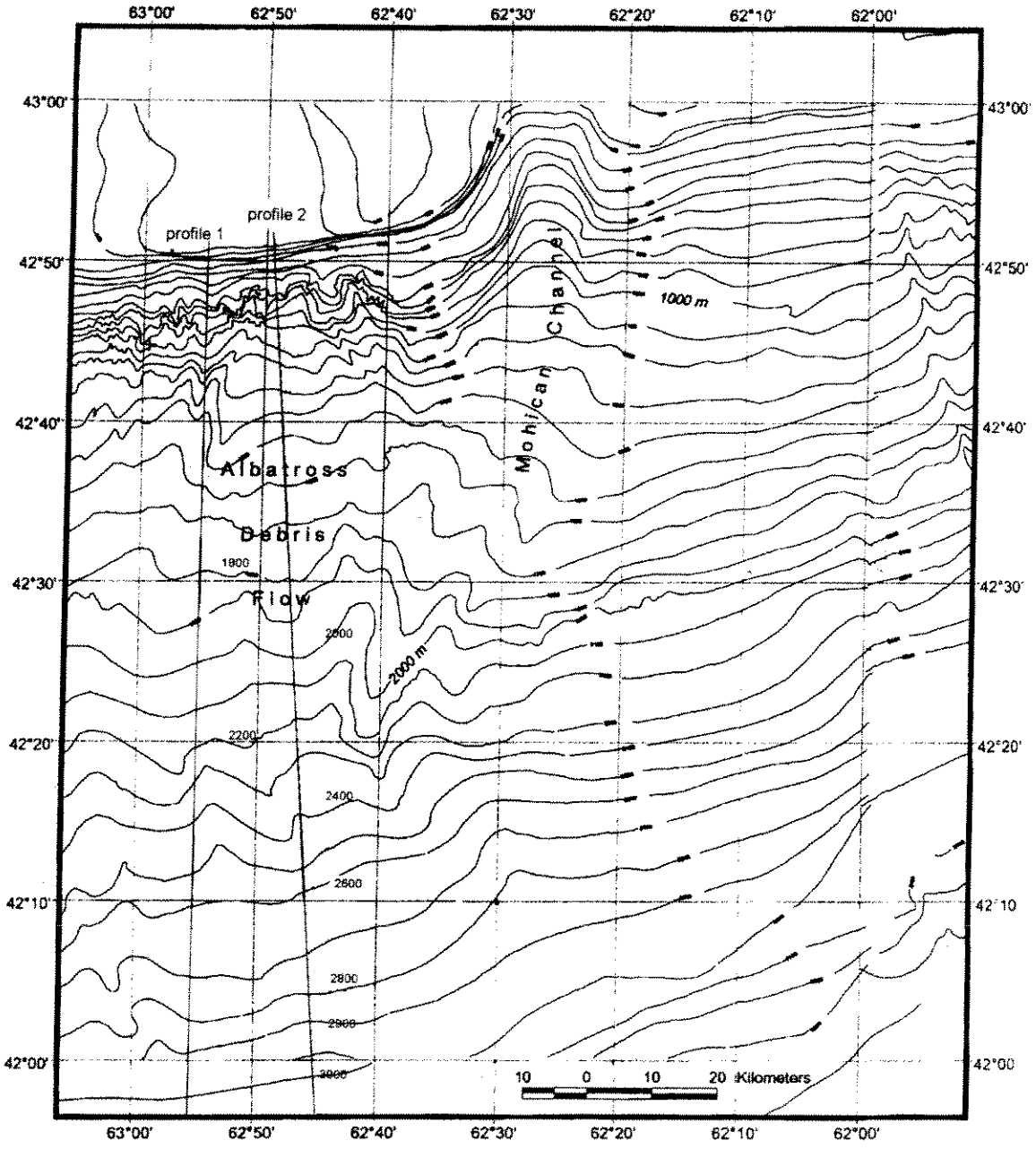

Figure 5-32: Locations of selected slope profiles at Albatross.

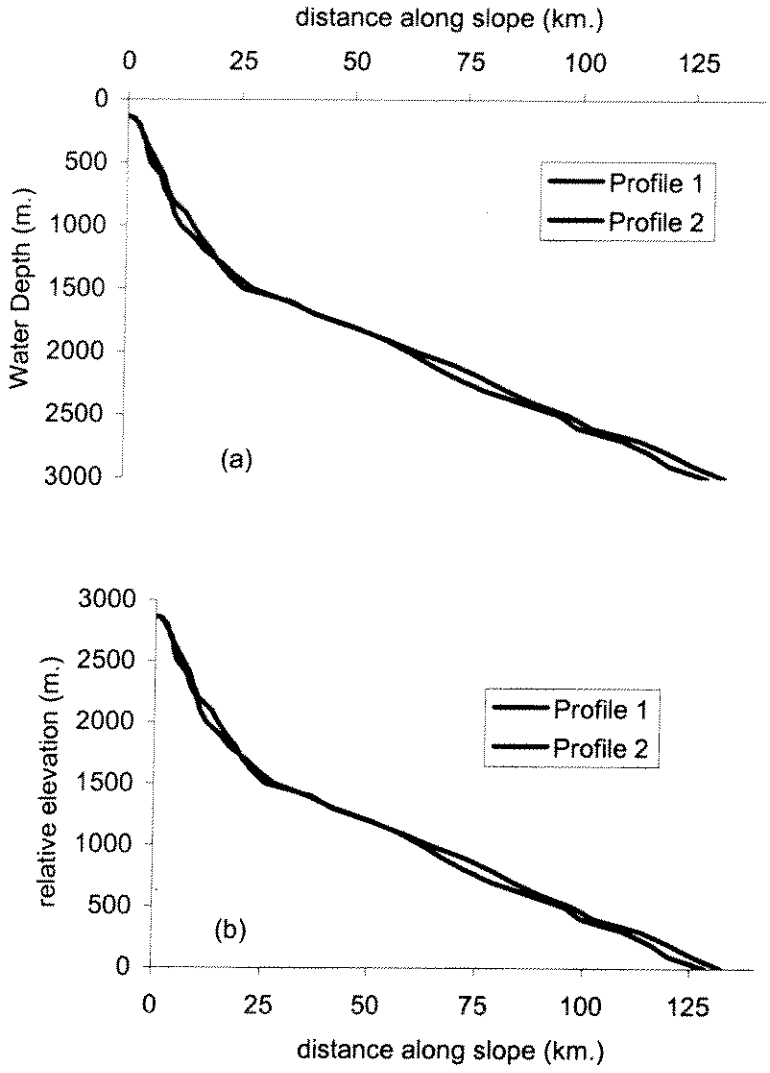

Figure 5-33: Slope profiles at Albatross: (a) Water depth; (b) relative elevation.

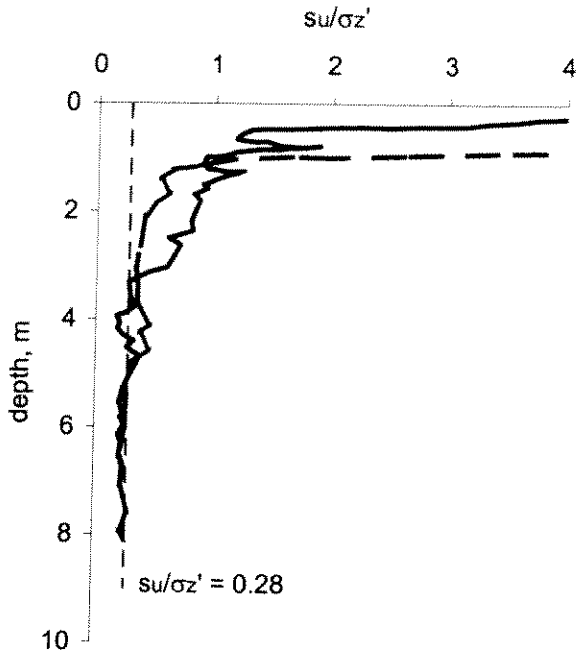

Figure 5-34: Down-core variation of shear strength ratio at Albatross.

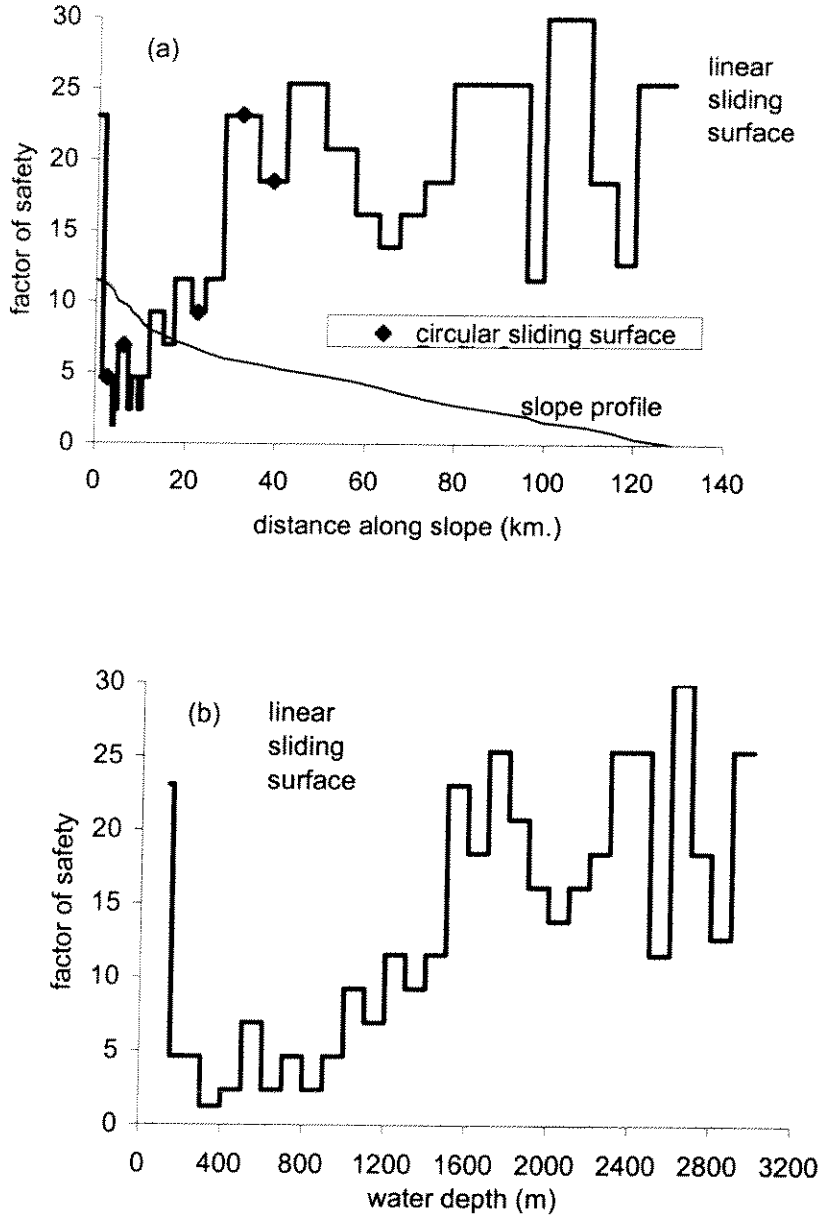

Figure 5-35: Factor of safety: linear and circular sliding surfaces along slope profile 2.

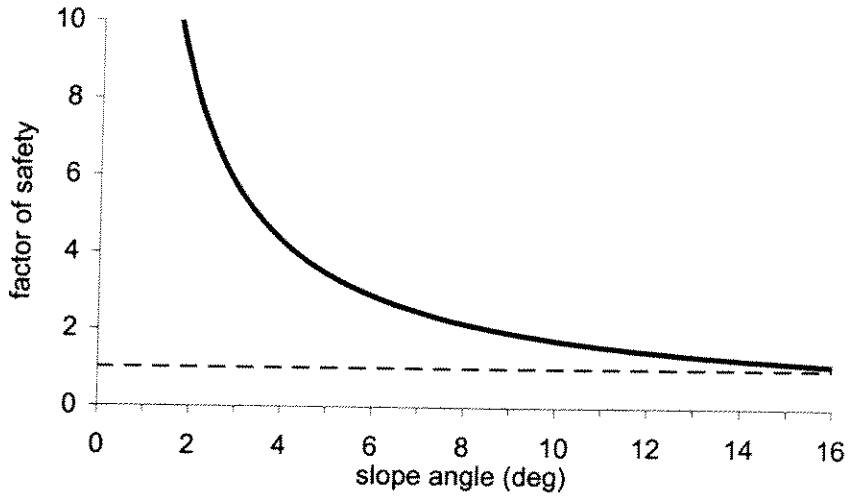

Figure 5-36: Variation of factor of safety with slope angle at Albatross.

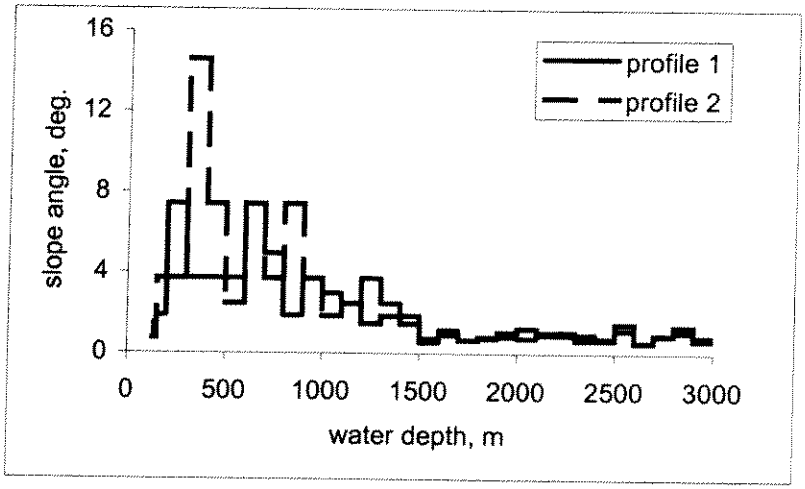

Figure 5-37: Slope angles at Albatross.

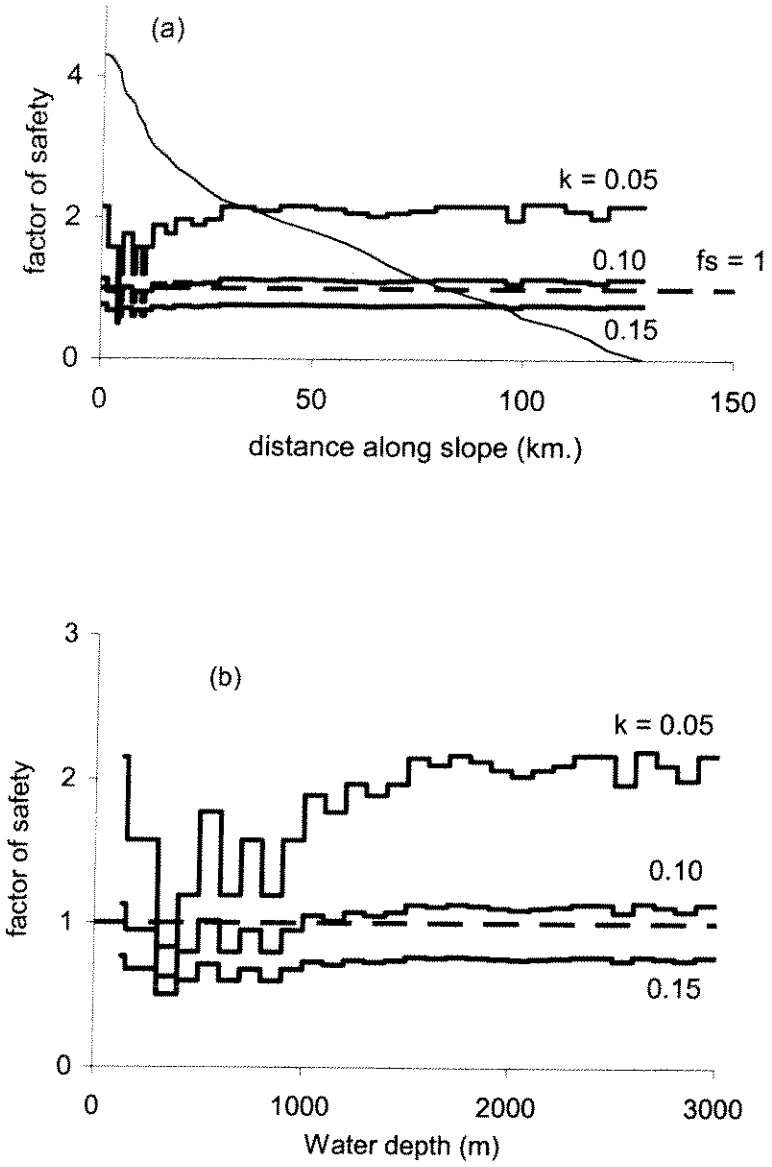

Figure 5-38: Slope stability during earthquake: Albatross.

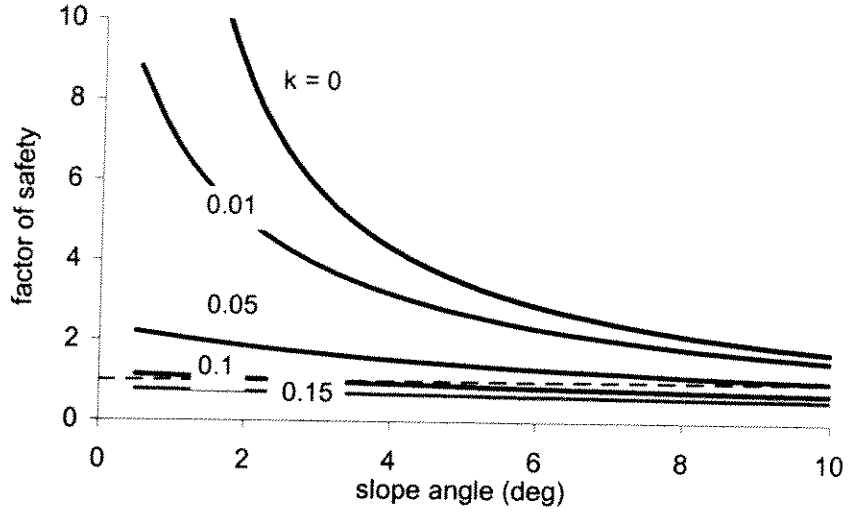

Figure 5-39: Effect of earthquake on slope stability at Albatross.

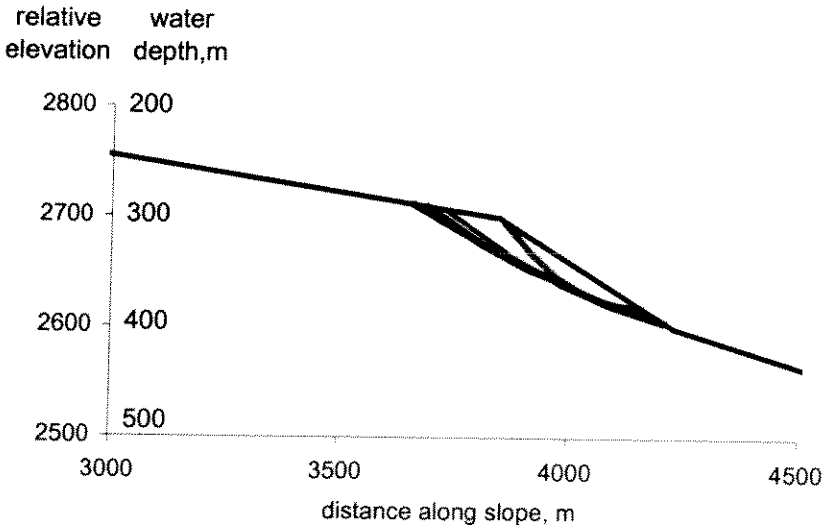

Figure 5-40: Retrogressive failure mechanism.

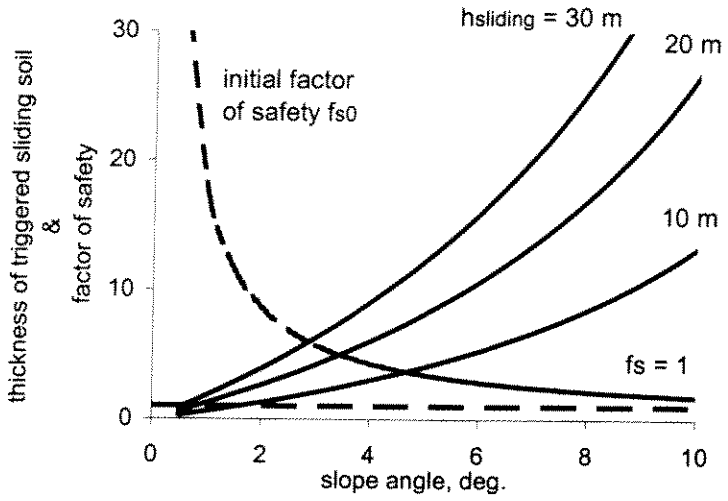

Figure 5-41: Thickness of triggered sliding soil due to upper stream slope failure.

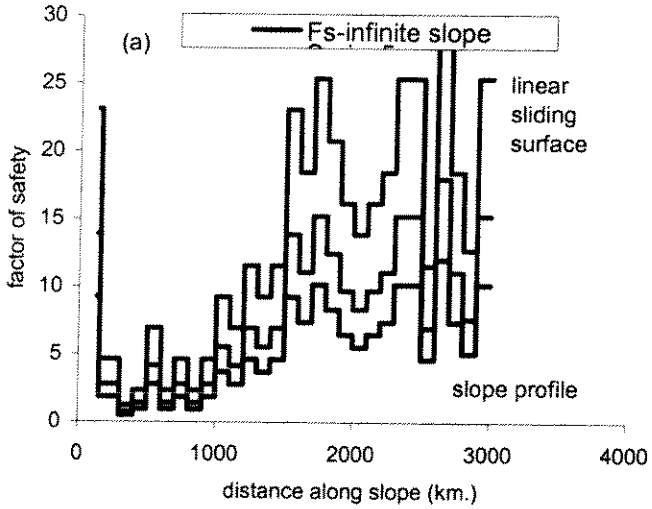

Figure 5-42: Factor of safety along slope.

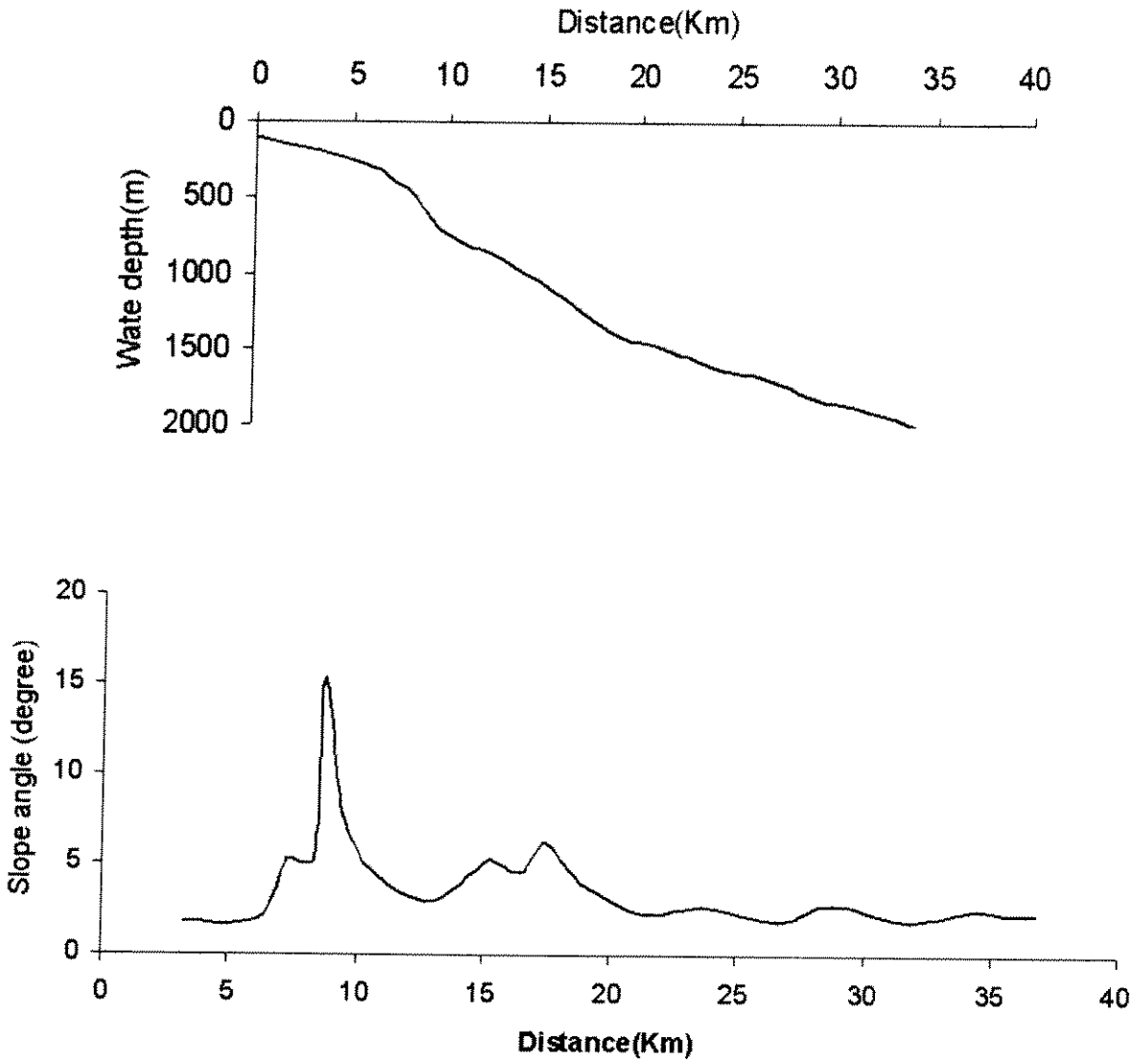

Figure 5-43: Slope profile of Logan.

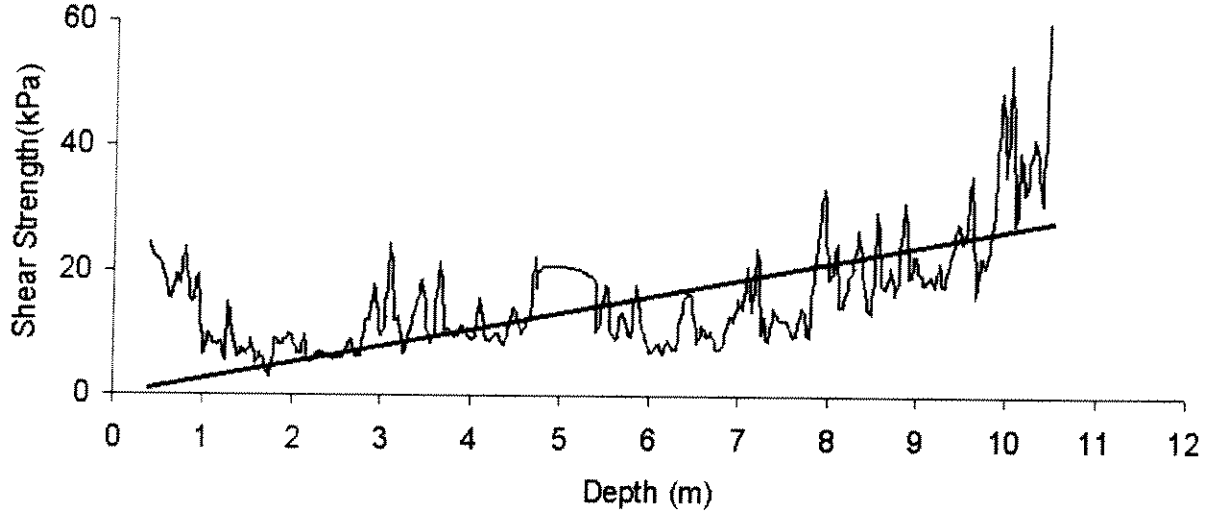

Figure 5-44: Geotechnical profile of Logan (Core99036-18).

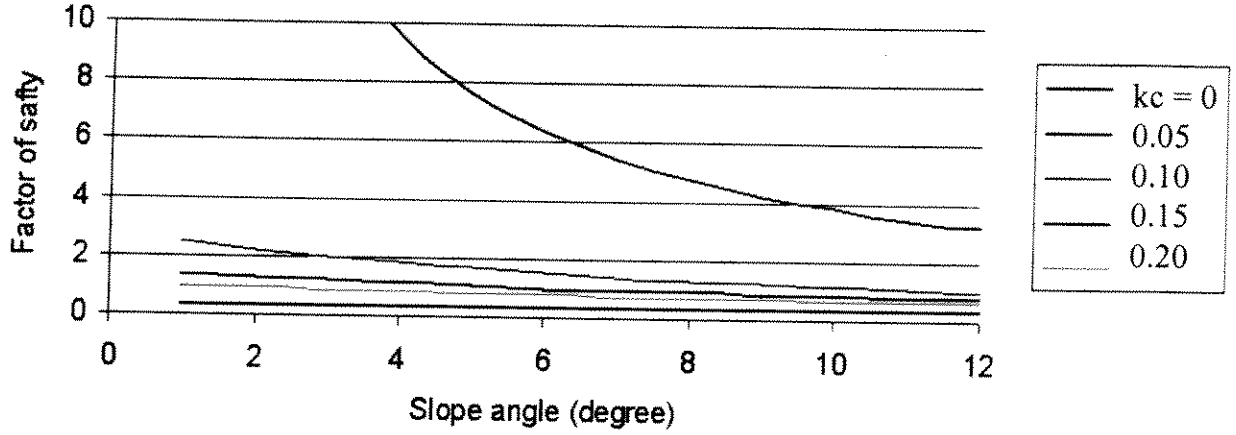

(a)

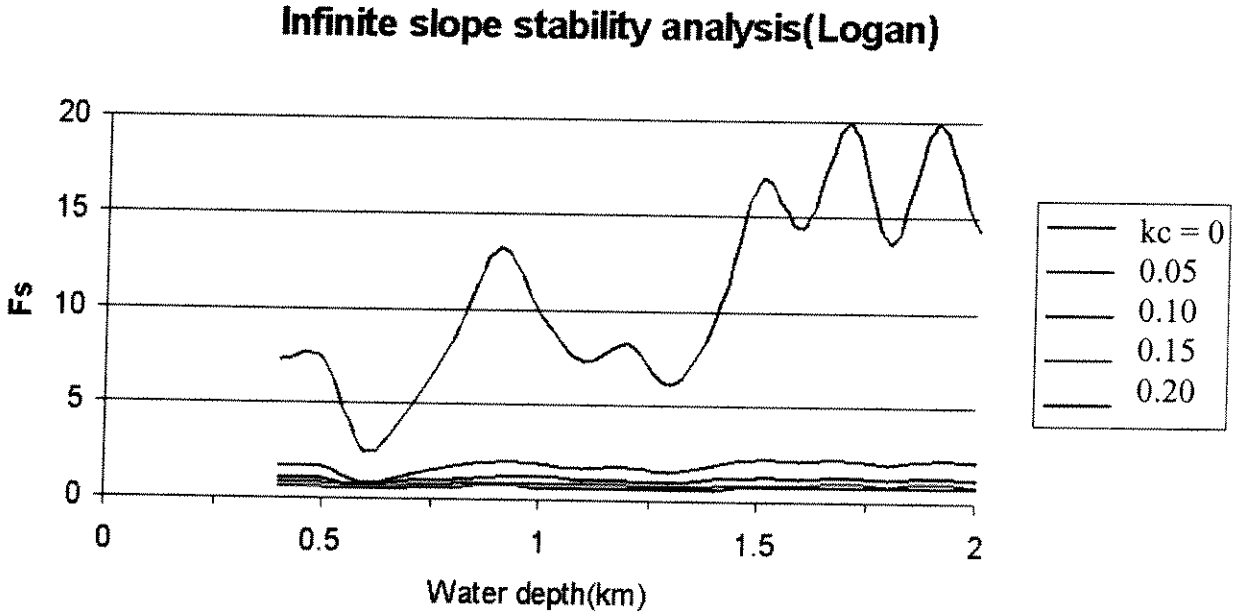

(b)

Figure 5-45: Infinite slope stability analysis for Logan.

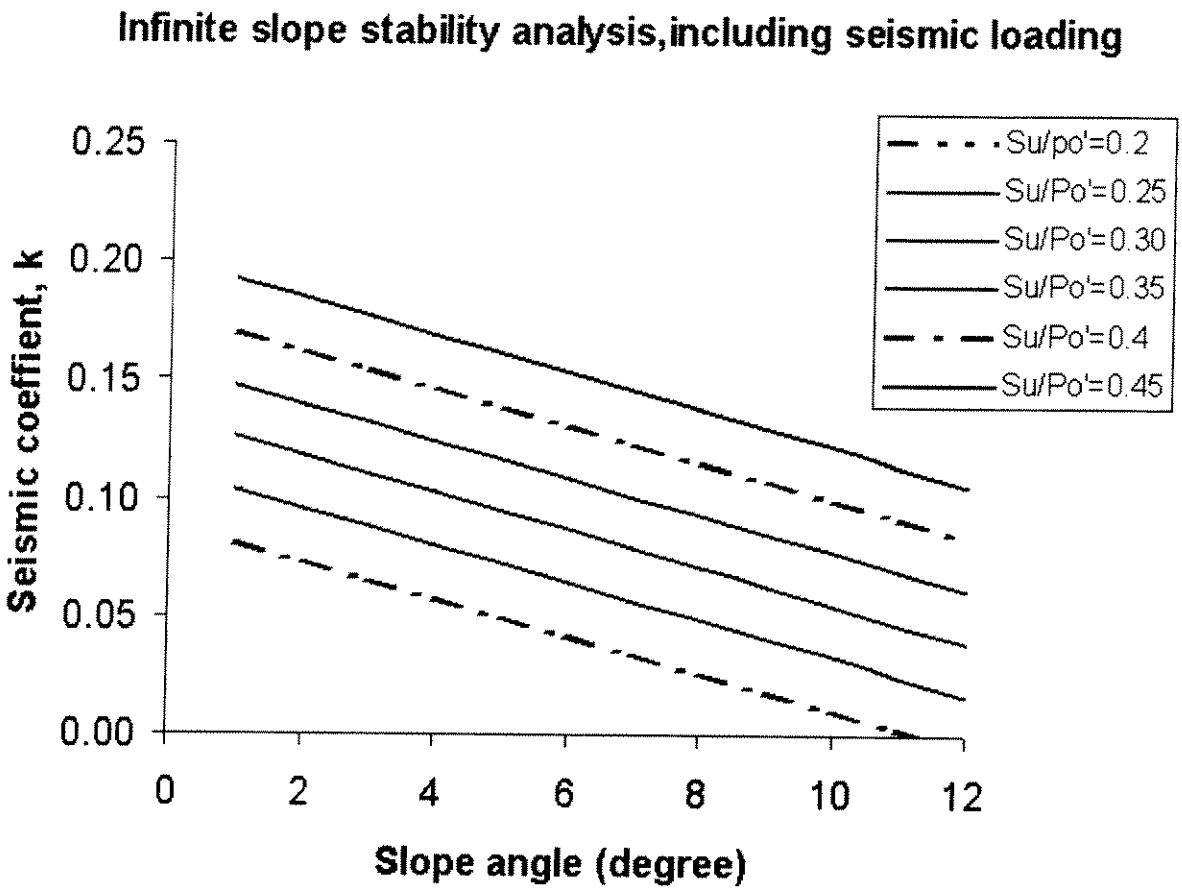

Figure 5-46: Infinite slope stability analyses, including seismic loading.

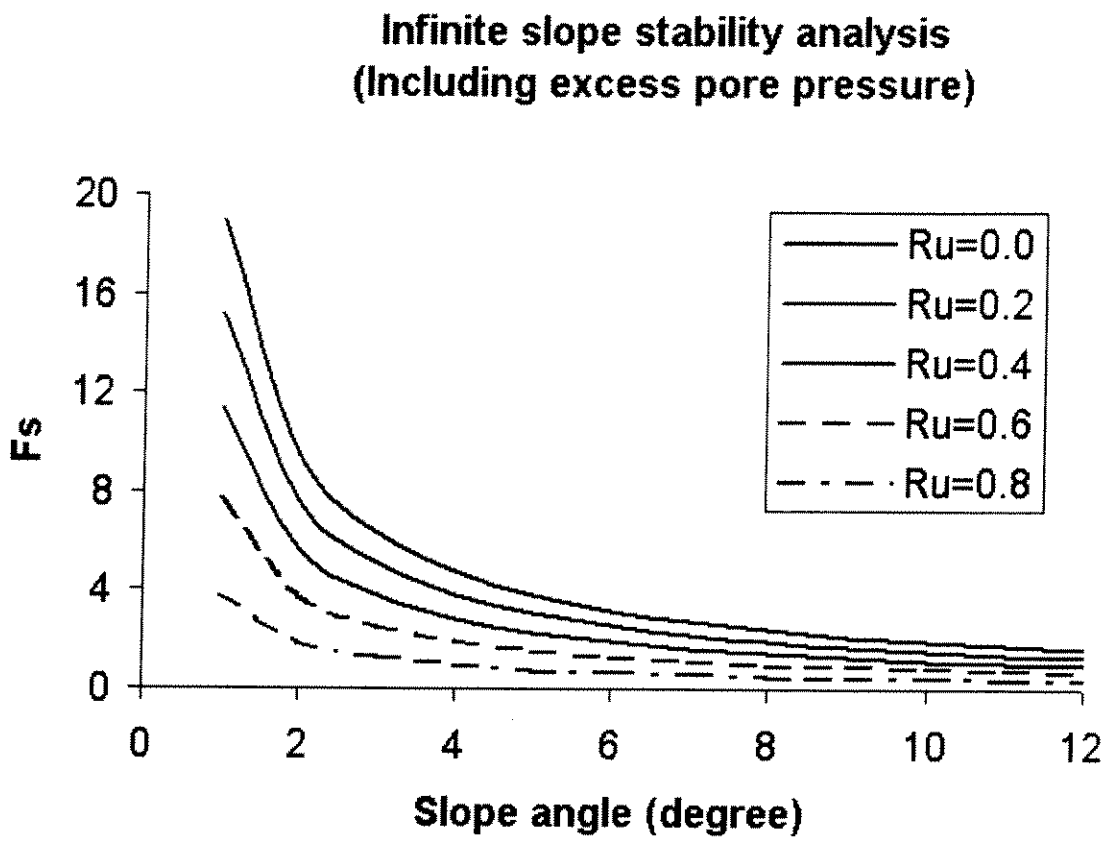

Figure 5-47: Infinite slope stability analysis, including excess pore pressure.

6 DESCRIPTION AND EVALUATION OF GRAND BANKS FAILURE

As part of the PODS Phase I task C-1 "Regional In Depth Study: Scotian Shelf/Slope, Flemish Pass and GOM", the Norwegian Geotechnical Institute (NGI) have evaluated the 1929 Grand Banks (GB) submarine slide failure. The description and evaluation of the failure, presented in this Section, are based on information provided by Geotechnical Survey of Canada - Atlantic (GSC-A). From the review of this information, support is found for a hypothesis that the GB slide failure was initiated in soil layers of mostly sensitive and strain-softening clay or clayey material by inertia loading from the GB earthquake of the same day.

However, it must be noted that the soil layering and geotechnical parameters are still very uncertain, due to the limited information of the GB area that has been available. Soil samples are available only from cores down to maximum 8 m depth below seabed. There exists, as far as we know, no comprehensive soil investigation report summarizing the available geotechnical information of the area. The same is true for the results from the sub-bottom seismic profiling.

6.1 Introduction

The Grand Banks submarine slide failure of November 18th 1929 is located south of the island St. Pierre on the continental slope outside of Newfoundland, Canada, see Figure 6.1. The failure is characterized by widespread clay slumping with small, 2-5 m deep, and large, 5-25 m deep slumps covering large areas today. The failure was initiated by the "Grand Banks earthquake" of the same day. The failure evolved into a turbidity current travelling at a velocity that peaked at more than 19 ms^{-1} and deposited >150 km^3 of sediments on the Sohm Abyssal Plain. The turbidity current broke cables up to 13 h after the earthquake.

In this Section the description and evaluation of the GB failure is given. The description of the failure in terms of series of events, geological setting and present-day seabed morphology, is more or less directly taken as a summary of the paper by Piper et al. (1999).

The soil conditions and geotechnical properties of the site area are presented. This is based on the material in Christian et al. (1991), Piper et al. (1999), Piper et al. (1987), Marsters (1986), Klohn (1993) and boring profiles from test on core samples. All the materials were provided by GSC-A, and interpreted by NGI. Special emphasis is devoted to the peak undrained shear strength and the strain-softening characteristics of the clay materials.

A back-calculation of the necessary earthquake acceleration forces to initiate the failure is presented. Also a probable mechanism causing the retrogressive spreading of the failure will be presented and discussed.

A summary with conclusions is included in a separate section at the end of Section 6.

6.2 Presentation of Slide Area

The slide area, denoted St. Pierre Slope, is located south of the island St. Pierre on the continental slope outside of Newfoundland, see Figure 6.1.

A bathymetric map of the present-day slide area, with contour interval 25 m, is given in Figure 6.2. The GB slide affected most of the area covered by this map. The epicenter of the M_s =7.2 "Grand Banks earthquake" of November 18th 1929 has been located on the western margin of St. Pierre Slope, in about 2000 m water depth. The slide was initiated by this earthquake.

The St. Pierre Slope is cut by several slope valleys with St. Pierre Valley being the largest (up to 300 m deep). The slope between 100 and 500 m water depth has a mean seabed gradient of about 2° which steepens to about 5° for the area between 500-2000 m.

6.2.1 Geological setting and soil conditions

During the Quaternary, glacial layered sediments where deposited (progradation) in the St. Pierre continental slope. The slope is located seaward of the Laurentian Channel, a major glacial outlet. The Quaternary ice margin followed more or less the present day continental shelf. The St. Pierre Slope is bounded to the west and east by the proglacial erosional pathways of the Eastern Valley of the Laurentian Fan and Halibut Channel, see Figure 6.2

The present day soil conditions display a unit of clay material in most of the area from seabed and down to 5-8 m depth. Evidence of this is found from core sampling (Marsters, 1986). Generally, due to the sedimentation environment, the material gets finer with increasing water depth. No sampling of material deeper than 8 m has been available, but geological history and interpretation from sub-bottom seismic profiling (Piper et al., 1999) indicates soil layering as presented in Table 6.1.

6.2.2 Morphology

A detailed description of the seabed morphology including the distribution of undisturbed seabed, seabed affected by slumps, debris flow deposits and channels are given by Piper et al. (1999).

The area seabed morphology is presented in Figure 6.3. The morphology has been derived from SeaMARC I sidescan surveys, and from IFREMER SAR deep-towed, high-resolution sidescan and sub-bottom profiler system (Piper et al., 1999).

The upper continental slope, to water depths of about 500 m, is undisturbed seabed (not affected by the failure). In many areas, gas escape craters (pockmarks), 30-50m in diameter, are common. Isolated 'islands' of undisturbed seabed are also visible down to water of 2000 m deep.

Slumps are found in large parts of the St. Pierre Slope, see Figure 6.3. They are visible as series of nearly parallel curved ridges. The slumps occur at two main scales: small slumps down to 2-5 m depth, and larger-scale slumps down to 5-30 m depth.

The small slumps have ridge spacing 10-30 m and are typically developed in areas with present-day seabed inclination 2-3°. They involve only the upper clay layer (Holocene mud), see Table 6.1.

The larger-scale slumps have ridge spacing >50 m. There is evidence of ridge spacing up to 200m, ridge height (height of backscarp) of 5-15 m and failure planes (bedding planes) up to 60°.

6.3 Geotechnical Properties

Core samples have been taken at several places in the St. Pierre slope area as shown in Figure 6.4. There is, as far as we know, no comprehensive soil investigation report presenting the results from these samplings. We have based our interpretation of geotechnical properties on the limited data given in references Marsters (1986) and Klohn (1993).

Core samples are taken only down to 8 m below seabed, and thus consists of material from the "Holocene mud" and possibly the "varegated clay" layers, see Table 6.1. There is uncertainty which cores have been taken in areas of undisturbed seabed and in areas where the soil masses have been affected by the slide. With reference to Table 6.1 and 6.2 it seems that cores 84003-4,5,18 and 910020-29 have been sampled in areas which may have been affected by the slide and that cores 84003-7,8,12,13,15 and 16 have been sampled from areas of undisturbed seabed.

6.3.1 Soil classification and results from index tests

Results from index testing and grain size analyses are summarized in Table 6.2, for water depth around 500 m, and Table 6.3 for water depths 1000-1500 m. The results are averaged for each core. The positions of core samples are given in Figure 6.4.

The soil material found in cores, Table 6.2, in the upper slope, from around 500 m water depth, can roughly be classified as either clayey, silty fine sands (SC) of low plasticity, or clays of low to medium plasticity (CL) that is silty and may be sandy. The clays found in cores, Table 6.3, from 1000-1500 m water depth can roughly be classified as clays of low to medium plasticity (CL) that is silty and occasionally sandy.

6.3.2 Sensitivity

Atterberg limits, reported by Marsters (1986), generally show a natural water content in excess of the liquidity limit, i.e. LI > 1.0, with a typical value of liquidity index being around 1.5. This indicates a quite sensitive and strain-softening clay material. Using Bjerrum's proposed relationship (Bjerrum, 1954) between the liquidity index and the sensitivity $S_t = 10^{(0.15+0.73LI)}$, the range of liquidity indexes in Tables 6.1 and 6.2 gives a range of sensitivity S_t = 5 - 60 with S_t = 18 for LI = 1.5.

On intact samples from core 91020-29, peak and residual vane shear strengths are reported by Klohn (1993). The resulting sensitivity falls within the range 3-30. A significant degree of strength loss at large strain is also supported by the triaxial test results reported by Klohn (1993).

6.3.3 *Effective stress strength parameters*

On three samples from core 91020-29, results from 5 undrained direct shear tests and 10 undrained triaxial compression tests (CIUC), are reported by Klohn (1993). Core 91020-29, 0-8 m, is sampled at water depth 1334 m. Tests where performed on samples at depths below seabed: 2.57-2.77 m (No. 1), 3.20-3.40 m (No. 2) and 5.60-5.80 m (No. 3).

An average friction angle of 34° and zero cohesion are reported for the medium plastic, silty clay (CL), with average initial water content of 40%. Samples are quite disturbed (poor quality according to NGI classification).

For the coarser grained material found in the upper slope, at water depths less than 500 m, higher friction angles must be expected.

6.3.4 *Undrained shear strength parameters*

In reference to the triaxial and direct shear tests (Klohn, 1993). described in subsection 6.3.3, three CIUC tests where performed on "natural" samples, though quite disturbed. The rest of the triaxial and direct shear tests where performed on remoulded specimens.

On cores obtained from the cruises 84003, 86034, 90015, 91020 and 92052, the undrained shear strength profiles (probably vane tests) in the depth range 0-8 m, are presented in *Boring Profiles from Test on Core Samples* as part of the borehole log.

Peak undrained shear strengths in compression from Klohn (1993) ("natural" samples) and one undrained shear strength profile (probably vane tests) from core 84003-4, are presented in Figure 6.5. The lines corresponding to $0.3\sigma'_{v0}$, $0.4\sigma'_{v0}$ and $0.5\sigma'_{v0}$ are also shown, with σ'_{v0} being the in situ vertical effective stress, assuming hydrostatic pore pressure. The shear strengths obtained from vane tests on core 84003-4 correspond quite well with the triaxial test results. It must be noted that several of the undrained shear strength profiles plots lower strength values compared to what is presented in Figure 6.5, but many samples are probably quite affected by sample disturbance.

The clay must be expected to display some anisotropy. There have been no test results available to directly evaluate the degree of anisotropy. Based on experience with similar clays, undrained shear strength in extension s_u^E could be expected to be in the order 0.6-0.7 times undrained shear strength in compression s_u^c, and direct simple shear strength s_u^{DSS} could be expected to be about 0.75-0.8 times s_u^c.

6.3.5 *Consolidation characteristics*

Consolidation tests are reported by Marsters (1986) with interpretation of vertical consolidation pressure, σ'_{vc}, and overconsolidation ratio OCR. The interpretation of σ'_{vc} is not very reliable

due to strong influence of sample disturbance. We will assume that most material in the slope is normally-consolidated or possibly lightly-overconsolidated.

Consolidation tests were also performed on core samples obtained on cruise 86034. Test results have been obtained from GSC-A (Marsters, 1986), but no index test results have been available to classify the soil material tested. Test results shows virgin compression indexes C_c in the range 0.35 - 0.7 with C_c = 0.45 being a representative value for material obtained from water depths 800-1500 m. Unloading compression indexes C_s are found to be in the range 0.08-0.15 with C_s = 0.1 being a representative value.

6.3.6 Summary of geotechnical properties

Based on the information presented in sections 6.2 and 6.3, it is assumed that for water depths greater than 500 m, the soil down to at least 25 m, mainly consists of normal-consolidated (lightly-overconsolidated in top) sensitive clays of low to medium plasticity (CL) that can be silty and sandy. It is assumed that the GB slide has been initiated in an area of such material.

In summary, the geotechnical properties recommended for evaluation of the GB slide, at this stage, are presented in Table 6.4.

6.4 Failure Type

The GB failure was triggered by the GB earthquake of 7.2 on Richter scale. The epicenter of the earthquake has been located on the western margin of the St. Pierre Slope at about 2000 m water depth. The commonly held model that the failure and the subsequent turbidity current was initiated by liquefaction of sandy sediments on the continental slope is not supported by Piper et. al. (1999). According to Piper et al. (1999), there is no evidence for a source of liquefied sandy sediment in the slope, see also Sections 6.2 and 6.3.

Again, according to Piper et al. (1999), the process of failure is slumping for each individual failure, but with many successive and overlapping slumps that have retrogressed over a widespread shear plane appearing at a depth < 25 m below the sea floor.

Between 700-900 m water depth in the middle St. Pierre Slope, failure appears to have been initiated in areas with local increase of seabed inclination at 10°, compared to 3° further up-slope. It is believed that, once initiated, small-scale slumps retrogressed up-slope from this area, but stopped at water depths of about 700 m. There is no change in seabed inclination that might be responsible for this up-slope limitation of the failure, but up-slope sediments generally have a higher proportion of coarse-grained material with higher strength (silt and fine sand), see sections 6.2 and 6.3. Up to 20 km of retrogression is probable, according to Piper et al. (1999).

The failure evolved into a debris flow and thereafter a turbidity current travelling at a velocity that peaked at more than 19 ms^{-1} and deposited >150 km^3 of sediments on the Sohm Abyssal Plain. Refer to (Piper et al., 1999) for a more detailed presentation and discussion of the slide evolution.

6.5 Slope Stability Analysis: Infinite Slope

A general discussion of the role of earthquakes in triggering submarine slide failures is presented in Appendix 2. Soil materials affected by the GB slide is mostly clay or clayey, see Sections 6.2 and 6.3. Their geotechnical properties are such that they have a low potential for liquefaction, see Appendix 2. It is more likely that the slide was initiated on the steeper slopes (seabed inclination of approximately 10^o) by horizontal loading from earthquake inertia forces in combination with strain-softening degradation of undrained strength.

Due to the clay material, and the short time duration, it is assumed that the initiation and retrogressive spreading of the slide is governed by undrained soil response, i.e. undrained shear strength parameters. Once initiated (on a relatively steep slope), the slide could spread up-slope retrogressively due to the high clay sensitivity, see discussion in Section 6.6.

One way to evaluate the pre-slide shear strength, or alternatively, if the shear strength is known, the minimum horizontal loading component exerted by the earthquake, is to assess the stability by a plane strain "infinite slope" analysis. Reference is made to Figure 6.6 and Appendix 2.

Areas of "infinite slope" conditions, i.e. large areas ($z/l << 1$) with approximately constant seabed inclination θ is found in the slide area, see Figure 6.2. The stability of an "infinite slope" clay layer of depth z is assessed. The layer, with submerged unit weight γ' and undrained shear strength profile $s_u(z)$, is inclined θ degrees to the horizontal. The layer is loaded by the vertical gravity force W_z and a horizontal force W_x, caused by the earthquake inertia. By equilibrium of the layer, over a horizontal length l, along the slope direction

$$R = W_z \sin(\theta) + W_x \cos(\theta)$$

where R is the base frictional resistance force. (In Figure 6.6 equilibrium at base failure with $R = s_u(z)\cdot\cos(\theta)$ is illustrated).

For the soil masses at-rest, prior to the slide, with the earthquake loading W_x equal to zero, a relationship between the necessary undrained shear strength and the layer inclination, can be calculated

$$s_u(z)/\sigma'_{v0}(z) = \tan(\theta)$$

where $\sigma'_{v0}(z)$ is the in situ vertical effective stress. The ratio of undrained shear strength to in situ effective vertical stress will be denoted b, i.e. $b = s_u(z)/\sigma'_{v0}(z)$.

For $\theta=10^o$, as indicated by (Piper et al., 1999) as the inclination where the slide was initiated, the normalized shear strength b necessary for stability can then be calculated to be about 0.18. Present day undrained shear strengths as presented in Figure 6.5, indicates that $b > 0.3$.

If the slope is subjected to an up-slope acceleration, a, parallel to the seabed, it will experience a down-slope mass inertia force. Then, if we assume the shear strength b known, the necessary

horizontal forces, exerted by the earthquake, to initiate a slide on an "infinite slope", can be calculated.

$$W_x = \frac{a}{g} \cdot \gamma \cdot lz / \cos^2(\theta)$$

where the term $lz/\cos^2(\theta)$ expresses the volume(area) of the layer and a/g is the earthquake acceleration component (with g being the gravitational acceleration).

At limit equilibrium, the earthquake body-force component a/g can then be expressed as

$$a/g = \frac{\gamma'}{\gamma}(b - \tan(\alpha))$$

For a range of b values the corresponding a/g values, necessary to initiate a slide on "infinite slopes" of inclination θ = 5, 10 and 15°, have been calculated. The results are presented in Figure 6.6.

Normalized undrained shear strength values in compression $s_u^C(z)/\sigma'_{v0}(z)$, Figure 6.5, suggests values in a range 0.3 to 0.5. Failure initiated on an "infinite slope" will probably be dominated by the DSS strength such that a reduced strength of 0.75-0.8 times $s_u^C(z)/\sigma'_{v0}(z)$ should be used. Because of the high strain rates induced by the earthquake loading, the peak undrained shear strength should be corrected by "strain-rate effects". For these medium plastic clays a "rate-effect" factor of 1.3-1.4 may be used.

Taking into account the effects of both anisotropy and strain-rate, the normalized peak undrained shear strength $s_u(z)/\sigma'_{v0}(z)$ governing the initiation of the failure can be estimated to be in the range 0.29-0.56. From this, the range of earthquake acceleration necessary to initiate a slide on an "infinite slope" with gradient 10°, can be calculated

$$a = 0.05g - 0.16g$$

No direct results of the ground acceleration from M_s = 7.2 GB earthquake has been available, but ground accelerations of up to 0.5g could be expected.

6.6 Mechanism for Retrogressive Spreading of the Failure

Section 6.5 assessed the local stability of an inclined clay layer subjected to earthquake inertia forces by a pseudo-static "infinite" slope analysis. It seems reasonable to believe that the GB slide was initiated on a locally steeper slope gradient by the mechanism discussed in section 6.5. In this section we are presenting the mechanism believed to cause the up-slope and laterally retrogressive spreading of such a local instability.

Since the maximum earthquake loads only last a fraction of a second the consequences of full mobilization of soil undrained shear strength could be only limited permanent deformations.

However, if the soil is strain-softening and experiences significant reduction of shear strength with increasing shear straining, a local instability may develop into a large slide.

Normally-consolidated (or light-overconsolidated) sensitive clays are known to display strain-softening characteristics with an idealized shear stress- shear strain (or shear stress -shear displacement) behavior as shown in Figure 6.7. The sensitivity S_t of such clays is known to depend mainly on the liquidity index as discussed in Section 6.3

Strain-softening effects

Strain-softening effects play roles both in slide triggering and development. Strain-softening clay may fail progressively when the peak shear strength is exceeded in only a limited zone of the soil volume, whereas perfectly plastic clay (with no strength loss with shear straining) fails when the (peak) shear strength is mobilized along a kinematically admissible failure mechanism. The shear stress distribution in a submarine slope caused by gravity and earthquake inertia loading will be highly non-uniform with stress concentrations in some areas. For a strain-softening clay slope the failure may then develop progressively once the shear stress in such a high stress area is exceeded and starts to loose strength (domino brick effect).

The presence of a relatively weaker layer at some depth within the slope, tends to concentrate the earthquake-induced strains in that layer. If such a layer is strain-softening, the failure will tend to follow the layer. Often, the observed submarine failure patterns (interpreted from seismic profiling) indicate a rather distinct block type failure with the lower extent of the failure following more or less a constant depth. The observed slide block pattern can be approximated by a series of triangular and possibly trapezoidal blocks. Failure along a relatively weaker (or relatively more sensitive) soil layer could explain such a failure pattern.

For the GB area, sub-bottom seismic profiling has revealed that the soil masses are layered, see also subsection 6.2.1, but there is no information of a layer being relatively weaker than others.

When a strain-softening clay slope is loaded, the soil masses will be in static equilibrium for increasing loads as long as the strength loss of locally failing soil masses are balanced by adjacent soil masses with rest capacity (soil where the shear stresses still are climbing towards peak shear strength). When a certain threshold load (the failure load) is reached (or exceeded) the soil mass reaches a state of structural instability where the strength increase (from the soil masses with rest capacity) can no longer balance the strength loss from the failing softening soil. At such a state of instability, the external load must be balanced by inertia forces from accelerating soil masses (dynamic equilibrium). The consequence may be a dramatic and rapid failure development.

As the peak loads from the earthquake last only for an extremely short period of time the clay slope may restabilize when the loading level decreases and the slope is only loaded by gravity. However, if the clay is quite sensitive, the residual (large strain) strength, mobilized during the earthquake loading, may not be sufficient to withstand the gravity loading and failure develops even if the earthquake loading has vanished.

With a sensitivity S_t the residual shear strength can be expressed as $s_{ur} = s_{up}/S_t$, where $s_{up} = b \cdot \sigma'_{v0}$ is the peak shear strength. With the "infinite slope" static shear stresses from the gravity loading being; $\tau = \tan(\theta) \cdot \sigma'_{v0}$, the necessary sensitivity for the slope to be unstable under only gravity loading can then be expressed as

$$S_t = b/\tan(\theta)$$

With b being in the range 0.3-0.6 and the slope gradient θ being in the range 2°-10°, the necessary sensitivity to avoid re-stabilization of the slope under gravity loading is calculated to be $S_t \approx 2$ - 17. From subsection 6.3.2 a sensitivity in the range 5-60 is estimated for the clay material found in the upper soil layers in the GB area.

Retrogressive sliding along strain-softening layer

The occurrence of a soil layer at a certain depth within the slope, which is relatively weaker (in peak strength) and/or relatively more sensitive (strain-softening), compared to the other soil layers could act as a sliding plane. This can explain why failures can retrogress large distances up-slope into areas of relatively flatter (low gradient) seabed. A possible scenario could be where a block of soil initially fails (first stage failure in Figure 6.8) along a shear-band following such a weak layer for a distance and then exposing a relatively steep backscarp. Block-like failure under undrained condition typically exposes scarps of 45° inclination to the weak layer.

Such a steep backscarp is normally not stable even if the seabed is flat. In perfect plastic clays, with no presence of a weak layer, the consequence could then be that the slide stops by several smaller rotational failures flattening out the backscarp as illustrated on Figure 6.8 a.

However, in the presence of a strain-softening layer, the slide could retrogress further up-slope into flatter areas by a block-like failure mechanism (each block failure exposing a new equally steep backscarp) as illustrated on Figure 6.8 b. The slide could spread unlimited even in flat areas unless the strain-softening layer vanishes or gets stronger (higher peak strength).

This effect has been demonstrated by numerical simulations in the NGI research project "Effect of strain-softening on stability analyses" (NGI, 2000). The NGI FEM program BIFURC (NGI, 1999) was applied using a strain-softening material model (NGI-3HC) to model the strain-softening layer. Figure 6.9 a shows the FE model and material assumptions made and Figure 6.9 b shows the failure mechanism. The failure mechanism gives a clear indication of shear band developing in between wedge-like blocks.

6.7 Summary and Conclusions

6.7.1 Summary

A description and evaluation of the Grand Banks submarine slide failure of November 18th 1929 have been presented in this section. This is based on information provided by Geological Survey of Canada - Atlantic (GSC-A). From the review of this information, support is found for a hypothesis that the GB slide failure was initiated in soil layers of mostly sensitive and strain-softening clay or clayey material by inertia loading from the GB earthquake of the same day.

However, it must be noted that the soil layering and geotechnical parameters are still very uncertain, due to the limited information of the GB area that has been available. Soil samples are available only from cores down to maximum 8 m depth below seabed. There exists, as far as we know, no comprehensive soil investigation report summarizing the available geotechnical information of the area. The same is true for the results from the sub-bottom seismic profiling.

Slide area

The slide area is located on the continental slope outside of Newfoundland, Canada. The source area of failing soil masses probably covered more than 2500 km^2 of the slope from 500 to 2500m water depth. The upper slope, to about 500m water depth has a mean gradient of about 2°, below this, the slope steepens to about 5°.

Slide evolution and damage

The slide evolved into a turbidity current travelling at velocity of more than 19 ms^{-1} and deposited > 150 km^3 of sediments on the Sohm Abyssal Plain. This indicate a run-out distance of about 400 km. The turbidity current broke cables up to 13 h after the earthquake.

Soil conditions

The present day soil conditions display clay material in most of the area from seabed and down to 5-8m depth. Evidence of this is found from core sampling (Marsters, 1986). No sampling of material deeper than 8m has been done, but geological history and interpretation from sub-bottom seismic profiling (Piper et al., 1999) indicates three clay (mud) layers for mid slope area with water depth deeper than 500m. One of these layers is described as thick. No evidence for a source of liquefaction susceptible sandy sediment is found (Piper et al., 1999).

Geotechnical properties

Clay material found in core samples (Marsters, 1986) can typically be classified as having low to medium plasticity (IP~14-20), with high liquidity index (IL~1.5), highly sensitive (S_t > 15), being normally consolidated (or possibly lightly over-consolidated). A few test of soil strength show friction angle of $\phi = 34°$ with zero cohesion and undrained shear strength in compression $s_u^C = 0.3\text{-}0.5 \cdot \sigma'_{v0}$. Total unit weight γ_t is typically about 17.5 kN/m^3. The sensitive clay found in the area is believed to display strong strain softening characteristics with a rapid decrease of shear strength for increasing shear strain after passing the peak shear strength.

Morphology

Present day surface sediments over most of St. Pierre slope are affected by the slide, interpreted as minor scarps or failure ridges and debris flows. These failures show a prominent line of headscarps on the upper slope between 700m and 500m water depth, above this, sediments are undisturbed of the failure.

Trigger source

The failure was triggered by the M_s 7.2 "Grand Banks earthquake" of the same day. The epicenter of the earthquake was located at 2000 m water depth central in the slide area. The failure was probably initiated in areas of locally steeper gradients (local gradient up to 10° is indicated by (Piper et al., 1999). Slope stability analyses presented herein indicate that an earthquake generated up-slope horizontal acceleration of 0.05g to 0.16g would have been

sufficient to initiate failures on the 10° slopes, for the range of undrained shear strength found for the clay layers in question. Earthquake ground accelerations of up to 0.5g is likely for the GB earthquake. It is likely that the failures have been initiated in thin clay layers (or interfaces between layers) with slightly less shear strength and shear modulus, or slightly higher sensitivity, relative to the other soil. Such "imperfections" are known to amplify shear straining caused by earthquake loading.

Because of the strain-softening characteristics of the clay, the soil did not re-stabilize after the short time period of earthquake loading. The earthquake loading probably induced large enough plastic shear strains to bring the shear strength down towards the residual strength level (at least in one layer). For this sensitive clay the residual strength is not high enough to withstand the static shear stresses caused by gravity loading. It is found that for sensitivities S_t in the range 2-17, this causes the clay layers of inclination 2°-10° to be unstable even after the earthquake loading has vanished.

Failure mechanism
Once initiated, the failure is believed to have spread retrogressively up-slope and laterally, also into areas with seabed gradient much less than 10°. The strain-softening clay (or clay layers) probably failed by developing thin shear-bands (or slip lines) of intense plastic straining. The slope failure mechanism in such clays may follow "imperfections" of weaker (or more sensitive clay) up-slope, successively exposing steep backscarps (daybreaks).

The initial failure pattern was probably dominated by wedge and trapezoidal blocks of more or less intact clay dissected by the shear-bands. Such failure patterns have been interpreted from seismic profiling of the slide masses at Storegga. A numerical simulation has been presented herein which illustrates this mechanism in strain-softening clay. The ridges observed in the Grand Banks slide area, interpreted as small and large rotational slumps, could also be evidence of such a failure pattern.

The up-slope failure retrogression eventually stopped in areas of more coarse grained material with higher shear strength or less sensitivity.

6.7.2 Conclusions

- The Grand Banks submarine slide failure of 18 November 1929 was triggered by additional shear stresses in the down-slope direction caused by earthquake mass inertia forces.

- The slope sediments consist mainly of normally and lightly over-consolidated low or medium plastic clays and silty clays, at least in the upper 5-10m, which are highly sensitive and probably display strong strain-softening characteristics.

Support is found for the following hypothesis:

- The earthquake loading, lasting only a fraction of a second, increased the shear stresses to the peak shear strength value (full mobilisation) in areas of locally higher seabed gradient of up

to 10°. Possibly this took place only in a limited clay layer or interface between two clay layers.

- Because of the strain-softening characteristics, the clay, in areas or zones, lost most of its shear strength during the earthquake cyclic loading. The residual strength was not enough to withstand the static shear stresses from gravity, at least in some areas. In this way the failure could start developing with large movements of soil masses.

- The strain-softening clay failed by developing shear-bands or slip lines possibly following a weaker or more sensitive layer up-slope. It has been shown, by numerical analyses, that this mechanism can cause retrogressive spreading of the failure into areas of relatively flat seabed.

6.8 References

Bjerrum (1954). Geotechnical properties of Norwegian marine clays. Geotechnique 4, pp. 49-69.

Bonifay, D. and Piper, D.J.W.(1988). Probable Late Wisconsinan ice margin on the upper continental slope off St. Pierre Bank, eastern Canada. Canadian Journal of Earth Sciences, Vol. 25, p.853-865.

Boring profiles from test on core samples. Cruise 84003, 86034, 90015, 90013, 90031, 91020 and 92052

CD with GIS data in ArcView format

Christian H.A., Piper, D.J.W., Cochonat, P. (1991). Excess Pore Pressure and Permeability Characteristics of Silty Quaternary Sediments, Southern Grand Banks of Newfoundland, Canadian Geotechnical Journal, Aug. 1991.

Datasheet with identification of most relevant (good quality) cores in the opinion of D. Piper

Klohn Leonoff (1993). Results of 5 direct shear tests and 10 triaxial compression tests performed on specimens from piston core samples. Depths 2.57 - 2.77, 3.20 - 3.40 m and 5.60 - 5.80 m

Map of St. Pierre Slope showing location of excess pore pressure determinations and interpreted values

Marsters, Janice C. (1986). Geotechnical analysis of sediments from the eastern Canadian continental slope, south of the St. Pierre Bank, Technical University of Nova Scotia.

NGI (1999). BIFURC-3D - A finite element program for 3-dimensional problems, Theory manual, NGI report 514065-1, 31 December 1999

NGI (2000). Effect of strain-softening on stability analyses. Submarine slide initiation and retrogressive spreading, NGI report 521001-10, In progress.

Piper D.J.W., Cochonat P. and Morrison L. (1999). The sequence of events around the epicentre of the 1929 Grand Banks erthquake: initiation of debris flows and turbidity current inferred from sidescan sonar. Sedimentology, 46, 79-97.

Piper, D.J.W., Sparkes R. and Mosher D. C. (1987). Seabed instability near the epicentre of the 1929 Grand Banks earthquake. A study funded by the Program of Energy Research and Development, Geological Survey of Canada Open File Report.

Sheet with stratigraphic setting of cores and module sites upper St. Pierre Slope.

Subbottom profiles, Interpretations from seismic profiling.

Table 6-1: Soil layering indicated by geological history and sub-bottom seismic profiling based on Bonifay and Piper 1988 and Piper et al. 1999)

Upper slope, water depth 400-600 mbsl	Thickness (m)
Clay, Holocene age, bioturbated (unit A)	3-10
Clay, thin sand beds, late Pleistocene (unit B)	3-6
Clay, proglacial with dropstones	8-12
Sandy glacial till	0-30
Clay, proglacial with dropstones	>20
Lower slope, water depth 1000-1500 mbsl	
Clay, Holocene age, bioturbated (unit A)	1-3
Clay, proglacial, with dropstones	>60

Table 6-2: Results from index tests and grain size analyses of cores from water depth ~500 m, data from Marsters (1986)

Core	Water depth (m)	Strati-graphic depth of top below original seabed (m)	Depth m	w (%)	w_L (%)	w_P (%)	IP (%)	LI	Sand %	Silt %	Clay %	e	γ_t kN/m^3
84003-8	560	0	2.12-2.31	43	35	26	9	1.9	NA	NA	NA	1.16	17.9
84003-12	571	10	0.0-5.9	51	36	23	14	2.2	6.3	66.8	27	1.38	17.1
84003-13	483	0	1.0-5.75	30	27	13	14	1.2	61.6	25.2	13.2	0.81	19.4
84003-15	516	0	0.93-1.08	115	95	38	57	1.4	NA	NA	NA	3.11	14.1
84003-16	494	0	0.75-0.85	29	21	14	8	1.9	61.8	25.0	13.2	0.78	19.6

Notes:

- w Natural water content
- w_L Liquid limit
- w_P Plastic limit
- IP Plasticity index
- LI Liquidity index
- e In situ void ratio
- γ_t Total unit weight

It is assumed a specific gravity for the soil solids of $G_s = 2.7$.

Table 6-3: Results from index tests and grain size analyses of cores from water depth 1000-1500m, data from Marsters (1986)

Core	Water depth (m)	Strati-graphic depth of top below original seabed (m)	Depth m	w (%)	w_L (%)	w_P (%)	IP (%)	LI	Sand %	Silt %	Clay %	e	γ_t kN/m^3
84003-4	1405	3	0.0-7.83	51	38	22	16	1.8	13.3	49.4	37.0	1.38	17.1
84003-5	1537	0	5.35-5.91	45	39	23	16	1.4	8.2	54.2	37.5	1.22	17.6
84003-7	1124	0	3.10-3.20	31	35	17	18	0.8	14.3	50.2	35.5	0.84	19.2
84003-18	1078	10	1.00-1.10	53	45	16	29	1.3	5.0	52.7	37.8	1.43	17.0
91020-29	1334	0	0.0-8.0	50									17.7

Table 6-4: Summary of geotechnical properties for GB slide evaluation

Property	**Value**
Total unit weight, γ_t (kN/m^3)	17.5
Sensitivity, S_t	~18
Friction angle, ϕ (Deg.)	34
Effective cohesion, c (kPa)	0
Normalized undrained shear strength in compression, s_u^C/σ'_{v0}	0.3 - 0.5
Undrained shear strength in extension, s_u^E (kPa)	$0.6 \cdot s_u^C$ - $0.7 \cdot s_u^C$
Undrained shear strength in DSS, s_u^{DSS} (kPa)	$0.75 \cdot s_u^C$ - $0.8 \cdot s_u^C$

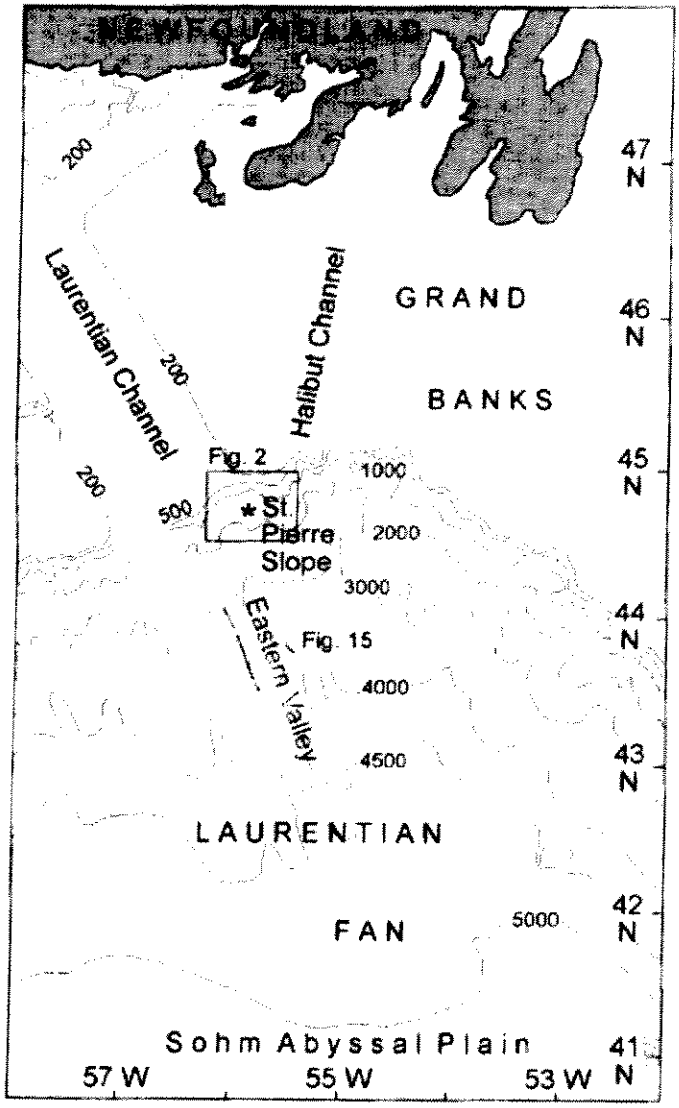

Figure 6-1: Location of St. Pierre Slope and the 1929 earthquake epicenter (*), from Piper et al. (1999)

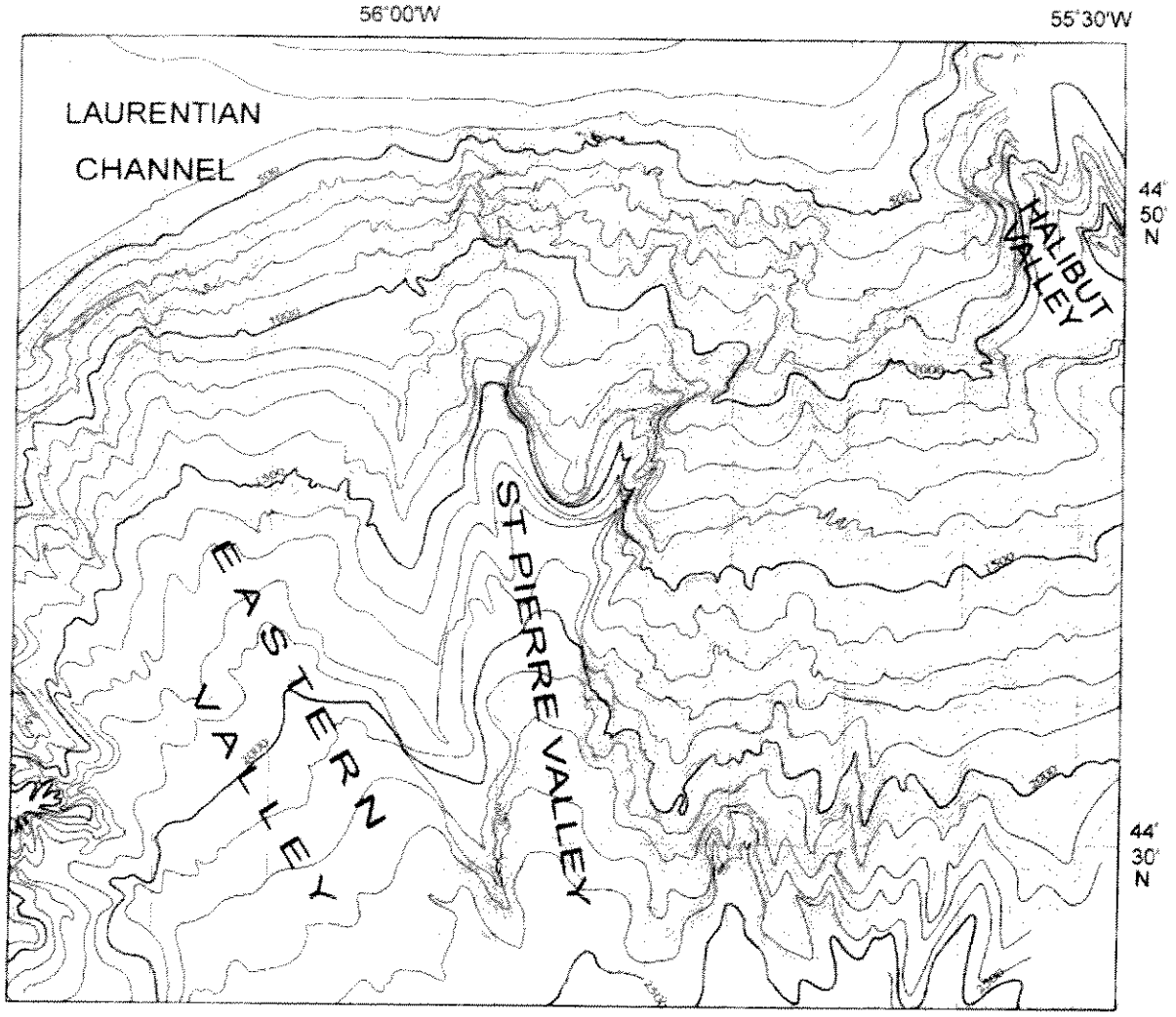

Figure 6-2: Contour map of St. Pierre Slope. Contour interval 25 m. From Piper et al. (1999)

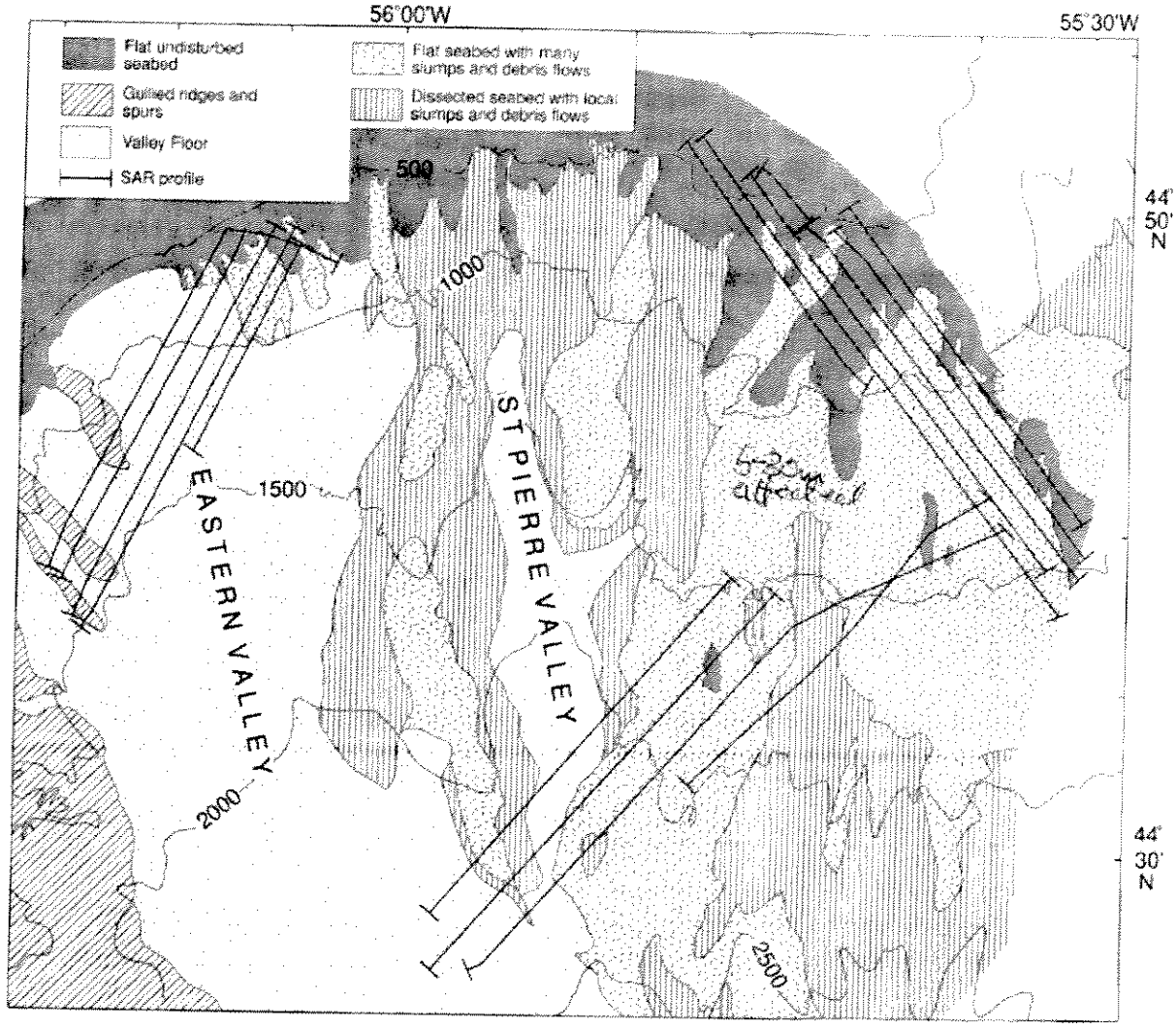

Figure 6-3: Present-day seabed morphology, from Piper et al. (1999)

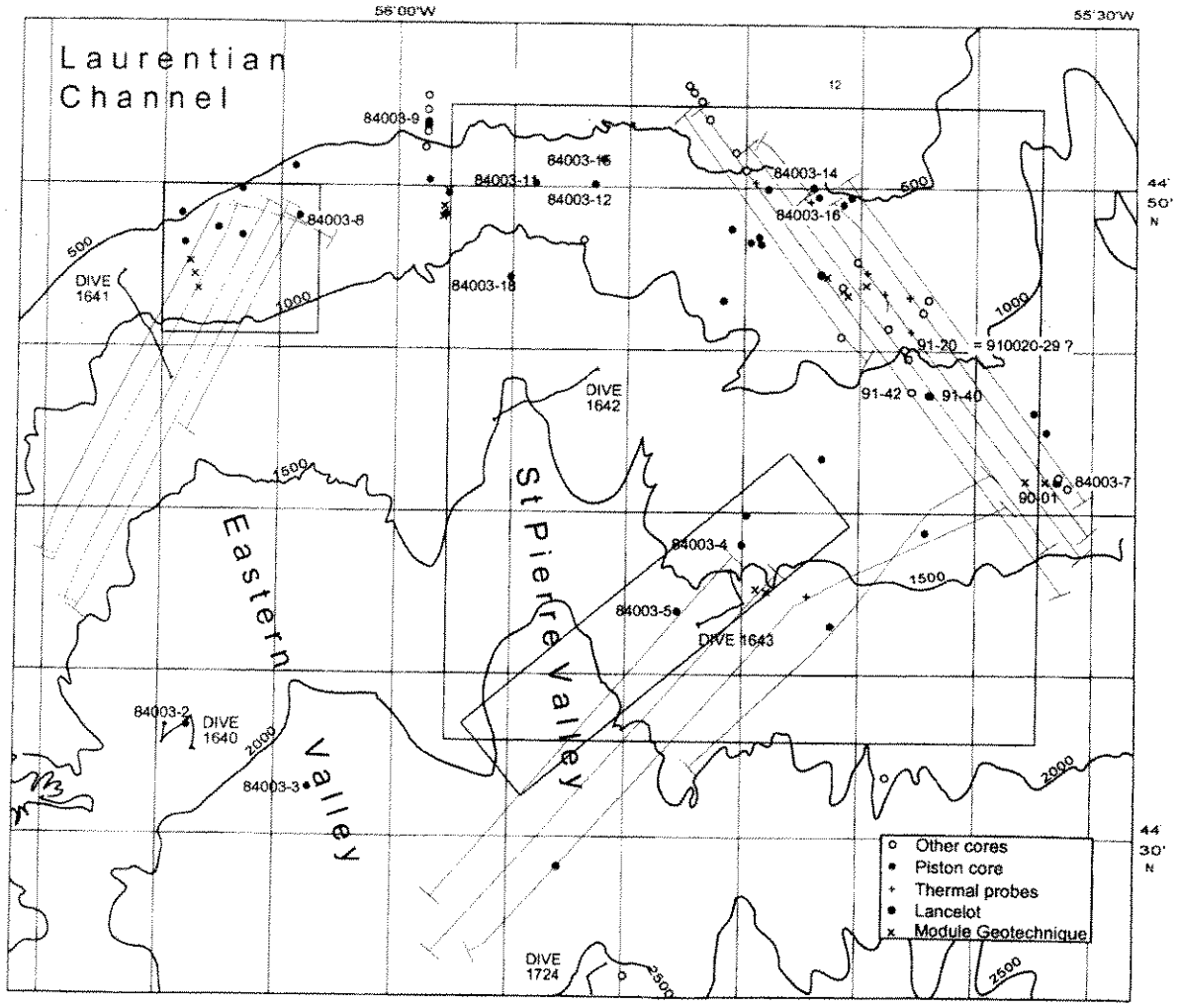

Figure 6-4: Map showing loaction of cores on St. Pierre Slope, from Piper et al. (1999)

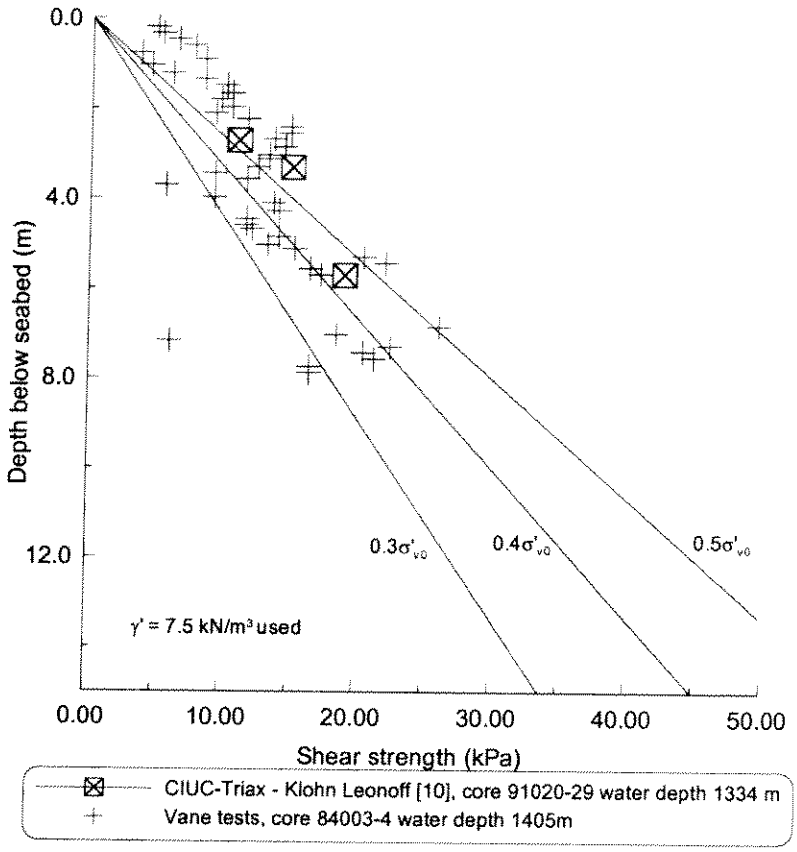

Figure 6-5: Undrained compression shear strength profile for water depth 1000-1500 m

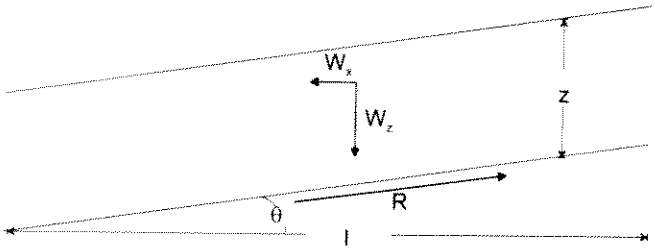

$R = W_z \sin(\theta) + W_x \cos(\theta)$
$R = s_u(z) l / \cos(\theta)$
$W_z = \gamma' l z / \cos^2(\theta)$
$W_x \quad (a/g) \gamma l z / \cos^2(\theta)$

$s_u(z)$ undrained shear strength parallel to seabed at depth z
a earthquake induced up-slope acceleration parallel to seabed
g gravitational acceleration = 9.81 m/s²
γ total unit weight
γ' submerged unit weight ($\gamma' = \gamma - \gamma_w$)

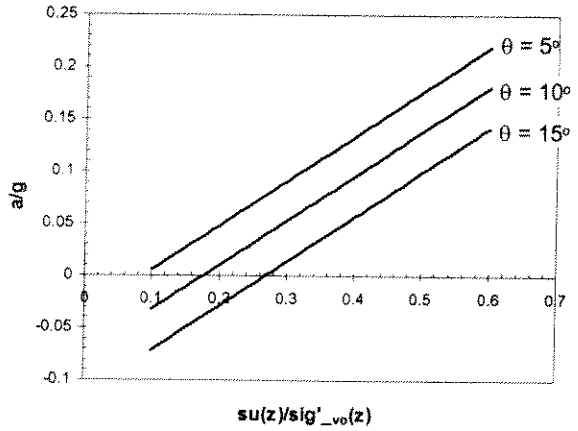

Figure 6-6: Total stress infinite slope stability, including horizontal force component from earthquake loading

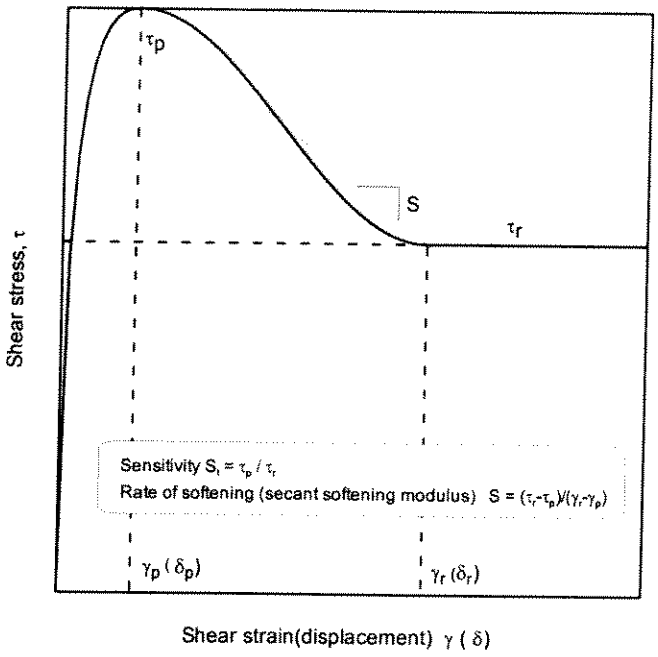

Figure 6-7: Relationship between shear stress and shear strain (displacement) for constitutive model NGI-3HC

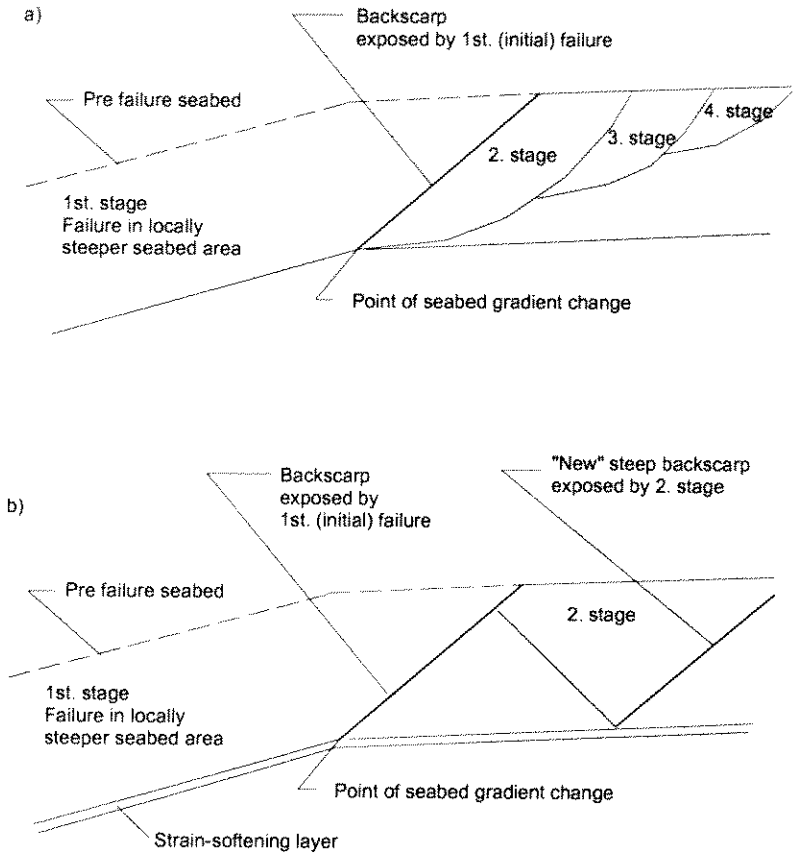

Figure 6-8: a) backscarp flattens out by rotational slumping and slide stops b) slide retrogresses up-slope by following base strain-softening layer

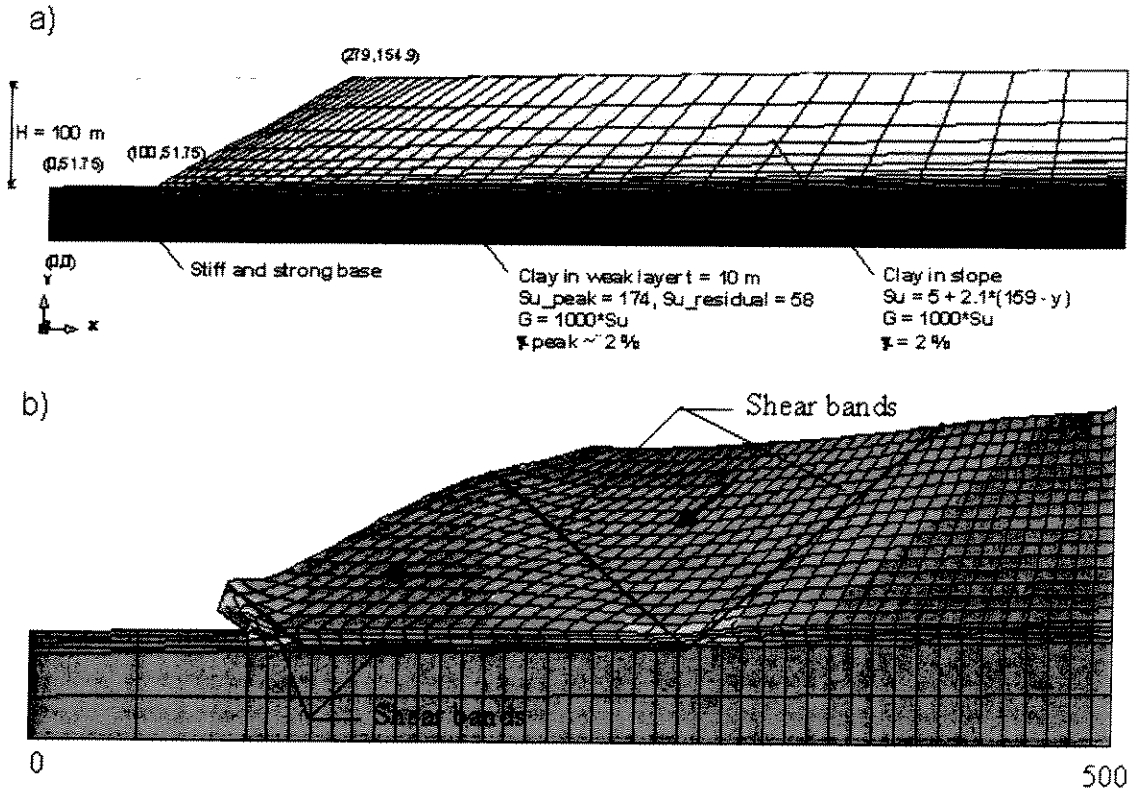

Figure 6-9: FEM study of retrogressive sliding along strain-softening layer: a) FE-model and material properties b) Failure mechanism

7 WAVE-INDUCED SEDIMENT MOVEMENTS

In 1969, a small but intense storm, Camille, struck the Mississippi delta area off the Louisiana coast, a prolific oil and gas producing area. In the aftermath of the storm, one platform was found toppled and two other platforms were damaged severely, all in the So. Pass area of the Mississippi delta (Bea, 1971). Subsequent investigations showed that the damage occurred not as a result of wind and wave forces on the platforms, but rather from wave-induced mudslides in the soft, underconsolidated sediments prevalent in the area. Although platform damage and pipeline breakages were well known in the area prior to Camille, this was the first major destruction of a large platform, and it sparked a multitude of studies on the topic of wave seabottom interaction. One of the first studies reported was by Henkel (1970) who used standard slope stability analysis with the forcing function being wave-induced bottom pressures. The only sediment properties required in this analysis were unit weight and undrained shear strength. Subsequently, Wright and Dunham (1972) developed a finite element approach which took into account the actual sediment properties at So. Pass 70, the location where the platform was destroyed during Camille. Other analytical studies have been conducted, many of which used Biot's formulation for poro-elastic bodies. In addition, a significant number of geological studies were conducted which developed the extent and magnitude of seafloor slides in the Mississippi delta area, as well as their morphology (e.g. Coleman et al., 1978 and 1980).

The study reported herein utilized results from research conducted for Chevron, Gulf and Mobil oil companies in response to needs for design of mudslide resistant platforms in the So. Pass 57-77 area. This research took three main paths: a) the development of constitutive relationships for the soft sediments involved, b) determination of sediment drag forces on platform members, mostly for piles, and c) development of the governing equations for sediment movement and numerical solution of these equations. The end product was a computer program which provided cyclic and downslope movement of the sediments in response to wave forces and calculated the drag forces of the sediment on platform members.

7.1 Sediment Constitutive Relationships

The constitutive relationship study was initiated by Stevenson (1973), who used a miniature vane rotated at four different rates in the sediment. A vane was chosen for the following reasons: the samples were often too soft to stand on their own, consequently they could not be trimmed or transferred to more sophisticated testing devices without causing significant disturbance, and the insitu vane which had recently become available showed promise for obtaining the same information insitu. Figure 7.1 is a typical torque-rotation plot. Calculations from these data are then plotted as shown in Fig. 7.2. These types of plots clearly show that the sediment behaves in a viscoelastic manner; the slope of the sets of lines in Fig. 7.2 represents the viscoelastic rate constant, n. King (1976) conducted a companion study using a long cylindrical vane installed along the axis of sediment samples which were contained in their original sampling liners. Studies by Marti (1976)and later by Riggins, (1980) who used a large simple shear device, further confirmed that the sediments behaved as nonlinear viscoelastic materials.

Subsequent tests on large numbers of Gulf of Mexico sediment samples established that the value of the constant, n, ranged from about 0.06 to 0.15 with the majority of values between 0.09

and 0.12. A relationship between the liquidity index of the sediment and n was developed. This relationship is coded into the computer program; alternatively, the actual values of n obtained by tests on sediment samples can be entered.

7.2 Sediment Drag Forces

The drag forces of moving sediment on platform elements is responsible for platform distress and destruction. Although the PODS study is concerned with the analysis of seafloor slides, the calculation of drag forces on structures provides a convenient method of determining the severity of the slide movement. Conventional geotechnical practice dictates a standard bearing capacity approach to this problem, usually with a bearing capacity factor of 9 or 10 applied to the frontal area of the structural element. However, the problem is more complicated than this as soft sediment, similar to a liquid, can actually flow around a structural shape. This requires an approach more akin to the classical Morison equations used for fluid flow around an object.

Marti (1976) studied this problem using experimental and theoretical approaches. He conducted an extensive set of experiments with model instrumented piles of various diameters buried in a soft, prepared sediment. The experimental equipment was capable of applying confining pressures up to 30 psi to the pile-sediment mass, it allowed the pile to move in the sediment at controlled velocities, and since the testing equipment was also a large scale simple shear device, it allowed for sediment movement against the model piles.

Based on a plastic limit analysis of the problem and the experimental results, Marti determined that the drag force per unit length of pile was:

$$F = 11.42(125.9n)^n(V/D)^n C_{uo} D$$

Where Cuo = vane shear strength determined at the standard rotation rate
V = velocity of sediment movement with respect to the pile
D = pile diameter
n = viscoelastic constant

Some time later, this approach was further validated during an AGA-sponsored project on sediment drag forces on buried pipelines (Schapery and Dunlap, 1984).

7.3 Mathematical Solution to Wave-Seabottom Interaction

Armed with knowledge of the sediment constitutive behavior, Schapery (1976) developed the governing equations for determining sediment movement induced by storm waves. After developing these equations, a computer program was written to solve the equations (Raju and Schapery, 1976). It is emphasized that this is not a finite element approach but rather a numerical solution of the closed form equations. The computer program is capable of providing:
a. horizontal and vertical sediment movements at desired locations below the mudline
b. downslope movement if the sediment is on a slope
c. drag forces against a pile of specified diameter at desired depths below the mudline
d. wave degeneration, i.e. distance required for a wave to lose a percentage of its height due to energy lost while traveling over a deformable bottom.

Key input parameters to the program are:
a. wave characteristics – length, height and period
b. sediment characteristics – undrained shear strength, Cu; viscoelastic rate parameter, n; unit weight; strength factor, G1/Cu; all with respect to depth
c. water depth and water unit weight
d. subbottom slope
There are other input parameters relevant to the internal operations of the program including an error tolerance applicable for certain iterative operations while solving the governing equations. An initial stress ratio – shear stress/shear strength – must also be entered; a reasonable guess will hasten the iterative process.

The strength factor, SF, is defined as the viscoelastic modulus, G1, divided by the undrained shear strength, Cu, determined by a vane shear at the standard rotation rate, i.e. SF = G1/Cu. Although actual values determined by test can be input into the program, early correlations established this ratio as 32. Later research using the large scale simple shear device (Riggins, 1980) determined that a value of 120 seemed more appropriate, especially for large strains.

The original program used a parallelogram model for cyclic stress-strain behavior of the sediment. Later a somewhat more realistic hyperbolic stress-strain equation was used to relate the maximum shear stress and strain. This was followed by the addition of a Ramberg-Osgood model. The user may specify which option is desired in the program; the hyperbolic law is generally preferred.

The sediment properties must be entered with respect to depth by assuming constant properties for each of several successive layers. Although there is no practical limit to the number of layers that can be used, the program in its present state utilizes a maximum of 10 layers plus a "hard bottom". This hard bottom is not necessarily perfectly rigid, but it is expected to be a zone that is significantly stronger and more rigid than the overlying sediments.

Finally, the program does not consider a change (degradation) in sediment properties with loading cycles although this could easily be done. The present procedure is to successively replace the original properties with new ones based on cyclic load test and rerun the program.

7.4 Program Validation

As with other wave-seabottom interaction programs, this program has not been tested in nature from the standpoint that no platforms designed using this approach have been subjected to large storms. There is, however, anecdotal evidence that supports its validity. One platform designed using the program was found at a later date to have more than 20 ft. of sediment that had accumulated against the legs since construction, but with no distress to the platform. This greatly exceeds normal sedimentation rates in the area and it must have been caused by sediment movement. But it is unknown whether this was a single slide or an accumulation of smaller slides. One validation approach is to test the program against the behavior of the one platform that is known to have failed during a storm event – So. Pass 70 B. The company records of this failure are not available, however, there are ample data available in the public records to reconstruct the important parameters.

Extensive studies were conducted on sediment strength using both laboratory and in situ vane measurements. Bea and Arnold (1973) reported a somewhat idealized strength profile which considered in situ vane measurements (Fig. 7.3). This shows an often observed "cutback zone" of strengths at sediment depths of 60 to 85 ft. Hooper (1980) suggested reasons why these zones of lower strength occur. If these cutback zones occur within the subbottom depth where maximum shear stresses due to waves occur (0.16L for an elastic material) the subbottom movements can be greatly magnified.

Wave parameters at the platform location were also reported by Bea and Arnold (1973) as follows:
Wave height = 65 ft.
Wave length = 1000 ft.
Wave period = 14 secs.
These are hindcast values and do not reflect API design standards.

Other sediment parameters such asn, strength factor and unit weight were varied over typical ranges with little effect on the results, probably because the shear strengths and the location of the cutback zone largely governed the magnitude of the movement. The results are illustrated in Figs. 7.4 and 7.5. Maximum downslope velocity was determined as 22.6 fps. These results do not consider a reduction in strength due to cyclic movement. The calculated cyclic movements (Fig. 7.4) are larger than those reported by others (Arnold, 1973, Bea and Arnold, 1973), however, they did not calculate continuous downslope velocities. Comparison of pre-and post-Camille soil borings by Sterling and Strohbeck (1973) showed significant strength reductions at the 70-80 ft. range after the storm which they interpreted as the depth to which the sediment was remolded as it translated downslope. Although this compares favorably with the wave-seabottom program results (Fig 7.4) this is not too surprising since the cutback zone occurs at roughly the 70-80 ft range.

One interesting aspect is that the lateral loading on the pile always occurs on the upslope side of the pile (Fig. 7.5) even though the cyclic sediment movement switches from one side of the pile to the other in concert with the waves. Running the program with the same parameters as before but using a 0% slope results in the lateral loading shown in Fig. 7.6. Obviously, the significant downslope velocity and the resulting drag forces on the pile overwhelm any lateral loads caused by cyclic upslope movement of the sediment.

In summary, the wave-seabottom interaction program calculates movements and forces which are consistent with failure of the So. Pass 70B platform. Significant downslope velocities and large cyclic sediment movements were predicted.

7.5 Parametric Study

A parametric study was conducted to provide guidance for estimating seafloor sliding potential. There are too many variations of near surface sediment properties with depth to be able to handle even a small number of them. The approach taken here was to use a range of properties consistent with the Gulf of Mexico but which are probably valid for a number of other near-surface cohesive sediment locations.

The single most important sediment property governing wave-seabottom interaction is shear strength. In slide prone areas in the Gulf of Mexico, surface sediments have an undrained shear strength of approximately 50 psf which then increases with depth depending on the state of consolidation: 5 psf for highly underconsolidated clays, 8 psf for lightly underconsolidated clays and 11 psf for normally consolidated sediments. These strength were used in the parametric study. The thickness of soft sediments prone to sliding also varies widely but it ranges generally from about 75 ft to 175 ft. Sediment unit weight, while obviously important , varies only slightly from 100 pcf for the soft sediments. As discussed earlier, an n value of 0.09 is an average value. Finally, a strength factor of 120 was used.

Water wave characteristics were selected from API guidelines for maximum height and length, and a period of 13 seconds was used. Water depths of 100, 200 and 300 ft. were used as shown below:

Water depth, ft	Maximum wave height, ft	Wave length, ft
100	57	648
200	66	794
300	68	845

Bottom slopes were 0, 0.5, 1.0 and 1.5%. Sediment forces were calculated on a 4 ft. diameter pile.

Results of the parametric study are presented in Figs. 7.7, 7.8 and 7.9. For the 75 ft. sediment thickness and 100 ft. water depth, large cyclic displacements and downslope velocities occurred for the highly underconsolidated and lightly underconsolidated sediments, while normally consolidated sediment exhibited only minor movement. However, this movement is probably still large enough to create cyclic strength degradation. In 200 ft water depth, only the highly underconsolidated sediment exhibited significant cyclic and downslope movement. Insignificant movements occurred with all states of consolidation in the 300 ft. water depth.

Increasing the sediment thickness up to 175 ft. had a relatively small effect (roughly a 10% increase) on cyclic displacement. Downslope movements were increased somewhat more, but again it was not a major change. Increasing the water depth had a more significant effect than increasing the sediment thickness.

Obviously, the potential exists for infrastructure damage in the 100 ft. water depth for underconsolidated sediments, and in the 200 ft. depth for highly underconsolidated sediments, but damage potential is very slight in 300 ft. water depth for even very weak sediments. This considers only linear increases of strength with depth, not cutback zones of lower shear strengths in the strength-depth profile. The calculated displacements should be considered as a snapshot in time. Continual movement, particularly downslope, may be modified by changes in slope, and by loss of strength due to large strains and mixing with moisture. The latter could lead to true debris flows with potentially higher velocities.

Attempts to place these results in dimensionless graphs have so far been unsuccessful, probably because of the highly nonlinear nature of the problem. However, interpolation between graphs should be fairly successful.

7.6 Conclusions

Shallow water storm waves of major proportions can cause significant movements in soft sediments. Two types of movements can occur: a cyclic back and forth movement in response to bottom pressures which can occur even if the bottom is flat, and a downslope movement if the bottom is sloped. Highly underconsolidated and slightly underconsolidated clays will suffer large movements whereas normally consolidated clays will be only marginally affected, although continued wave loading in water depths less than 200 ft. may cause cyclic reduction of strength which can lead to more significant movements. These conclusions are based on shear strengths that increase fairly linearly with depth. If the strength-depth profile contains cut back zones where the strength decreases at depth, the sediment movements can become much larger. This depends greatly on the depth of the cutback zone in relation to the wave length.

Graphs have been presented which can be helpful as a first estimation of whether sediment movement will be a problem.

7.7 References

Arnold, P., (1973), "Finite Element Analysis-A Basis for Seafloor Soil Movement Design Criteria", Proceedings, Offshore Technology Conference, Houston, Texas.

Bea, R. G., (1971), "How Sea-Floor Slides Affect Offshore Structures", The Oil and Gas Journal, November 29, 1971, pp 88-92.

Henkel, D. J., (1970), "The Role of Waves in Causing Submarine Landslides", Geo-technique, Volume 20.

Hooper, J. R., (1980), "Crustal Layers on the Mississippi Delta Mudflows", Proceedings, Offshore Technology Conference, Houston, Texas.

King, J. B., W. A. Dunlap, and R. A. Schapery, (1976), "Characterization of Viscoelastic Properties of Submarine Sediments", Texas A&M University Report No. MM 3008-76-3.

Marti, J., (1976), "Lateral Loads Exerted on Offshore Piles by Subbottom Movements", Ph.D. Dissertation in Civil Engineering, Texas A&M University.

Raju, S. B. and R. A. Schapery, (1976), "Wave-Sea Bottom Interaction (Final Report) Part 2. Computer Program Guide", Texas A&M University Report No. MM 3008-76-1.

Riggins, M., (1981), "The Viscoelastic Characterization of Marine Sediment in Large Scale Simple Shear", Ph.D. Dissertation in Civil Engineering, Texas A&M University.

Schapery, R. A., (1976), "Wave-Sea Bottom Interaction Study (Final Report) Part 1: Theory and Results", Texas A&M University Report No. 3008-76-9.

Schapery, R. and W. Dunlap, (1978), "Prediction of Storm Induced Sea Bottom Movement and Platform Forces", Proceedings, Offshore Technology Conference, Houston.

Schapery, R. and W. Dunlap, (1984), "Theoretical and Experimental Investigation of Mud Forces on Offshore Pipelines", Report to American Gas Association, Center for Marine Geotechnical Engineering, Texas A&M University.

Sterling, G. H. and E. E. Strohbeck, (1973), "The Failure of South Pass 70 "B" Platform in Hurricane Camille", Proceedings, Offshore Technology Conference, Houston, Texas.

Stevenson, H. S., (1973), "Vane Shear Determination of the Viscoelastic Shear Modulus of Submarine Sediments", M.S. Thesis in Civil Engineering, Texas A&M Universtiy.

Wright, S. G. and R. S. Dunham, (1972), "Bottom Stability Under Wave Induced Loading", Proceedings, Offshore Technology Conference, Houston, Texas, Paper No. OTC 1603.

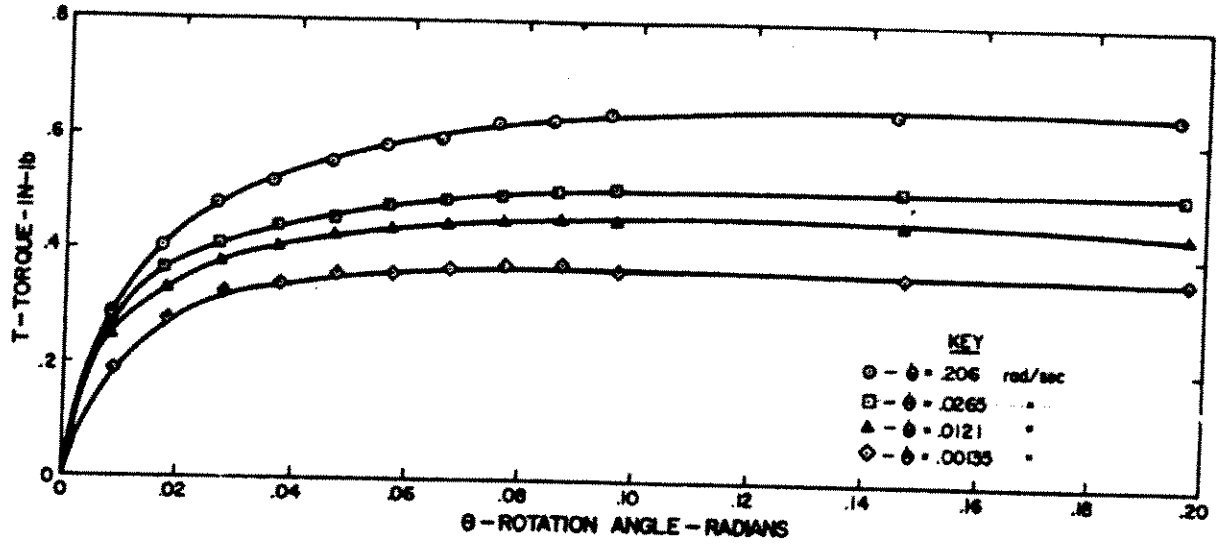

Figure 7-1 Typical torque vs. rotation data

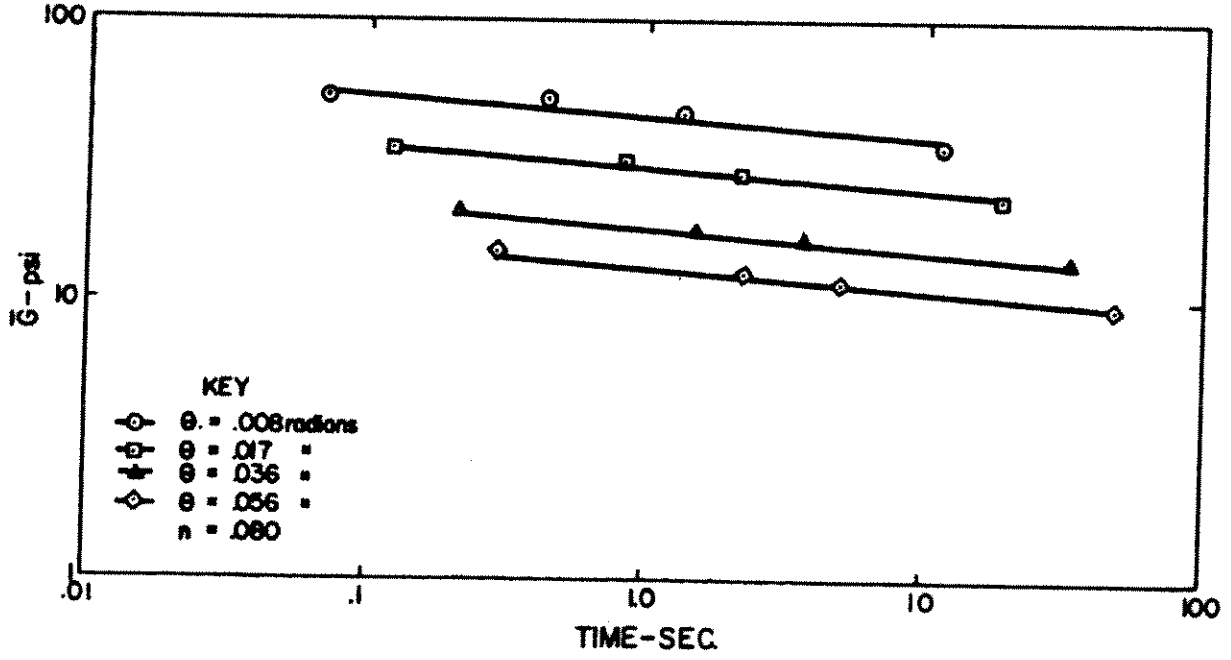

Figure 7-2 Relationship between stiffness G and time for results shown in Figure 7.1

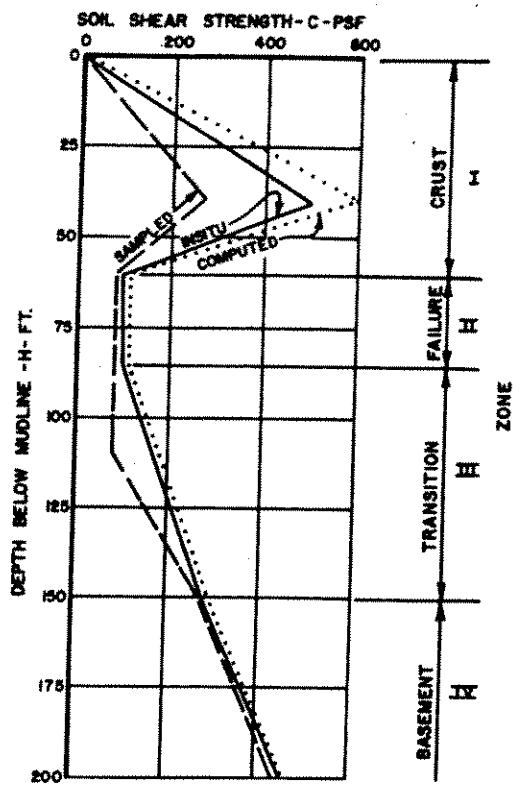

Figure 7-3 Idealized shear strength profile for So. Pass 70B platform. *In-situ* strength was used for analysis

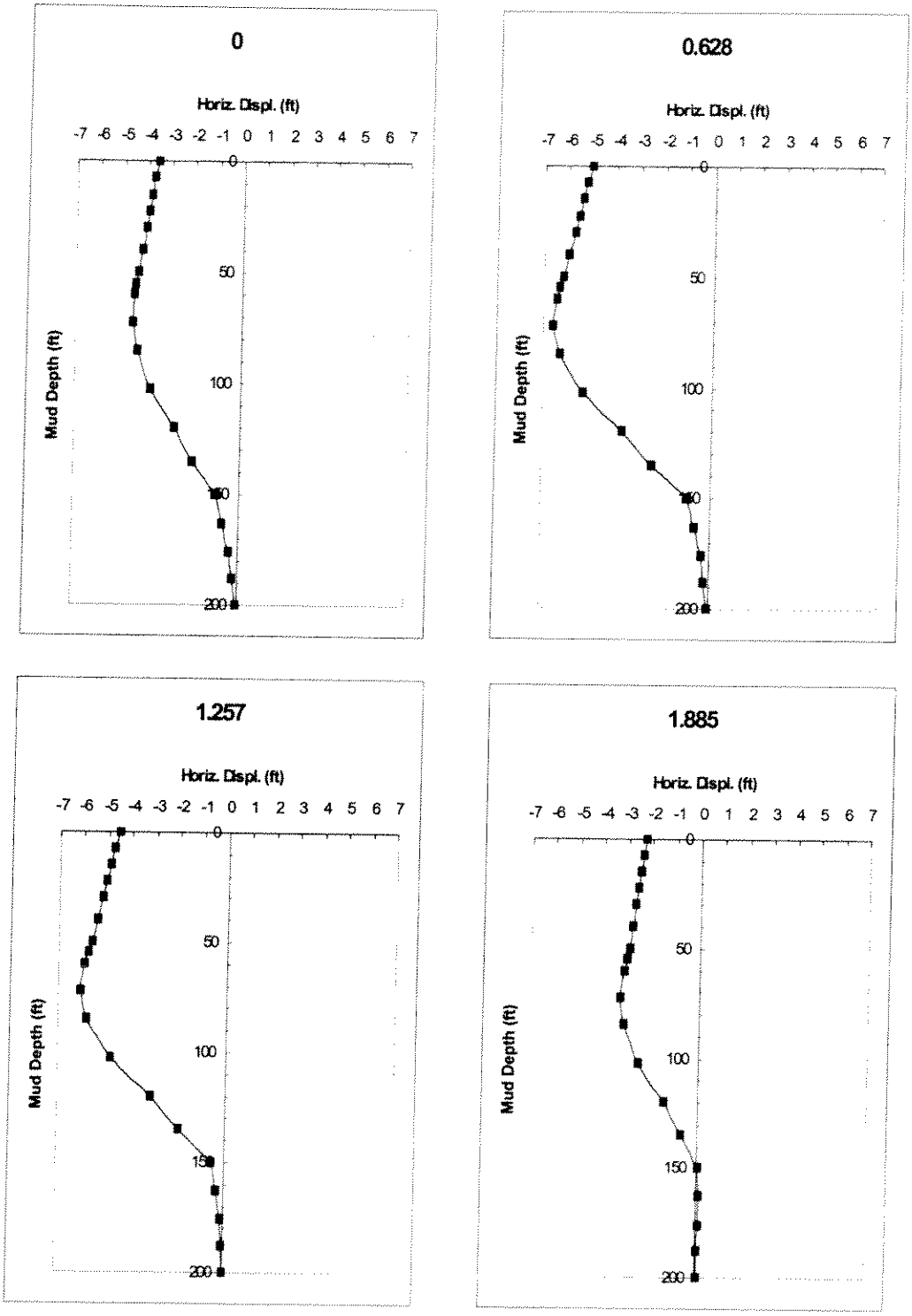

Figure 7-4 (a) Calculated cyclic sediment movements for So. Pass 70B platform. Bold numbers on top of each graph indicate distance along the wave length of 2pi.

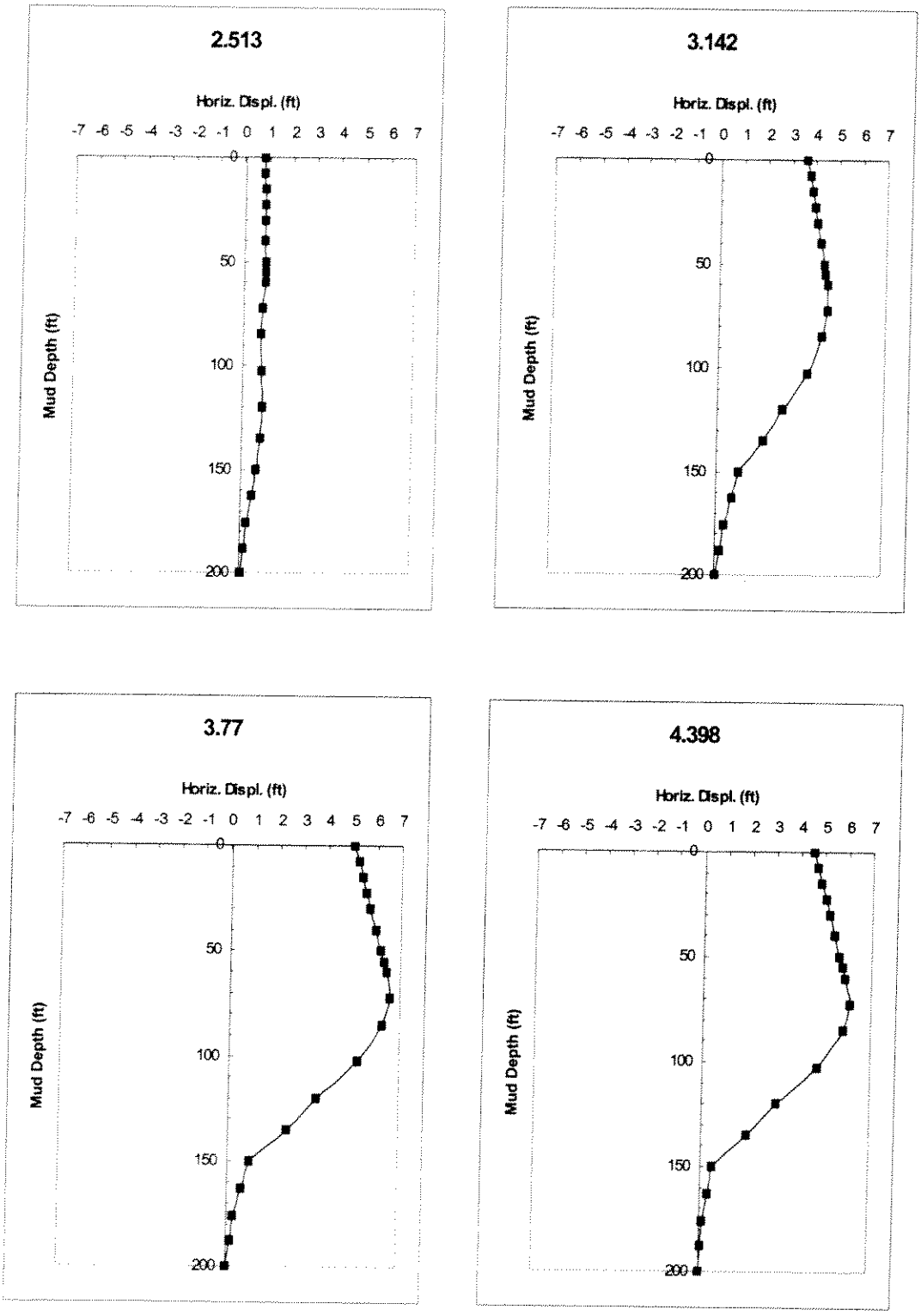

Figure 7.4 (b) Calculated cyclic sediment movements for So. Pass 70B platform. Bold numbers on top of each graph indicate distance along the wave length of 2pi (Continued)

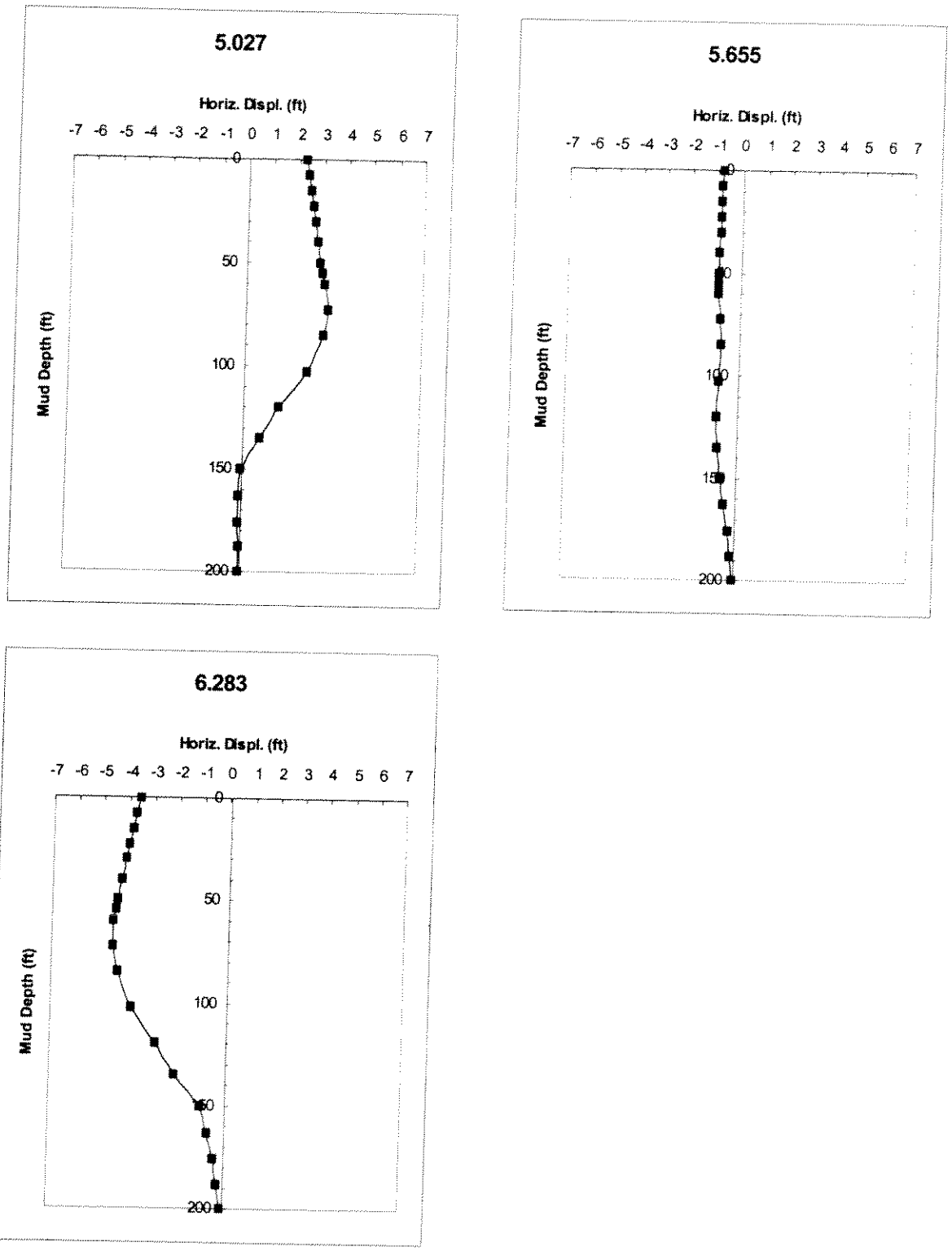

Figure 7.4 (c) Calculated cyclic sediment movements for So. Pass 70B platform. Bold numbers on top of each graph indicate distance along the wave length of 2pi (Continued)

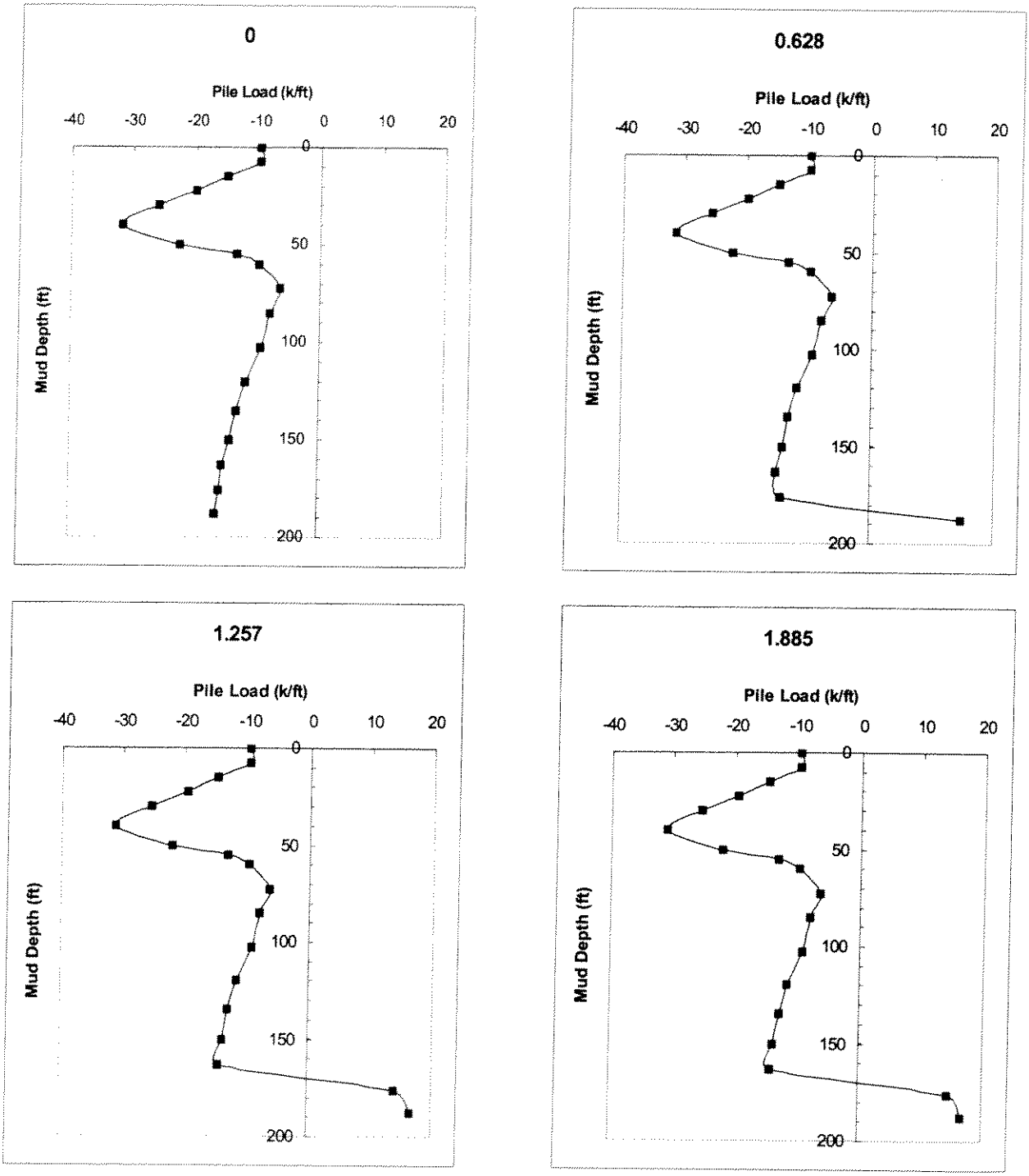

Figure 7-5 (a) Calculated sediment forces along 4 ft. diameters pile with 1% bottom slope for So. Pass 70B platform.

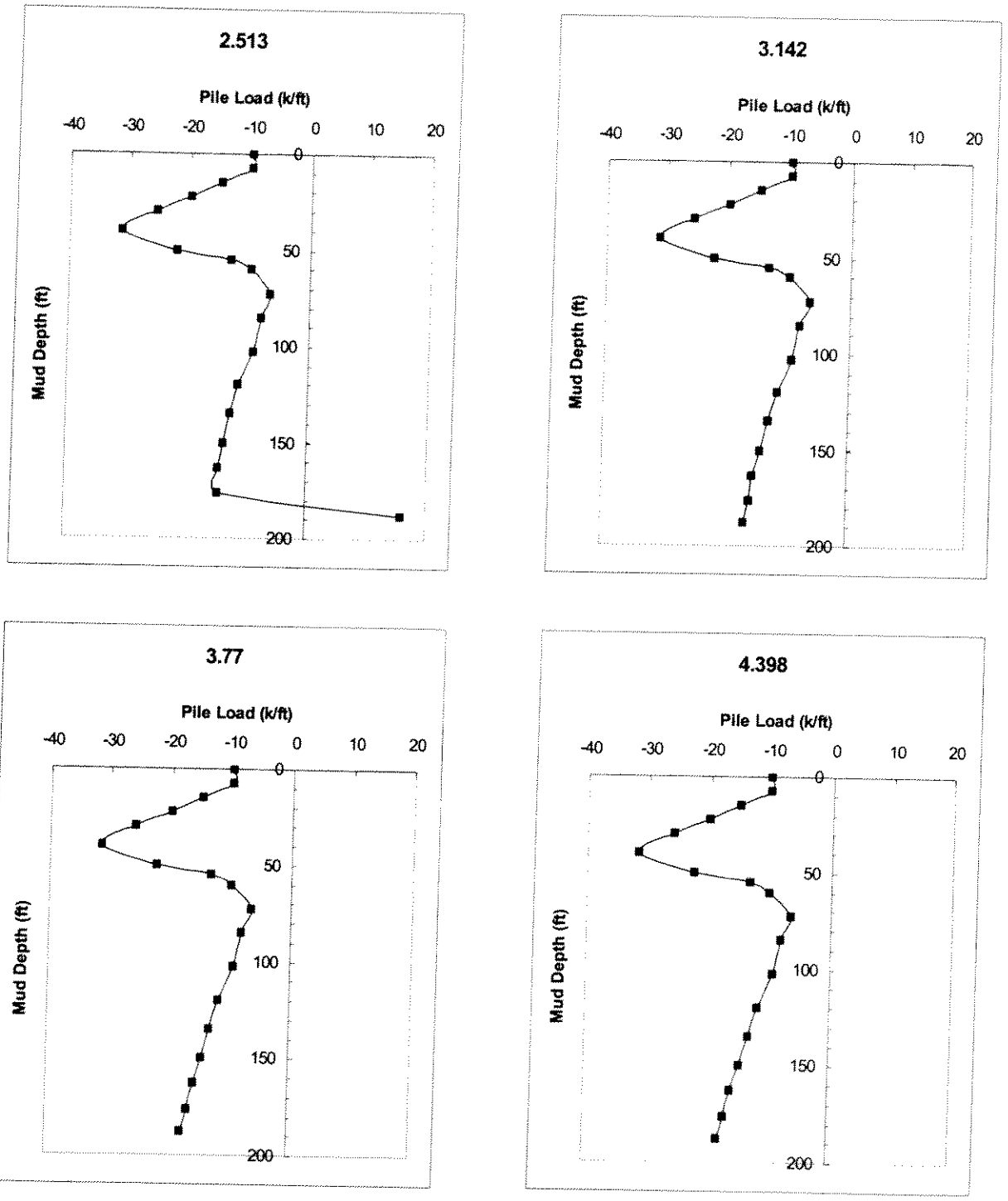

Figure 7.5 (b) Calculated sediment forces along 4 ft. diameters pile with 1% bottom slope for So. Pass 70B platform (Continued)

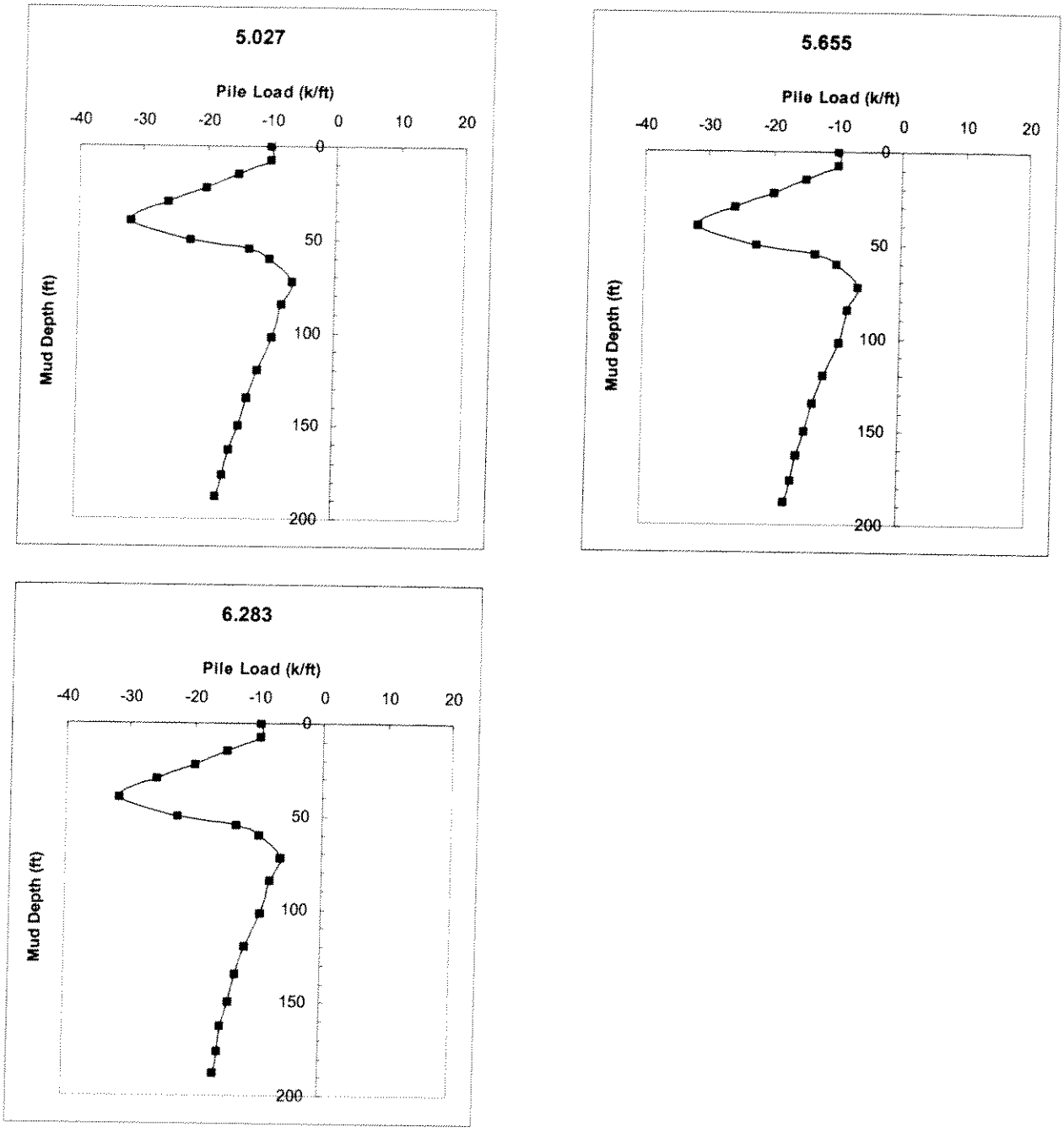

Figure 7.5(c) Calculated sediment forces along 4 ft. diameters pile with 1% bottom slope for So. Pass 70B platform (Continued)

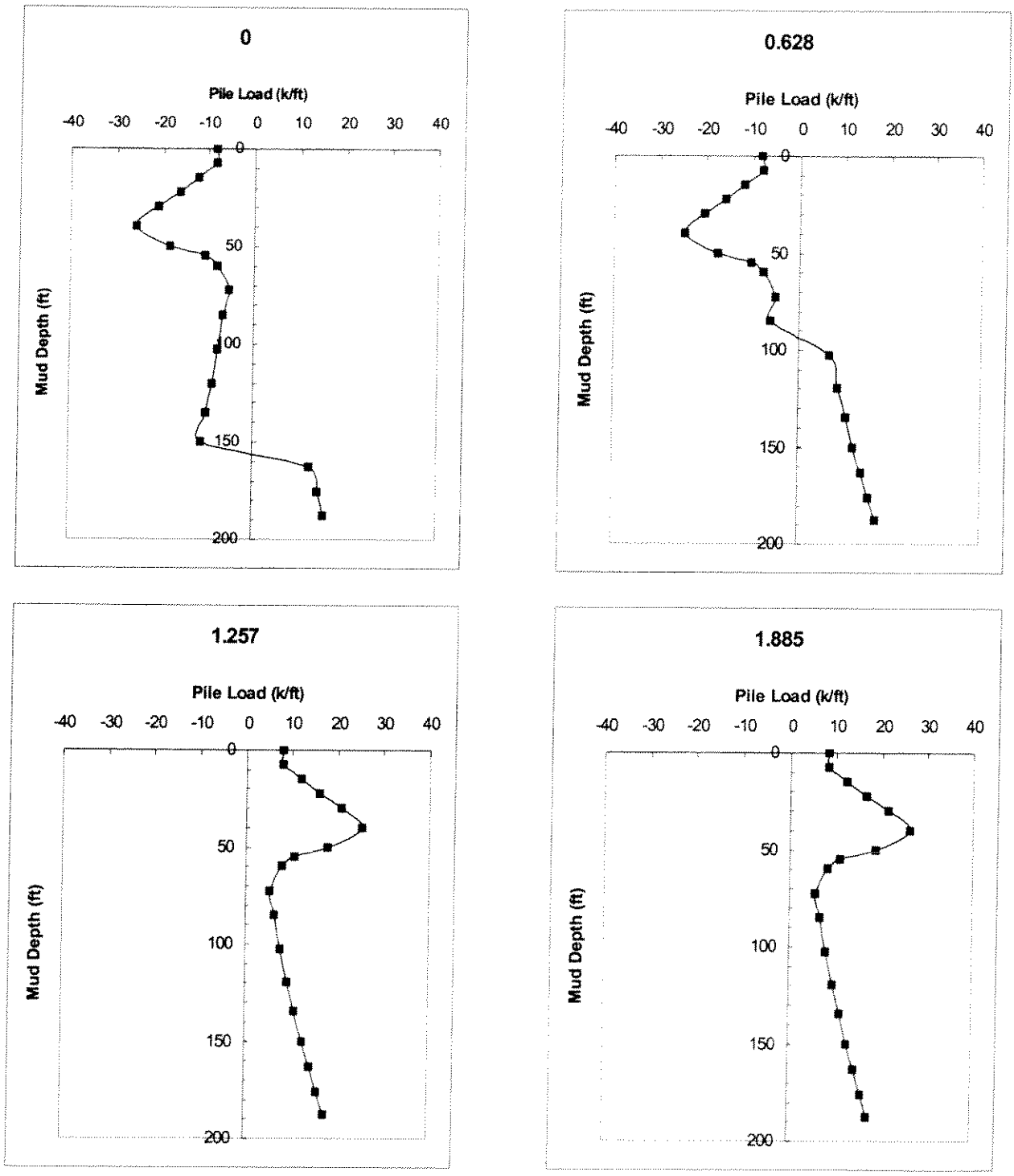

Figure 7-6 (a) Calculated sediment forces along 4 ft. diameters pile with 0% bottom slope for So. Pass 70B platform

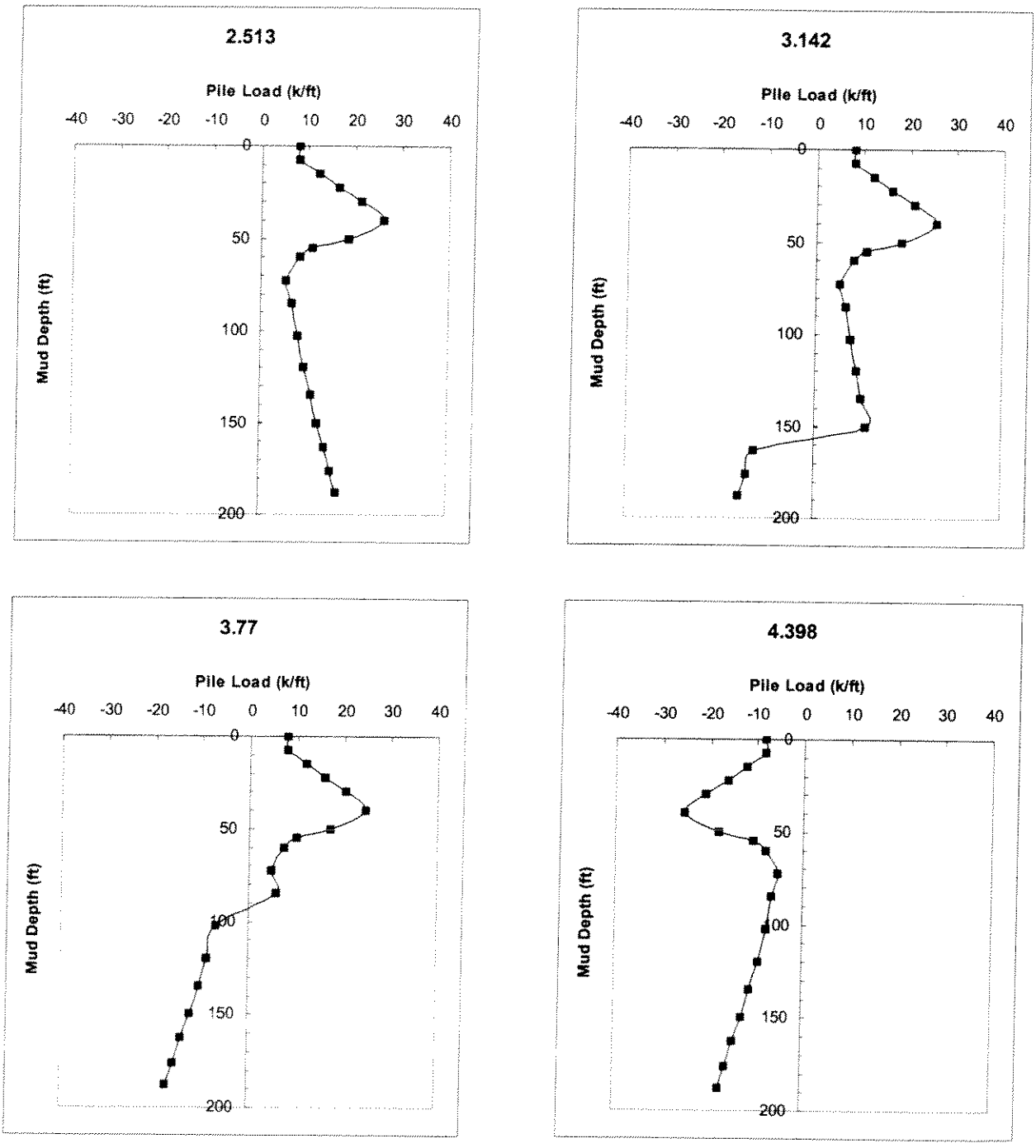

Figure 7.6(b) Calculated sediment forces along 4 ft. diameters pile with 0% bottom slope for So. Pass 70B platform (Continued)

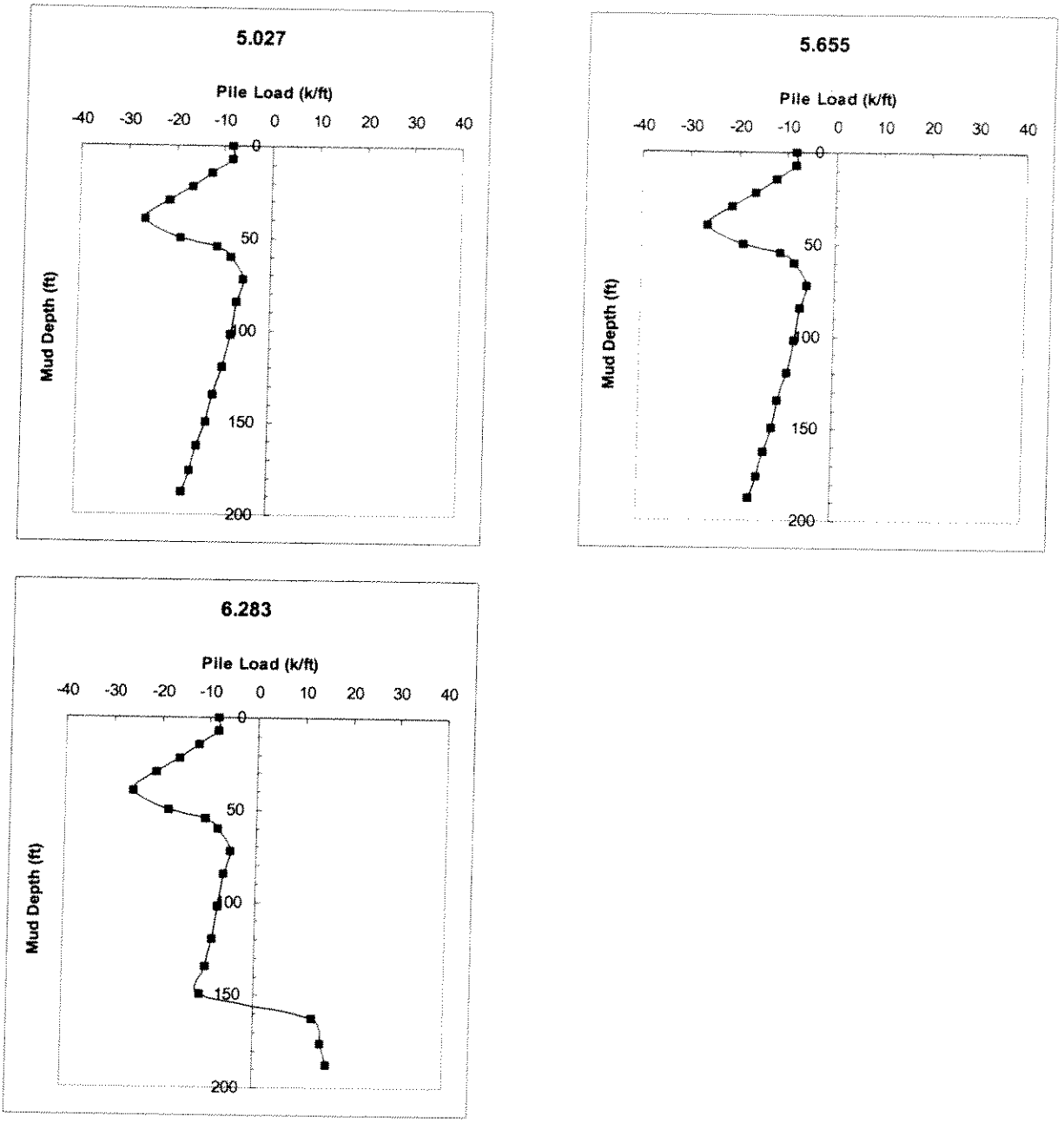

Figure 7.6(c) Calculated sediment forces along 4 ft. diameters pile with 0% bottom slope for So. Pass 70B platform (Continued)

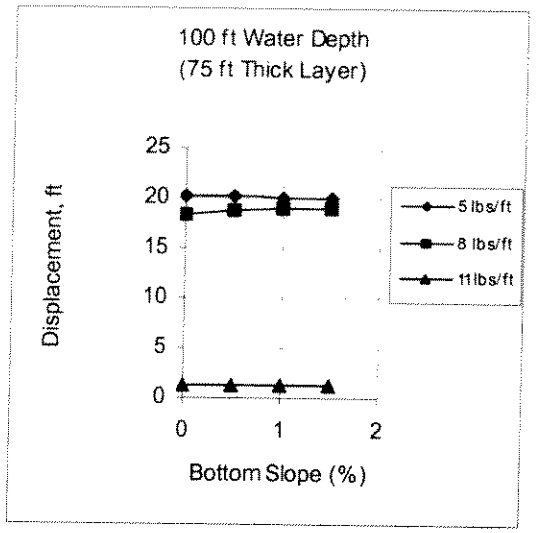

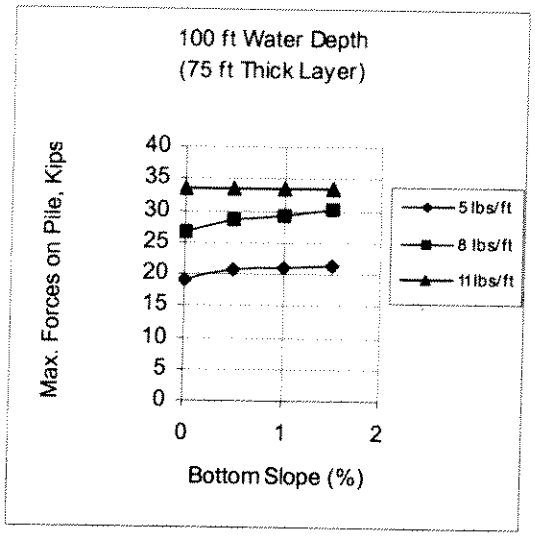

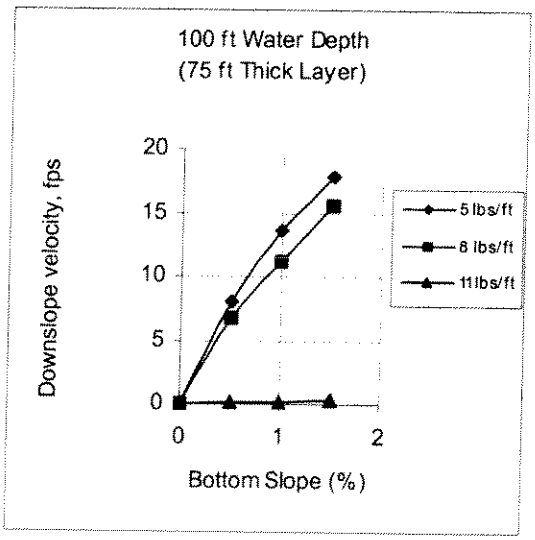

Figure 7-7 (a) Sediment movements and pile forces for 100ft. water depth and 75 ft. sediment thickness

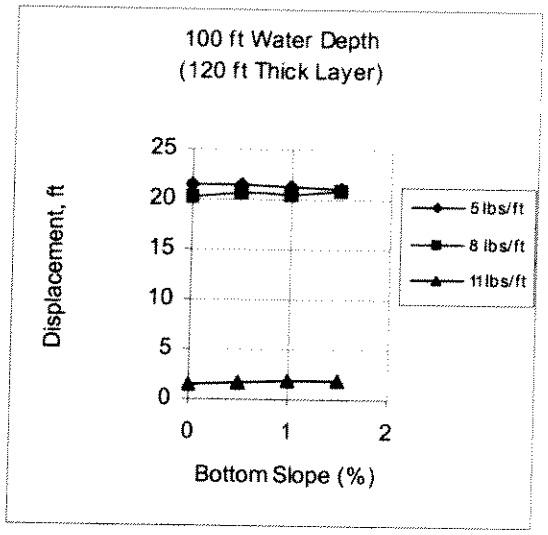

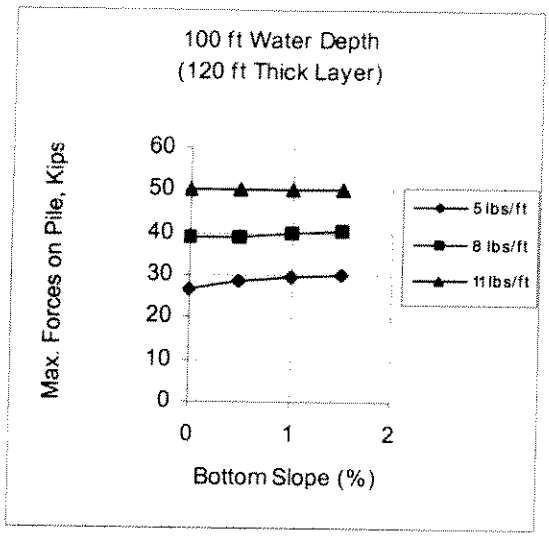

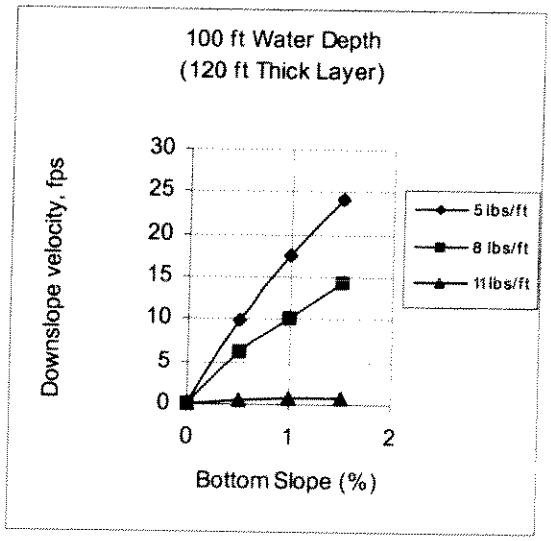

Figure 7.7(b) Sediment movements and pile forces for 100ft. water depth and 120 ft. sediment thickness

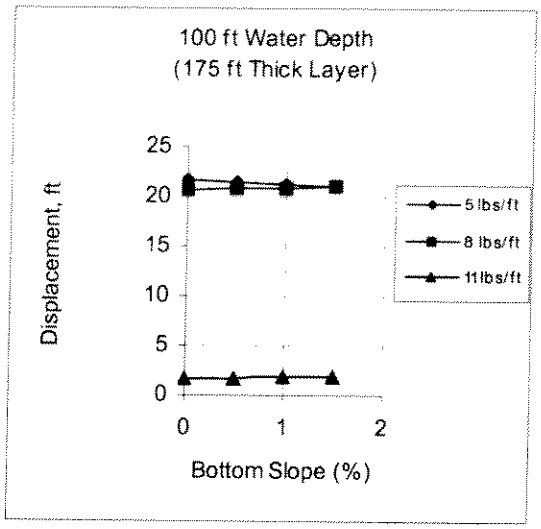

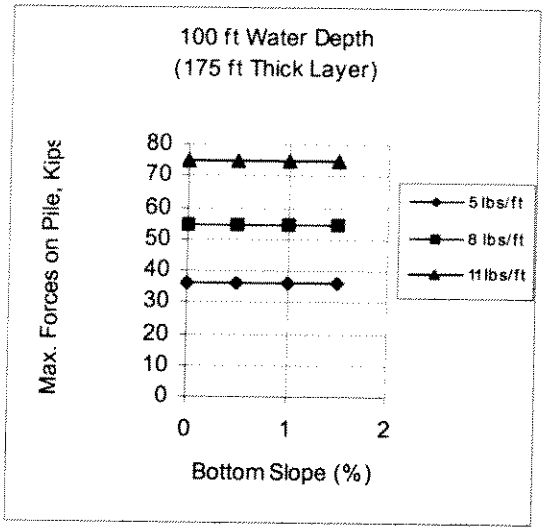

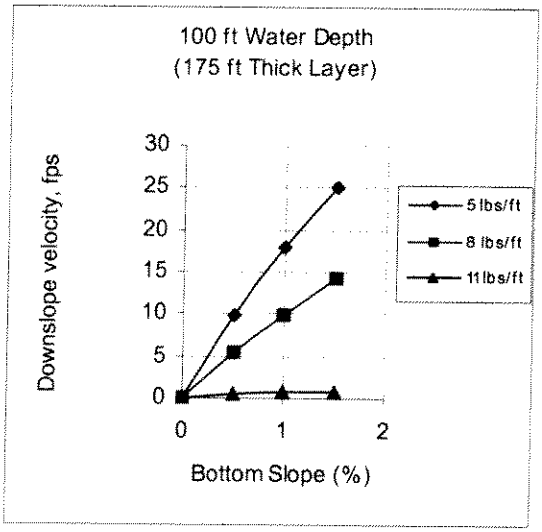

Figure 7.7(c) Sediment movements and pile forces for 100ft. water depth and 175 ft. sediment thickness

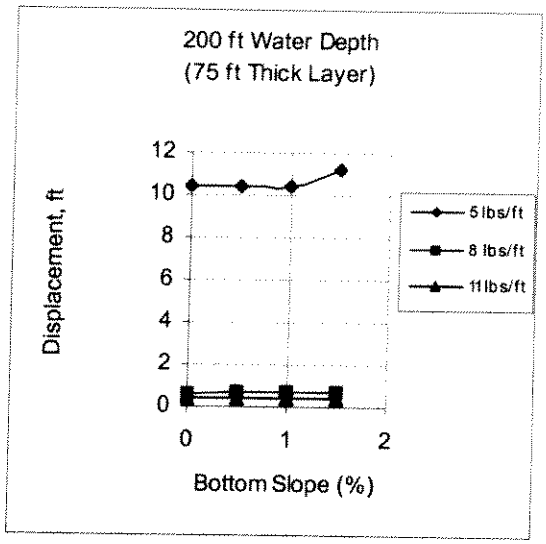

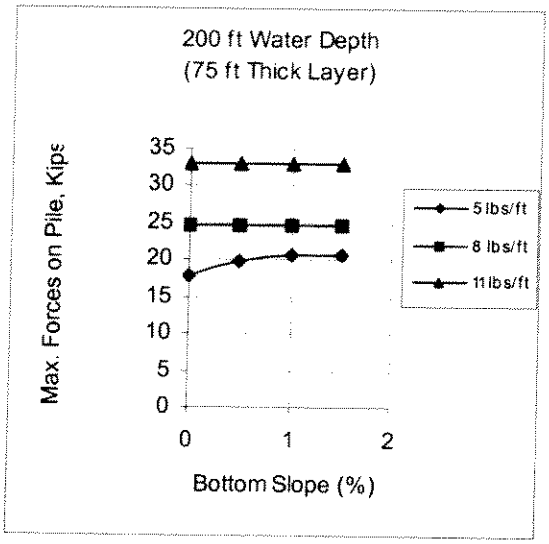

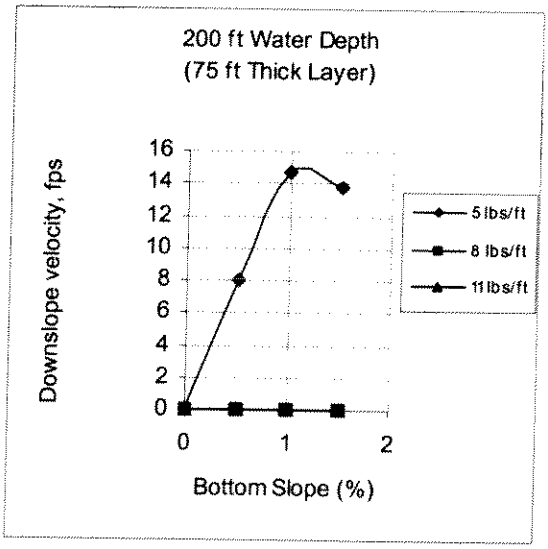

Figure 7-8 (a) Sediment movements and pile forces for 200ft. water depth and 75 ft. sediment thickness

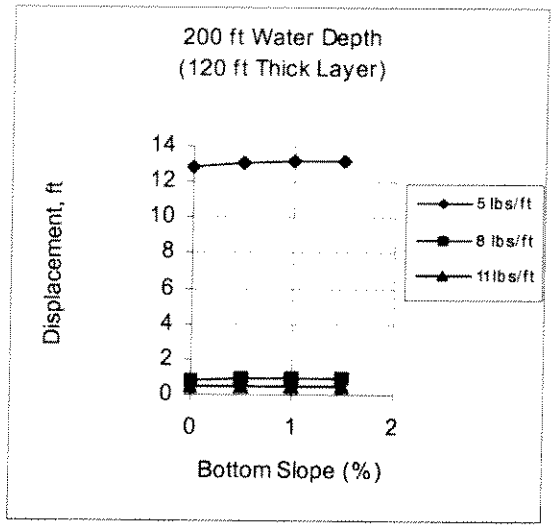

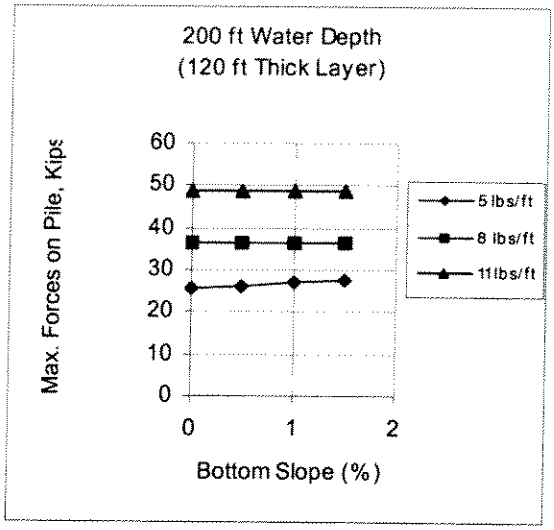

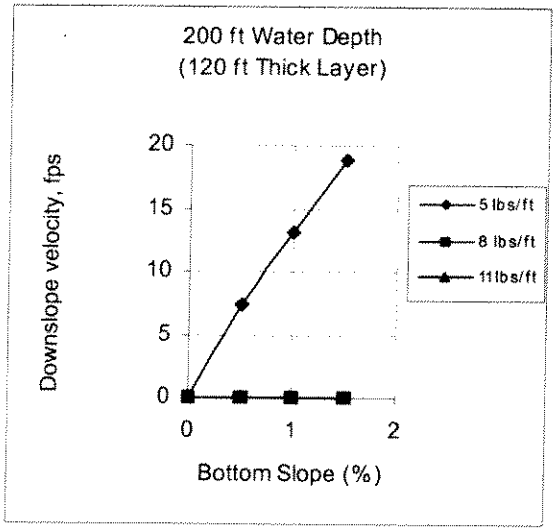

Figure 7.8(b) Sediment movements and pile forces for 200ft. water depth and 120 ft. sediment thickness

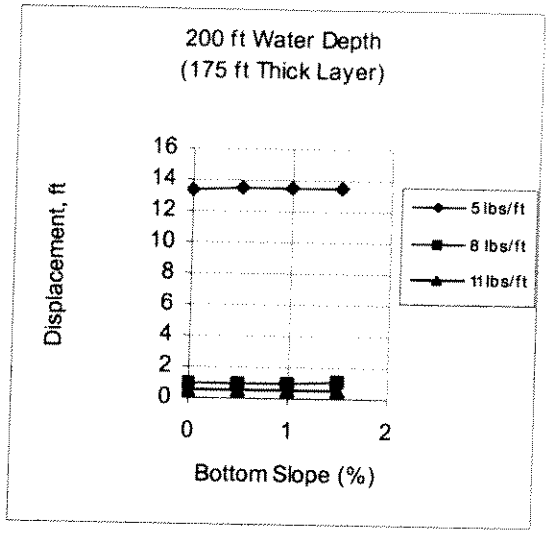

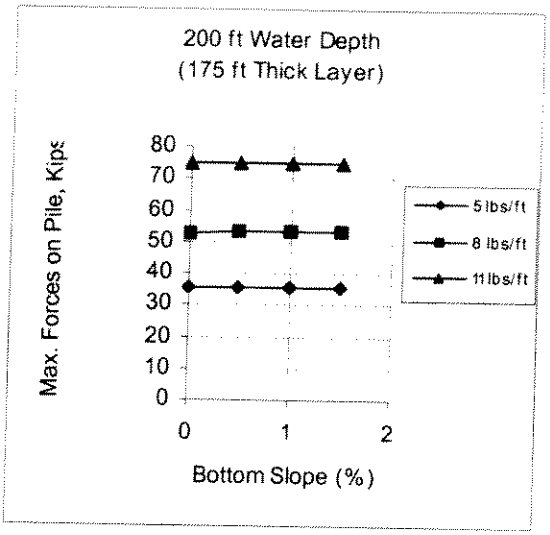

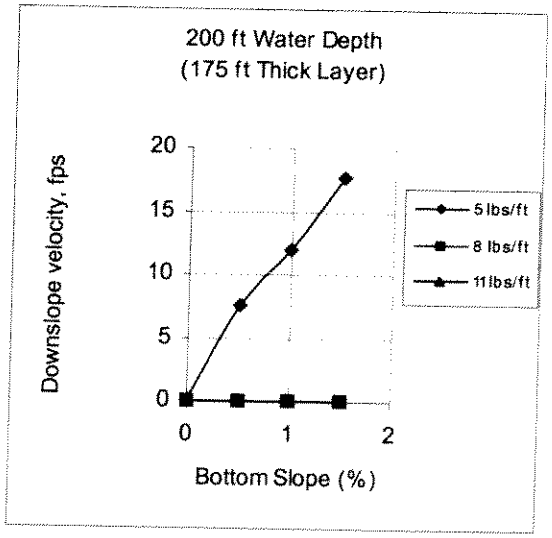

Figure 7.8(c) Sediment movements and pile forces for 200ft. water depth and 175 ft. sediment thickness

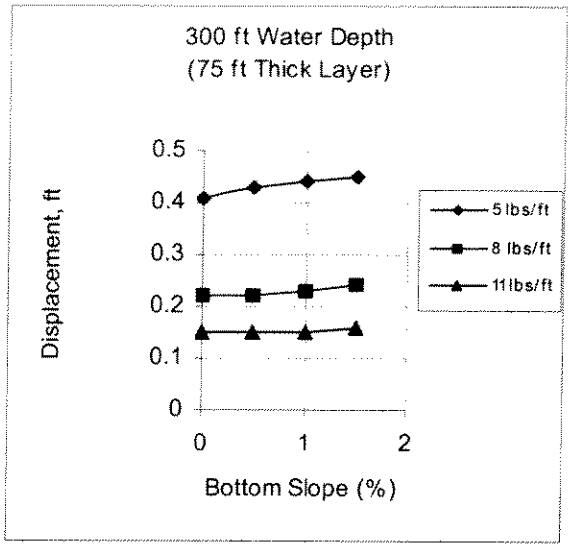

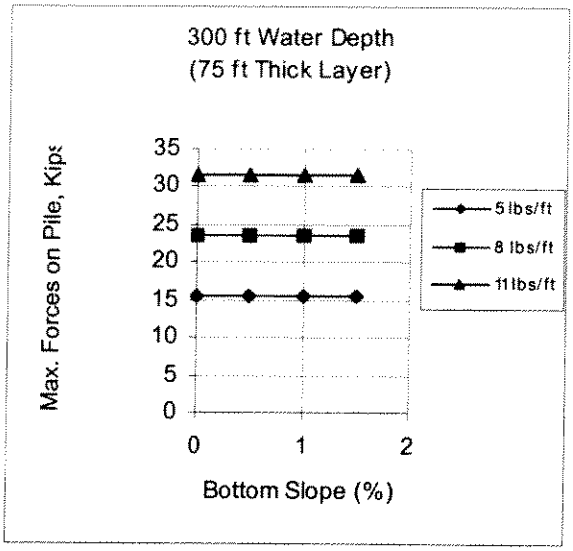

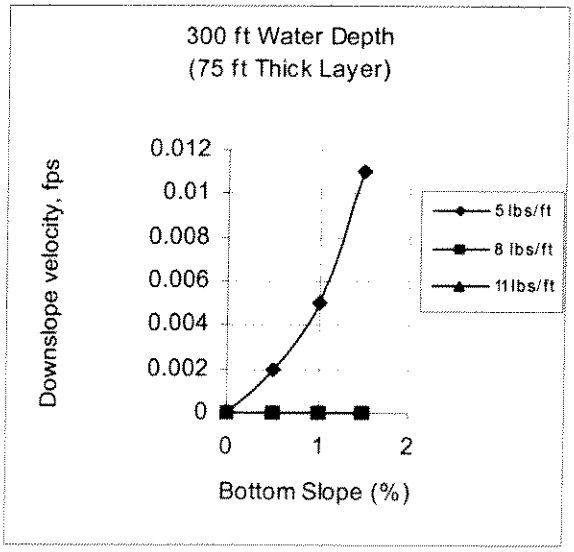

Figure 7-9 (a) Sediment movements and pile forces for 300ft. water depth and 75 ft. sediment thickness

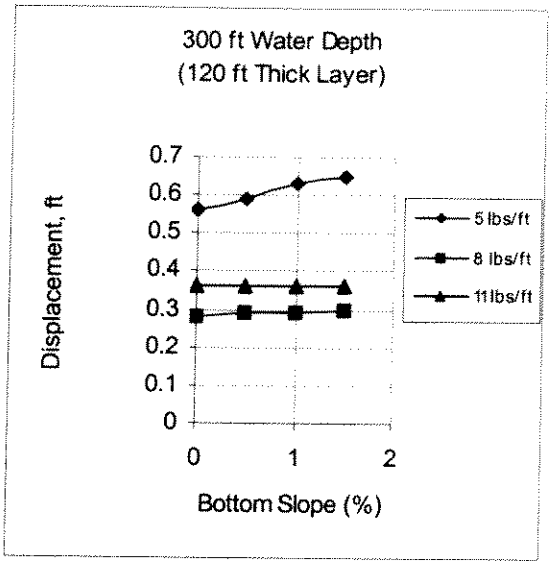

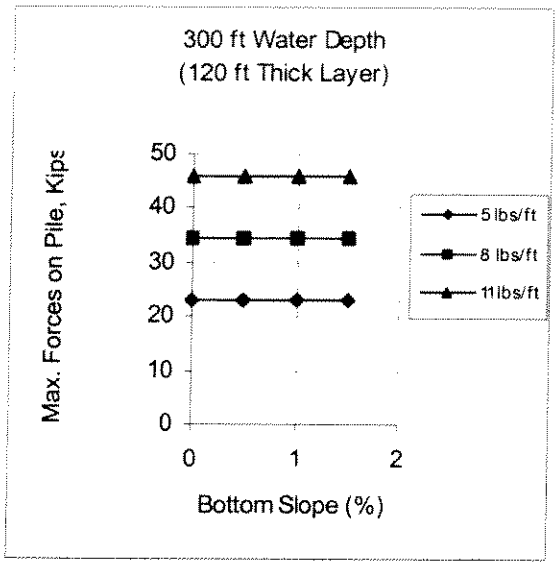

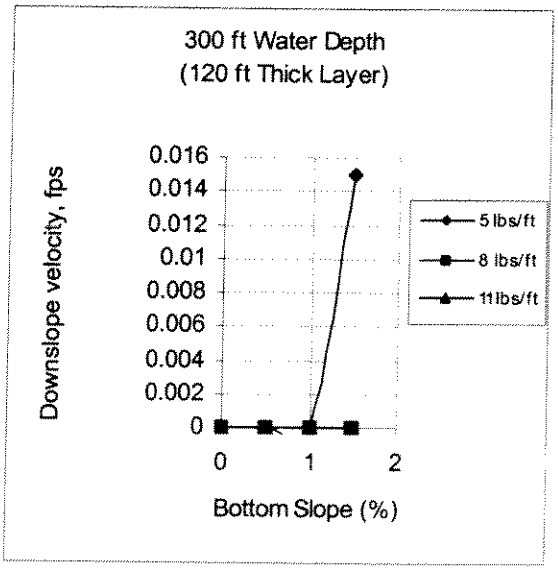

Figure 7.9(b) Sediment movements and pile forces for 300ft. water depth and 120 ft. sediment thickness

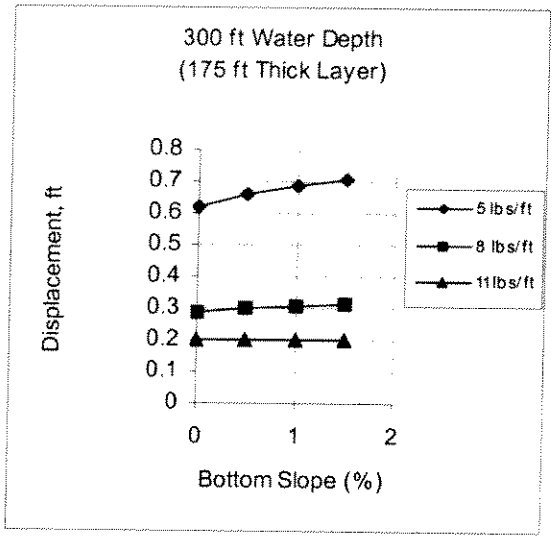

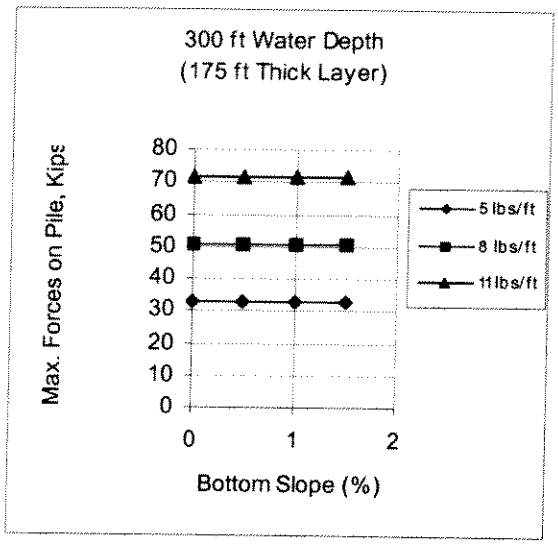

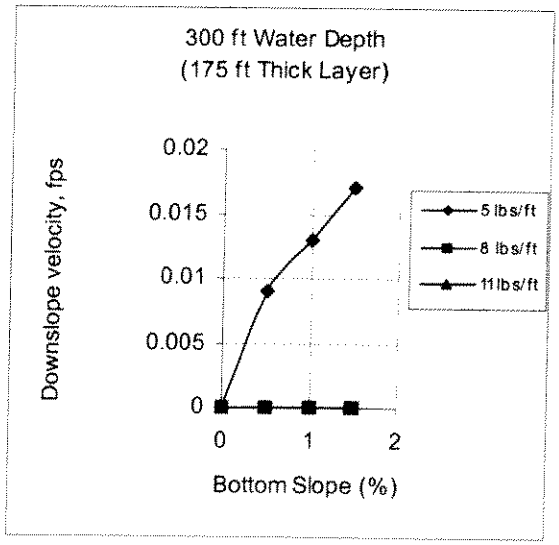

Figure 7.9(c) Sediment movements and pile forces for 300ft. water depth and 175 ft. sediment thickness

8 GEOTECHNICAL ASPECTS OF GAS HYDRATES

8.1 Introduction

Gas hydrates are ice-like materials composed of water molecules that encapsulate natural gas molecules in a very compact form. Immense quantities of gas hydrates exist in permafrost and offshore regions around the world. Figure 8.1 shows the worldwide locations of known and inferred gas hydrate deposits (Kvenvolden 2000). In Canada, gas hydrates have been identified onshore within the permafrost in the Arctic and offshore in the Beaufort Sea, off Vancouver Island, and off the coast of Newfoundland and Labrador.

Naturally occurring deposits of hydrates are common throughout the ocean basins of the world. Judge et al. (1994) have mapped the locations of natural gas hydrate deposits in Canada. Onshore deposits have been identified in the Canadian Arctic, trapped within the permafrost soils of the Yukon, Northwest Territories, and the Mackenzie Delta. Offshore Canadian deposits are located in the Beaufort Sea, off Vancouver Island, and off the coast of Newfoundland and Labrador. These deposits exist both on the seabed and more commonly trapped within the seabed sediments.

8.2 Human interest in Gas Hydrates

Gas hydrates came into awareness in the 1930s when hydrate formations were discovered to be the cause of pipeline blockage during the transmission of natural gas. Figure 8.2 presents the phenomenon of burning hydrate. Sloan (1998) summarizes the history of gas hydrate research and includes reference to the first observations of naturally occurring hydrates found in permafrost regions in 1965. By the 1970s, it was recognized that gas hydrates occur naturally in the sediments underlying 'deep' water (Claypool & Kaplan 1974). Interest in hydrates has continued in the last 30 years. Hydrates affect humans in three distinct ways: (1) as a potential energy resource, (2) as a factor in global climate change, and (3) as a submarine geohazard (Kvenvolden 1993).

Although gas hydrates were recognized as an energy source in the 1960s, there was a general lack of interest in extraction of methane from hydrates due in part to abundant conventional gas supplies and lack of economic incentives. Interest in methane extraction from hydrates has increased dramatically over the last few years. Worldwide, the total amount of carbon in hydrate form is believed to be twice that of all conventional reserves (coal, oil, natural gas) combined (Suess et al. 1999). Research wells have been drilled in Northern Canada, Offshore USA, and Western Siberia where the Siberian well has produced methane gas for a number of years now. However, many challenges still face scientists and engineers before full-scale production of methane for energy from gas hydrates can occur. Perhaps one of the greatest is "complicated geological and technological problems" (Kvenvolden 2000).

Methane gas is greenhouse gas, which is ten times more productive than carbon dioxide at adsorbing heat from the sun and warming the earth. The earth has a number of sources and sinks of atmospheric methane including gas hydrates. A vast quantity of methane is stored within hydrates, which if released, could have a substantial impact on atmospheric conditions and thus

affect global climate change. As the earth warms, gas hydrates will dissociate (melt) and release further methane thus causing further warming. The exact role of hydrates on global climate change is uncertain as illustrated in Figure 8.3, however we do know that continual practices leading to global warming will result in gas hydrate dissociation (Kvenvolden 2000).

There are many examples of a possible connection between gas hydrates and submarine slope failures. Kvenvolden (1993; 1999) summarized slope failures on the continental slope and rise of the west coast of Africa, on the US Atlantic continental slope, on the Norwegian continental margin, in the fjords of British Columbia, and on the Alaskan Beaufort Sea continental margin. Sloan (1998) indicates that there is substantial observational evidence that links major seafloor collapses, submarine slides, and drilling hazards to the presence of hydrates. Geohazards resulting from gas hydrates place offshore drilling and production facilities at considerable risk of damage.

In order to assess the role that hydrates play in submarine slope stability and the other human-interest areas, we need to have a better understanding of the fundamental issues. Sloan (1998) cites four underlying issues or areas in which research is needed:

a) distribution – We need to determine the occurrence, distribution, and concentration of gas hydrates. Estimates of hydrate quantities are based on extrapolation of local measurements or from crude estimates from parameters considered proxies for gas hydrate concentration. Certainly a better understanding of the volumes, distribution, geologic settings, and controlling processes would lead to a better estimate of hydrate resources.
b) detection – We currently rely on geochemical proxies, seismic reflection methods, and core samples to detect the presence of hydrates. Work is needed on sampling, transport and handling of hydrate cores with the objective of retrieving and testing in-site hydrate-sediment properties with confidence. Remote sensing methods also need to be further developed and surveys carried out to determine the relationships between hydrate distribution and geologic processes.
c) sediment properties – Formation and dissociation of gas hydrate in sediments causes immense changes in shear strength, as well as many other physical parameters, the results of which are mass movements, collapse, and loss of bearing capacity (Sloan 1998). Studies of the geotechnical properties of hydrate-sediment mixtures are necessary to understand the fundamental behavioural changes induced by formation and dissociation. An improved fundamental knowledge combined with a greater understanding of the in situ characteristics compared to an increased database of field observations will lead to understanding the role of hydrates in submarine slope failures.
d) hydrate controls – We must obtain a better understanding of the dynamics of hydrate equilibrium before we can investigate their response to fluxes such as commercial production, earthquakes, and climate change.

Sloan (1998) goes on to recommend the approach to hydrate problems should be to: (a) identify the best sites appropriate to hydrates as either a potential resource, an agent in global change, or a factor in seafloor hazards; b) assess any target sites in terms of cross-cutting scientific needs;

and c) evaluate experiments to be performed at these sites, along with laboratory experiments relative to the field observations.

8.3 Hydrate properties

8.3.1 Structure

Natural gas hydrates belong to a class of solids known as clathrates. Several different structures of clathrates exist which accommodate guest molecules of different sizes, see Figure 8.4 for example. The hydrate forming gases include light alkanes, carbon dioxide, hydrogen sulphide, nitrogen and oxygen. Methane gas, the most common clathrate, forms a Structure-I hydrate in which one volume of water will enclathrate (adsorb) 207 volumes of methane gas. This translates to 1 m^3 of hydrate containing 0.9 m^3 of water and 164.5 m^3 of methane gas, at standard conditions, or 1.1 m^3 of methane gas at 1000 m water depth and 2 °C.

8.3.2 Acoustic properties

Acoustic properties (P and S waves) provide important information on the soil structure. Knowledge of the material occupying the pore space and the consolidation stress is critical to understanding the implications of the velocity measurements (Winters et al. 1999). Table 8-1 summarizes some published acoustic properties (based on Anderson 1992).

Table 8-1. Summary of acoustic properties of gas hydrates (from Anderson 1992).

Parameter	Pure hydrates	Water-saturated sediments	Hydrate-sediment mixture
Compression wave, V_p (km/sec)	3.25-3.6	1.6-2.5	2.05-4.5
Shear wave, V_s (km/sec)	1.65	0.38-0.39	0.14-1.56
Bulk density (g/cm^3)	-	1.26-2.42	1.15-2.4

Winters et al. (1999) performed studies on the properties of hydrate-sediment mixtures using core samples obtained from the Mallik Well. Their investigation into the acoustic properties indicated that the P-wave velocity of specimens containing hydrates decreased at least 25% after dissociation. Booth et al. (1998) presented a correlation between the change in compression wave velocity and the presence of hydrates.

8.3.3 Electrical resistance

Gas hydrate formation is accompanied by a sharp increase in the electrical resistance (Makogon et al. 1997; Booth et al. 1998). The resistance of hydrate-saturated sediments varies from approximately 10^3 to 10^6 Ohm-m (Tzirita 1991). Water has a resistance of approximately 10 Ohm-m, sand approximately 10^2-10^3 Ohm-m, and ice about 10^5 to 10^6 Ohm-m. Electrical properties have been used to estimate hydrate content (Buffet & Zatsepina 2000; Booth et al. 1998) but further work on the electrical resistance of hydrate-sediment mixtures is required.

8.3.4 Density

The density of pure methane gas hydrates ranges from 0.895 g/cm^3 at 1 MPa to 1.053 g/cm^3 at 1000 MPa (Makogon et al. 1997). The density of hydrate-sediment mixtures will depend on the density of the sediment and the percentage of the void spaces occupied by hydrates.

8.3.5 Strength properties

The strength of hydrates and hydrate sediment mixtures is influenced by a number of factors including strain rate, temperature, confining pressure, grain size, and density and most likely by hydrate cage occupancy. Studies on the strength of hydrates and hydrate saturated media have been performed by Parameswaran et al. (1989), Cameron and Handa (1990), and Winters et al. (1999). Results of these tests indicate that specimens containing gas hydrates have undrained shear strengths in the order of three times greater than similar specimens without hydrates. The strength of hydrate bearing sand is in the same range as the strength of ice bearing sand. Although the hydrates will increase the strength of the soils, it is essential to consider the significant strength loss if dissociation of the hydrates occur.

8.3.6 Hydraulic conductivity

There is considerable variation in the hydraulic conductivity of hydrate-sediment mixtures (Winters et al. 1999). Factors affecting the in situ hydraulic conductivity will include grain size, porosity, structure, discontinuities, and tortuousity of the sediments and viscosity of the fluids.

8.4 Hydrate Stability

Gas hydrates form under specific conditions of low temperature and high pressure. Oceanic hydrates are stable in a zone extending downward from the seafloor in water depths greater than 400 m to a depth determined by the geothermal gradient. The hydrate stability zone is a function of the water depth, seafloor temperature, and geothermal gradient. For offshore conditions, the pressure-temperature correlation shown in Figure 8. 5(a) can be used to determine the hydrate stability zone in pure water (Kamath et al. 1987). For hydrates in seawater, the temperature is shifted approximately – 1.5°C, i.e. salt water inhibits hydrate formation to a certain extent (Dickens and Quinsby-Hunt 1994).

For onshore conditions, the hydrate stability is a function of the stress state (i.e. depth of burial in the sediments) and the ambient ground temperature. Figure 8.5(b) illustrates an example of the hydrate stability zone for hydrates buried within permafrost soils.

At pressure and temperature conditions outside the stability range, dissociation or melting of gas hydrates will occur. Pressure decreases may occur due to sea level variations or removal of mass by slumping or sliding. Temperature increases may develop due to increased seawater temperatures, due to sedimentation, or due to heat from producing wells.

8.5 Formation of Gas Hydrates

Gas hydrates form under conditions of high pressure and low temperature. Hydrates are found offshore on and beneath the seafloor in water depths greater than approximately 300-500 m and on land beneath permafrost soils in arctic regions. Figure 6 shows a picture of hydrate mound on the seafloor. Natural gas hydrates are formed from both biogenic and thermogenic gas sources. Biogenic gas is the product of anaerobic bacterial activity and is found in areas where there is a rapid accumulation of organic matter and sediments. Thermogenic gas has been altered by time and pressure and is found along faults, vents and seeps. Most scientists believe that most natural gas hydrates are formed from biogenic methane gas. In general, biogenic hydrates are more evenly distributed throughout the sediment except when the organic matter has been concentrated or the methane gas has migrated to the bottom of a less permeable layer. Thermogenic hydrates are likely to be more concentrated and can often mound on the seafloor near the fault.

Gas hydrates have been observed in coarse sediments, such as sand and sandstone; fine-grained sediments, such as clays; deep-sea ooze and mudstones; and also filling in fractures within sediments (Kvenvolden 1993; Makogon 1981). The tendency for hydrates to form in sediments of higher porosity has been observed but a clear-cut relationship does not exist. Clennel at al. (2000) have investigated how pore size and capillary action affect hydrate stability and determined that hydrate growth is inhibited within fine-grained sediments. Clennel and co-workers also developed a model to predict the way in which hydrate is distributed on the microscale to mesoscale within sediments.

The geologic history will also affect the formation of hydrates within sediments. Hydrate layers may melt and reform. Seasonal or climatic fluctuations will affect the stability of hydrates as will earthquakes or other mechanical disturbances. Hydrates may form caps, which seal off faults or they may fill in sediment pore spaces effectively sealing them (Rowe & Gettrust 1993). In permafrost regions, the frozen ground often creates a seal which prevents gas from escaping and initiated hydrate formation.

8.5.1 Formation of gas hydrates in soil specimens

The majority of information in the literature regarding gas hydrates in porous media is actually with respect to specimen preparation. The original studies on the properties of gas hydrates in porous media used tetrahydrofuran (THF) to form a structure II hydrate where the resulting specimen consisted of THF hydrate and frozen soil (Parameswaran et al. 1989; Sego and Wittebolle 1984). Synthetic hydrates have also been formed using other refrigerants such as R11; using R11 a sand specimen containing both synthetic hydrate and free water could be formed. More recently researchers have formed hydrates under higher pressures by exposing sand specimens to carbon dioxide saturated water (Buffet and Zatsepina 2000) or exposing sand to methane gas (Wright et al. 1998). Grozic and Kvalstad (2001) formed gas hydrates by exposing a clay specimen to methane saturated water at high pressure and low temperatures. Methods of forming hydrates by exposing the specimen to free and/or dissolved gas simulate the in situ formation of hydrates and have therefore become more popular in recent years.

8.6 Dissociation of Gas Hydrates

8.6.1 Theory

At pressures and temperatures outside the hydrate stability range, dissociation (melting) of gas hydrates will occur. Dissociation will result in the release of water and methane gas but requires heat input through heat flow. Makogon et al. (1997) gives an expression for calculating the heat of formation/dissociation from natural gases. Complicating the dissociation process are the effects of time dependency, soil permeability, and diffusion.

As dissociation occurs, the released gas and water creates a volume expansion that depending on the drainage conditions, can cause an increase in the pore fluid (gas and water) pressures and a resulting decrease in the effective stress. The following discussion on the effect of methane hydrate on the soil response to temperature and total stress changes is based on Grozic & Kvalstad (2001).

Dissociation of gas hydrate will release gas and generate a volume expansion. If the temperature/heat transport and the pressure change processes are fast compared with pore pressure dissipation processes, the excess pore pressure and reduction in effective stress can be estimated as follows:

$$-0.13 \cdot n \cdot (1 - S_w) + \frac{164.6 \cdot n \cdot (1 - S_w) \cdot 1atm \cdot T_{eq}}{298.15K \cdot p_{eq}} = -\frac{\Delta\sigma'}{M(\sigma')}$$

where n is the soil porosity, S_w is the degree of water saturation, (1-S_w) is the degree of saturation of gas hydrates assuming no free gas in the hydrate stability zone, T_{eq} is the equilibrium temperature of gas hydrate in K, p_{eq} is the equilibrium pressure of gas hydrate in atm, $\Delta\sigma'$ is the change in effective stress caused by melting of gas hydrate, and M is the confined compression modulus of soil. The first term represents the difference between the hydrate volume and melted water volume (1.0 m^3 – 0.87 m^3), the second term represents the volume of released gas at equilibrium temperature and pressure and the final term represents the volume change of the soil.

If it is assumed that the pore water pressure and the pore gas pressure are equal then:

$$\Delta p = \Delta u + \Delta\sigma'$$

where Δp is the change in total stress and Δu is the change in pore pressure. For a pure temperature induced melting, $\Delta p = 0$ and $\Delta u = -\Delta\sigma'$, and thus:

$$\Delta\sigma' = -\Delta u = M(\sigma') \cdot n \cdot (1 - S_w)\left[0.13 - 164.6\frac{T_{eq}}{298.15}\frac{1atm}{p_{eq}}\right]$$

The above equation is valid until the effective stress reduction reaches the overburden pressure, resulting in zero effective stress, or until the gas starts to form bubbles.

The effect of hydrate dissociation has been predicted using the above equation. Figure 8. 7 shows a plot of hydrate content (percentage of voids occupied by hydrates) versus the normalized effective stress. This Figure 8.7 illustrates that if even as little as 5% hydrates occupy the soil voids, changes in equilibrium leading to dissociated could bring about soil failure.

8.6.2 Laboratory studies

A few laboratory studies have investigated the soil response to hydrate dissociation. Grozic and Kvalstad (2001) investigated the response of clay soil to hydrate dissociation in the laboratory. The results indicate that the specimen will undergo an increase in pore fluid (water and gas) pressures during dissociation which results in a decrease in effective stress and a loss of shear strength. Comparison of the theoretical results predicted using the theory presented above and observed test results showed a correspondence, however considerable uncertainty existed regarding estimates of the hydrate content in the laboratory and further testing was recommended. Kvalstad (personal communications 2001) confirms that the gas hydrate testing is ongoing at the Norwegian Geotechnical Institute.

Wright et al. (1999) formed and dissociated gas hydrates within fine sand to investigate the pressure temperature conditions and kinetics of hydrate formation/dissociation. They noted a small but measurable shift in the pressure – temperature equilibrium threshold during hydrate dissociation which may be related to weakly bound water in association with soil particles surfaces in unsaturated fine sands.

Makami et al. (2000) used granular core samples, containing natural gas hydrates within the pore spaces, from the Mallik 2L-38 well drilled in the Mackenzie Delta. They warmed the samples from –18 to +4 °C while the samples were contained within at CT (computerized tomography) scanner. Dissociation of the hydrates was controlled through controlled pressure reductions to bring the samples out of the hydrate stability range. The important conclusion from this experiment was that dissociation was initiated nearly simultaneously within the interior of the sample and at the sample surface, although this could be due to the pore spaces not being completely filled with hydrate.

8.7 Gas Hydrates and Submarine Slope Stability

Observational evidence suggests that gas hydrates have a role in the failure of submarine slopes. Kvenvolden (1993; 1999) present several cases where hydrates are believed to play a role in the failure of submarine sediments. Many of these slides are on gentle slopes which should be stable. Analysis of the failures on the Atlantic continental margin indicates that the slide scars are near the top of the hydrate zone and that there is less hydrate is the sediment beneath the slide scars. Failures on the continental margin seem to occur at the base of the hydrate layer where the hydrates tend to break down and free methane is found (Dillion 1992).

The results of theoretical and laboratory programs show that the soil will experience a dramatic reduction in effective stress and an associated reduction in shear strength due to hydrate dissociation. Dissociation of oceanic hydrates may be due to pressure reductions such as sea level changes, localized sliding and slumping, or temperature increases such as global warming, sedimentation, or reservoir production. The reduced shear strength of the sediments may ultimately lead to soil collapse and triggering of submarine slope failures. Little research has been done on this topic and certainly a better understanding of the influence of hydrate formation and dissociation on the soil response is necessary before quantitative analysis of the role of gas hydrate dissociation on submarine slope stability can be determined.

The dissociation of gas hydrates can induce high fluid pressures and ultimately result in the loss of strength and collapse of the sediments resulting in slope failure or collapse of engineering structures. Risks associated with the presence of gas hydrates also include blowouts and casing failures as described by Yakushev and Collett (1992) and Bagrov and Lerche (1997). We can therefore conclude that gas hydrate is a significant geohazard of immediate and increasing importance as society moved to exploit ever-deeper seabed resources (Kvenvolden 2000).

8.8 Conclusions

Gas hydrates represent a potentially vast energy resource yet also a significant geohazard. In addition, they may play an important role in global climate change. The physical properties of gas hydrates are relatively well studied yet little is known about the properties of gas hydrates in porous media. The few laboratory and theoretical programs reported in the literature have mainly focused on specimen preparation and determination of hydrate quantity and distribution. Studies evaluating the influence of hydrate dissociation on the response of the surrounding soil confirm antidotal evidence that gas hydrate dissociation plays a role in submarine slope failure. Before quantitative analysis of the stability of submarine slopes containing gas hydrates can be determined, further research is required on 1) the fundamental behavioural properties of gas hydrate-sediment mixtures; 2) the dynamic equilibrium of gas hydrate-sediment mixtures including the effects of perturbations to this system; 3) in situ detection and distribution of gas hydrates.

8.9 References

Anderson, A.L. 1992. Remote acoustic characterization of the seafloor including gassy and hydrated sediment regions. *In* 2nd International Offshore and Polar Engineering Conference proceedings, v. 1: International Society of Offshore and Polar Engineering, Golden Colorado, p. 674-683.

Bagrov, E. and Lerche, I. 1997. Hydrates represent gas source, drilling hazard. Oil and Gas Journal, **95(48)**: 99-104.

Booth, J.S., Clennell, M.B., Pecher, I.A., Winters, W.J., Relle, M.K., and Dillon, W.P. 1998. Laboratory investigation of gas hydrate genesis in sediments; Modes of occurrence, volumes, and growth patterns. Poster presentation to European Geophysical Society XXII General Assembly, 1998, Nice, France.

Buffett, B.A. and Zatsepina, O.Y. 2000. Formation of gas hydrate from dissolved gas in natural porous media. Marine Geology, **164**: 69-77.

Cameron, I. and Handa, P. 1990. Compressive strength and creep behaviour of hydrate-consolidated sand. Canadian Geotechnical Journal, **27**: 255-258.

Claypool, G.E. and Kaplan, I.R. 1974. The origin and distribution of methane in marine sediments. *In* Natural Gases in Marine Sediments. *Edited by*: I.R. Kaplan, Plenum, New York, pp. 99-139.

Clennell, M.B., Henry, P., Hovland, M., Booth, J.S., Winters, W.J., and Thomas, M. 2000. Formation of natural gas hydrates in marine sediments; Gas hydrate growth and stability conditioned by host sediment properties. *In* Gas Hydrates; Challenges for the Future. *Edited by*: G.D. Holder & P.R. Bishnoi, Ann. N.Y. Acad. Sci., Vol. 912, pp. 887-897.

Dickens, R., Quinsby-Hunt, M.S. 1994. Methane hydrate stability in seawater, Geophysical Research Letters, Vol. 21, No. 19 pp. 2115-2118, Sept. 15, 1994.

Dillon, W. 1992. Gas (methane) hydrates – A new frontier. U.S. Geological Survey Fact Sheets.

Ginsburg, G.D. and Soloviev, V. 1998. Submarine gas hydrates. VNHOkeangeologia/Norma, St. Petersburg.

Grozic, J.L.H. and Kvalstad, T.J. 2001. Effect of gas on deepwater marine sediments. In Proceedings of the XVth International Conference on Soil Mechanics and Geotechnical Engineering, August 27-31,2001, Istanbul, Turkey, pp. 2289-2294.

Judge, A.S., Smith, S.L. and Majorowicz, J.A. 1994. *In* Proceedings IVth International Offshore and Polar Engineers Conference, Osaka, Japan, Vol. 1, pp. 307-314.

Kamath, A., Godbole, S.P., Ostermann, R.D., Collett, T.S. 1987. Evaluation of the stability of gas hydrates in northern Alaska, Cold Regions Science and Technology, Vol. 14, pp 107-119, Elsevier Science Publishers B.V. Amsterdam, 1987.

Kvalstad, 2001. Personal communications.

Kvenvolden, K.A. 1993. Gas hydrates – geological perspective and global climate change. Rev. Geophys. **31:** 173-187.

Kvenvolden, K.A. 1999. Potential effects of gas hydrate on human welfare: Proc. Natl. Acad. Sci. USA, **96**: 3420-3426.

Kvenvolden, K.A. 2000. Gas hydrate and humans. *In* Gas Hydrates; Challenges for the Future. *Edited by*: G.D. Holder & P.R. Bishnoi, Ann. N.Y. Acad. Sci., Vol. 912, pp. 17-22.

Makogon, Y.F. 1981. Hydrates of Natural Gas. Penwell, Tulsa.

Makogon, Y.F., Dunlap, W.A. and Holditch, S.A. 1997. Recent research on properties of gas hydrates. *In* Proceedings Offshore Technology Conference, Houston, Texas, 5-8 May, 21 pgs.

Mikami, J., Masuda, Y., Uchida, T., Satoh, T. and Takeda, H. 2000. Dissociation of natural gas hydrates observed by X-ray CT scanner. *In* Gas Hydrates; Challenges for the Future. *Edited by*: G.D. Holder & P.R. Bishnoi, Ann. N.Y. Acad. Sci., Vol. 912, pp. 1011-1020.

Parameswaran, V.R., Paradis, M. & Handa, Y.P. 1989. Strength of frozen sand containing tetrahydrofuran hydrate. Canadian Geotechnical Journal **26**: 479-483.

Rowe, M.M. and Gettrust, J. F. 1993. Methane hydrate content of Blake Outer Ridge sediments. New York Academy of Science International Conference on Natural Gas Hydrates, 1993.

Sassen, R. 1997. Gas Hydrate Gardens of the Gulf of Mexico. Texas A&M University, Dept.of Oceanography, Quarterdeck Vol. 5 Issue 3, Dec. 1997.

Sego, D.C. and Wittebolle, R.J. 1984. Engineering behaviour of a sand containing gas hydrates. *In* Proc. Cold Regions Spec. Conf., pp. 589-601.

Sloan, E.D. 1998. Clathrate Hydrates of Natural Gas, 2nd Edition. Marcel Dekker, New York.

Suess, E., Bohrmann, G., Greinert, J. and Lausch, E. 1999. Flammable Ice. Scientific American, **281(5)**: 76-83.

Tzirta, A. 1991. Rec. TraV. CHIM, 79, 582.

Winters, W.J., Pecher, I.A., Booth, J.S., Mason, D.H., Relle, M.K. and Dillon, W.P. 1999. Properties of samples containing gas hydrate from the JAPEX/JNOC/GSC Mallik 2L-38 gas hydrate research well, determined using Gas Hydrate And Sediment Test Laboratory Instrument (GHASTLI). *In* Scientific Results from JAPEX/JNOC/GSC Mallik 2L-38 Gas Hydrate Research-Well, Mackenzie Delta, Northwest Territories, Canada, *Edited by*: S.R. Dallimore, T. Uchida, and T.S. Collett: Geological Survey of Canada, Bulletin 544, p. 241-250.

Wright J.F., Chuvillin, E.M., Dallimore, S.D., Yakushev, V.S. and Nixon, F.M. 1998. Methane hydrate formation and dissociation in fine sands at temperatures near 0°C. In Proceedings of the 7th International Permafrost Conference, Yellowknife, N.W.T., pp. 1147-1153.

Wright, J.F., Dallimore, S.R., and Nixon, F.M. 1999. Influences of grain size and salinity on pressure-temperature thresholds for methane hydrate stability in JAPEX/JNOC/GSC Mallik 2L-38 gas hydrate research-well sediments. *In* Scientific Results from JAPEX/JNOC/GSC Mallik 2L-38 Gas Hydrate Research-Well, Mackenzie Delta, Northwest Territories, Canada, *Edited by*: S.R. Dallimore, T. Uchida, and T.S. Collett: Geological Survey of Canada, Bulletin 544, p. 229-240.

Yakushev, V.S. and Collett, T.S. 1992. Gas hydrates in Arctic regions; Risk to drilling and production. *In* Proceedings of the 2nd International Offshore and Polar Engineering Conference, Vol.1, pp. 668-673.

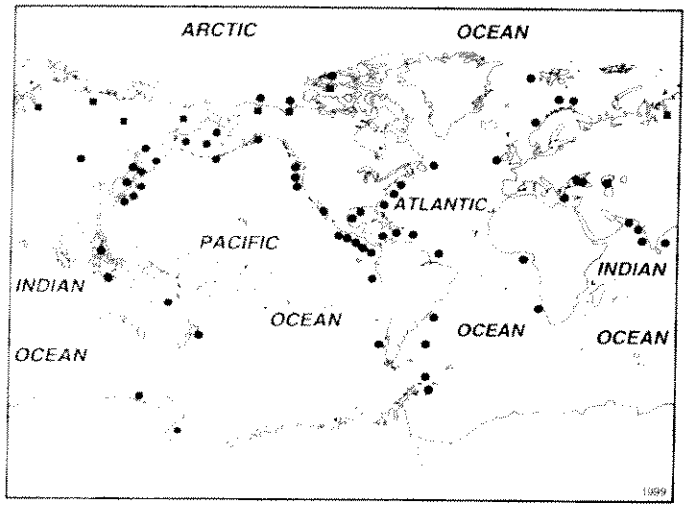

Figure 8-1: Map showing worldwide locations of known and inferred gas hydrate deposits (Kvenvolden 2000).

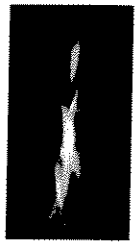

Figure 8-2: Burning hydrate (**www.hydrate.org**)

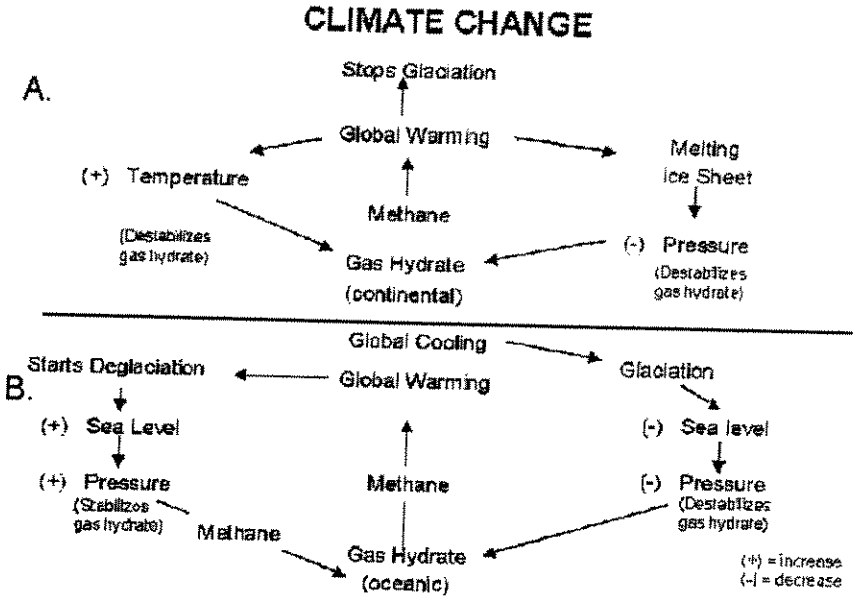

Figure 8-3: How gas hydrate dissociation may affect glacial cycles. A) Continental gas hydrate (positive environmental feedback loop); B) Oceanic gas hydrate (negative feedback loop) (Kvenolden 1993).

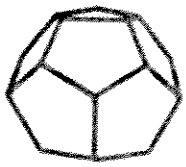

Figure 8-4: Structure I hydrate (Sassen 1997)

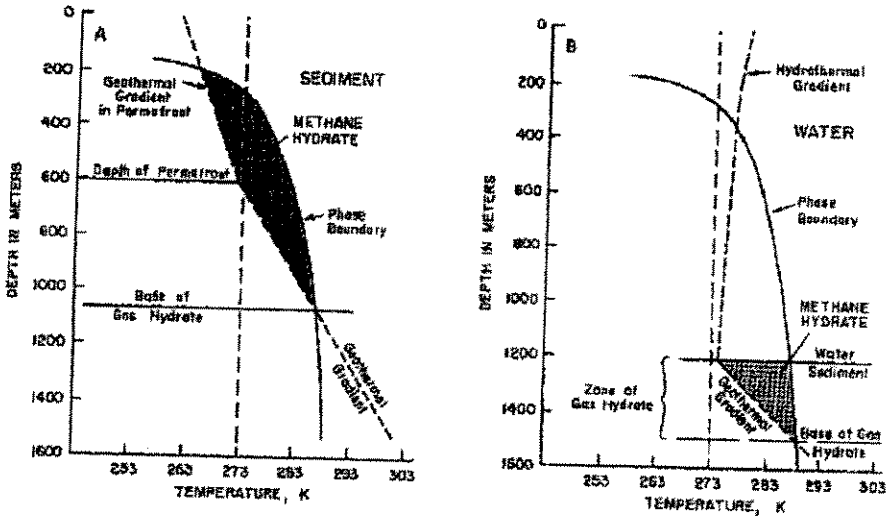

Figure 8-5: Hydrate stability diagram (a) in permafrost and (b) in ocean sediments (Kvenvolden 1988).

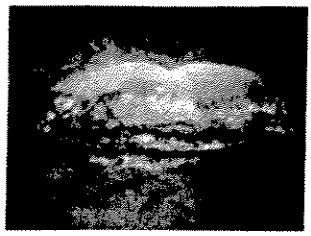

Figure 8-6: Hydrate mound on the seafloor (**www.hydrates.org**)

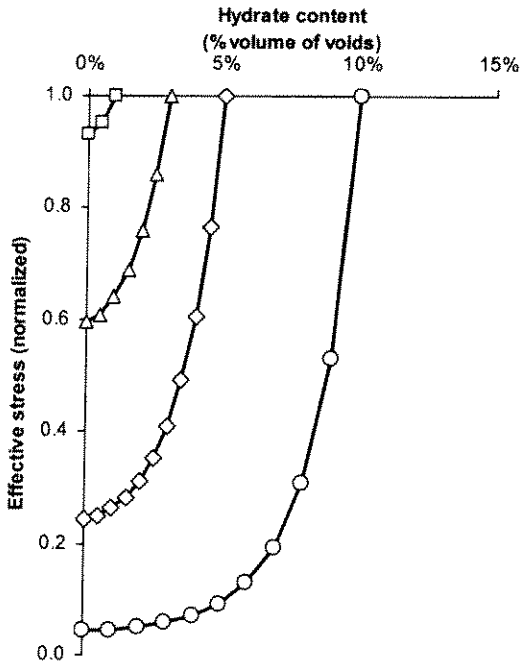

Figure 8-7: Theoretical stress change with hydrate dissociation (Grozic & Kvalstad 2001)

9 CENTRIFUGE DEMONSTRATION TESTS

9.1 Objectives

As part of Phase I of the PODS project, C-CORE undertook a centrifuge demonstration. The purpose of the test was to demonstrate the applicability of the centrifuge technology to submarine slope failure and to illustrate how centrifuge tests could contribute to the understanding of the initiation and mechanics of failures. The tasks involved included: conducting a literature review of previous similar tests; designing the centrifuge demonstration test to illustrate various failure triggering mechanisms; constructing the test equipment; preparing the instrumented strong box (test box); performing the centrifuge test; determining soil properties, presenting and analyzing the results and making recommendations regarding future tests.

9.2 Test Design

Centrifuge modeling is currently the most reliable technique of using small-scale tests of geotechnical phenomena to predict full-scale conditions. Murff (1996) and Taylor (1995) describe the principles, scaling laws and some applications of centrifuge modelling. C-CORE applies its geotechnical centrifuge testing to offshore structures, including offshore production platforms, pipelines, breakwaters and wharves; and onshore structures such as dams, pipelines, landfills, mines, and large buildings. Tests are routinely conducted in soil statics, soil dynamics, and environmental engineering. The C-CORE centrifuge is shown in Figure 9.1.

The initiation of submarine slope instability has been attributed to triggers such as earthquakes, waves, tides, sedimentation, gas, erosion and diapirism, Hampton et al. (1996). Centrifuge modelling has been used to simulate many of these loading conditions and relevant soil conditions in similar seafloor stability studies. Examples presented by Phillips (2001) include submarine failures from:

a) Material softening,
b) Sedimentation,
c) Wave loading, and
d) Earthquakes.

Material Softening

The Canadian Liquefaction Experiment (CANLEX) by Robertson et al (2000) investigated the liquefaction potential of loose sand deposits under monotonic shear stress increments. The program included high quality soils testing, numerical analyses and a full-scale field event designed to cause a flowslide. Centrifuge model tests were added to the CANLEX program to provide additional physical data and to simulate the physical response of the field event. The oil sand tailings from the field site used in the model tests were strain softening under triaxial extension. One centrifuge model simulated the failure of a 16°, 8.8m high loose sand submerged slope, Phillips and Byrne (1994). Surcharging the slope crest caused the model slope to liquefy and flow with deep-seated lateral movements to an angle of 7°, Figure 9.2. This submarine slope

failure occurred primarily due to the strain softening response of the sand at the toe of the slope that caused pore pressure increases and destabilisation of the slope.

Sedimentation

There are other external loading conditions that can cause pore pressure increases in the vicinity of slopes. Continuous sedimentation has been identified as one such loading condition. Hurley (1999) has modelled the sedimentation and primary consolidation of a highly permeable cohesive kaolin sediment from 580% water content. The equivalent of 10m depth of aqueous slurry sedimented and consolidated into a 2m thick silty clay layer, Figure 9.3. Continuous measurements of bulk density (from gamma ray attenuation), pore pressure and shear and compression wave velocities were made at 100g. The excess pore pressures generated by this sedimentation process may be sufficient to destabilise a submarine slope, Figure 9.4. The excess pore pressure at PPT6 5m down in the consolidating clay layer was 30kPa at the equivalent of 2 years (100 mins.) after commencement of sedimentation. This is equivalent to an excess pore pressure ratio, r_u, of about unity. The associated effective shear strength is low. If sufficient material is subject to such pore pressures, then seafloor instability can ensue.

Wave Loading

Wave loads can also cause excess pore pressures leading to seabed mobility and liquefaction. The techniques for modelling wave seabed interaction were developed by Phillips and Sekiguchi (1992). Sekiguchi et al (2000) simulated at 50g the response of a 4.5m thick sand layer under 4m water depth subjected to 0.3m high waves with a 6 second period, Figure 9.5. A 50-centistoke pore fluid was used to allow simultaneous time scaling of diffusion and inertial processes.

Significant seabed mobility and liquefaction was observed to propagate down from the seafloor to base of the sand layer. Figure 9.6 shows the excess pore pressure response, u_e, at the sand base to pressure cycles at the seafloor. Three additional configurations were modelled with a gravel cap of various lengths on the seabed to develop a mitigation strategy to minimise damage to the seafloor.

Earthquake Effects

The VELACS (Verification of Earthquake Liquefaction Analysis by Centrifuge Studies) program considered the effects of earthquake-like loading on a variety of soil models, Arulanandan and Scott (1993 &1994) and http://ceor.princeton.edu/~radu/soil/velacs/. VELACS was aimed at better understanding the mechanisms of soil liquefaction and at acquiring data for the verification of various analysis procedures. The response of each of nine boundary value configurations was predicted by between 4 to 16 numerical analysts. The Class-A predictions were then compared to the measured response from nominally the same physical model test conducted at between 1 to 3 centrifuge centres.

Model 2 involved the simulation of lateral spreading of a submerged slope due to earthquake effects, Figure 9.7. The submerged 2^0 slope comprised a saturated 10m deep layer of Nevada sand at 40% relative density. The base of the layer was subjected to about 22 cycles to 0.1g

lateral acceleration at 2Hz. The toe of the slope at the seafloor, LVDT 3 was observed to move downslope a distance of 0.5m due to this earthquake, Figure 9.8.

Other work in the area of centrifuge modelled flow slides due to earthquakes has been conducted by Dean and Schofield (1983).

The C-CORE demonstration test design covered four main areas: the model material, the slope geometry, the instrumentation, and the triggering mechanism. As the expected focus of future centrifuge tests would be the initiation of the slide, the design of the centrifuge test concentrated on the triggering mechanisms.

The model material was selected such that it had sensitivity but not too high a permeability such that undrained conditions could be maintained during a rapid slope failure. The model material was placed in the test box as a slurry then normally consolidated. The test box measures 425 mm in height, 900 mm in length by 300mm in width and has a plexiglass side to permit viewing of the slope movement during the test. The fully instrumented test box includes pore pressure transducers, displacement markers, a CPT and two video cameras. The sediment consolidation phase and the instrumented strong box are shown in Figures 9.9a) and 9.9b). The test design called for an 8° slope on the sediment as shown in Figure 9.10a).

There were three independent triggering mechanisms included in the demonstration test, to ensure that failure could be initiated. The triggers were addition of a surcharge of gravel on the head of the slope (Figure 9.10b), increase in pore water pressure in the sediment at approximately mid slope (Figure 9.11a) and removal of the toe of the slope (Figure 9.11b). The increase in pore water pressure was accomplished by opening a valve to a standpipe on the strong box and the erosion of sediment at the toe of the slope was by injecting water under pressure.

Details of the instrumentation and the test up for Demonstration Test 1 and 2 are provided in Appendix 3.

9.3 Centrifuge Demonstration Test 1

9.3.1 Demonstration Test I Procedure

The silty clay slurry was consolidated during centrifuge operation under 80g. The slurry was allowed to drain to both the free surface and through the sand drainage layer at the base. This consolidation stage had an approximate duration of $4^{1}/_{2}$ hours. The test container was placed on a 4° wedge and then rotated 180° after primary consolidation to create an 8° incline of the soil surface with respect to the normal gravitational axis. The valve on the base drain was turned off and the surface water was removed prior to rotation of the wedge. Two additional pore pressure transducers (PPT) were installed within the head of the slope. Spaghetti strands were placed vertically in the soil adjacent to the plexi-window at 20 mm intervals. Sitting in the saturated soil, the spaghetti softens and became flexible thereby enabling one to visualize the soil movement. The surface was then covered with a plastic sheet until testing resumed the following day.

During the primary consolidation phase from the slurry state, the surface water was reinstated and the external valve of the pore pressure induction nozzle was left open to purge any air out of the lines leading from the nozzle to the reservoir. During the secondary consolidation phase (8° slope), this valve was closed off and the elevated reservoir was full. After sitting for about 13 hours, the model was accelerated towards 80g to continue the consolidation process. Slope failure was observed at about 35g, as shown in the photographs in Figure 9.12.

After spindown, moisture contents were taken through a series of eight borings shown in Figure A3.1. Vane tests were also conducted in the soil. Six tests were carried out in all; 3 in the head, 1 at mid body, and 2 in the toe of the slope.

9.3.2 Demonstration Test 1 Results

The slide during secondary consolidation involved the movement of 4,725 cm^3 of slurry. This movement changed the slope angle of the slurry surface. Prior to failure, the sediment surface sloped downward toward the toe at an angle of 8°. After failure, the slope of the sediment was downward toward the head at an angle of 2°.

The water content decreased with depth, Figure 9.13. Percentage water content *w*% ranged from 61.1% at the uppermost water content site (boring no. 1) to 36.9% at the lowest water content site (boring no. 8). After the test was completed, vane shear tests were conducted in the slide. Results of the tests ranged from 0.5 kPa at the toe, up to 3.25 kPa in the head of the slope. The strength increased with depth, Figure 9.14. Table A3.1 and A3.2 in Appendix 3 show the moisture content data taken from each of the 8 borings and the vane test results respectively.

Pore water pressures (pwp) were monitored in the sand and at the head, toe, mid body and mid body nozzle as shown in Figure 9.15. During the primary consolidation, as the centrifuge accelerated to 80g, the pore water pressure increased then at 80g the pwp at most locations gradually decreased as the soil consolidated. During the secondary consolidation with the surface inclined, the pore water pressure again increased rapidly as the centrifuge accelerated to 10g then 35g. Slope failure occurred once 35g was obtained, Approximate values of the pore water pressures and depth at the time of failure are presented in Table 9.1. At failure, the highest pore water pressure was observed in the toe, followed by the mid body nozzle. A more detailed account of the pore water pressures during both consolidations of PODS Centrifuge Demonstration 1 is displayed in Figure A3.5 & A3.6.

9.4 Centrifuge Demonstration Test 2

9.4.1 Purpose of Demonstration Test 2

The first test slope's premature failure prevented the demonstration from accomplishing its objectives as the failure was not from one of the intended triggering mechanisms. C-CORE revised the test 1 procedure in an attempt to keep the slide stable during consolidation until failure was triggered.

9.4.2 Demonstration Test 2 Procedure

The procedure for Demonstration Test 2 was similar to Test 1 except as noted below. In Test 2, the soil depth was decreased by about 20%. The Phase 1 consolidation was increased from 4.5 to about 8.5 hours. The decreased depth and increased time provided three times more primary consolidation of the soil than in test 1. The centrifuge was then stopped, the base drain closed, surface water was removed and the wedge rotated to form an 8° slope of the sediment surface with respect to the normal gravitational axis. Strands of spaghetti, surface markers and two additional PPT's were installed in the test bed.

During the secondary consolidation phase, rather than spinning up to the 80g immediately for this consolidation, the speed was incrementally increased. First the package was spun to 10g. Thirty minutes later, the acceleration increased to 20g, then 40, and 60g. Slope failure again occurred prematurely at 60g. The slope movement was not as significant as test 1. The test was continued to test the intended triggering mechanisms. The observed slope failure is shown in Figure 9.16.

Once 80g had been attained, the 3 triggering mechanisms were applied. First, a surcharge of fine gravelly sand was tipped onto the head of the slope. No further change in the slope along the surface of the sediment was evident from the cameras in the centrifuge control room. Next the PWP injector was opened, increasing the PWP in the sediment followed by the toe injector. No further slope failures were apparent. The test package was spun down to 1g and a cone penetrometer test was conducted.

Moisture content and vane tests were conducted in the soil. Moisture contents were taken at a series of 9 sites throughout the sediment. Vane tests were also conducted on the soil. Six tests were carried out in all; 3 in the head, 1 at mid body, and 2 in the toe of the slope.

9.4.3 Demonstration Test 2 Results

The slide during secondary consolidation involved the movement of 3,756 cm^3 of sediment. This movement caused a lower change in the angle of the slurry surface. Prior to failure, the sediment surface sloped downward toward the toe at an angle of +8°. After failure, the slope of the sediment surface had been reduced to +5°.

The water content decreased with depth and remained fairly constant along the slope, Figure 9.17 a) and b). Percentage water content ranged from 45.3% nearest the surface (site No. 1) to 35.3% nearest the base of the test box (site no. 8). Results of the vane tests ranged from 0.5 kPa at the toe, up to 3.25 kPa in the head of the slope. The vane test results show an increase in strength with depth, Figure 9.18). The remoulded strength was 35 to 70 percent of the anticipated inflight strength. The positions of the vane test and moisture contents samples are shown in Figures A3.3 and A3.4, Appendix 3.

Pore water pressures were monitored in the sand and at the Head, Head 1, Head 2, Mid Body, Toe, PWP Injector and their location is shown in Figure 9.19. During the primary consolidation (Figure A3.7, Appendix 3), as the centrifuge accelerated to attain 80g, the pore water pressures increased rapidly and then decreased gradually by 15 to 35 percent over the eight and a half hour

consolidation period. During the secondary consolidation, the pore water pressure increased as the g force was increased (Figure A3.8). The pore water pressure gradually decreased until the g level was raised again.

At the point of failure at, 60g, the pore water pressure experienced a slight dip in all locations (Figure A3.9 in Appendix 3). Approximate values of the pore water pressures at the time of failure are presented in Table 9.2 and are graphed for various depths in Figure 9.20. Adding the sand surcharge to the head of the slope resulted in a sharp dive of the pore water pressures at the Head, Head 1, and Head 2, and the pore water pressure increased slightly in the other locations at the same time (shown in Figure A3.10, Appendix 3). When the PWP Injector was released, the pore water pressure at Mid Body and at the injector both increased slightly however little effect was evident on the transducers in any other section of the slope.

9.5 Analysis of Demonstration Test Results

Slope failure occurred prematurely in both demonstration tests as the 8° slope in normally consolidating silty clay was being accelerated towards test speed of 80g. The slopes failed at 35g and 60g in tests 1 and 2 respectively as shown in Figures 9.12 and 9.16. The cause of both these slope failures is believed to be excess pore pressures in the slope during the secondary consolidation phase.

The effect of these excess pore pressures is demonstrated using an infinite slope type analysis of Test 2. The ratio, λ_m, of undrained (vane) shear strength to effective stress of the normally consolidated silty clay is

$$\lambda_m = (S_u/\gamma' z)_m = (S_u/z)_m/(\gamma' N) = 0.25$$

from Lin (1995). This undrained shear strength ratio in prototype is the same as that in model, i.e. $\lambda_p = \lambda_m = 0.25$. The factor of safety of an infinite slope at an angle β is then

$$F = 2\lambda\gamma' z(1 - r_u)/(\sigma_z' \sin 2\beta) = 2\lambda(1 - r_u)/\sin 2\beta \quad \text{where } s_u = \lambda\sigma_z' = \lambda\gamma' z$$

with r_u being excess pore pressure ratio defined as $r_u = u/\gamma' z$. The effect of initial shear stresses in the slope are neglected.The critical slope angle can then be calculated as follows:

$$\sin 2\beta_{cr} = 2\lambda(1 - r_u) = 2(1 - r_u) \times 0.25 = 0.50(1 - r_u)$$

The variation of critical slope angle different excess pore pressure is presented in Figure 9.21. Since the critical slope angle does not change with scale factor, the results shown in Figure 9.21 is applicable to centrifuge tests under any acceleration. For $\beta_{cr} = 8^0$, $r_u = 0.45$.

The critical pore pressure in a slope with $\beta = 8^0$ is plotted in Figure 9.22 by a straight line. The measured total pore pressures in the soil at failure are also shown. The changing depth of free water down the slope affects these measured pressures. The measured pressures are corrected to an assumed surface water depth of 25 mm as shown in Figure 9.22. Below 140 mm, the measured excess pore pressures are high enough to cause slope failure. If the slope angle had been 5^0, the slope may have been stable. This is consistent with the observation that the slope in test 2 stabilized at $\beta = 5^0$ after failure.

9.6 Recommendations for Future Centrifuge Tests

A number of changes will be considered for future centrifuge tests.

- Increase the degree of primary consolidation of the flat test bed by further reductions in the sample thickness (to say 150mm) and by increasing the primary consolidation time (to say 12 hours).
- Increase the intervals (to say 1 hour) between centrifuge speed increases during secondary consolidation of the inclined test bed to dissipate the excess pore pressures in the slope.
- Reduce the initial slope angle, possibly to 6°. It will however be more difficult to trigger a slope failure in shallower slopes until a mechanism has been identified.
- Cover the head of the slope with plastic strips to prevent embedment of the sand surcharge into the slope and to slow dissipation of excess pore pressures in this region due to surcharging.
- Move mid-slope and base of slope injection points closer to the soil surface, to say within 50mm.

9.7 References

Almeida, M.S.S., Davies, M.C.R., Parry, R.H.G. (1985), Centrifuge tests of embankments on strengthened and unstrengthened clay foundations, Geotechnique 37, No.1, 127-130.

Almeida, M.S.S., Britto, A.M., Parry, R.H.G. (1986), Numerical Modelling of a centrifuged embankment on soft clay, Canadian Geotechnical Journal, No.23, 103-114.

Arulanandan, K., and Scott, R. F. (1993 & 1994) Verification of numerical procedures for the analysis of soil liquefaction problems. Proceedings of the International Conference on the Verification of Numerical Procedures for the Analysis of Soil Liquefaction Problems, Vols. 1 and 2, A. A. Balkema, Rotterdam, Netherlands.

Dean, E.T.R., Schofield, A.N. (1983), Two centrifuge model test: earthquakes on submerged embankments, Attidel XV Convegno Nazionale di Geotechnica Spotela Vol.1, 115-129.

Hurley, S.J. (1999) Development of a Settling Column and Associated Primary Consolidation Monitoring Systems for use in a Geotechnical Centrifuge. Master of Engineering Thesis, Memorial University Newfoundland.

Hampton, M.A., Lee, H.J. and Locat, J. (1996) Submarine landslides. Reviews of Geophysics, 34:33-59.

Lin, L (1995) Strength characteristics of a modelling silty clay. Masters thesis. Memorial University of Newfoundland, Faculty of Engineering & Applied Science.

Murff, J.D. (1996) The geotechnical centrifuge in offshore engineering. OTRC Honors Lecturer, Proceedings of Offshore Technology Conference, Houston, Texas.

Phillips, R. (2001) Simulating Submarine Slope Instability Initiation Using Centrifuge Model Testing. Canadian Geotechnical Conference, Calgary, AB, Paper G-12.

Phillips, R. and Sekiguchi, H. (1992) Generation of Water Waves in a Drum Centrifuge. Proceedings of Techo-Ocean '92, Yokohama, Japan, Volume 1, p29-34.

Phillips, R. and Byrne, P.M. (1994) Modelling slope liquefaction due to static loading. 47th Canadian Geotechnical Conference, Halifax, NB 1994, pp 317-326.

Robertson, PK, ...Phillips, R... et al. (34 authors) (2000) The Canadian Liquefaction Experiment: An Overview. Canadian Geotechnical Journal Vol. 37, No. 3, pp. 499-504.

Sekiguchi, H., Sassa, S., Sugioka, K. and Miyamoto, J. (2000) Wave induced liquefaction, flow deformation and particle transport in sand beds. GeoEng 2000, Melbourne.

Taylor, R.N. (1995) Geotechnical Centrifuge Technology, Blackie Academic & Professional, Chapman & Hall, London.

Table 9-1: Centrifuge Test 1, Pore Water Pressure During Phase 2 Consolidation At Failure

Location	**PWP After Acceleration (approx. 700s.) kPa**	**PWP Before Deceleration (approx. 14000s.) kPa**	**PWP Difference** kPa
Sand	310	263	-47
Head	258	224	-34
Toe	218	198	-20
Mid Body	125	141	16
Mid Body (nozzle)	105	183	78

Table 9-2: Centrifuge Test 2, Pore Water Pressure At Failure (Phase 2 Consolidation, 60g)

Location	**PWP At Failure (approx. 567s.) kPa**
Sand	71
Head	74
Head 1	84
Head 2	50
Mid Body	53
Mid Body (nozzle)	91
Toe	103

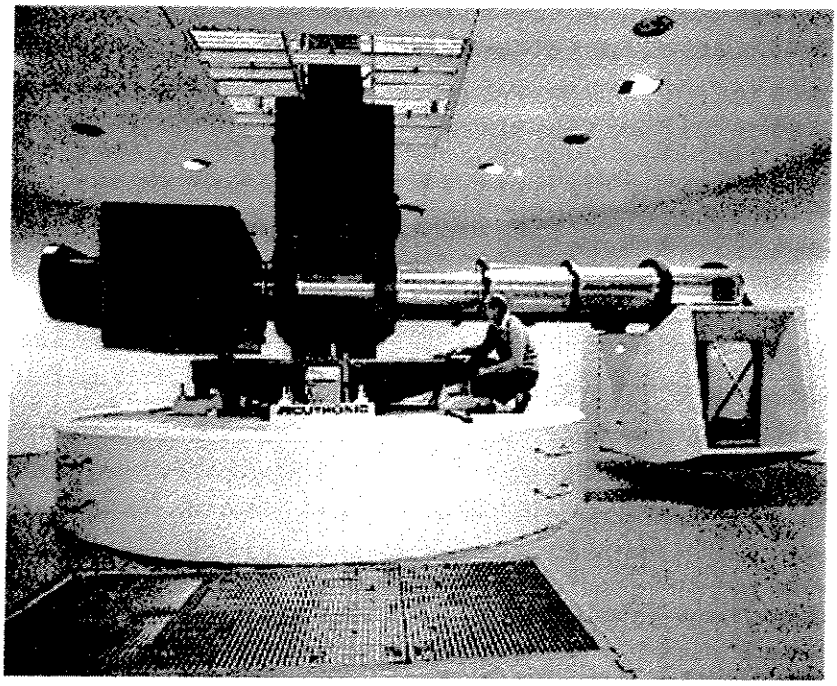

Figure 9-1: C-CORE's Acutronic 680-2 Centrifuge Facility

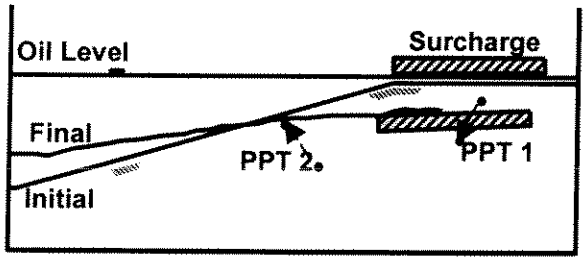

Figure 9-2: CANLEX Submerged Slope Flowslide Failure

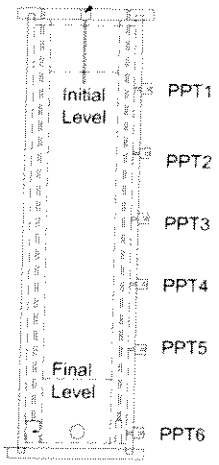

Figure 9-3: Sediment Column Test Setup

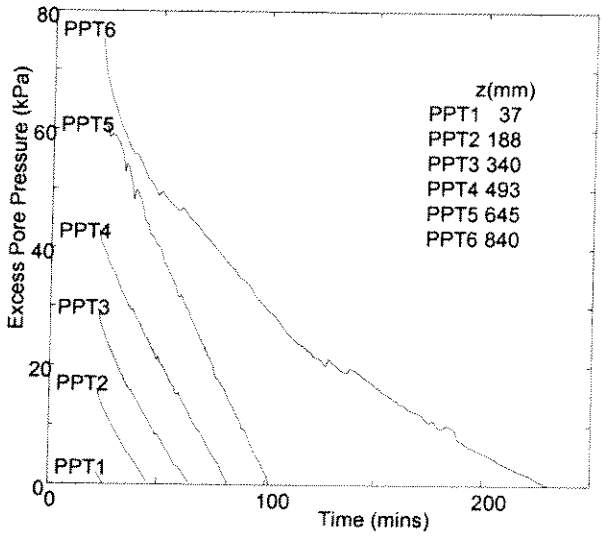

Figure 9-4: Excess Pore Pressures in Slurry Sediment

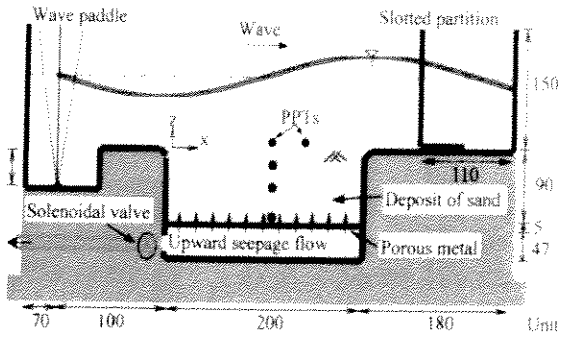

Figure 9-5: Wave Loading Model Test Setup

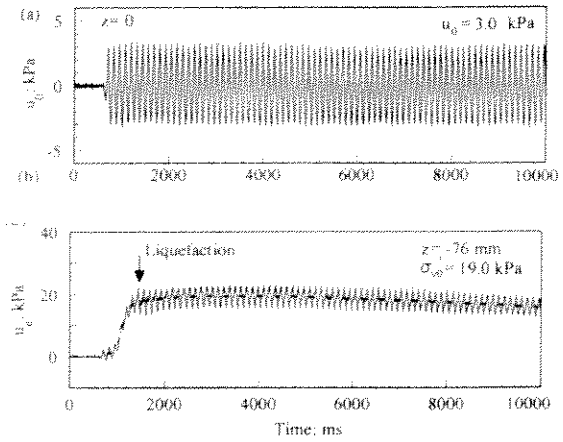

Figure 9-6: Excess Pore Pressure Response in Seabed

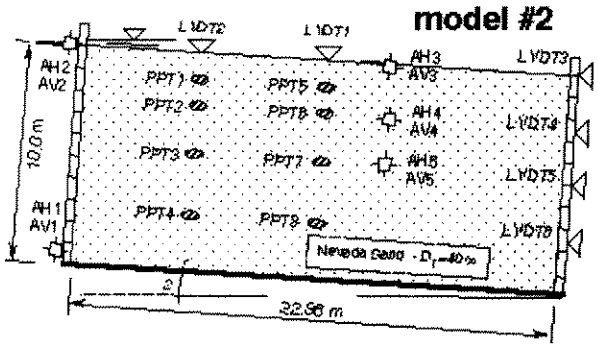

Figure 9-7: VELACS Model 2 test setup

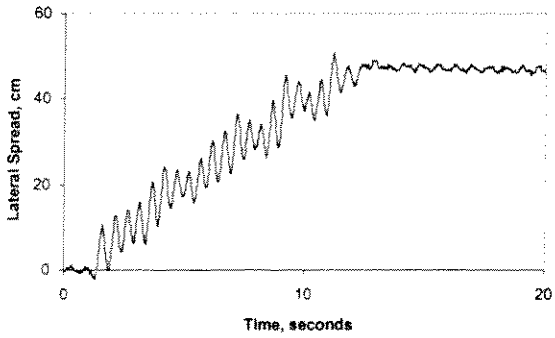

Figure 9-8: VELACS Model 2 Lateral Spread

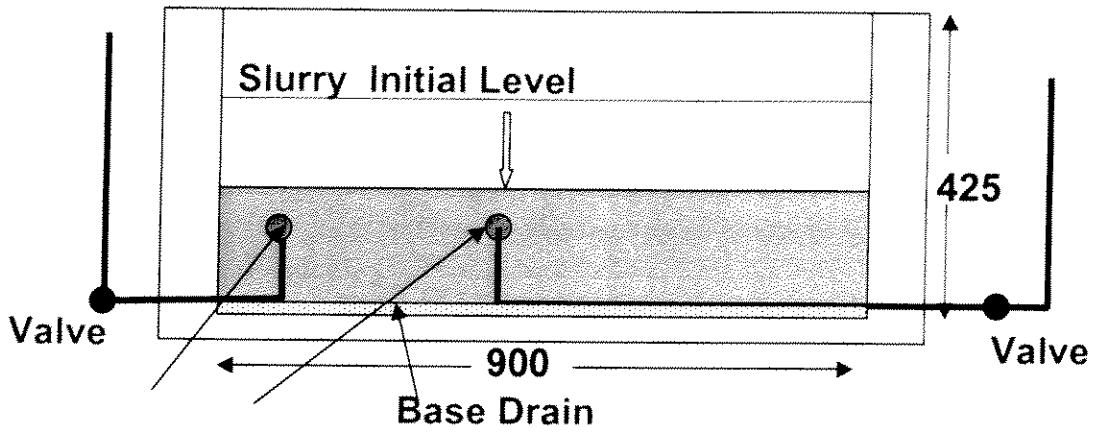

(a)

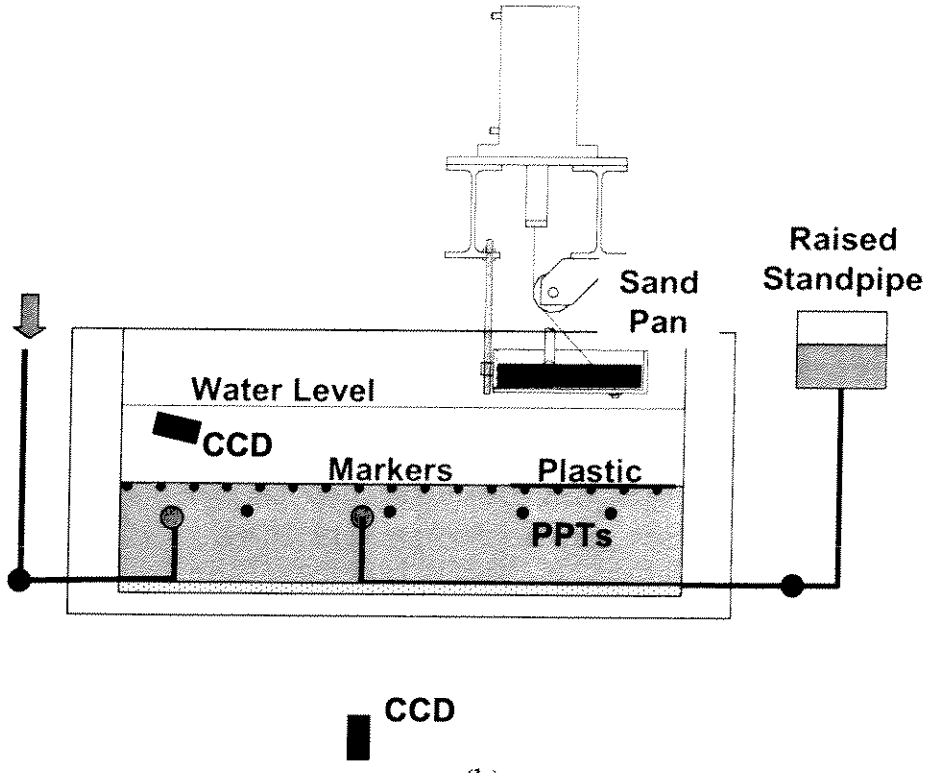

(b)

Figure 9-9: (a) Centrifuge Test, Sediment Consolidation Phase; (b) Centrifuge Test, Instrumented Strong Box

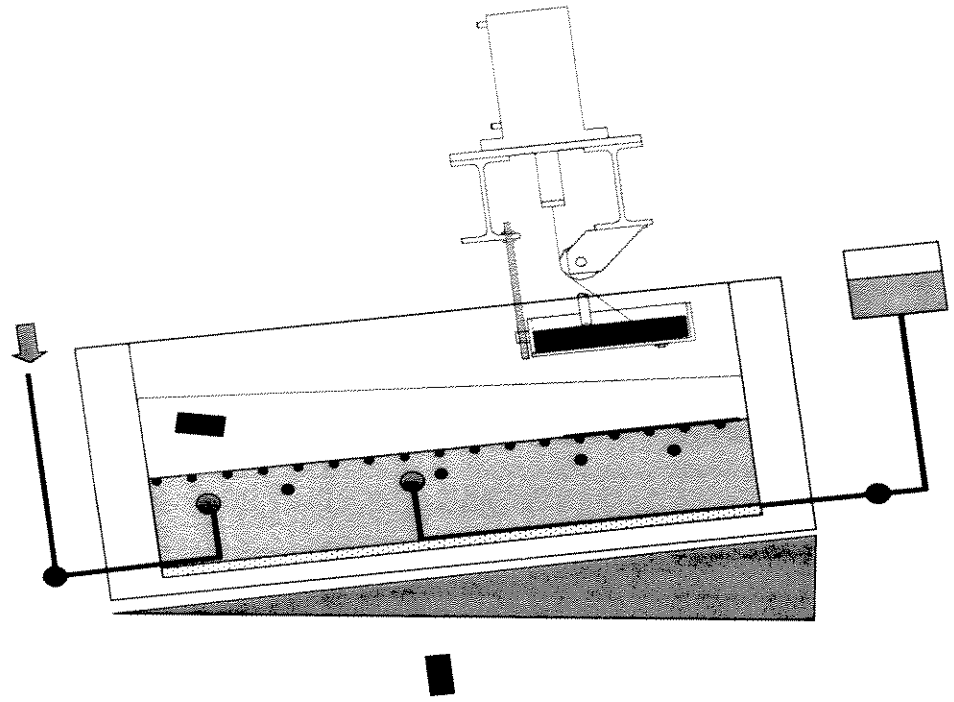

(a)

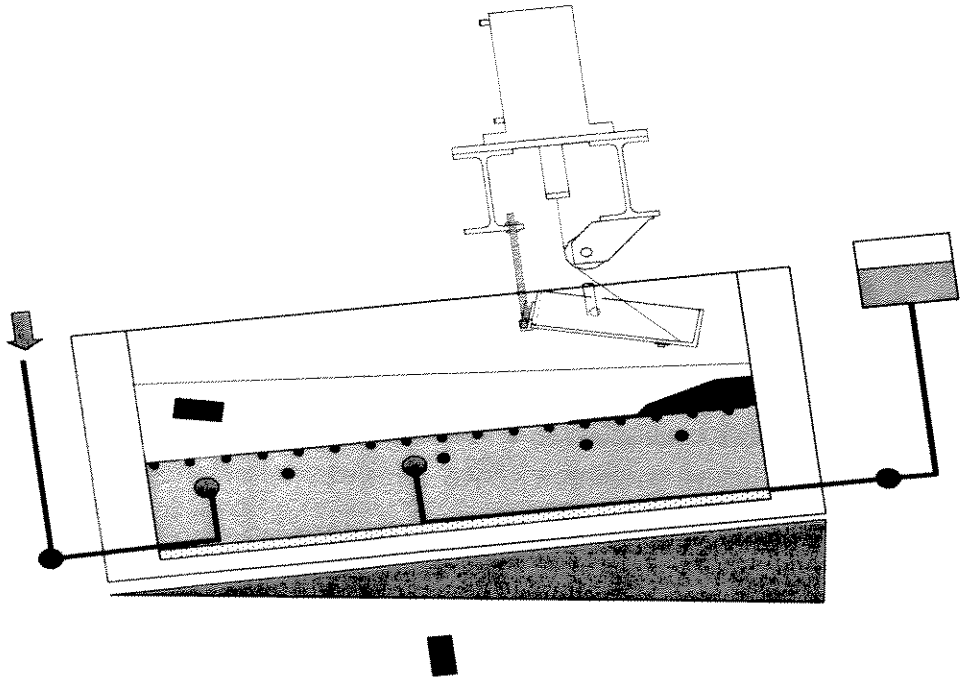

(b)

Figure 9-10: (a) Centrifuge Test, 8 Degree Slope; (b) Centrifuge Test, Surcharge Application

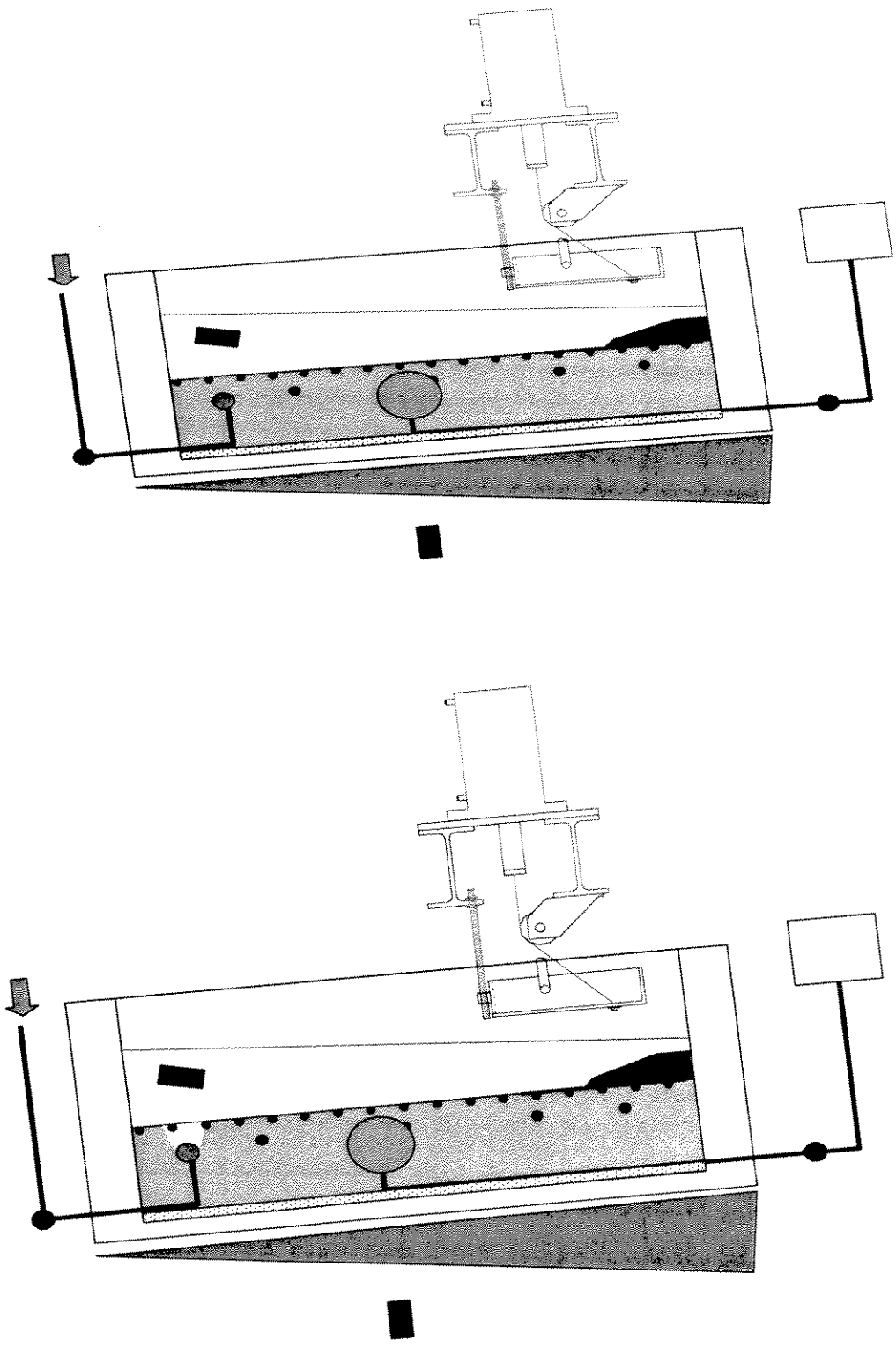

Figure 9-11: (a) Centrifuge Test, Increase in PWP; (b) Centrifuge Test, Removal of Toe of Slope

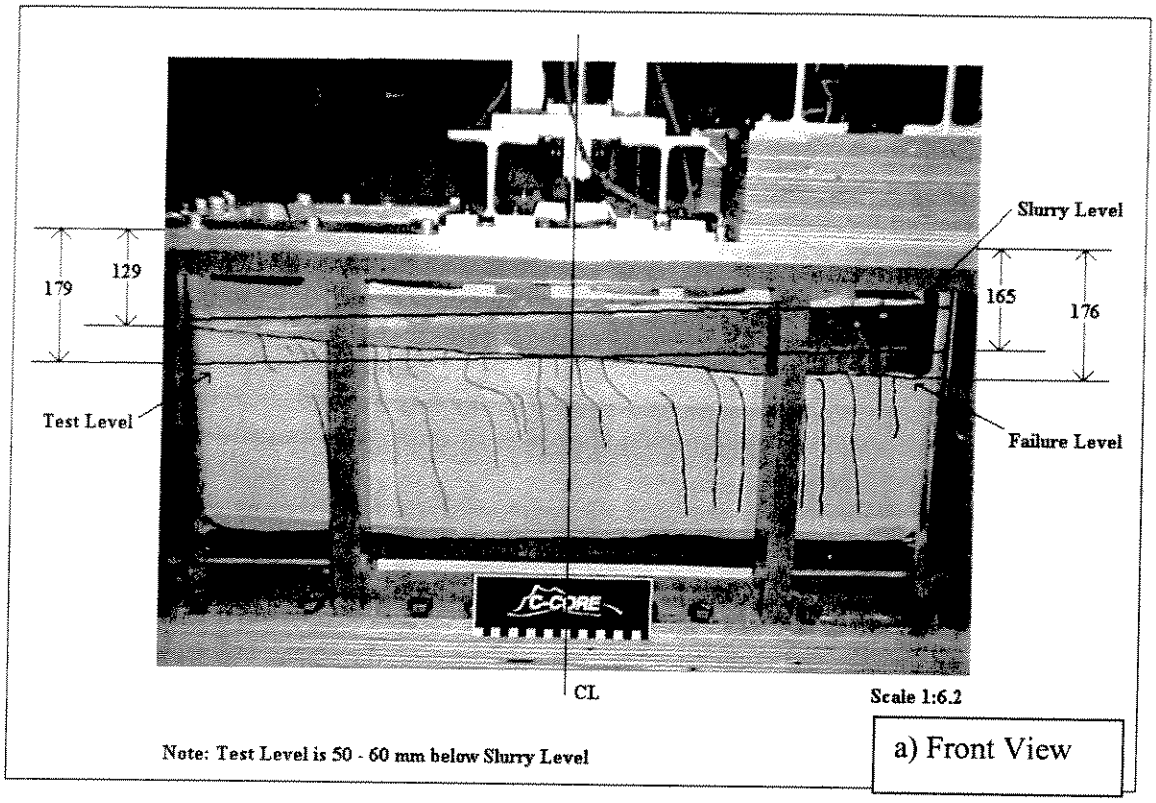

Figure 9-12: Strongbox Model After Failure Centrifuge Test 1

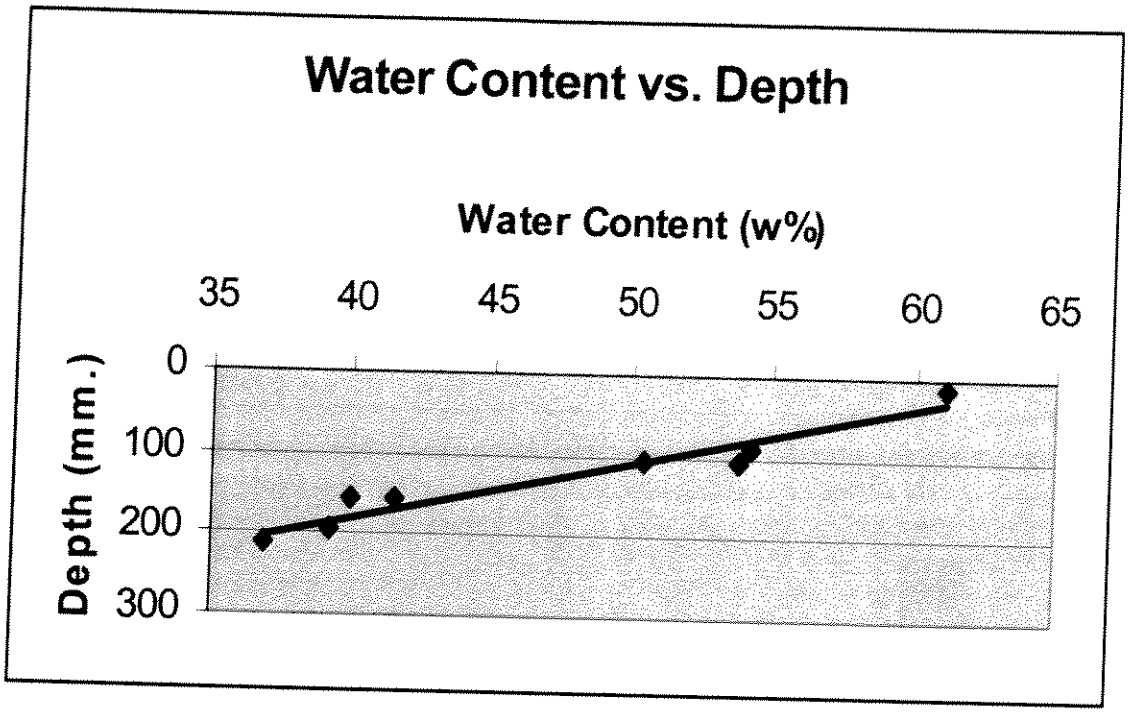

Figure 9-13: Water Content Determinations after Centrifuge Test 1

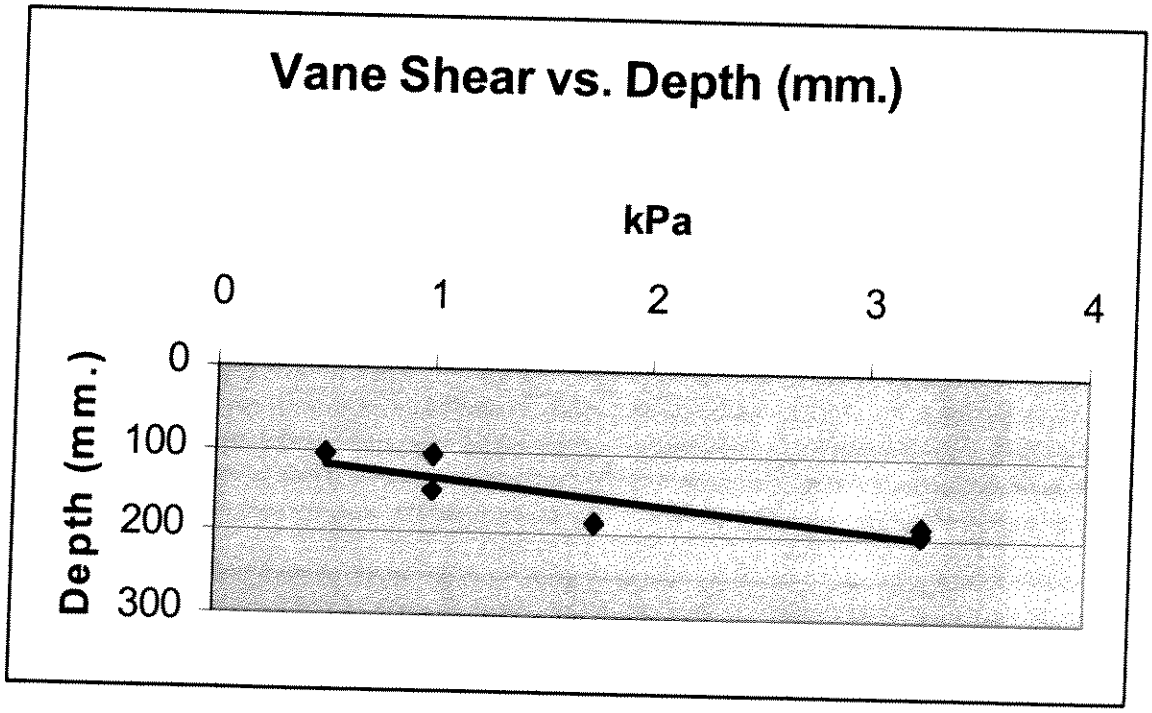

Figure 9-14: Vane Strength determinations after Centrifuge Test 1

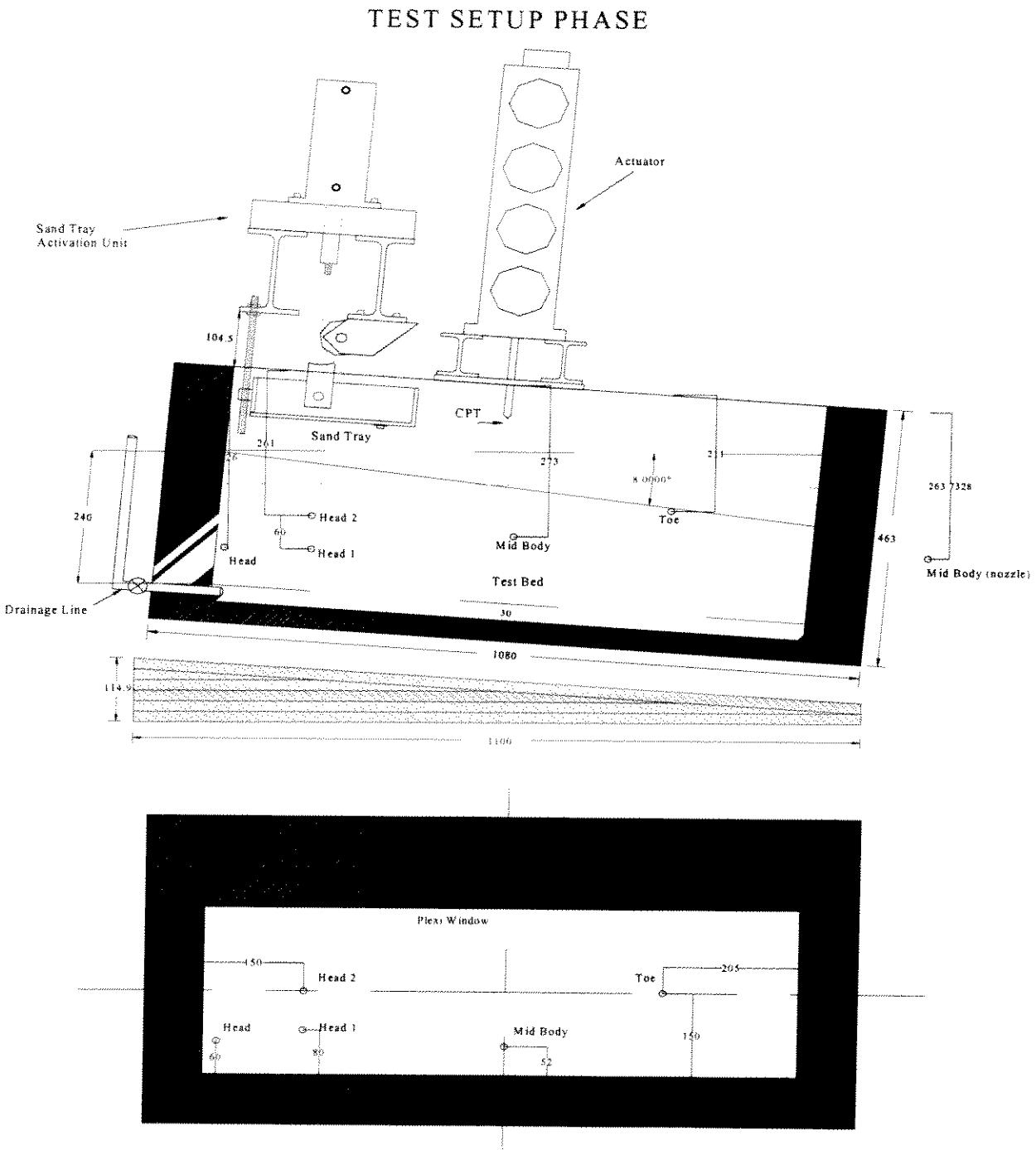

Figure 9-15: Centrifuge Test 1 PPT Locations

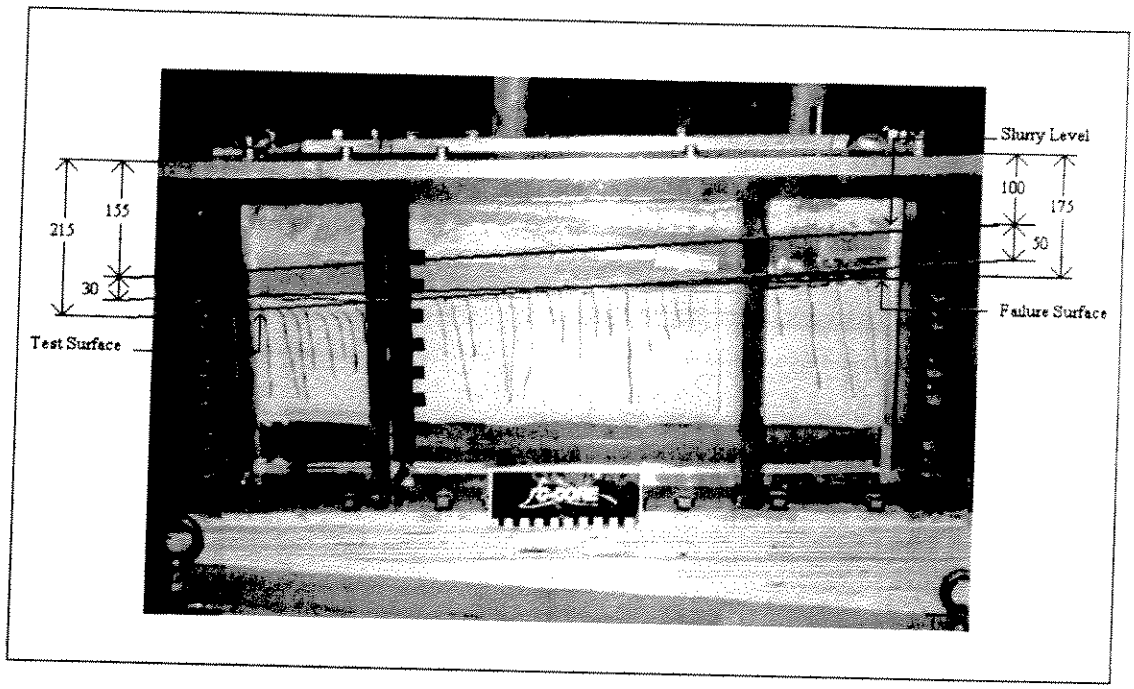

Figure 9-16: Strongbox Model after Failure, Centrifuge Test 2

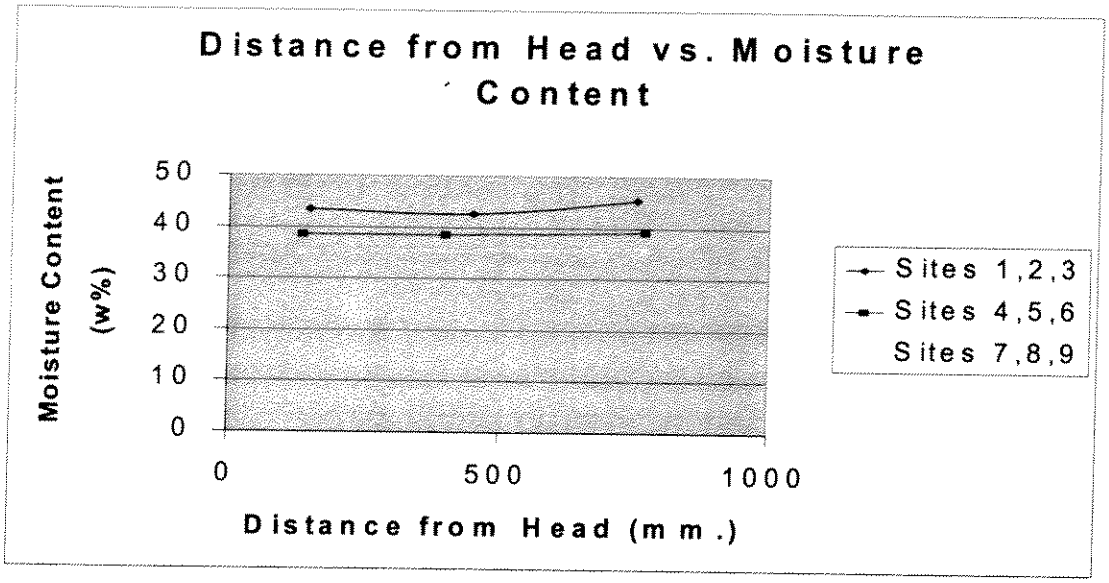

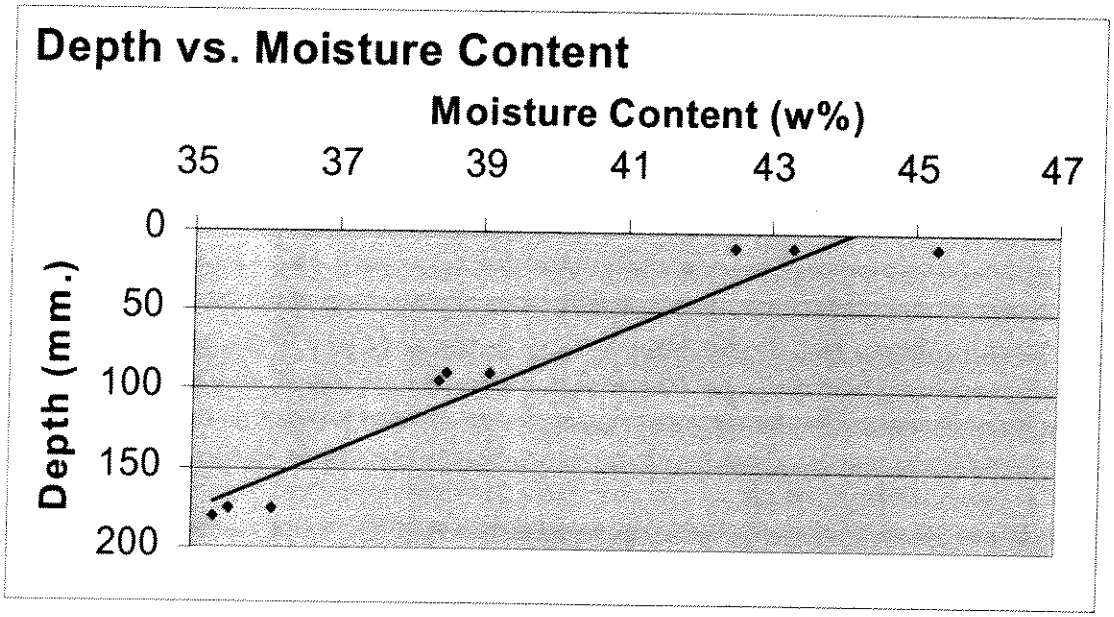

Figure 9-17: Water Content Determinations after Centrifuge Test 2

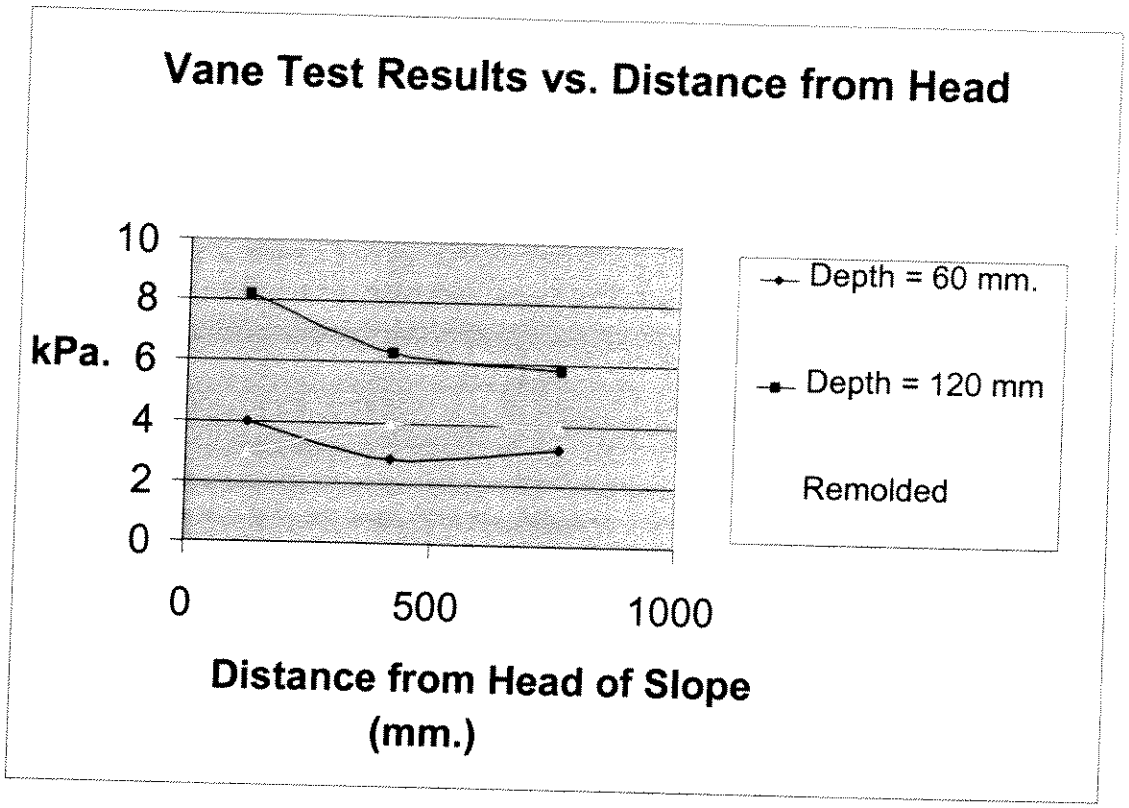

Figure 9-18: Vane Strength Determinations, Centrifuge Test 2

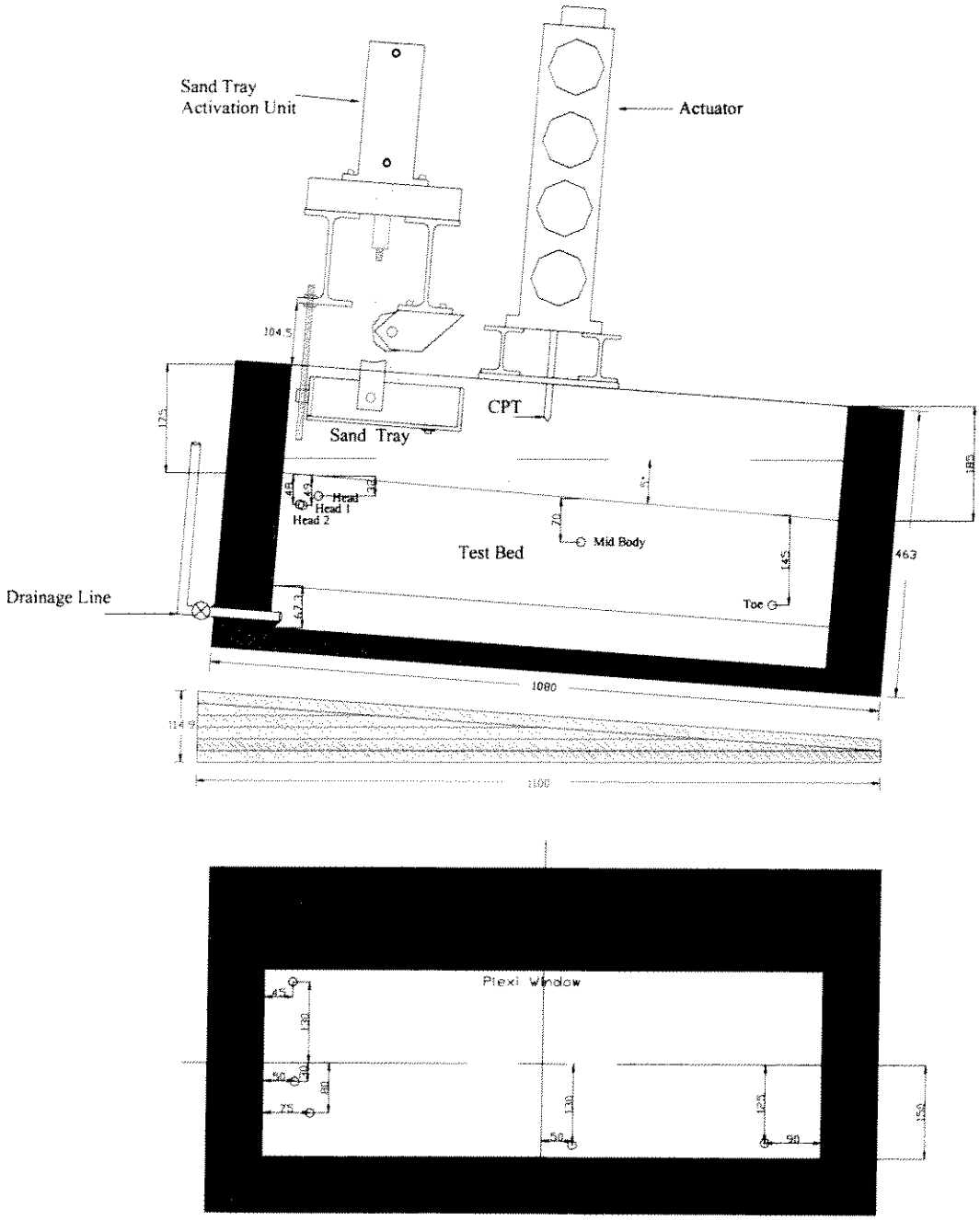

Figure 9-19: PPT Locations For Centrifuge Test 2

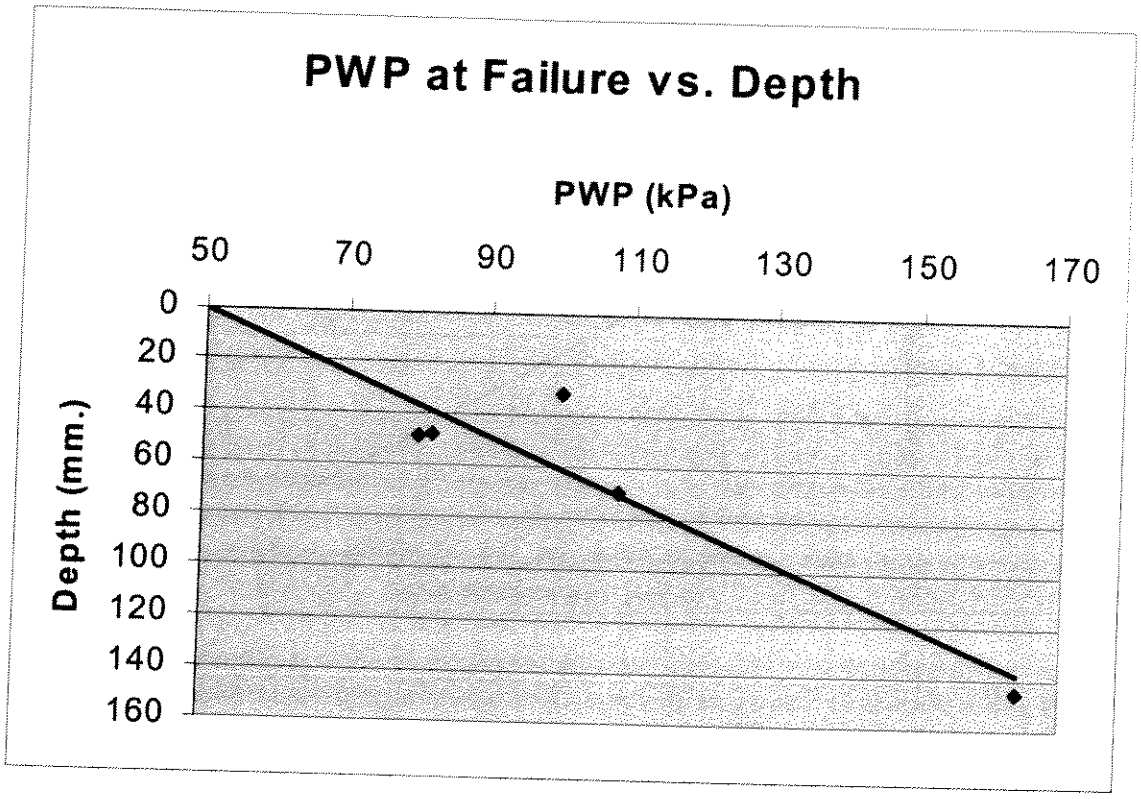

Figure 9-20: PWP Measurements at Failure Centrifuge Test 2

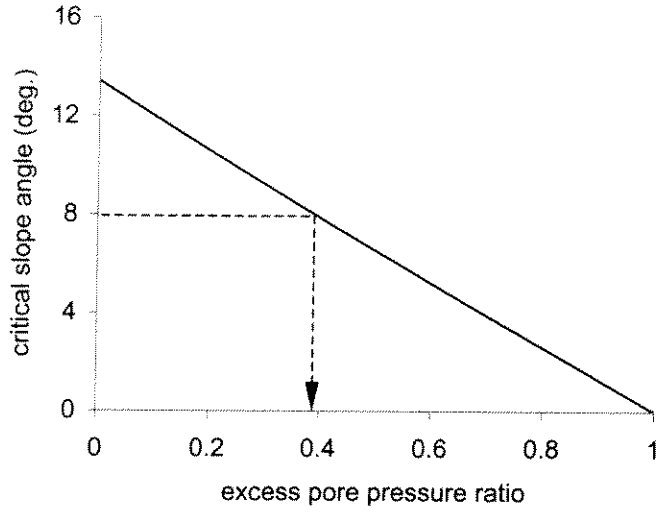

Figure 9-21: Variation of critical slope angle with excess pore pressure ratio

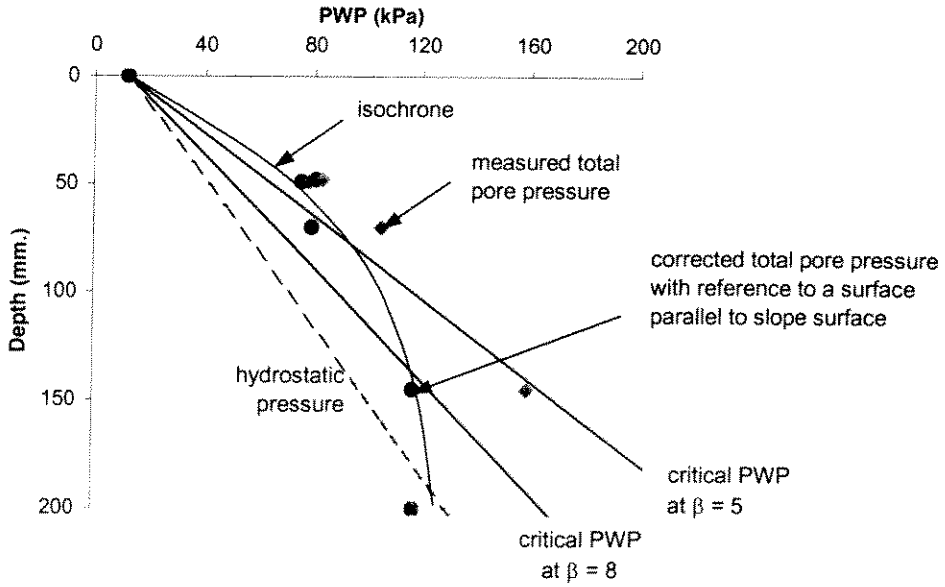

Figure 9-22: Measured pore pressure at failure in Test 2

10 FRAMEWORK FOR RISK ANALYSIS

10.1 Objectives

Due to the random nature of soil properties and triggering mechanisms, it is necessary to assess slope stability in terms of probabilistic methods. Probabilistic analysis would also account for uncertainties in mechanistic models used and associated parameters. The objectives of this Section are:

- to outline a framework for risk analysis of slope stability,
- to identify the dominant releasing agents and their governing parameters,
- to characterise the dominant releasing agents, where information is available,
- to provide a description of mechanistic models for releasing agents where available, and
- to make recommendations for specific numerical and physical modelling work based on the characterisation and framework provided.

10.2 Outline of Risk Analysis Framework

Development of an outline for a risk analysis framework for submarine slides is based on four main components:

1. Releasing Agents,
2. Site Parameters,
3. Mechanistic Models, and
4. Event Consequence and Frequency.

The flowchart shown in Figure 10.1 outlines the framework for assessment of risk for submarine slides. In order to assess risk in this instance, it is important to determine both the frequency and consequence of an event (i.e. a submarine slide).

Event frequency is based on the rate at which the releasing agents occur and the magnitude of these events. If the magnitude of an event is greater than some critical level required to trigger a sliding mechanism, then an event is said to have occurred. The critical magnitude is calculated using the site characteristics and a model for the relevant mechanisms in the study region. Determination of event frequency is based on past measurements of the releasing agents in a given study region.

Event consequence is based on the overall magnitude of the event, assuming the releasing agent magnitude is above the critical magnitude for triggering a sliding mechanism. The higher the magnitude of the releasing agent, the greater the consequence of the event. These data are usually collected and presented as case studies of a given region.

Each component of this framework is described in more detail in the sections that follow.

10.3 Description of Releasing Agents

The study region for this work is primarily the Scotian Self and the Grand Banks (Figure 10.2). Eight different submarine slide releasing agents have been identified for this region which are presented in Figure 10.3.

These mechanisms are described in some detail here (as outlined in Schwarz, 1982), along with any related sub-types associated with each.

1) Sedimentation: Four subtypes exist:

a) Long-term, high sedimentation rates which occur at near-shore canyons and steep trench slopes. Generally this process is combined with an additional trigger mechanism.
b) Short-term heavy sediment supplies which are self-sufficient to release slope failure at shelf breaks.
c) Overloading of insufficiently consolidated slopes and near slope areas, resulting from processes such as loss of buoyancy in tidal flats and prograding marine foreset beds.
d) Oversteepening of depositional slope to the critical angle of failure at trench slopes possibly as a result of tectonic movements.

2) Tidal Changes: In near shore regions, tidal changes can induce excess pore water pressure and reduce the strength of soil. This will decrease the stability of submarine slope stabilities.

3) Wave Loading: Wave-induced loads can cause submarine slides due to increased pore pressures in ocean floor deposits (Seed & Rahman, 1978).

4) Tectonics: While too slow to be considered direct, a direct release agent, tectonics can prepare favorable conditions for slope failure.

5) Emergence: Implies loss of buoyancy and an increase of effective load upon a potential shear face.

6) Erosion: In water depths of up to 200m, a close interaction exists between surface water movements and seabed sediments. Such processes may trigger considerable secondary gravitational mass movements. Three subgroups exist within current and wave contributions to erosion:

a) Contribution from normal ocean currents,
b) Contribution from hurricanes and heavy waves at canyon heads, and
c) Tsunamis and seiches along affected coastlines with weak sediments.

7) Physical/Chemical: Changes in physico-chemical properties may reduce shear strength and contribute to sliding, such as the chemical decomposition of organic or inorganic sedimentary components. The possibility of

"artificial" (human intervention) slope failures can also be grouped under this heading. These events can be triggered by offshore activities such as drilling of wells, construction of underwater structures and collision of underwater vehicles/objects with sloped soil surfaces.

8) Earthquake: Generally thought to be one of the most effective releasing agents whereby a horizontal acceleration of the seabed is, at times, sufficient to cause slope failure.

The physics involved in submarine mass movements has been classified by the International Society for Soil Mechanics and Geotechnical Engineering (ISSMGE) technical committee on landslides (TC-11). Locat & Lee (2000) presented an adjustment to this classification, making it applicable to the marine environment.

10.4 Description of Site Characteristics

Site characteristics (Figure 10.4) include subsurface stratigraphy, presence of geohazards and bathymetry. These are used in slide models (Figure 10.5) to determine critical trigger levels for releasing agents in the region of interest.

Subsurface stratigraphy for a site includes the type and extent for each soil layer. Soil types can be either fully drained, consolidated or unconsolidated and the properties of interest may include: Cohesion (C'), internal angle of friction (ϕ'), unit weight (γ'), OCR, K_c, shear strength, water content, grain size, excess pore water pressure, plasticity (liquid limit and plasticity index) and sensitivity.

Geohazards include existing failures and gas presence at a site. Existing failures may lead to porewater overpressure and make a site more prone to a slide.

The bathymetry of a given site includes the seabed slope and the water depth throughout the region. For obvious reasons, seabed slope is an important factor in computing risk for submarine slides. Water depth is important since it gives an indication of pressures acting on the seabed.

Uncertainty of each of these parameters plays an important role in the assessment of risk for submarine slides. Some characteristics are difficult to treat formally, such as geological details missed in exploration programs, while others are readily dealt with using statistical analysis, such as soil properties (Christian, et al., 1994). Christian et al. (1994) states that uncertainties in soil properties can come from either data scatter or systematic error in the estimates. Data scatter consists of real spatial variations in the properties or random testing errors in the measurements. Systematic errors come from either statistical errors in the mean or bias in the measurement methods. For a more in-depth discussion of assessing uncertainties in site characteristics for risk assessment of submarine slopes, the reader is referred to the works of Chowdhury (1991) and Yong et al. (1976).

10.5 Mechanistic Models for Releasing Agents

For the eight releasing agents identified, five mechanistic models reported in the literature have been examined, namely earthquakes, wave loading, sedimentation, erosion and sea level changes. These models are presented briefly in this section with references to the literature for further information.

Estimating earthquake induced slope failures is based on a reasonably simple formulation. Details of this method are given in Christian and Urzua (1998). The method of assessment is based on a modification of the commonly used static safety factor for sloped surfaces which is used to compute the probability of static slope failure. Calculation of the new (dynamic) factor of safety includes details of the soil and slope, as well as the horizontal ground acceleration and an amplification factor. The new factor is used along with standard formulations for calculating probability of slope failure and gives an estimate of the probability of slope failure due to an earthquake. Calculation of earthquake recurrence rates are also explained by Christian and Uzrua (1998) in terms of standard statistical methods and using earthquake data specific to the region of interest. In order to calculate the annual probability of failure due to an earthquake, the probability of slope failure and recurrence rate must be combined and integrated over the entire range of possible ground accelerations. A method similar to that present by Christian and Urzua (1998) is given in Athanasiou-Grivas (1980). The Athanasiou-Grivas (1980) model was based on calculation of the probability of failure due to an earthquake loading and was used to examine the reliability of an existing natural slope. A simple method for determining pore pressure response of sand deposits on the ocean floor was developed by Seed and Idriss (1971) for evaluating the cyclic mobility or liquifaction potential of sand deposits during earthquakes.

Wave loading plays an important role in the buildup of pore pressures in seabed soils. As storm waves move across the sea surface, the seafloor is subjected to changing pressures which are a function of wave, water depth and seafloor motion characteristics (Bea et al., 1983). This will induce cyclic stresses within the profile which may cause a progressive buildup of pore pressure (Seed and Rahman, 1978). The amount and rate of pore pressure buildup will depend on the storm characteristics (wave height, period and length), cyclic loading characteristics of the soil deposits and drainage and compressibility of the soil strata that make-up the soil profile. Wave induced pressures on the seafloor due to each wave component in a storm can be computed using linear wave theory.

Seed and Rahman (1978) state that stresses can be computed by directly using the theory of elasticity formulation or finite element methods. To remove over conservatisms, it is important to consider the effects of pore pressure dissipation during the period of storm loading, since this would normally be quite significant. Once pore pressures reach a sufficiently high level, the soil becomes liquefied, significantly reducing the stability of the seabed.

Three type of numerical models have been developed to assess the effects of ocean waves on the stability and movement of clay sediments. These are: limit equilibrium, finite element and continuum mechanics models. These models are described in this context by Bea et al. (1983). A more detailed discussion of models and the effect of wave-induced submarine slides is given in the works of Seed and Rahman (1978), Bea et al. (1983), and Kraft and Watkins (1976).

Little information has been found regarding models developed for sedimentation and it's effect on pore pressure. Pratson and Mello (1995) note that through their analysis, it was found that for sedimentation rates in which accumulation occurs faster than dewatering during compaction,

pore pressures increase while the effective stress on the slope sediments decreases thus promoting frictional slope failure.

The Pratson and Mello (1995) model for erosion predicts that rapid erosion tends to reduce the pore pressure and increase the effective stress thus lowering the possibility of frictional slope failure on a slope.

Sea level changes have no effect on slope stability according to Pratson and Mello (1995). While changing water depth does cause a corresponding change in pore pressure, the effective stress on the slope sediments does not change, regardless of the rate of sea level rise or fall.

10.6 Inputs to Regional Geohazard Mapping

Where available, data have been collected which are applicable to the study region. These data include epicenter locations for seismic activity on the Grand Banks and the Scotian Shelf (Figures 10.6 and 10.7), along with relative Richter scale magnitudes of the events. Figure 10.8 gives the frequency and magnitude of these events, from about 1915 to the present day.

Wave loading data for four sites on the Scotian Shelf are shown in Figure 10.9. Figure 10.10 gives the geographic location of the significant wave height data shown in Figure 10.9 along with resulting slides near each site.

Figure 10.11 shows the slope intensities for the Scotian Shelf for water depths between 50m and 3000m. Figure 10.12 shows the slope intensities for the Grand Banks.

10.7 Recommendations for Specific Numerical and Physical Modelling Work

While certain mechanistic models and data do exist for the study region and can be used for the assessment of risk for submarine slopes, other information are still required to develop a full risk assessment. Further work is required to develop mechanistic models for the releasing agents: tectonics, sedimentation, erosion, emergence, tidal changes and physico-chemical change, as these models have not been found in the literature. Data specific to the study region appear to be lacking somewhat as well.

10.8 References

Athanasiou-Grivas, D. (1980). Probabilistic Seismic Stability Analysis – A Case Study. Canadian Geotechnical Journal, Vol. 17.

Bea, R.G., Wright, S.G., Sircar, P. and Niedoroda, A.W. (1983). Wave-Induced Slides in South Pass Block 70, Mississippi Delta. Journal of Geotechnical Engineering, Vol 109, No.4.

Chowdhury, R.N. (1991). Simulation of Risk of Progressive Slope Failure. Canadian Geotechnical Journal, Vol 29.

Christian, J.T., Ladd, C.C. and Baecher, G.B. (1994). Reliability Applied to Slope Stability Analysis. Journal of Geotechnical Engineering, Vol 120, No. 12.

Christian, J.T. and Urzua, A. (1998). Probabilistic Evaluation of Earthquake-Induced Slope Failure. Journal of Geotechnical and Geoenvironmental Engineering, Vol 124, No. 11.

Kraft, L.M. and Watkins, D.J. (1976). Prediction of Wave-Induced Seafloor Movements. Proceedings of the 15th Coastal Engineering Conference, Honalulu, Hawaii.

Locat, J. and Lee, H.J. (2000). Submarine Landslides: Advances and Challenges. Keynote Lecture, 8th International Symposium on Landslides, Cardiff, U.K.

Pratson, L.F. and Mello, U.T. (1995). Pore Pressure Response to Sedimentation, Erosion and Sea Level Change and their Influence on Submarine Slope Stability (Abstract). EOS supplement (Nov 7, 1995), Presented at AGU 1995 Fall meeting, Dec. 11-15, 1995 , San Francisco, California. pg. F192.

Schwarz, H.U., (1982). Subaqueous Slope Failures – Experiments and Modern Occurrences. Contributions to Sedimentology #11.

Seed, H.B. and Idriss, I.M. (1971). Simplified Procedure for Evaluating Soil Liquefaction Potential. Journal of the Soil Mechanics and Foundations Division, Proceedings of the American Society of Civil Engineers, Vol. 97, No. SM9, pp. 1249-1273.

Seed, H.B. and Rahman, M.S. (1978). Wave-Induced Pore Pressure in Relation to Ocean Floor Stability of Cohesionless Soils. Marine Geotechnology, Vol. 3, No. 2.

Yong, R.N., Alonso, P.B., Fransham, P.B. and Tabba, M.M. (1976). Application of Risk Analysis to Prediction of Slope Instability.

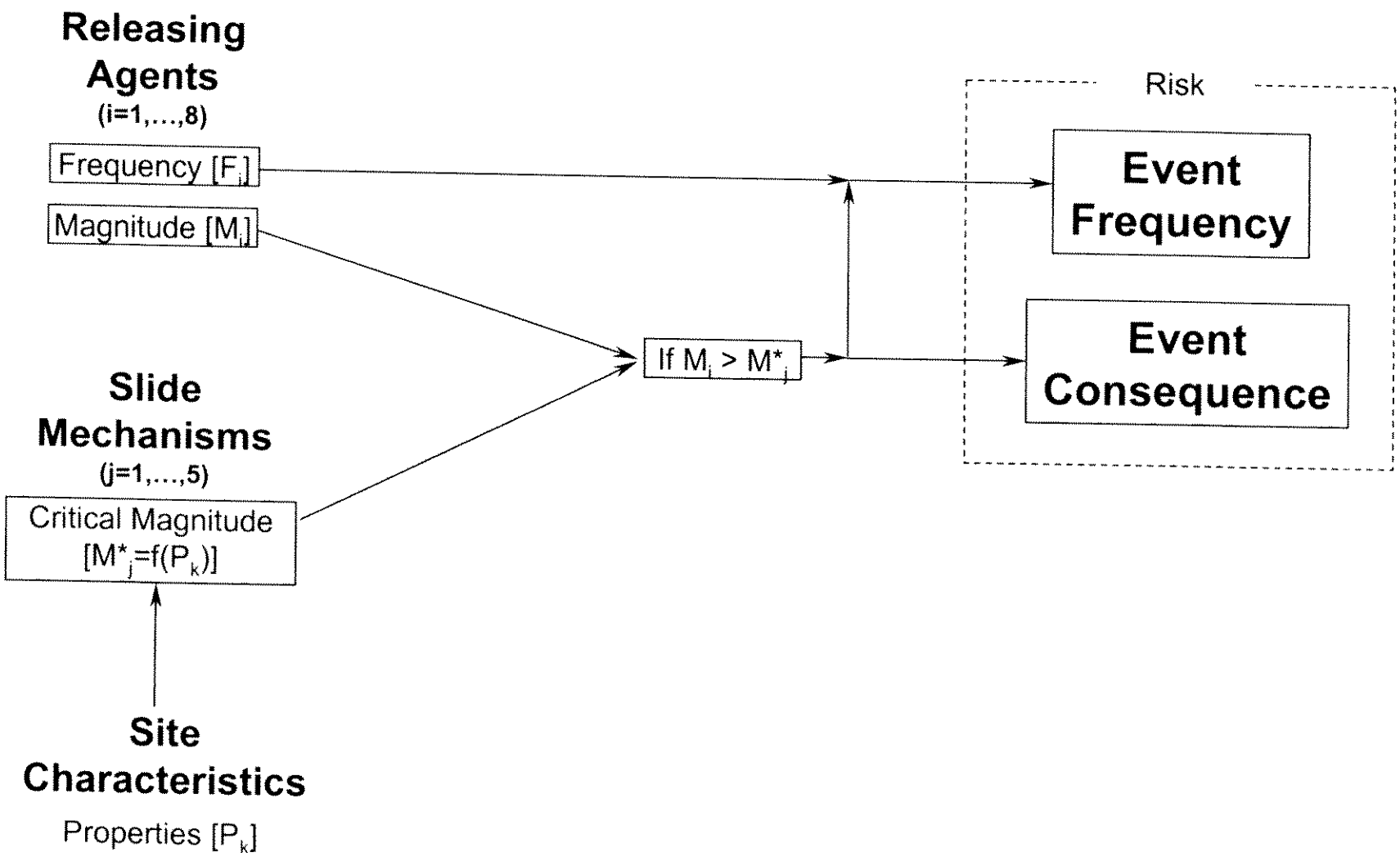

Figure 10-1: General risk assessment framework for submarine slides.

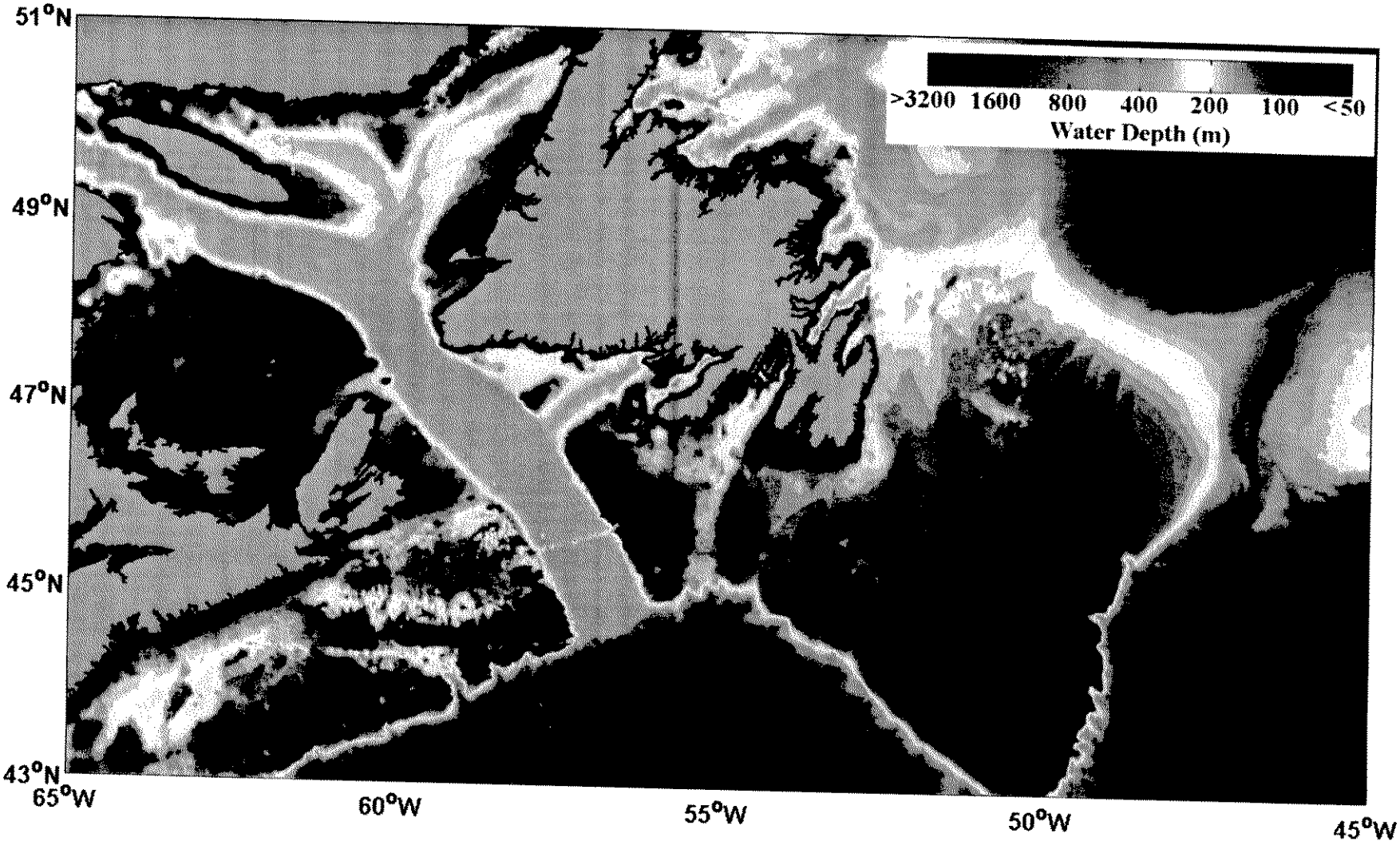

Figure 10-2: Study Region.

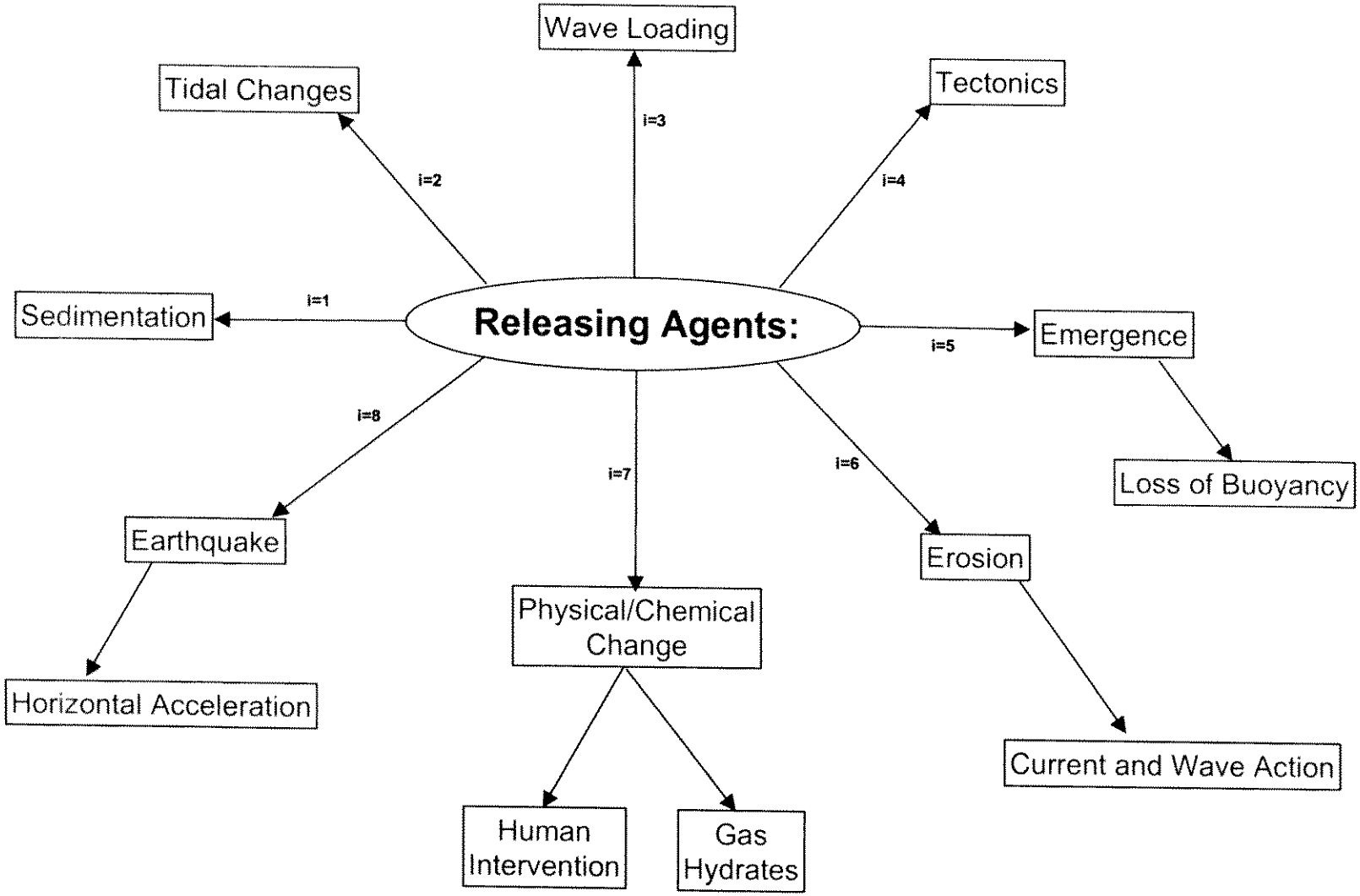

Figure 10-3: Eight different releasing agents identified for submarine slides.

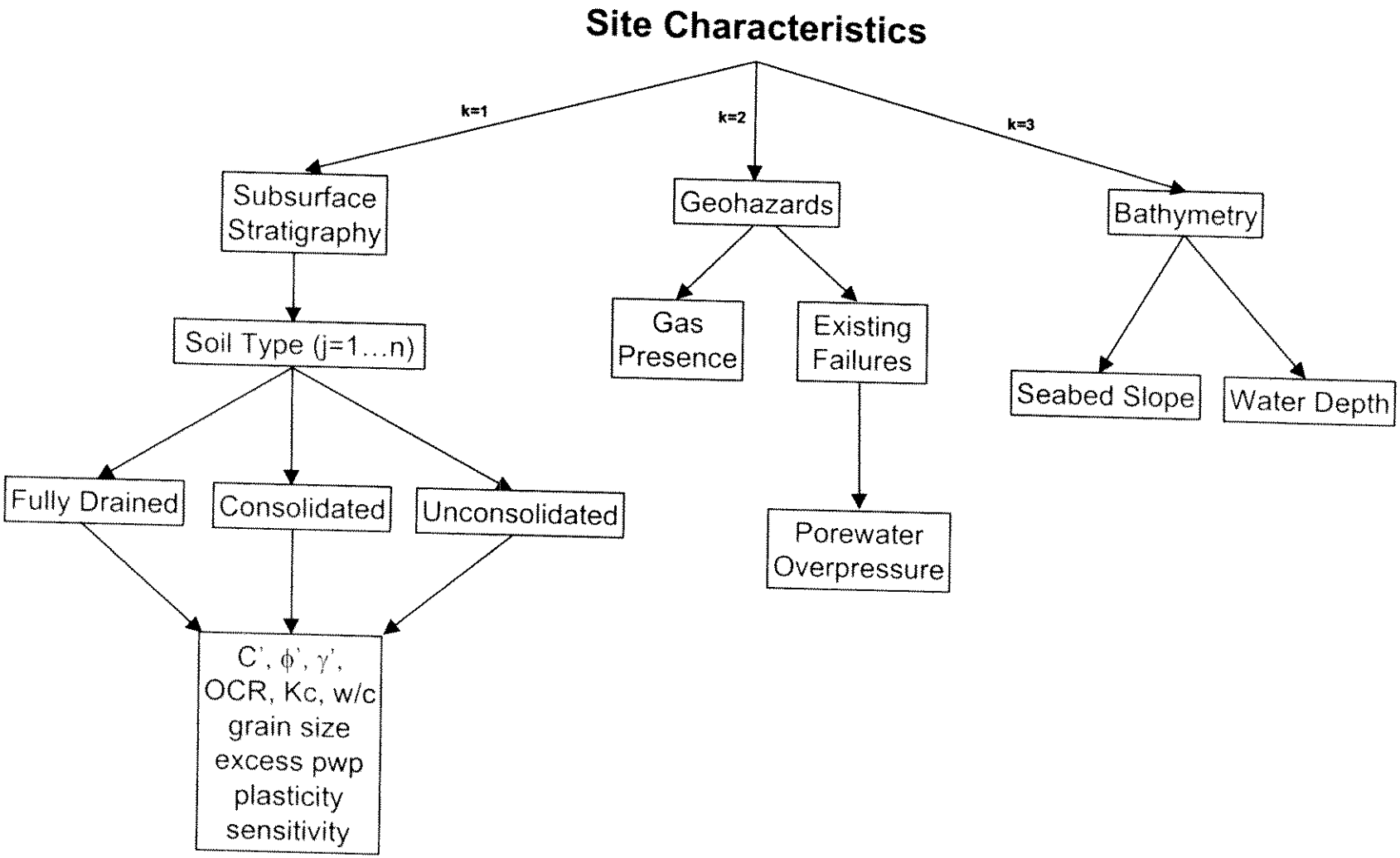

Figure 10-4: Breakdown of the various site characteristics important to risk assessment of submarine slides.

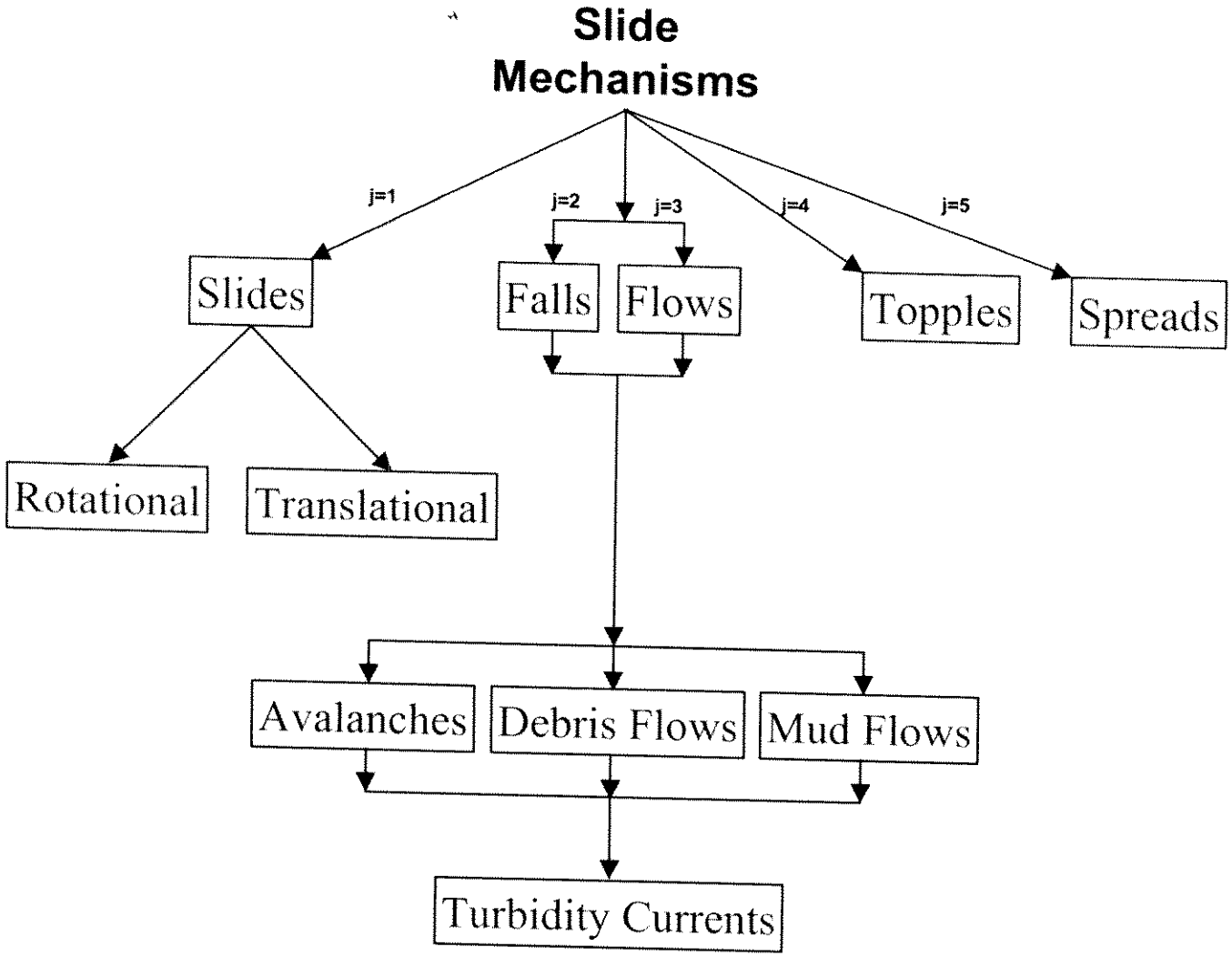

Figure 10-5: Mechanisms associated with submarine slides

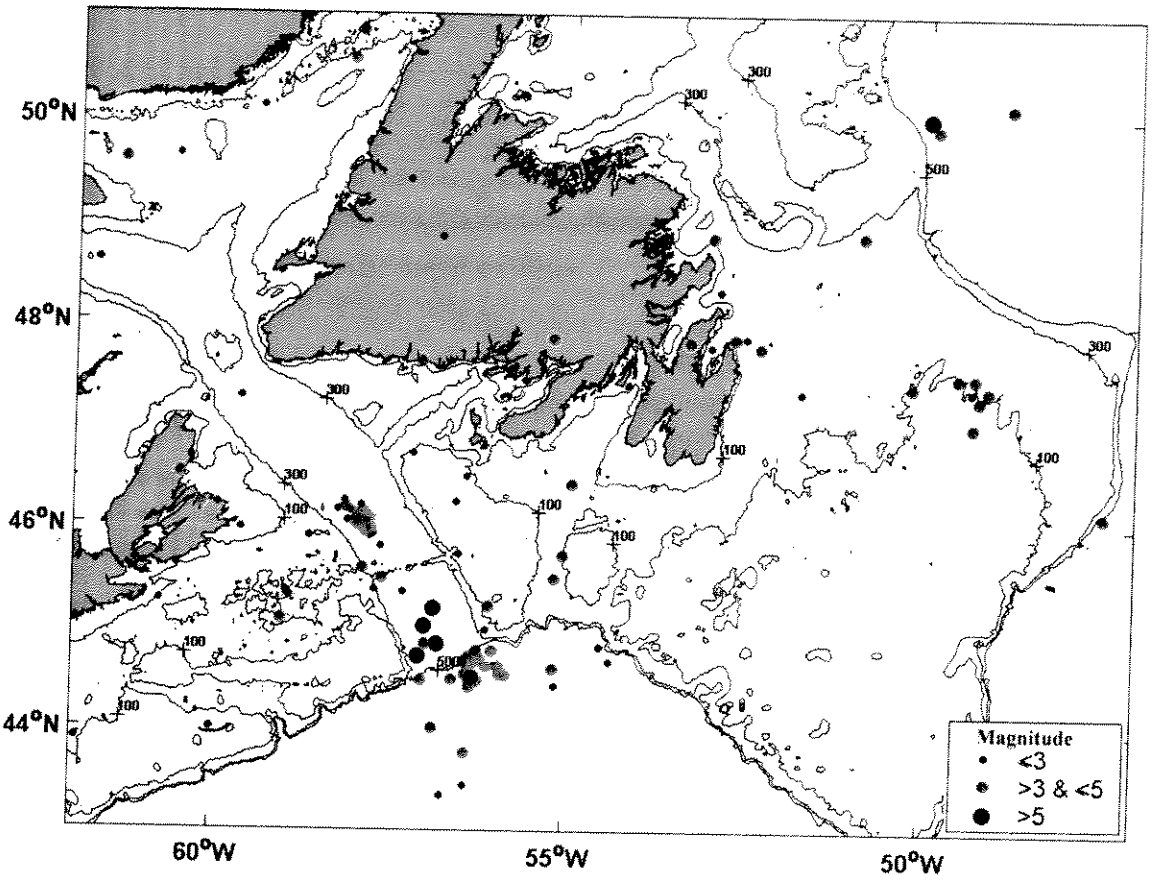

Figure 10-6: Epicenter locations for seismic activity in and around Newfoundland and the Grand Banks.

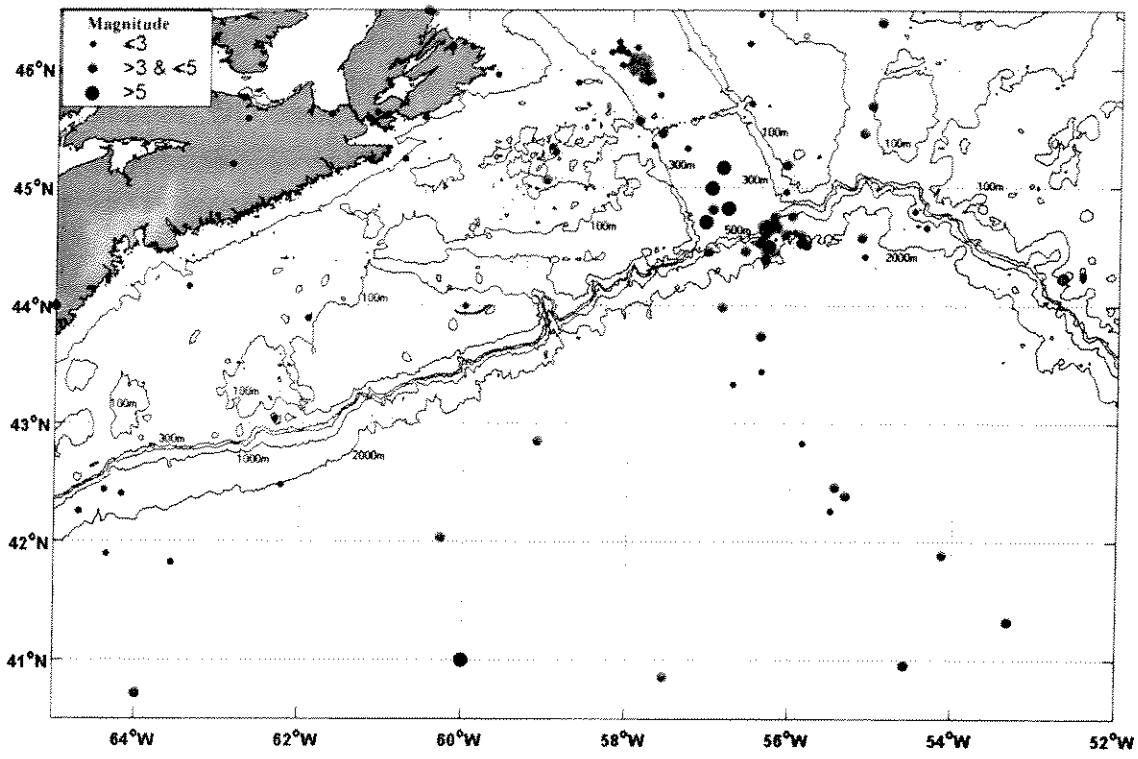

Figure 10-7: Epicenter locations for seismic activity in and around Nova Scotia and the Scotian Shelf.

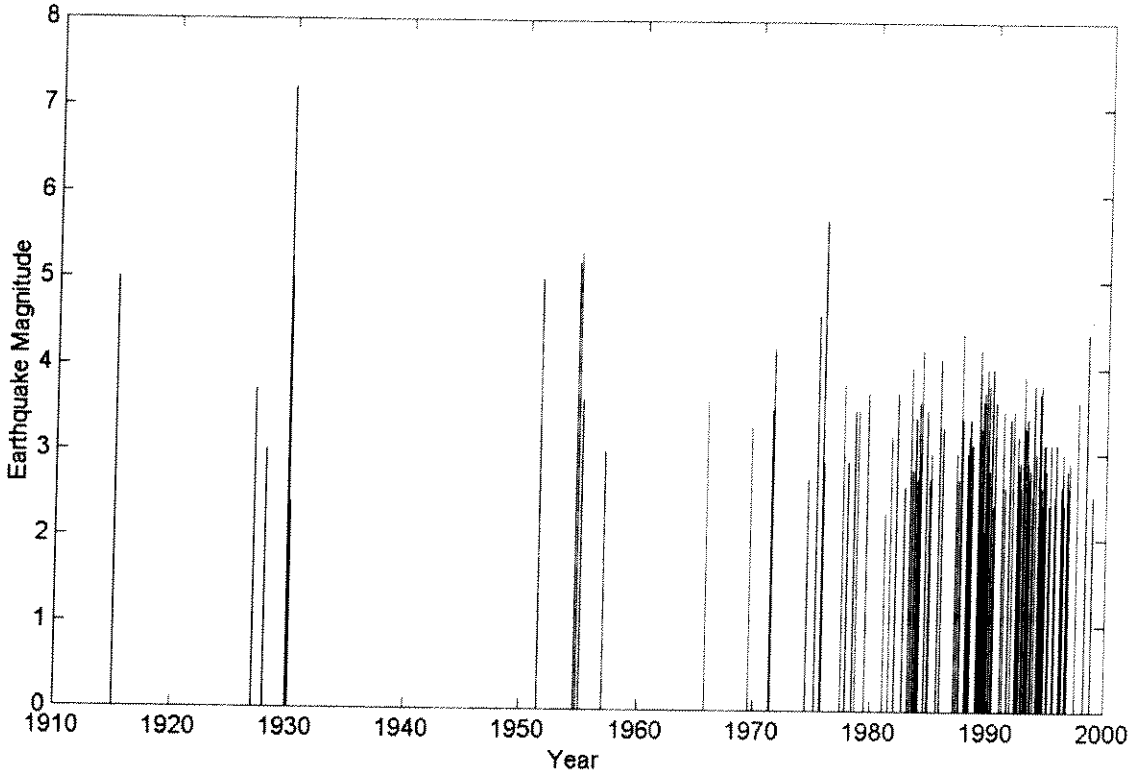

Figure 10-8: Time history and magnitude of earthquake events in the study region.

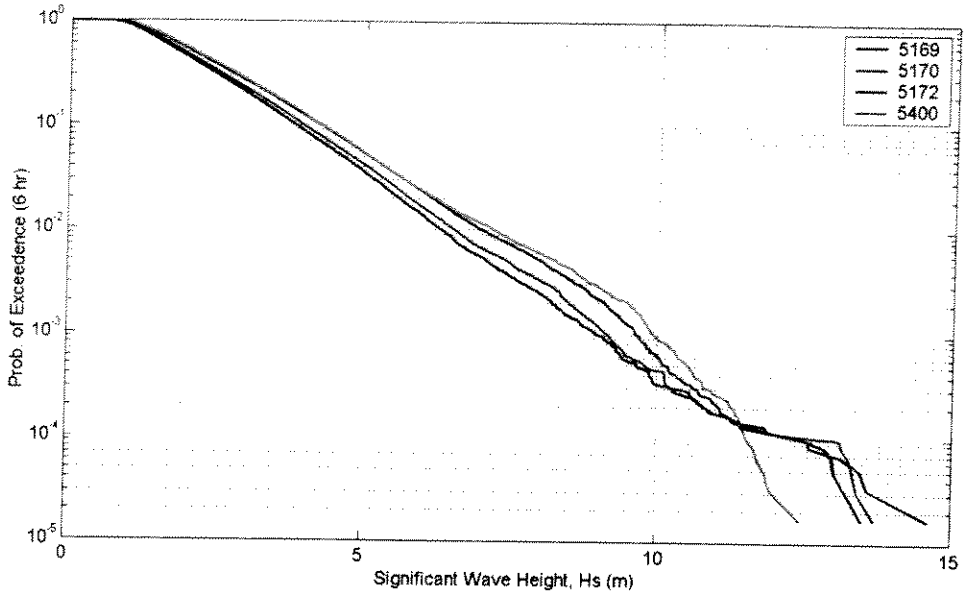

Figure 10-9: Probability of exceedance plot of significant wave height for four event locations on the Scotian Shelf.

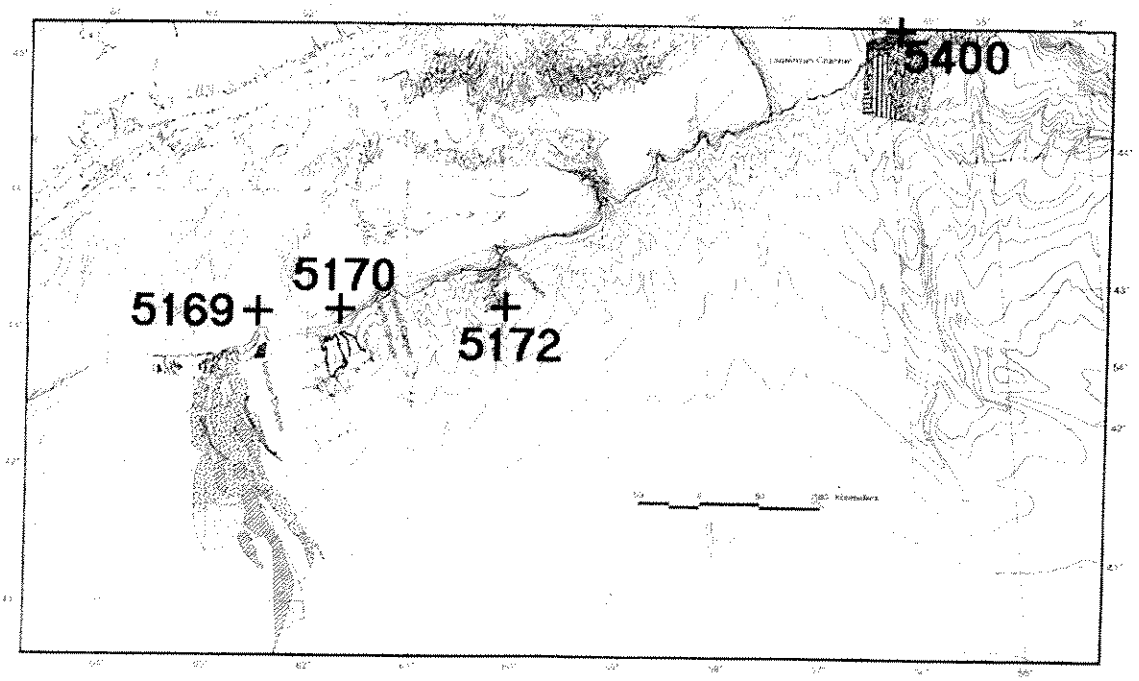

Figure 10-10: Map of Scotian Shelf showing locations of significant wave height calculations and submarine slide events.

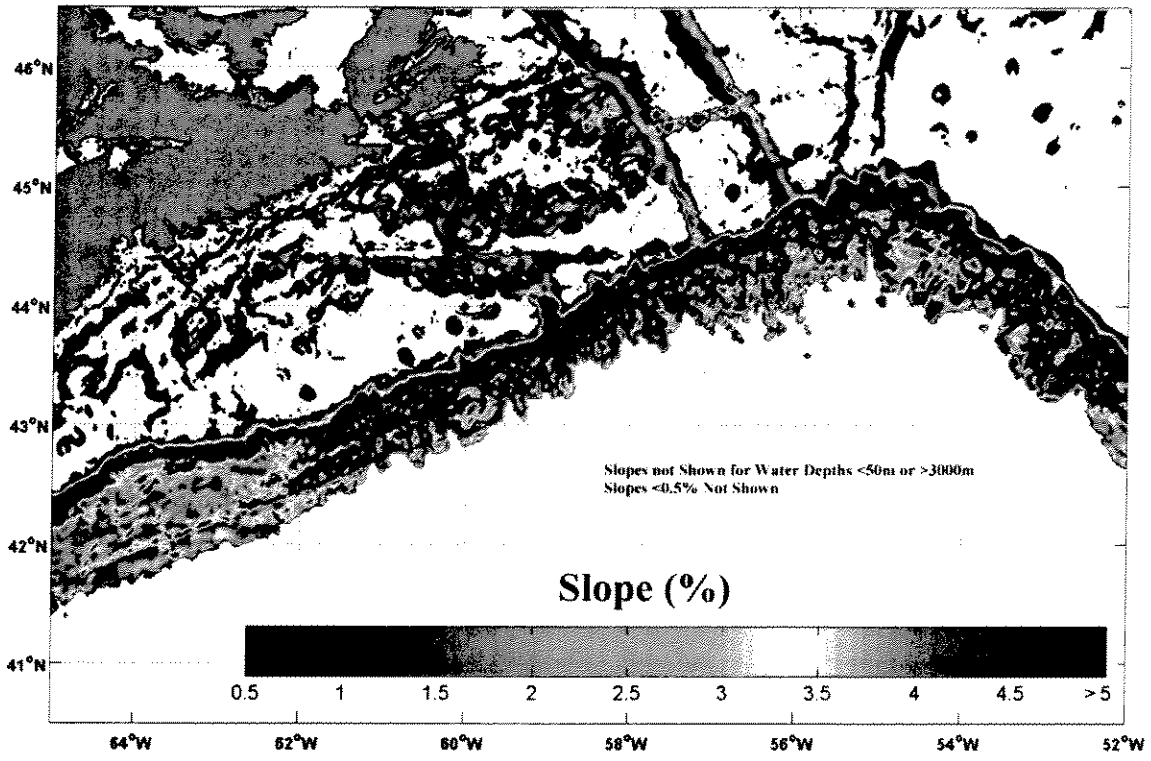

Figure 10-11: Map showing slope intensities on the Scotian Shelf for water depths between 50m and 3000 m for slopes >0.5%.

11 SUMMARY OF PHASE I WORK AND PHASE II WORK SCOPE

11.1 Summary of Phase I Work

11.1.1 Phase I Objectives

The objective of the Phase I work was four-fold: to review existing case histories of submarine failures, to examine failure sites on the Scotian Slope, St. Pierre Slope and in the Gulf of Mexico and to analyze these failures by appropriate methodologies. Next, centrifuge demonstration tests of submarine failures were conducted and the framework for the risk analysis of submarine slope instability was outlined. These objectives were divided into a number of tasks that are described subsequently.

11.1.2 Phase I Work

Background Information

Background information was presented on a number of aspects of submarine failures. The classification of slides was presented along with an approach to submarine slope stability analysis. The classification of information relating to submarine slides was summarized and the ratios and indices used to describe slide were outlined. Concepts relating to the cyclic loading of soils were presented and finally examples other types of analysis conducted during case histories were summarized.

Study of Case Histories and Loading Conditions

Well-known case histories of submarine slides in offshore areas worldwide were selected for examination to gain an understanding of the nature of submarine slides. A summary of submarine failure morphology, the potential loading conditions and failure mechanisms was conducted. In addition, information on the analysis of the slides was provided, along with an integrated synopsis of the analytical methods used by researchers for these failures.

Regional In-depth Studies: Scotian Slope, St. Pierre Slope and Gulf of Mexico

The existing loading conditions, geohazards, geotechnical and geological conditions for the eastern Scotian Slope were identified and summarized. The three failures on the Scotian Slope; the Verrill, the Albatross and the Logan, were described in detail through consideration of the slide morphology, sediment types and properties and previous analysis. Transects through each of the failures were analyzed for existing slope stability through use of the infinite slope and limit equilibrium approach. How the existing failure could have evolved was assessed. Next, the effect of excess pore water pressure and seismic loading on the selected profiles was considered. The St. Pierre Slope was analysed in a similar manner as the Scotian Slope failures. Work on the Gulf of Mexico seafloor failure has not been included with this draft report.

Gulf of Mexico Specific Geohazard

A summary of analyses related to a failure of a platform triggered by Hurricane Camille in 1969 is presented. Program validation and parametric studies were carried out for a range of water depths, soft clay strengths and seabed slope angles.

Geotechnical Aspects of Gas Hydrates

Evidence suggests that gas hydrates have had triggered a number of slope failures. Details of gas hydrates with respect to slope stability issues are described.

Centrifuge Demonstration Test

The results of two centrifuge demonstration tests were presented in order to determine the applicability of the centrifuge to understanding the mechanics of submarine slope failure. The tests were designed to highlight a variety of triggering mechanisms. Soil deformation characteristics, soil properties and slope stability were considered in the analysis of results.

Framework of the Risk Analysis

At this stage, a framework of risk analysis was presented in order to identify dominant failure mechanisms and highlight the governing parameters for those mechanisms. The releasing agents were described, the data required for the models and the site parameters were outlined. Where readily available, mechanistic models governing the effect of the releasing agents were presented, and data relating to the occurrence of failure triggers for the marine slope was presented.

Design of the Experimental Program

Results of Phase I were reviewed with the project team and will be reviewed with the industry sponsors. The review from the project team has provided a basis from which the experimental program has been designed. A proposal for Phase II, including recommendations from the team, has been presented in the following section. The proposal focuses on the experimental program that incorporates aspects relating to the configuration of the experimental program and analytical modeling approaches. The project team welcomes comments from the sponsors on the draft proposal for Phase II of PODS.

11.2 Phase II Proposed Work Scope

11.2.1 Description of Phase II Work

Phase II moves towards quantification of slope stability based on the phenomenological evidence gathered in Phase I and the analytical work carried out to set up a basic predictive model. Verification of the predicted model by analyzing an actual slope failure would be almost impossible to do without a recent failure that could be assessed with relevant site information. In addition, it is possible to reliably assess the predictive model, and to verify its applicability to offshore development design, by analyzing a range of submarine slope failures that are induced

in a large-scale centrifuge. The potential for use of large centrifuges in geotechnical problem solving has been demonstrated over 70 years. There are now very few major engineering offshore structures that do not benefit from either present or past centrifuge modeling of such phenomena or structures as foundation behaviors, anchors, piles, suction caissons, ice scours, pipelines and so on. The centrifuge has been used extensively for analyzing slope stability for natural slopes and embankments. The reliability is proven.

The use of a centrifuge for modeling submarine slopes has not been developed to the same degree as other experimental modeling applications. However, based on the extensive experience that is now compiled at C-CORE, we believe that it would be possible to model the various triggering mechanisms. The slopes that fail are in one way or another induced by excess pore pressure. The centrifuge lends itself particularly well to replicating this phenomenon and therefore it is a part of the Phase II activities to verify what has been learned from Phase I and to enhance the capability to predict potential submarine slope behavior with a proven numerical model.

The work on understanding the effect of gas hydrates will be continued and incorporated into the numerical modeling. The objective is to be able to predict the effects of hydrate melting on the pore pressure in sediments and hence the stability of slopes where gas hydrates are expected.

Finally, the results of previous work will be incorporated into a risk analysis framework that will incorporate material hazard effects including earthquakes, gas hydrates, sedimentation and erosion. Within this framework, a series of regional maps for the Scotian Slope that describe significant risk features in the development areas will be prepared for use by owners and contractors.

11.2.2 Proposed Work Approach

An outline of the proposed tasks to be conducted in Phase II is provided in the following paragraphs. The involvement of the team is indicated beside each task. It is anticipated that additional team participants will be brought to the project in order to address specific objectives.

TASK A: *Laboratory Testing & Design of Centrifuge Experiments (NGI, GSC, C-CORE)*
The Phase I work demonstrated that centrifuge modeling is an applicable technology for use in the evaluation submarine slope failures. In Phase II a series of focused centrifuge experiments will be designed. Possible loading mechanisms during the centrifuge tests include: wave loading through a wave actuator, surcharge loading and earthquake loading.

Laboratory testing will be conducted under both static and cyclic loading to replicate wave and earthquake loading and to determine representative soil parameters for use in the centrifuge tests. Soil cores taken from the Scotian Slope, including slide sites, will be subjected to laboratory testing and analysis. Results will be correlated to down hole testing where feasible.

TASK B: *Centrifuge Experiments (C-CORE)*
The designed centrifuge tests will be conducted. Submarine slopes have previously been tested in the centrifuge and a similar test set-up and apparatus can be used. The actual design of the test set-up will depend on the test conditions.

TASK C: *Analysis of Centrifuge Results (NGI, C-CORE)*
The results of the centrifuge experiments will be analyzed and presented. Prediction, back-calculation and interpretation of centrifuge experiments will be conducted at NGI and C-CORE.

TASK D: *Numerical Analysis Work (OTRC, NGI, C-CORE)*
Each centrifuge experiment will focus on understanding more about specific aspects of the offshore slope stability problem. Using the information from the centrifuge tests, numerical model tests will be run based on results of centrifuge experiments. In addition, work will be done on a model for predicting the effect of earthquake loading on inducing submarine slope failure in soft sediments.

TASK E: *Gas Hydrate Work (U of C, OTRC)*
Work on the effect of gas hydrates will be continued. Various scenarios will be considered that could lead to gas hydrate dissociation. Theories will be developed on the effects of hydrate melting on the pore pressure in sediments.

TASK F: *Risk Analysis Framework (NGI, C-CORE, GSC, other researchers)*
The framework for the risk analysis will be further developed using information from the centrifuge tests and numerical analyses. Work will be compared with NGI calculation models. Regional maps for the Scotian Slope describing the significant risk features will be compiled.

11.2.3 Schedule

The schedule for the project and its tasks are shown on Figure 11.1. The anticipated start date for the project is November 2001. The project will take approximately 18 months to complete.

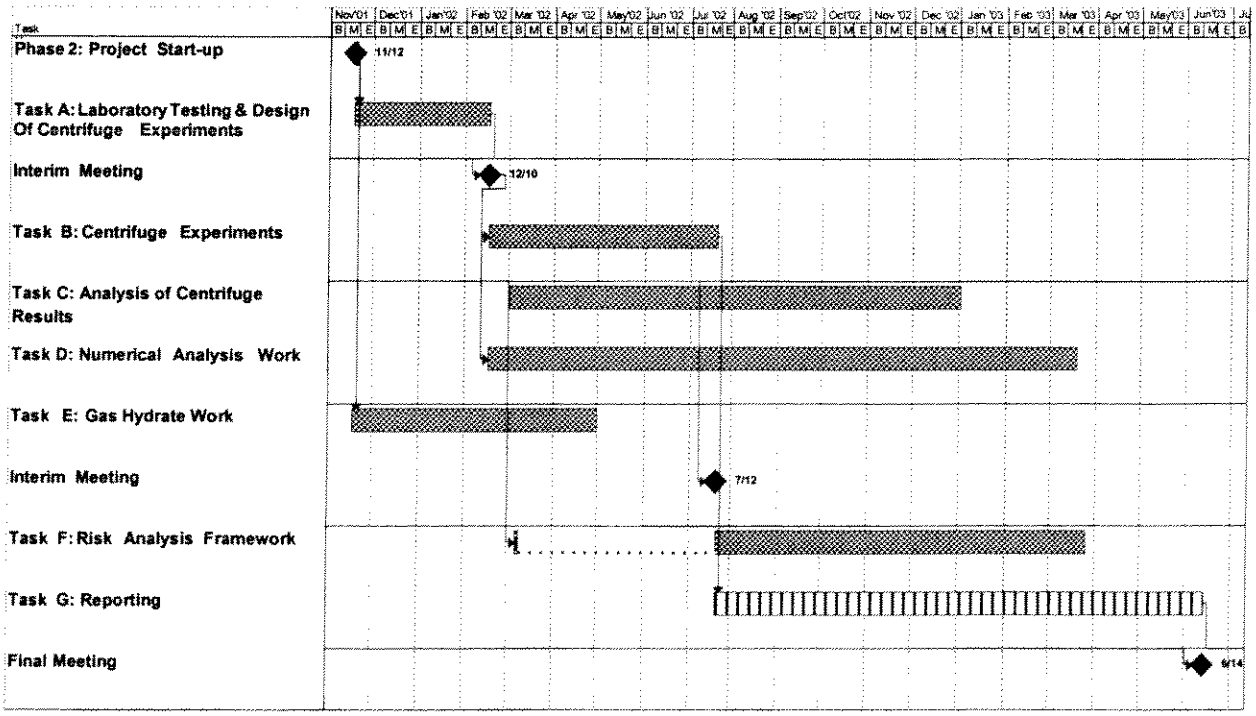

Figure 11-1: Proposed Schedule for Project Offshore Deep Slopes, Phase II

11.2.4 Budget

The budget for Phase II of the project is $180,000 US. C-CORE is requesting industry support of $30,000 US per sponsor. The project funding will be received by C-CORE, GSC, OTRC, NGI and the other researchers involved in the project.

11.2.5 Confidentiality

The information obtained from the work conducted for Phase II of PODS must remain confidential to the participants and project sponsors for a period of two years from the completion of the project.

11.2.6 Corporation Information

C-CORE

C-CORE is an applied engineering research and development corporation in St. John's, Newfoundland, Canada. We encompass a wide spectrum of engineering and business skills required by resource industries operating in global markets. At C-CORE we collaborate closely with industrial partners, research institutes, universities, and government agencies to identify and respond to global technological challenges. Since 1975, our activities have grown to include applied research and development, technology transfer and demonstration, commercialization of intellectual property, and specialized advisory services to a wide range of industries, the largest being pipeline, oil and gas, mining, and fisheries. Demonstrated abilities to lead and develop alliances have made C-CORE a recognized resource for industry and government.

The collaborative work environment at C-CORE allows us to apply the fullest range of expertise to client needs. We undertake major programs in ice engineering, remote sensing, geotechnical engineering, and intelligent systems. A major initiative at C-CORE is the adaptation of space technologies to resource sectors such as mining, oil and gas, and forestry that operate in harsh terrestrial and marine environments.

Geotechnical engineering at C-CORE focuses primarily on physical and numerical modeling. C-CORE has considerable expertise in investigating gravity dependent phenomena using reduced scale physical modeling in its centrifuge facility. C-CORE's geotechnical expertise encompasses centrifuge modeling, full-scale modeling, pipeline testing, ice/seabed interaction, soil/structure interaction, and risk and numerical analysis. Besides PODS, C-CORE is currently involved in another project relating to offshore slope stability, COSTA-Canada (Continental Slope STAbility) whose participants include researchers at universities across Canada. This project is linked to a similar project undertaking among European researchers.

Centrifuge modeling is currently the most reliable technique of using small-scale tests of geotechnical phenomena to predict full-scale conditions. C-CORE applies its geotechnical centrifuge testing to offshore structures, including offshore production platforms, pipelines, breakwaters and wharves; and onshore structures such as dams, pipelines, landfills, mines, and large buildings. Tests are routinely conducted in soil statics, soil dynamics, and environmental engineering.

C-CORE maintains a full-scale pipeline testing facility and a world class centrifuge facility. The centrifuge machine is capable of carrying a cargo payload up to 200g's. Through our highly qualified staff, excellent facilities, and collaborative partnerships with industry, government, institutes, and universities, C-CORE has developed considerable expertise in the provision of geotechnical engineering services and technologies in the oil and gas, pipeline, and environmental sectors.

Offshore Technology Research Center

The Offshore Technology Research Center (OTRC) is a National Science Federation (NSF) Engineering Research Center created in support of the offshore oil and gas industry. The center was founded in 1988 by Texas A&M University and the University of Texas at Austin, to facilitate basic engineering research pertaining to optimal resource development in deep offshore waters. The OTRC's mission is to reduce the cost and increase the reliability of producing oil and natural gas at great water depths so reserves can be economically produced while protecting sensitive coastal and marine environments. Through the usage of facilities at both universities, the center concentrates its study in three main areas: fluid/structures interaction, material and structural system integrity and structures/seafloor interactions. Since its inception, the center has taken on a leadership role in cutting-edge research within deepwater production problems. Presently, the center is in a position to address the need for new and evolving technologies, larger and more complex facilities, modification of procedures, and additional environmental protection issues.

Geological Survey of Canada

The Geological Survey of Canada (GSC) plays an integral role in Canadian geoscientific research. Firstly, GSC supplies a national geoscience knowledge base in support of mineral and hydrocarbon exploration and development in Canada. Secondly, GSC provides a geological basis that is necessary to understand and address health, safety and environmental issues. Finally, GSC advocates the interest of Canadian geoscience at an international level. GSC has particular fortitude in onshore and offshore surveys and in the interpretation and mapping of geoscience information. GSC adheres to a number of working principles including continuing development of a dedicated, internationally renowned staff as well as demonstrating and promoting scientific excellence in improving its products and services. GSC applies these strengths within industry, universities and other government organizations in Canada and throughout the world.

Norwegian Geotechnical Institute

The forerunner to the Norwegian Geotechnical Institue (NGI), the "Officer for Geotechnics" was formed in 1950. Since that time, this private foundation has worked to meet its goal, "to promote geotechnical research and work for the implementation of the results in practice." To accomplish this goal, NGI has completed a great deal of consulting work alongside research projects. Many textbooks at technical colleges and universities incorporate results and methods developed at NGI. Being a diverse organization allows NGI to maintain a high standard of excellence in a number of professional areas including onshore foundations, marine structures, rock engineering, soil investigation, and so on. NGI has been a key player in Norway's oil industry. The institute has played a particularly significant role in solving problems of underwater soil sampling and the foundation of large platforms in the North Sea. NGI's efforts to this regard have earned them, distinction for "outstanding contributions in the field of offshore geotechnical engineering" from the International Society for Soil Mechanics and Foundation of Engineering.